国立病院機構鹿児島医療センター

研究業績集　第24号

令和5年4月～令和6年3月(2023年4月～2024年3月)

国立病院機構鹿児島医療センター
臨床研究部

巻頭言

鹿児島医療センター研究業績集第 24 号の発刊にあたって

令和 5 年度（2023 年度）研究業績集第 24 号を発刊する運びとなりました。平成 11 年（1999 年）に始まり、24 冊目となります。今回の論文数は総説を含めて 41 編（英文 27 編、和文 14 編）、学会報告 128 件（国外 6 件、国内 122 件）でした。昨年と比べ、かなり増加しています。コロナ感染症が5類相当となり、学会活動がコロナ前に戻りつつあるようです。これからますます盛んになることを期待しております。鹿児島医療センターの研究成果を発信し続けることが重要と考えています。

2024年度から鹿児島医療センターの鹿児島大学連携講座名を先端医療学講座の「生理活性物質制御学」から「臨床情報医工学分野」に変更し、今年度就任した松下茂人臨床研究部長を中心に活動を開始しました。今まで生化学関連の研究が中心でしたが、それに加え、予防・診断や治療医学など、実践的・包括的な臨床研究も可能となりました。大学院生にとって基礎的研究から臨床的研究まで幅広い選択ができるようになっています。今年度秋より1名、来年度（2025 年度）さらに1名の大学院生が増え、指導教官（客員教授）も以前より充実することになりました。若い研究家が研究の面白みを感じ、きちんとした成果が出るように手助けをしたいものです。

最近、日本の研究は論文数が減少し、さらに信頼性も揺らいでいます。2014 年 1 月、STAP 細胞の論文が撤回された事件は話題になりましたが、その後の 10 年間に研究不正などで論文を撤回、または取り消しをしている撤回論文数世界のランキング上位 10 名中 5 名が、日本の医師で有ったと報告されています。日本の研究の復活が喫緊の課題です。若い人たちの新鮮な感覚で研究を行い、質の高い研究発表に期待しています。臨床成果と同時に研究でも実績を上げ、自分自身の努力をしっかりと形に残してもらいたいものです。鹿児島医療センターが、若者が集まる臨床も研究も強い医療施設になることを祈念しております。

独立行政法人国立病院機構鹿児島医療センター
院長　田中　康博

目次

1. 臨床研究部の組織概要

1. 名称・所在地

独立行政法人国立病院機構鹿児島医療センター臨床研究部

鹿児島県鹿児島市城山町８－１

2. 沿革

臨床研究部は 1999 年 10 月に設置されました。当初は病態生理研究室、医用工学研究室、画像診断研究室、臨床疫学研究室、治療評価研究室の 5 室で運営されていましたが、2007 年に治療評価研究室を臨床研究推進室と名称変更を行い、さらに 2013 年からは治験管理室を加え、現在 1 部 6 室で活動しています。2006 年からは東病棟 8 階に臨床研究部・治験管理室がありましたが、2018 年 4 月の逓信病院機能移転に伴い、2017 年 11 月に臨床研究部は旧更衣棟に、治験管理室は事務棟に移転しました。

3. 組織構成

臨床研究部長の総括のもとに以下の研究室を設置しています。

1. 病態生理研究室
2. 医用工学研究室
3. 画像診断研究室
4. 臨床疫学研究室
5. 臨床研究推進室
6. 治験管理室

令和2年度の臨床研究部の各室の体制は以下に示す通りです。

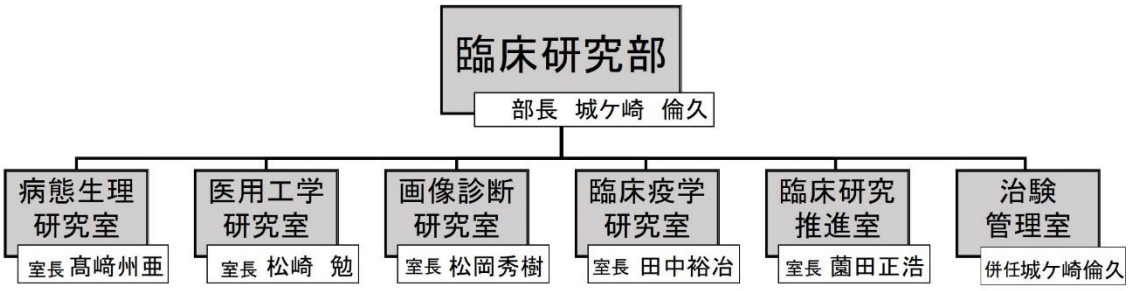

4. 鹿児島大学大学院医歯学総合研究科

当院は 2009 年より、鹿児島大学の連携大学院となっており、先進医療学講座（連携講座）生理活性物質制御学を開講しています。

これまでに 5 人の学生が臨床研究部で研究を行い、鹿児島大学大学院医歯学総合研究科の大学院博士号を取得しました。

2. 臨床研究と治験

① 臨床研究

(ア) NHO 共同臨床研究

領域・課題番号	研究責任医師	研究課題名
NHO 共同研究	城ケ崎倫久	自己炎症性疾患特異的 iPSC 細胞の培養ストックの作成及び分化誘導
H26-遺伝子-03	郡山暢之	日本人の肥満症の発症と治療効果・抵抗性に関連する遺伝素因の探索 -オーダーメイド医療の確立-(G-FORCE 研究)
特定臨床研究 H27-EBM(介入)-01	塗木健介	免疫抑制患者に対する 13 価蛋白結合型肺炎球菌ワクチンと 23 価莢膜多糖体型肺炎球菌ワクチンの連続摂取と 23 価莢膜多糖体型肺炎球菌ワクチン単独摂取の有効性の比較 -二重盲検無作為化比較試験-(CPI Study)
H29-EBM(観察)-02	中島 均	我が国における左冠動脈主幹部インターベンションに対するコホート研究(LM-JANHO)
H28-NHO(血液)-02	大塚眞紀	成人初発未治療びまん性大細胞型 B 細胞リンパ腫における R-CHOP 単独治療と放射線併用療法の治療成績、QOL、費用、費用対効果の多施設共同前向きコホート研究
H28-NHO(多共)-02	野元三治	メトトレキサート(MTX)関連リンパ増殖性疾患の病態解明のための多施設共同研究
H30-NHO(糖尿病)-01	郡山暢之	多面的管理達成者の糖尿病性腎臓病(DKD)予後改善効果評価法の確立と、効果予測のための非侵襲的指標の確立(DKDrem-2 研究)
H30-NHO(外科)-01	塗木健介	本邦における成人鼠経ヘルニア術後慢性疼痛の実態調査とそのリスク因子解析 -多施設共同前向きコホート研究- (HERNIA STUDY)
H31-NHO(血液)-01	大塚眞紀	未治療濾胞性リンパ腫における Obinutuzumab の治療成績、QOL、費用対効果、予後に関する多施設前向きコホート研究(PEACE-FL)
H31-NHO(多共)-02	野元三治	メトトレキサート(MTX)関連リンパ増殖性疾患の遺伝子変異プロファイルの解析
R2－NHO(心脳)-04	城ケ崎倫久	がん化学療法関連心筋症の予測、早期発見、早期治療 ～心臓超音波検査 speckle tracking 法、タイチン truncating 変異の検出、尿中タイチン N フラグメント測定、血中心筋トロポニン I 高感度測定の比較検討～
R3－NHO(血液)-01	大塚眞紀	レジストリーデータを利用した AYA 世代 DLBCL の臨床的・生物学的特性を明らかにする観察研究(NHO-DLBCL-AYA 研究)
R3-NHO(他研)-01	中村康典	DOAC 服用患者における抜歯の安全性の確立に関する研究:ガイドライン確立のための多施設共同前向き研究
R4－NHO(心脳)-01	松岡秀樹	急性期 BAD 型脳梗塞に対する抗血栓療法の種類と神経学的予後に関する前向き探索研究

（イ）競争的研究費等

I. 公費臨床試験

財源	課題名	研究者名	金額（円）
厚生労働省 厚生労働科学研究費補助金	小児から成人期発症遺伝性 QT 延長症候群の突然死予防に関する研究	分担研究者 吉永正夫	100,000
日本医療研究開発機構研究費	進行性悪性黒色腫治療における抗 PD-1 抗体との TM5614 の安全性・有効性を検討する第 II 相試験	分担研究者 松下茂人	259,872
日本医療研究開発機構研究費	頭頸部基底細胞癌縮小マージン切除による新たな低侵襲標準治療の開発	分担研究者 松下茂人	1,300,000
日本医療研究開発機構研究費	爪部悪性黒色腫への指趾骨温存切除による新たな低侵襲標準治療の開発	分担研究者 松下茂人	650,000
日本医療研究開発機構研究費	ロメリジン塩酸塩による CADASIL 患者に対する脳虚血イベント再発抑制	分担研究者 松岡秀樹	650,000
文部科学省 科学研究費助成事業　基盤研究（C）	心臓弁膜症術後合併症制御に対する医学管理における系統的口腔管理の構築（21K10389）	主任研究者 中村康典	793,000
		分担研究者 金城玉洋	39,000
		分担研究者 片岡哲郎	39,000
		分担研究者 平峯聖久	39,000
文部科学省 科学研究費助成事業　基盤研究（C）	口腔機能評価と健康指標のデータビジュアライズと口腔機能管理アウトカムの検討（23K09483）	分担研究者 中村康典	65,000
文部科学省 科学研究費助成事業　基盤研究（C）	唇裂患者の顔貌評価を三次元から四次元へ進化させる分析方法の開発（22K10125）	主任研究者 大河内孝子	468,000
		分担研究者 中村康典	260,000

II. 民間セクターからの寄付金

課題名/依頼業者名	研究者名	金額（円）
弁膜症外科治療における研究（心臓血管外科）	金城玉洋	500,000
高齢者の血管疾患に対する外科治療の研究助成	金城玉洋	600,000
201T 心筋シンチにおける心筋外集積抑制手法の至適画像処理パラメータの検討	宮島隆一	300,000
肝細胞がんに対する冠動脈塞栓療法に関する研究	櫻井一宏	200,000
難治性創傷における wound hygiene コンセプトに基づいたケアでのバイオフィルム形成能と筋線維芽細胞の動的変化の相関解析	松下茂人	100,000

課題名/依頼業者名	研究者名	金額(円)
安全な消化器外科手術	塗木健介	100,000
教育研究の助成	金城玉洋	100,000

(ウ)臨床研究課題

	研究内容・課題名	部署・研究者名
1	動脈硬化を基盤とした虚血性心臓病における新規血液マーカーの確立	第 1 循環器内科
2	エベロリムス溶出性コバルトクロムステント(CoCr-EES[XIENCE])留置後の DAPT 投与期間を 1 か月に短縮することの安全性を評価する多施設前向きオープンラベル無作為化比較試験(ShorT and Optimal duration of Dual AntiPlatelet Therapy study-2(STOPDAPT-2)	第 1 循環器内科 中島　均
3	日本心血管インターベンション学会内登録データを用いた統合的解析	第 1 循環器内科
4	日本経カテーテル心臓弁治療学会(JTVT)内登録データを用いた統合的解析	第 1 循環器内科
5	至適な血管内超音波ガイド経皮的冠動脈インターベンションの複雑性病変における臨床経過を評価する前向き観察研究(OPTIVUS)	第 1 循環器内科
6	鹿児島県における急性冠症候群(ACS)のレジストリー(OK－ACS　Registry)	第 1 循環器内科
7	1・2世代薬剤溶出性ステント留置後のステント血栓症に関するレトロスペクティブ多施設レジストリー(REAL-ST)	第 1 循環器内科
8	胸部正中切開創の表皮細菌が及ぼす影響と皮膚ドレッシング剤の効果	心臓血管外科 立石直毅
9	非弁膜症性心房細動とアテローム血栓症を合併する脳梗塞例の二次予防における最適な抗血栓療法に関する多施設共同ランダム化比較試験 (Optimal Antithrombotic Therapy in Ischemic Stroke Patients with Non-Valvular Atrial Fibrillation and Atherothrombosis：ATIS-NVAF)	脳血管内科 松岡秀樹
10	K-RESOLVE Network 研究	脳血管内科 松岡秀樹
11	機械的血栓回収療法による再開通後の脳循環時間と再潅流障害との関連についての研究	脳血管内科 濵田祐樹
12	レセプト等情報を用いた脳卒中・脳神経外科医療疫学調査(J-ASPECT study : Nationwide survey of Acute Stroke care capacity for Proper dEsignation of Comprehensive stroke CenTer in Japan)	脳血管内科 松岡秀樹
13	血管モデルを用いた有効な血栓回収療法手技の確立に関する研究	脳血管内科 濵田祐樹
14	脳梗塞再発のリスク因子を有する急性期アテローム血栓性脳梗塞及びハイリスク TIA 患者を対象としたプラスグレルのクロピドグレルとの血小板凝集能の比較臨床研究	脳血管内科 松岡秀樹
15	第 Xa 因子阻害薬による治療下で大出血を認めた患者の特性、医療介入、健康状態の転帰を記録する、多国籍、縦断的、観察研究(REVERXaL)	脳血管内科 松岡秀樹
16	血栓吸引カテーテルを用いた機械的血栓回収療法の効果と安全性に関する多施設共同登録研究(REACT AIS Registry)	脳血管内科 濵田祐樹
17	最終健常確認時刻から 24-72 時間経過した前方循環主幹動脈閉塞を有する脳梗塞例に対する血管内治療の有効性検証の為の多施設共同ランダム化比較研究	脳血管内科 濵田祐樹

	研究内容・課題名	部署・研究者名
18	急性期脳主幹動脈閉塞における機械的血栓回収療法例の後ろ向きコホート研究	脳血管内科 濵田祐樹
19	後方循環の主幹動脈閉塞・高度狭窄症に対する急性期治療の現状	脳血管内科 濵田祐樹
20	未治療 CCR4 陽性高齢者 ATL に対するモガムリズマブ併用 CHOP-14 の第Ⅱ相試験	血液内科 大塚眞紀
21	骨髄増殖性腫瘍の実態と遺伝子変異検索	血液内科 大塚眞紀
22	B 細胞性急性リンパ性白血病におけるターゲットキャプチャーRNA-seq を用いたサブタイプ診断の実行可能性に関する研究	血液内科 大塚眞紀
23	成人 T 細胞白血病リンパ腫における CCR4 遺伝子変異と予後の検討	血液内科 大塚眞紀
24	血小板減少を呈する患者における酵素測定法によるゴーシェ病スクリーニング	血液内科 大塚眞紀
25	80 歳以上未治療びまん性大細胞型 B 細胞リンパ腫に対するポラツズマブベドチン＋R-miniCHP 療法の有効性と安全性を検証する多施設共同非盲検無対象試験	血液内科 大塚眞紀
26	肝細胞癌に対するアテゾリズマブ＋ベバシズマブ併用療法の治療効果と安全性の検討	消化器内科 森内昭博
27	C 型肝炎ウイルス排除治療による肝硬変患者のアウトカムに関する多施設共同観察研究	消化器内科 櫻井一宏
28	CIN の再発因子の検討	婦人科 神尾真樹
29	婦人科領域における DWIBS の有用性に関する研究	婦人科 神尾真樹
30	頭頸部がん再発症例に対する光免疫療法の有効性と適応範囲の検討	耳鼻咽喉科 西元謙吾
31	副甲状腺腫瘍による高 Ca 血症の臨床検査との関連	耳鼻咽喉科 西元謙吾
32	Experience of radiotherapy during the nosocomial cluster of coronavirus disease-19 in a regional core hospital	放射線科 上山友子
33	放射線治療の治療効果評価法・合併症低減法	放射線科
34	オクトレオスキャン症例の解析	放射線科
35	骨転移のある前立腺癌に対する塩化ラジウム治療	放射線科
36	塩化ラジウム治療における MRI の評価	放射線科
37	ブルーリ潰瘍（M.ulcerans 感染症）における無痛性病態メカニズムの解明	病理診断科 後藤正道
38	呼吸上皮腺腫様過誤腫の病理学的特徴と疫学に関する研究	病理診断科 後藤正道
39	耳下腺ワルチン腫瘍の病理学的特徴と疫学に関する研究	病理診断科 後藤正道
40	心臓弁膜症術後合併症制御に対する医学管理における系統的口腔管理の構築	歯科口腔外科 中村康典

	研究内容・課題名	部署・研究者名
41	摂食機能評価に基づいた栄養食事指導の有効性と体組成改善への影響の検討	歯科口腔外科 中村康典
42	メラノサイト系の悪性腫瘍に関する角層解析の有用性	皮膚腫瘍科・皮膚科 松下茂人
43	皮膚腫瘍における免疫応答解析に基づくがん免疫療法予測診断法の確立	皮膚腫瘍科・皮膚科 松下茂人
44	JCOG1605：パクリタキセル既治療原発性皮膚血管肉腫に対するパゾパニブ療法の非ランダム化検証的試験	皮膚腫瘍科・皮膚科 松下茂人
45	ニボルマブ+イピリムマブで治療される悪性黒色腫患者における腸内細菌代謝産物の臨床的意義に関する前向き観察研究	皮膚腫瘍科・皮膚科 松下茂人
46	結合組織性皮膚疾患における病態解明	皮膚腫瘍科・皮膚科 松下茂人
47	皮膚疾患画像ナショナルデータベースの構築とAI活用診療支援システムの開発	皮膚腫瘍科・皮膚科 松下茂人
48	BRAF 陽性悪性黒色腫に対する BRAF･MEK 阻害薬および免疫チェックポイント阻害薬の臨床効果に関する多機関共同後ろ向き観察研究	皮膚腫瘍科・皮膚科 松下茂人
49	悪性黒色腫のリンパ節郭清範囲に関する多施設共同観察研究	皮膚腫瘍科・皮膚科 松下茂人
50	超高齢者の有棘細胞癌の再発率に対する観察研究	皮膚腫瘍科・皮膚科 佐々木奈津子
51	基底細胞癌のスクリーニング効果に対する観察研究	皮膚腫瘍科・皮膚科 青木恵美
52	毛巣洞の外科的治療に関する多施設共同後ろ向き研究	皮膚腫瘍科・皮膚科 松下茂人
53	汗孔癌の予後および再発に関する観察研究	皮膚腫瘍科・皮膚科 松下茂人
54	皮膚原発 NUT 癌の解析検討	皮膚腫瘍科・皮膚科 後藤啓介
55	apocrine carcinoma with sebaceous differentiation の一例	皮膚腫瘍科・皮膚科 松下茂人
56	JCOG-バイオバンク・ジャパン連携バイオバンク	皮膚腫瘍科・皮膚科 松下茂人
57	掌蹠末端黒子型黒色腫の外科的深部マージンと予後に関する多機関共同後方視的観察研究　Correlation between surgical deep margin and prognosis of palm and sole acral melanoma: A multi-institutional retrospective study	皮膚腫瘍科・皮膚科 松下茂人
58	メルケル細胞癌の治療に関する多施設共同後ろ向き観察研究	皮膚腫瘍科・皮膚科 松下茂人
59	BRAF 陽性悪性黒色腫に対する BRAF･MEK 阻害薬および抗 PD-1 抗体を用いた術後補助療法の臨床効果に関する多機関共同後ろ向き観察研究	皮膚腫瘍科・皮膚科 松下茂人
60	アポクリン腺過形成から発生するアポクリン癌の PIK3CA 遺伝子変異の解析検討	皮膚腫瘍科・皮膚科 後藤啓介
61	皮膚悪性腫瘍(non-melanoma skin cancer)の Sentinel node 同定に関する研究	皮膚腫瘍科・皮膚科 松下茂人
62	センチネルリンパ節陽性メラノーマの治療選択と予後に関する多機関共同観察研究	皮膚腫瘍科・皮膚科 松下茂人
63	皮膚リンパ腫臨床統計調査研究	皮膚腫瘍科・皮膚科 松下茂人

	研究内容・課題名	部署・研究者名
64	Cryo AF グローバルレジストリ研究	不整脈治療科 塗木徳人
65	カテーテルアブレーション症例全例登録プロジェクト（J-AB レジストリ）	不整脈治療科 塗木徳人
66	リード抜去症例の実態調査（J-LEX レジストリ）	不整脈治療科 塗木徳人
67	Micra Acute Performance（MAP）AV Japan Registry	不整脈治療科 塗木徳人
68	循環器疾患診療実態調査（JROAD）のデータベースと CRT 患者の予後に関わる因子に関する研究	不整脈治療科 塗木徳人
69	循環器疾患診療実態調査（JROAD)データベースと二次調査に基づく致死性心室性不整脈患者の診断・治療・予後に関する研究	不整脈治療科 塗木徳人
70	鼻腔拭い液及び唾液検体を用いた「ケミルミ SARS-CoV-2Ag」による SARS-CoV-2 感染の臨床性能の検証	臨床検査科 梅橋功征
71	SARS-CoV-2 検査の評価研究	臨床検査科 梅橋功征
72	冠動脈 CT における撮影条件の最適化	診療放射線科 木原　諒
73	経皮的カテーテル心筋焼灼術における被ばく線量の推移	診療放射線科 久木野豊
74	カテーテルアブレーション術前単純 3D-CT における、3 次元ワークステーションの自動抽出精度と画像再構成条件の検討	診療放射線科 山口英明
75	防護板の使用率及び防護効果の向上に向けた検討	診療放射線科 松下真優
76	骨シンチグラフィ解析ソフトウェアの研究・開発・評価等のためのデータ収集	診療放射線科 宮島隆一
77	201Tl 心筋血流 SPECT における横隔膜下集積の影響抑制法の検討	診療放射線科 宮島隆一
78	放射線診療における多施設被ばく線量の実態調査と診断参考レベルとの比較	診療放射線科 宮島隆一
79	X線撮影における再撮影の発生状況と要因分析	診療放射線科 宮島隆一，阿南圭吾
80	MUS 法を用いた 201Tl 心筋血流シンチにおける至適画像処理パラメータの検討	診療放射線科 市野凌資
81	サージカルマスク装着が心臓血管手術を受けた酸素療法中患者に与える影響因子	看護部 立宅由佳
82	混合病棟での小児看護における患児・家族が医療者に期待する看護	看護部 前田明歩
83	意識障害のある患者のベッドサイドの療養環境を整えるためのアプローチ～シミュレーション、環境ラウンド、環境ラウンドチェックリストを用いて～	看護部 福留美那
84	腹膜透析を継続している方が生活の中で大切にしていること	看護部 森山佳奈
85	TAVI へのスタッフの心情に対してアプローチをすることでの意識変化	看護部 神野　愛
86	喉頭摘出患者の意思決定支援でのかかわりで看護師が抱くコミュニケーションの困難さと要因	看護部 俵積田麻衣

	研究内容・課題名	部署・研究者名
87	面会制限下における病棟看護師の介護支援専門員との連携上の課題～効果的な支援に繋げるために～	看護部 石原由貴
88	手術室看護師の周術期看護の指導に対する「思い」	看護部 田中佑介
89	クラスターが発生した病棟の看護師が看護師長に求める支援	看護部 中本　恵
90	ハイパフォーマーなジェネラリスト看護師のワーク・エンゲージメントに影響する因子	看護部 今吉弥生
91	周手術期看護における看護学生の臨床判断能力育成に向けた ICU 看護師の実習指導の実際	看護学校 西園里美
92	(仮)A 市における医療的ケア児を受け入れている保育園等に勤務する看護師の語りからみえてきた課題	看護学校 今田南生人
93	看護学生の小児看護学実習経験が及ぼす倫理的感受性への影響～子どもに携わる看護師の子どもの権利擁護実践能力尺度を用いて～	看護学校 澁谷幸子
94	ARCS モデルを活用した学習活動による自己教育力と主体性への影響	看護学校 濱﨑友実

② 治験実績

(ア) 治験

以下に 2023 年度の治験の実績を示す。

2023 年度(令和 5 年度)治験内容　　2023.4～2024.3

	医薬品		医療機器		再生医療		合計
	新規契約	継続契約	新規契約	継続契約	新規契約	継続契約	
治験　第Ⅱ相	0(O)	1(1)	0(0)	0(0)	0(0)	0(1)	1(2)
治験　第Ⅲ相	2(1)	1(0)	0(0)	0(0)	0(0)	0(0)	3(1)
合計	2(1)	2(1)	0(0)	0(0)	0(0)	0(1)	4(3)

(　)内は昨年の実数

実施率(2023 年度に終了した治験)

	契約件数(件)	契約症例・調査数	実施症例・調査票	実施率(%)
治験	1(1)	6(4)	4(4)	66(100)

(　)内は昨年の実数

細目

研究課題名	研究依頼者	責任医師
Elezanumab の前期第 II 相試験	アッヴィ合同会社	松岡秀樹
脳卒中リスクのある 18 歳以上の心房細動の患者の有効性及び安全性をアピキサバンと比較する多施設共同、無作為化、実薬対照、二重盲検、ダブルダミー、二群間並行群間比較、第Ⅲ相国際共同試験	バイエル薬品株式会社	薗田正浩
急性期虚血性脳卒中又は高リスク一過性脳虚血発作後の脳卒中の再発抑制を目的とした経口第 XIa 因子阻害剤 Milvexian の有効性及び安全性を評価する第 3 相, ランダム化, 二重盲検, 並行群間, プラセボ対照試験	ヤンセンファーマ株式会社	松岡秀樹
切除したステージ III 又はステージ IV の黒色腫患者を対象としたアジュバント治療における ABP 206 とオプジーボ® (ニボルマブ) の薬物動態の類似性を評価する試験	アムジェン株式会社	松下茂人

（イ） 製造販売後調査（新規）

研究課題名	研究依頼者	責任医師
エドワーズ　サピエン 3（TAV in TAV）使用成績調査	エドワーズライフサイエンス株式会社	片岡哲郎
エドワーズ　サピエン 3（TAV in TAV）使用成績調査	エドワーズライフサイエンス株式会社	平峯聖久
サムタス一般使用成績調査（心性浮腫）	大塚製薬株式会社	東　健作
コセルゴ®特定使用成績調査神経線維腫症 1 型における叢状神経線維腫に関する全例調査	アレクシオンファーマ合同会社	松下茂人
オプジーボ点滴静注 20mg・100mg・120mg・240mg、ヤーボイ点滴静注液 20mg・50mg、ビラフトビカプセル 50mg・75mg、メクトビ錠 15mg　副作用・感染症詳細調査	小野薬品工業株式会社	青木恵美
ヤーボイ点滴静注液 20mg・50mg、ビラフトビカプセル 50mg・75mg、メクトビ錠 15mg　副作用・感染症詳細調査	小野薬品工業株式会社	青木恵美
エジャイモ点滴静注 1.1g特定使用成績調査＜寒冷凝集素症患者＞	サノフィ株式会社	原口浩一
ゼジューラ特定使用成績調査「卵巣癌」	武田薬品工業株式会社	神尾真樹
オプジーボ点滴静注 20mg・100mg・120mg・240mg、ヤーボイ点滴静注液 20mg・50mg　副作用・感染症詳細調査	小野薬品工業株式会社	西原克彦
エザルミア錠一般使用成績調査	第一三共株式会社	大渡五月
レクビオ皮下注　特定使用成績調査［家族性高コレステロール血症又は高コレステロール血症］	ノバルティスファーマ株式会社	東　健作

製造販売後調査（継続）

研究課題名	研究依頼者	責任医師
献血グロベニン-I静注用　使用成績調査（再審査用）「スティーブンス・ジョンソン症候群及び中毒性表皮壊死症」	武田薬品工業株式会社	松下茂人
ジャカビ®錠　5mg　特定使用成績調査（真性多血症）	ノバルティスファーマ株式会社	大塚眞紀
ジャカビ®錠　5mg　特定使用成績調査（真性多血症）	ノバルティスファーマ株式会社	魚住公治
アイノフロー吸入用 800ppm　使用成績調査	エア・ウォーター・メディカル株式会社	金城玉洋
自家培養表皮ジェイスの先天性巨大色素性母斑に対する使用成績調査	株式会社ジャパン・ティッシュエンジニアリング	松下茂人
サデルガカプセル 100mg　特定使用成績調査	サノフィ株式会社	大塚眞紀
ウプトラビ錠 0.2mg・0.4mg　特定使用成績調査 「長期使用に関する調査」	日本新薬株式会社	田中裕治
ベスポンサ®点滴静注用 1mg　特定使用成績調査（プロトコール No.:B1931024）	ファイザー株式会社	原口浩一
ゾスパタ錠　一般使用成績調査〔プロトコル No.XSP001〕	アステラス製薬株式会社	大塚眞紀

研究課題名	研究依頼者	責任医師
ヴァンフリタ錠一般使用成績調査	第一三共株式会社	大塚眞紀
レパーサ皮下注 特定使用成績調査(長期使用)	アムジェン株式会社	片岡哲郎
レパーサ皮下注 特定使用成績調査(長期使用)	アムジェン株式会社	東 健作
デファイテリオ静注 200mg 一般使用成績調査	日本新薬株式会社	大塚眞紀
ベレキシブル®錠 特定使用成績調査 再発又は難治性の中枢神経系原発リンパ腫(PCNSL)	小野薬品工業株式会社	魚住公治
サピエン 3(TAV in SAV)使用成績調査	エドワーズライフサイエンス株式会社	片岡哲郎
サピエン 3(TAV in SAV)使用成績調査	エドワーズライフサイエンス株式会社	平峯聖久
コララン®特定使用成績調査(洞調律かつ投与開始時の安静時心拍数が 75 回/分以上の慢性心不全:ただし、β 遮断薬を含む慢性心不全の標準的な治療を受けている患者に限る。)	小野薬品工業株式会社	中島 均
コララン®特定使用成績調査(洞調律かつ投与開始時の安静時心拍数が 75 回/分以上の慢性心不全:ただし、β 遮断薬を含む慢性心不全の標準的な治療を受けている患者に限る。)	小野薬品工業株式会社	東 健作
ビンダケルカプセル特定使用成績調査 ートランスサイレチン型心アミロイドーシス患者に対する調査ー (プロトコール№B3461064)	ファイザー株式会社	薗田正浩
エドルミズ®特定使用成績調査〔がん悪液質:非小細胞肺癌、胃癌、膵癌、大腸癌〕	小野薬品工業株式会社	魚住公治
ダラキューロ配合皮下注 ベルケイド注射用 3mg 全身性 AL アミロイドーシス患者を対象とした特定使用成績調査	ヤンセンファーマ株式会社	大塚眞紀
ハイヤスタ錠®10mg 再発または難治性の成人 T 細胞白血病リンパ腫(ATL)患者における一般使用成績調査(全例調査)	Meiji Seika ファルマ株式会社	大塚眞紀
ジャディアンス®錠 特定使用成績調査(慢性心不全患者を対象とした長期使用に関する調査)	日本ベーリンガーインゲルハイム株式会社	中島 均
ジャディアンス®錠 特定使用成績調査(慢性心不全患者を対象とした長期使用に関する調査)	日本ベーリンガーインゲルハイム株式会社	東 健作
オンデキサ®静注用 200mg 一般使用成績調査	アストラゼネカ株式会社	城ヶ崎倫久
エフィエント錠特定使用成績調査−脳梗塞発症リスクが高い虚血性脳血管障害患者−	第一三共株式会社	松岡秀樹
レブラミド®カプセル一般使用成績調査〔再発又は難治性の FL 及び MZL〕	ブリストル・マイヤーズスクイブ㈱	大塚眞紀
ハイヤスタ錠 10mg 再発又は難治性の末梢性 T 細胞リンパ腫(PTCL)患者における一般使用成績調査(全例調査)	Meiji Seika ファルマ株式会社	大塚眞紀
タケキャブ錠 副作用・感染症調査	大塚製薬株式会社	今田 涼
ダラキューロ配合皮下注の副作用・感染症等詳細調査(ヤンセン症例管理番号:J 22064667)	ヤンセンファーマ株式会社	鎌田勇平
ソグルーヤ®皮下注 5 mg,10 mg 特定使用成績調査 「ソグルーヤ®長期使用に関する特定使用成績調査」	ノボノルディスク ファーマ株式会社	郡山暢之

研究課題名	研究依頼者	責任医師
フォシーガ錠 副作用・感染症詳細調査	アストラゼネカ株式会社	牧野美和
アキャルックス点滴静注 250 mg一般使用成績調査（全例調査）－切除不能な局所進行又は局所再発の頭頸部癌－	楽天メディカル株式会社	西元謙吾

治験・受託研究請求額推移

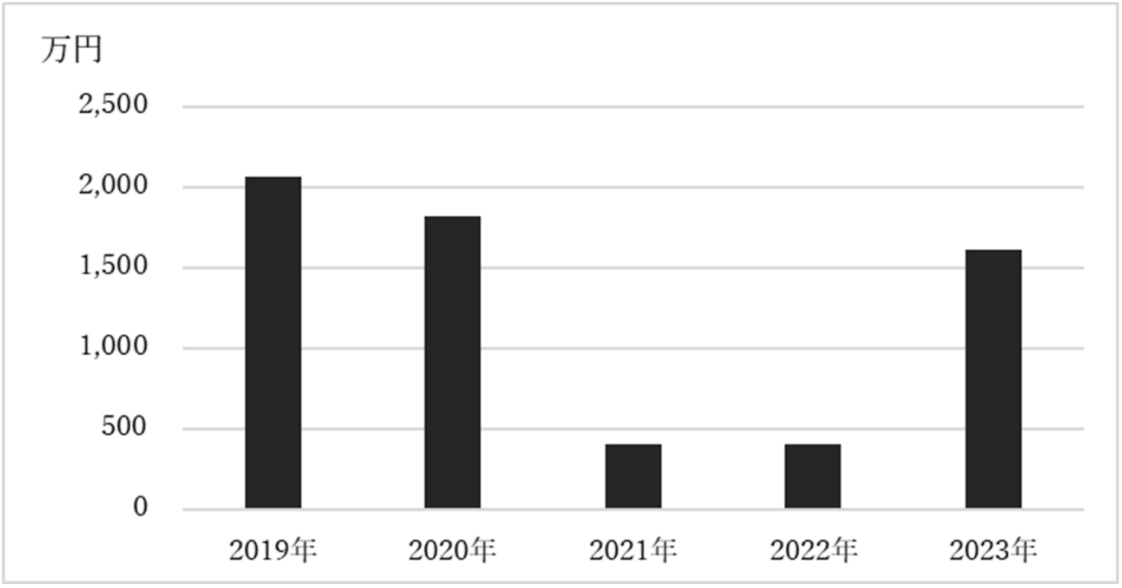

3. 業績報告

① 英文原著論文等

※2023 年度中に Epub (online)で公開された論文も含みます。

■第2循環器内科

Nakabeppu M, Ijuin S, Tateishi N.
Constrictive pericarditis with massive pericardial effusion.
Eur Heart J. 2023; 44(26): 2411. (Epub 2023 Apr 8)

Ijuin S, Yamashita Y, Kinjo T.
Right heart failure due to compression of right ventricular outflow tract by post-operative aortic pseudoaneurysm
Eur Heart J-Case Rep. 2024; 8(1): 1-2 (Epub 2024 Jan 25)

■心臓血管外科

Yasumura H, Tao K, Imada R, Yamashita Y, Tateishi N, Kinjo T.
Successful sutureless repair of multiple left ventricular free wall ruptures due to Takotsubo cardiomyopathy: a case report.
Surg Case Rep. 2024; 10(1): 47. (Epub 2024 Feb 23)

■脳血管内科

Takei J, Higuchi Y, Ando M, Yoshimura A, Yuan JH, Fujisaki N, Tokashiki T, Kanzato N, Jonosono M, Sueyoshi T, Kanda N, **Matsuoka H**, Okubo R, Suehara M, Matsuura E, Takashima H.
Microbleed clustering in thalamus sign in CADASIL patients with NOTCH3 R75P mutation.
Front Neurol. 2023; 14: 1241678.

Hamada Y, Miyashita F**, Matsuoka H**, **Nishinakama Y**, **Kai Y**, **Yamashita Y**, **Ikeda M**, **Takaguchi G**, Masuda K, Kubo F, Takashima H.
Alternative Proximal Protection Method during Carotid Artery Stenting Using Combined Transbrachial and Transradial Artery Approaches.
NMC Case Rep J. 2023; 10: 273-278.

Masuda A, Hamada Y, Matsuoka H, Takashima H.
Eagle Syndrome Induced by the Head Retroflexion.
Intern Med. 2024; 63(11): 1669-1670. (Epub 2023 Oct 6)

■小児科

Yoshinaga M, Ninomiya Y, Tanaka Y, Fukuyama M, Kato K, Ohno S, Horie M, Ogata H.
Holter Electrocardiographic Approach to Predicting Outcomes of Pediatric Patients With Long QT Syndrome.
Circ J. 2024; 88(7): 1176-1184. (Epub 2023 Dec 1)

■血液内科

Arai A, Yoshimitsu M, **Otsuka M**, Ito Y, Miyazono T, Nakano N, Obama K, Nakashima H, **Hanada S**, **Owatari S**, Nakamura D, Tokunaga M, Kamada Y, Utsunomiya A, **Haraguchi K**, Hayashida M, **Fujino S**, Odawara J, Tabuchi T, Suzuki S, Hamada H, Kawamoto Y, Uchida Y, Hachiman M, Ishitsuka K.
Identification of putative noncanonical driver mutations in patients with essential thrombocythemia.
Eur J Haematol. 2023; 110(6): 639-647. (Epub 2023 Mar 14)

■糖尿病・内分泌内科

Makino M, **Koriyama N**, **Kojima N**, **Tobo T**, Nishio Y.
Food-dependent Cushing's syndrome due to unilateral adrenocortical adenoma with cortisol secretion without ACTH elevation detected in peripheral blood by the CRH test: a case report.
Endocr J. 2023; 70(7): 745-753. (Epub 2023 May 15)

Makino M, **Koriyama N**, **Kojima N**, Nishio Y.
A Rare Case of Painless Destructive Thyroiditis Resulting in Thyroid Storm.
Intern Med. 2023; 62(22): 3373-3379. (Epub 2023 Apr 7)

■消化器内科

Tahata Y, Hikita H, Mochida S, Enomoto N, Ido A, Kuroda H, Miki D, Kurosaki M, Hiasa Y, Sakamori R, Kawada N, Yamashita T, Suda G, Yatsuhashi H, Yoshiji H, Kato N, Takami T, Nakao K, Matsuura K, Asahina Y, Itoh Y, Tateishi R, Nakamoto Y, Kakazu E, Terai S, Shimizu M, Ueno Y, Akuta N, Miyazaki M, Nozaki Y, Kabayama M, Sobue S, **Moriuchi A**, Miyaki T, Kodama T, Tatsumi T, Yamada T, Takehara T.
Posttreatment liver function, but not baseline liver function stratifies patient survival after direct-acting antiviral treatment in decompensated cirrhosis with hepatitis C virus.
J Gastroenterol. 2023; 58(12): 1211-1221. (Epub 2023 Oct 13)

■病理診断科

Hoshida Y, Tsujii A, Ohshima S, Saeki Y, Yagita M, Miyamura T, Katayama M, Kawasaki T, Hiramatsu Y, Oshima H, Murayama T, Higa S, Kuraoka K, Hirano F, Ichikawa K, Kurosawa M, Suzuki H, Chiba N, Sugiyama T, Minami Y, Niino H, Ihata A, Saito I, Mitsuo A, Maejima T, Kawashima A, Tsutani H, Takahi K, Kasai T, Shinno Y, Tachiyama Y, Teramoto N, Taguchi K, Naito S, Yoshizawa S, Ito M, Suenaga Y, Mori S, Nagakura S, Yoshikawa N, **Nomoto M**, Ueda A, Nagaoka S, Tsuura Y, Setoguchi K, Sugii S, Abe A, Sugaya T, Sugahara H, Fujita S, Kunugiza Y, Iizuka N, Yoshihara R, Yabe H, Fujisaki T, Morii E, Takeshita M, Sato M, Saito K, Matsui K, Tomita Y, Furukawa H, Tohma S.
Effect of Recent Antirheumatic Drug on Features of Rheumatoid Arthritis-Associated Lymphoproliferative Disorders.
Arthritis Rheumatol. 2024; 76(6): 869-881. (Epub 2024 Jan 25)

■歯科口腔外科

Yoshimura T, Hirano Y, Hamada T, Yokoyama S, Suzuki H, Takayama H, Migita H, Ishida T, **Nakamura Y**, Ohsawa M, Asakawa A, Ishihata K, Tanimoto A.
Exercise Suppresses Head and Neck Squamous Cell Carcinoma Growth via Oncostatin M.
Cancers (Basel). 2024; 16(6): 1187. (Epub 2024 Mar 18)

■皮膚腫瘍科・皮膚科

Inozume T, Namikawa K, Kato H, Yoshikawa S, Kiniwa Y, Yoshino K, Mizuhashi S, Ito T, Takenouchi T, **Matsushita S**, Fujisawa Y, Matsuzawa T, Sugihara S, Asai J, Kitagawa H, Maekawa T, Isei T, Yasuda M, Yamazaki N, Uhara H, Nakamura Y.
Analyzing the relationship between the efficacy of first-line immune checkpoint inhibitors and cumulative sun damage in Japanese patients with advanced BRAF wild-type nonacral cutaneous melanoma: A retrospective real-world, multicenter study.
J Dermatol Sci. 2023; 110(1): 19-26. (Epub 2023 Mar 31)

Doi R, Baba N, Kato H, Nakamura M, **Matsushita S**, **Aoki M**, Fujimoto N, Kato T, Iino S, Saito S, Yasuda M, Asai J, Ishikawa M, Yatsushiro H, Kawahara Y, Inafuku K, Matsuya T, Araki R, Teramoto Y, Hasegawa M, Nakama T, Nakamura Y.
Evaluation of prognostic prediction ability of the novel Japanese risk factor scoring system in a Japanese cohort of resectable cutaneous squamous cell carcinoma: A retrospective cross-sectional study.
Exp Dermatol. 2023; 32(10): 1682-1693. (Epub 2023 Jul 3)

Fujisawa Y, Namikawa K, Yoshino K, Kiniwa Y, Ito T, Kato H, **Matsushita S**, Hoashi T, Nakamura Y, Yoshikawa S, Miyagawa T, Asai J, Matsuya T, Fukushima S, Kato J, Takenouchi T, Uchi H, Masuzawa M, Yanagi T, Maekawa T.
Combined use of nivolumab and ipilimumab in Japanese patients with melanoma: a multicentre retrospective study of 111 cases.
Br J Dermatol. 2023; 189(2): 223-250.

Muto Y, Kambayashi Y, Kato H, Fukushima S, Ito T, Maekawa T, Fujisawa Y, Yoshino K, Uchi H, **Matsushita S**, Yamamoto Y, Amagai R, Ohuchi K, Hashimoto A, Asano Y, Fujimura T.
Adverse events associated with postoperative outcomes of adjuvant anti-PD-1 antibody therapy in both acral and non-acral cutaneous melanomas: A multicenter, observational, post hoc analysis study.
J Dermatol. 2024; 51(3): 458-462. (Epub 2023 Jul 30)

Mori T, Namikawa K, Yamazaki N, Kiniwa Y, Yamasaki O, Yoshikawa S, Inozume T, Kato H, Nakai Y, Fukushima S, Takenouchi T, Maekawa T, **Matsushita S**, Otsuka A, Nomura M, Baba N, Isei T, Saito S, Fujimoto N, Tanaka R, Kaneko T, Kuwatsuka Y, Matsuya T, Nagase K, Onishi M, Onuma T, Nakamura Y.
Efficacy of salvage therapies for advanced acral melanoma after anti-PD-1 monotherapy failure: a multicenter retrospective study of 108 Japanese patients.
Front Med (Lausanne). 2023; 10:1229937. (Epub 2023 Aug 10)

Namikawa K, Ito T, Yoshikawa S, Yoshino K, Kiniwa Y, Ohe S, Isei T, Takenouchi T, Kato H, Mizuhashi S, Fukushima S, Yamamoto Y, Inozume T, Fujisawa Y, Yamasaki O, Nakamura Y, Asai J, Maekawa T, Funakoshi T, **Matsushita S**, Nakano E, Oashi K, Kato J, Uhara H, Miyagawa T, Uchi H, Hatta N, Tsutsui K, Maeda T, Matsuya T, Yanagisawa H, Muto I, Okumura M, Ogata D, Yamazaki N.
Systemic therapy for Asian patients with advanced BRAF V600-mutant melanoma in a real-world setting: A multi-center retrospective study in Japan (B-CHECK-RWD study).
*Cancer Med.*2023; 12(17): 17967-17980. (Epub 2023 Aug 16)

Fujimura T, Yoshino K, Nakamura M, Kato H, Ito T, Maekawa T, Fujisawa Y, **Matsushita S**, Amagai R, Yamazaki E, Takahashi M, Tamabuchi E, Hashimoto A, Kambayashi Y, Yamazaki N, Miyata T, Asano Y.
Efficacy and safety of TM5614 in combination with paclitaxel in the treatment of paclitaxel-resistant cutaneous angiosarcoma: Phase II study protocol.
Exp Dermatol. 2024; 33(1): e14976. (Epub 2023 Nov 9)

Muto Y, Kambayashi Y, Kato H, Fukushima S, Ito T, Maekawa T, Shoichiro I, Uchi H, **Matsushita S**, Yamamoto Y, Yoshino K, Fujisawa Y, Amagai R, Ohuchi K, Hashimoto A, Asano Y, Fujimura T.
Postoperative adjuvant therapy for 120 patients with melanoma, including acral and mucosal subtypes: a multicentre, observational study of 2-year follow-up results.
Br J Dermatol. 2023; 189(4): 476-478. (Epub 2023 May 27)

Nishida H, Sasaki T, Taga Y, Murasawa Y, Simizu S, **Matsushita S**, Isogai Z, Hattori S, Daa T, Nagamine N, Sekine A, Fujiwara S.
Presence of microfibril associated glycoprotein 4 and type V collagen and the possible absence of fibrillin-1 in bead-like structures in elastofibroma.
J Dermatol Sci. 2023; 112(2): 112-116. (Epub 2023 Sep 28)

Goto K, Kiniwa Y, Hishima T, Honma K, **Matsushita S**, **Aoki M**, **Nishihara K**, Hiraki T.
PIK3CA mutation status in apocrine carcinoma arising in apocrine gland hyperplasia/apocrine nevus: A study of four cases.
J Cutan Pathol. 2024; 51(6): 399-402. (Epub 2024 Jan 18)

Sasaki-Saito N, Goto K, **Aoki M**, **Nishihara K**, Hiraki T, Yoshikawa S, **Matsushita S**.
Apocrine carcinoma with marked sebocyte-like cytological features: A report of two cases.
J Cutan Pathol. 2024; 51(2): 92-98. (Epub 2023 Sep 24)

■臨床研究部

Umebashi K, Yamamoto M, Tokito A, Sudou K, Takenoshita Y, Jougasaki M.
Inhibitory Effects of Simvastatin on IL-33-Induced MCP-1 via the Suppression of the JNK Pathway in Human Vascular Endothelial Cells.
Int J Mol Sci. 2023; 24(16): 13015. (Epub 2023 Aug 21)

Jougasaki M, Takenoshita Y, Umebashi K, Yamamoto M, Sudou K, Nakashima H, Sonoda M, Kinjo T.
Autocrine Regulation of Interleukin-6 via the Activation of STAT3 and Akt in Cardiac Myxoma Cells.
Int J Mol Sci. 2024; 25(4): 2232. (Epub 2024 Feb 13)

Takenoshita Y, Tokito A, Jougasaki M.
Inhibitory Effects of Eicosapentaenoic Acid on Vascular Endothelial Growth Factor-Induced Monocyte Chemoattractant Protein-1, Interleukin-6, and Interleukin-8 in Human Vascular Endothelial Cells.
Int J Mol Sci. 2024; 25(5): 2749. (Epub 2024 Feb 27)

② 和文原著・著書等

松岡秀樹
心原性脳塞栓症とは
心臓財団季報; 253 巻, 2023 年 12 月 10 日

濵田祐樹, 池田め衣, 松岡秀樹
脳梗塞軽症例に rt-PA を投与してもよいか？
脳卒中 Controversy; 50-53, 2023 年 3 月

森内昭博
糖尿病との関連を含めた肝疾患フォローアップの勘所
鹿児島県内科医会報, 2024 年 1 月

吉永正夫
予期せぬ乳幼児の突然死 (SUDI) ～対策と予防を考える～ : (7) SIDS と鑑別すべき疾患 (3) ～循環器疾患と突然死～
チャイルドヘルス; 26(10): 750−752, 2023 年 9 月

吉永正夫
QT 延長症候群
日本小児循環器学会雑誌; 39(3): 132-143, 2023 年 12 月

古庄正英
高齢者に腹膜透析という選択肢を届ける
鹿児島市医報; 62(9): 36-, 2023 年 9 月

安庭愛子
鹿児島医療センターにおけるせん妄診療について
鹿児島市医報; 63(3):23-25, 2024 年 3 月

吉野 歩, 橋本剛志, 松元亜由美, 本郷 剛, 一瀬康浩, 吉原正保
臨床検査システム内物品管理ソフトを用いた管理体制の構築と導入効果
医学検査; 72(4): 588-596, 2023 年 10 月

吉野 歩, 橋本剛志, 松元亜由美, 本郷 剛, 吉原正保, 林 尚子, 古橋 聡, 栗脇一三
男性乳腺嚢胞内癌の一例
国臨協九州; 23(2): 12-17, 2023 年 5 月

中釜美乃里, 宮﨑明信, 原田美里, 日野出勇次, 梅橋功征, 渡辺秀明, 馬場善政, 西方菜穂子
Bentall 術後の大動脈弁位人工弁機能不全に対し経胸壁心エコー図検査による左室圧推定が有用であった 1 症例
超音波検査技術; 48(5): 489-498, 2023 年 10 月

草原 智, 岡村優樹, 久保祐子, 日野出勇次, 梅橋功征, 西方菜穂子
胸痛消失後に特徴的な心電図波形を呈した wellens 症候群の一症例
国臨協九州; 24 (1): 1-8, 2023 年 10 月

樋渡まこ, 梅橋功征, 山口 俊, 西方菜穂子, 藤野達也
SARS-CoV-2 感染症診断におけるケミルミ SARS-CoV-2Ag の臨床的有用性の検討
医学と薬学; 80 (4): 423-430, 2023 年 3 月 27 日

大井邦治, 宮島隆一, 増井飛沙人, 渋谷 充, 太田一郎, 財前 誠, 市川和幸, 池田敏久, 阿南恵吾, 松井謙典, 筒井昭詔
Ｘ線撮影における再撮影の発生状況と要因分析について 第 2 報
九州国立病院機構日本診療放射線技師会誌; 70(10): 1122, 2023 年 9 月 1 日

宮島隆一
X 線透視における被ばく管理
放射線防護部会誌; 23(1): 32-38, 2023 年 10 月

③ 学会発表

筆頭演者が鹿児島医療センターの職員

＜国際学会＞

Kensaku Higashi
Impact on effectiveness of Carvedilol and Bisoprolol for patients with heart failure aged 80 years old and older
AHA Scientific sessions 2023, Philadelphia, 2023/11/12

Kodai Murayama
Conduction System Pacing contributes to Left Ventricular Reverse Remodeling and Improvement of Left Atrial Function.
The 88th Annual Scientific Meeting of the Japanese Circulation Society (JCS2024), Kobe, 2024/03/10

Shun Ijuin
Left Bundle Branch Block and Left Ventricular Enlargement Deteriorate Prognosis after Leadless Pacemaker Implantation.
The 88th Annual Scientific Meeting of the Japanese Circulation Society (JCS2024), Kobe, 2024/03/10

Shigeto Matsushita
From resection to reconstruction: surgical procedures for skin cancers in Japan
The 7th Asian Congress of Dermatologic Surgery, Seoul, 2023/05/20

Shigeto Matsushita
Treatment of cutaneous squamous cell carcinoma in Japan in the Era of Super-aged Society
25th World Congress of Dermatology, Singapore, 2023/07/07

Natsuko Sasaki-Saito, Megumi Aoki, Katsuhiko Nishihara , Shigeto Matsushita
Over 90-year-old is unfavorable prognostic factor of cutaneous squamous cell carcinoma patients.
FIRST INTERNATIONAL SOCIETIES FOR INVESTIGATIVE DERMATOLOGY MEETING, Tokyo, 2023/05/10-14

＜国内学会＞

片岡哲郎, 福永研吾, 野元裕太朗, 沖野秀人, 平峯聖久, 髙﨑州亜, 風呂井敦, 塗木健介, 中島 均
超重症大動脈弁狭窄症と出血性ショックを来した小腸腫瘍に対して経カテーテル的大動脈弁置換術(TAVI)と小腸腫瘍切除術を同一入院中に段階的に施行した 1 例
第 341 回日本内科学会九州地方会, 北九州, 2023 年 5 月 27 日

福﨑 篤, 髙﨑州亜, 今田 涼, 金城玉洋, 川畑深怜, 稲津真穂人, 沖野秀人, 野元裕太朗, 福永研吾, 片岡哲郎, 中島 均, 大石 充
胸痛を契機に診断に至った巨大左房粘液腫の 1 例
第 134 回日本循環器学会九州地方会, 熊本, 2023 年 6 月 24 日

稲津真穂人, 髙﨑州亜, 川畑深怜, 福﨑 篤, 沖野秀人, 野元裕太朗, 福永研吾, 片岡哲郎, 立石直毅, 金城玉洋, 城ケ崎倫久, 中島 均, 大石 充
僧帽弁閉鎖不全症に対する精査にて、冠動脈瘤・冠動脈静脈瘻を認めた一例
第 134 回日本循環器学会九州地方会, 熊本, 2023 年 6 月 24 日

福永研吾, 片岡哲郎, 野元裕太朗, 平峯聖久, 薗田正浩, 中島 均, 大石 充
当院における「CHIP TAVI」3症例の検討
第 31 回日本心血管インターベンション治療学会学術集会, 福岡, 2023 年 8 月 4 日

片岡哲郎
右心カテーテル検査の際に肺動脈損傷をきたしカバードステントを使用してベイルアウトした閉塞性肥大型心筋症患者の 1 例
第 31 回日本心血管インターベンション治療学会学術集会, 福岡, 2023 年 8 月 5 日

沖野秀人, 片岡哲郎, 川畑深怜, 隈元健吾, 田方健人, 野元裕太朗, 福永研吾, 髙﨑州亜, 中島 均, 大石 充
右心カテーテル検査中に肺動脈損傷を合併した 1 例
日本内科学会九州支部第 342 回九州地方会, 佐賀, 2023 年 8 月 5 日

野元裕太朗, 片岡哲郎, 川畑深怜, 沖野秀人, 福永研吾, 髙﨑州亜, 中島 均, 池田め衣, 金城玉洋, 大石 充
僧帽弁形成術後に脳塞栓症を繰り返した 1 例
日本内科学会九州支部 第 342 回九州地方会, 佐賀, 2023 年 8 月 5 日

川畑深怜, 髙﨑州亜, 隈元健吾, 田方健人, 沖野秀人, 野元裕太朗, 福永研吾, 片岡哲郎, 中島 均, 大石 充
Bentall 術後に仮性動脈瘤を発症した高安動脈炎の 1 例
日本内科学会九州支部 第 342 回九州地方会, 佐賀, 2023 年 8 月 5 日

沖野秀人
造影剤使用後に第 1 世代薬剤溶出ステントで血栓症を生じた Kounis 症候群の 1 例
第 71 回日本心臓病学会学術集会, 東京, 2023 年 9 月 10 日

福永研吾
当院における極小弁輪に対する Sapien3 を用いた TAVR の治療成績
第 71 回日本心臓病学会学術集会, 東京, 2023 年 9 月 10 日

窪田唯伊, 片岡哲郎, 大渡五月, 隈元健吾, 田方健人, 沖野秀人, 野元裕太朗, 福永研吾, 髙﨑州亜, 大石 充
急性前骨髄球性白血病再発に対し三酸化ヒ素での治療中、房室ブロックによる徐脈を認め、リードレスペースメーカーを留置した1例
第 343 回日本内科学会九州地方会, 長崎, 2023 年 11 月 26 日

片岡哲郎, 福永研吾, 野元裕太朗, 沖野秀人, 田方健人, 隈元健吾, 窪田唯伊, 平峯聖久, 園田幸一郎, 松本洋之, 馬場善政, 髙﨑州亜, 中島 均
大動脈弁狭窄症に対する経カテーテル的大動脈弁置換術における Sapien3 (20mm)弁の連続 56 例の使用経験
第 135 回日本循環器学会九州地方会, 福岡, 2023 年 12 月 2 日

野元裕太朗, 片岡哲郎, 隈元健吾, 窪田唯伊, 田方健人, 沖野秀人, 福永研吾, 髙﨑州亜, 中島　均, 大石　充
当院における Shockwave IVL　カテーテルの使用経験
第 135 回日本循環器学会九州地方会, 福岡, 2023 年 12 月 2 日

野元裕太朗, 片岡哲郎, 隈元健吾, 窪田唯伊, 田方健人, 沖野秀人, 福永研吾, 髙﨑州亜, 安村拓人, 峠　幸志, 金城玉洋, 中島　均, 大石充
左室修復術を行った特発性心破裂の一例
第 135 回日本循環器学会九州地方会, 福岡, 2023 年 12 月 2 日

隈元健吾, 福永研吾, 窪田唯伊, 田方健人, 沖野秀人, 野元裕太朗, 髙﨑州亜, 片岡哲郎, 井手上淳一, 中島均, 大石　充
特発性気管支動脈瘤破裂に対しコイル塞栓術を施行した1例
第 135 回日本循環器学会九州地方会, 福岡, 2023 年 12 月 2 日

田方健人, 片岡哲郎, 隈元健吾, 窪田唯伊, 沖野秀人, 野元裕太朗, 福永研吾, 髙﨑州亜, 中島　均, 大石　充
大伏在静脈グラフトの高度狭窄に対してエキシマレーザー使用した急性冠症候群の一例
第 36 回日本心血管インターベンション治療学会九州・沖縄地方会, 福岡, 2024 年 1 月 13 日

隈元健吾, 福永研吾, 窪田唯伊, 田方健人, 沖野秀人, 野元裕太朗, 髙﨑州亜, 片岡哲郎, 中島　均, 大石　充
高度石灰化病変を有する急性冠症候群患者に対し Rotablator を使用し冠動脈ステント留置した 1 例
第 36 回日本心血管インターベンション治療学会九州・沖縄地方会, 福岡, 2024 年 1 月 13 日

窪田唯伊, 片岡哲郎, 隈元健吾, 田方健人, 沖野秀人, 野元裕太朗, 福永研吾, 髙﨑州亜
診断に苦慮した汎血球減少を伴う Mycobacterium chelonae による非結核性抗酸菌症の 1 例
第 344 回日本内科学会九州地方会, 福岡, 2024 年 1 月 27 日

片岡哲郎
Assessment of Procedure Outcomes and Short-term Prognosis in Patients Aged 90 and Elder Undergoing Transcatheter Aortic Valve Implantation.
第 88 回日本循環器学会学術集会, 神戸, 2024 年 3 月 10 日

福永研吾
The Feasibility of 20-mm Balloon-Expandable Transcatheter Heart Valve Implantation in Aortic Stenosis Patients with Small Aortic Annulus
第 88 回日本循環器学会学術集会, 神戸, 2024 年 3 月 10 日

田方健人
Impact of Vascular Complication during Transcatheter Aortic Valve Implantation with Balloon Expandable Transcatheter Heart Valve on Early and Short-term Prognosis.
第 88 回日本循環器学会学術集会, 神戸, 2024 年 3 月 10 日

園田幸一郎
当院での MitraClip 導入初期 20 例についての経過
第 31 回日本心血管インターベンション治療学会学術集会, 福岡, 2023 年 8 月 4 日

中馬洋介
ECPELLA 管理にて救命し得た劇症型リンパ球性心筋炎の 1 例
鹿児島救急医学会第 87 回学術集会, 鹿児島, 2023 年 9 月 2 日

塚田光助
V-A ECMO 導入により救命し得た肺高血圧クリーゼの 1 例
鹿児島救急医学会第 87 回学術集会, 鹿児島, 2023 年 9 月 2 日

石川裕輔
心臓移植術前術後の栄養管理
第 59 回 日本移植学会総会, 京都, 2023 年 9 月 23 日

中別府麻里, 伊集院駿, 村山剛大, 松本洋之, 園田幸一郎, 石川裕輔, 馬場善政, 蔡 榮鴻, 平峯聖久, 東 健作, 田中秀樹, 片岡哲郎, 塗木徳人, 薗田正浩
当院の心不全患者における, サクビトリル・バルサルタンによる予後と左室駆出率改善についての検討
第 135 回日本循環器学会九州地方会, 福岡, 2023 年 12 月 2 日

伊集院駿, 中別府麻里, 村山剛大, 松本洋之, 石川裕輔, 馬場善政, 園田幸一郎, 蔡 榮鴻, 平峯聖久, 東 健作, 田中秀樹, 塗木徳人, 薗田正浩
リードレスペースメーカ植込み前の左脚ブロックは予後に関連する
第 135 回日本循環器学会九州地方会, 福岡, 2023 年 12 月 2 日

塚田光助, 伊集院駿, 村山剛大, 中別府麻里, 松本洋之, 園田幸一郎, 石川裕輔, 馬場善政, 蔡 榮鴻, 平峯聖久, 東 健作, 田中秀樹, 塗木徳人, 薗田正浩
V-A ECMO 導入により救命し得た肺高血圧クリーゼの一例
第 135 回日本循環器学会九州地方会, 福岡, 2023 年 12 月 2 日

中別府麻里
Heart Rate is Predictor of Left Ventricular Reverse Remodeling with Sacubitril/Valsartan
第 88 回日本循環器学会学術集会, 神戸, 2024 年 3 月 10 日

立石直毅
心内異物肉芽腫の一例
第 56 回日本胸部外科学会九州地方会, 大分, 2023 年 7 月 28 日

今田 涼, 安村拓人, 山下雄史, 立石直毅, 峠 幸志, 金城玉洋
ステンレスワイヤーにより人工血管損傷をきたした 1 例
第 56 回日本胸部外科学会九州地方会, 大分, 2023 年 7 月 28 日

大野文也, 立石直毅, 今田 涼, 山下雄史, 川津祥和, 金城玉洋
右房内海綿状血管腫の 1 種
第 56 回日本胸部外科学会九州地方会, 大分, 2023 年 7 月 28 日

今田 涼, 金城玉洋, 峠 幸二, 立石直毅, 山下雄史, 安村拓人
SSI ハイリスク症例における閉鎖切開陰圧療法を用いた術後 SSI 予防効果の検討
第 54 回日本心臓血管外科学会学術総会, 浜松, 2024 年 2 月 24 日

濵田祐樹, 吉江智秀, 植田敏浩,西 萌生, 池田め衣, 岡田敬史, 髙口 剛, 松岡秀樹
脳血管領域の no reflow phenomenon は存在するのか～120 例の再開通療法例における検討～
JSVIN2023, 岩手, 2023 年 8 月 19 日

増田愛子, 濵田祐樹, 西 萌生, 池田め衣, 岡田敬史, 髙口 剛, 松岡秀樹
後屈位で誘発された頸部内頚動脈解離により脳梗塞を発症した Eagle 症候群の 1 例
第 241 回日本神経学会九州地方会, 大分, 2023 年 9 月 23 日

濵田祐樹, 西 萌生, 池田め衣, 岡田敬史, 髙口 剛, 松岡秀樹
広範脳梗塞に対する機械的血栓回収療法単独と rt-PA 併用との治療結果の比較: プロペンシ ティスコアマッチング解析を用いた検討
第 39 回日本脳神経血管内治療学会総会, 京都, 2023 年 11 月 23 日

山中菜央, 濵田祐樹, 野間美織, 隈元菜々子, 西久保省吾, 吉留 萌, 西 萌生, 岡田敬史, 髙口 剛, 松岡秀樹
Carotid Web による脳梗塞の 1 例
第 243 回日本神経学会九州地方会, 福岡, 2024 年 3 月 2 日

石丸綺梨, 濵田祐樹, 吉留 萌, 西 萌生, 池田め衣, 岡田敬史, 髙口 剛, 松岡秀樹
直接作用型抗凝固薬内服中に発症した主幹動脈閉塞例に対する機械的血栓回収療法の特徴
脳卒中学会総会 Stroke2024, 横浜, 2024 年 3 月 7 日

鎌田勇平, 山本 花, 原口浩一, 大渡五月, 大塚眞紀
高齢者 AML 患者におけるアザシチジン＋ベネトクラックス療法の治療、有害事象軽減、入院日数短縮効果
第 85 回日本血液学会学術集会, 東京, 2023 年 10 月 15 日

二宮由美子，田中裕治，吉永正夫
学校心臓検診で診断された QT 延長症候群患児の予後を予測するための新たなアプローチ
第 59 回日本小児循環器学会総会・学術集会，横浜, 2023 年 7 月 6 日

二宮由美子，田中裕治，吉永正夫
低 K 血症の悪化から Gitelman 症候群と診断した QT 延長症候群の一例
第 59 回日本小児循環器学会総会・学術集会　横浜　2023 年 7 月 6 日

田中裕治
術後に心室仮性瘤を形成し、感染性心内膜炎のため死亡した両大血管右室起始症の成人例
第 59 回日本小児循環器学会総会・学術集会，横浜, 2023 年 7 月 7 日

椙松貴成
早期再発小児 B 前駆細胞性急性リンパ性白血病に対する骨髄移植後のブリナツモマブ維持療法
第 65 回日本小児血液・がん学会学術集会，札幌, 2023 年 9 月 29 日

吉永正夫，西原栄起，畑 忠善，阿部勝巳，太田邦雄，立野 滋，野村裕一，堀米仁志，廣野恵一，岩本眞理，長嶋正實
学校心臓検診における肥大型心筋症の心エコー抽出基準値に関する検討
第 59 回日本小児循環器学会総会，横浜, 2023 年 7 月 8 日

吉永正夫，牛之濱大也，佐藤誠一，畑 忠善，堀米仁志，田内宣生，住友直方，西原 栄，市田蕗子，野村裕一，塚野真也，二宮由美子，高橋秀人，緒方裕光，長嶋正實
Screening of 1-month-old Infants with a Prolonged QT Interval and Its Cut-off Value.
第 88 回日本循環器学会学術集会，神戸, 2024 年 3 月 8 日

郡山暢之
日本糖尿病学会，日本糖尿病医療学学会合同シンポジウムー心・身と人の結びつきがつくる糖尿病医療学維新
「有痛性神経障害をきたした若年発症 2 型糖尿病者」
第 66 回 日本糖尿病学会年次学術集会，鹿児島, 2023 年 5 月 12 日

児島奈弥，郡山暢之，當房卓也，牧野美和，西尾善彦
当院におけるセマグルチドの有効性についての検討
第 66 回 日本糖尿病学会年次学術集会，鹿児島, 2023 年 5 月 12 日

牧野美和，郡山暢之，當房卓也，児島奈弥，楠元公士，西尾善彦
異なる膵島関連自己抗体，疾患感受性 HLA ハプロタイプを示した 1 型糖尿病姉妹例
ー発症時の病態と経過よりー
第 66 回 日本糖尿病学会年次学術集会，鹿児島, 2023 年 5 月 12 日

郡山暢之
教育講演 糖尿病医療学 Update
第 66 回 日本糖尿病学会年次学術集会，鹿児島, 2023 年 5 月 13 日

牧野美和，郡山暢之，向井 舞，児島奈弥，野津 寛大，西尾 善彦
QT 延長症候群のフォローー中に低 K 血症が顕在化し，遺伝子解析により Gitelman 症候群の確定診断に至った一例
第 23 回 日本内分泌学会九州支部学術集会，長崎, 2023 年 9 月 2 日

児島奈弥，郡山暢之，向井 舞，牧野美和，西尾善彦
副腎 black adenoma によるサブクリニカルクッシング症候群の 1 例
第 23 回日本内分泌学会九州支部学術集会，長崎, 2023 年 9 月 2 日

向井 舞，郡山暢之，牧野美和，児島奈弥，西尾善彦
Ketosis-prone type 2 diabetes と考えられた若年発症糖尿病性ケトアシドーシスの 1 例
第 61 回日本糖尿病学会九州地方会，熊本, 2023 年 12 月 1 日

郡山暢之
シンポジウム心と体に寄り添う糖尿病医療学「糖尿病医療学の実践ー聴き、続け、待つ」
第 58 回糖尿病学の進歩，京都, 2024 年 2 月 16 日

和田竣太郎, 福森　光, 梶原　涼, 井上和彦, 森内昭博, 櫻井一宏, 野元三治, 橋元慎一, 井戸章雄
術後病理検査で淡明細胞型腎細胞癌の膵転移と診断されたが、原発巣が同定できなかった1例
第 122 回　日本消化器病学会九州支部例会, 那覇, 2023 年 11 月 24 日

平川雄太, 安留龍太郎, 髙取寛之, 塗木健介
当院で経験した悪性黒色腫消化管転移の 2 例
第 87 回鹿児島県臨床外科学会医学会 第 73 回日本臨床外科学会地方会, 鹿児島, 2024 年 3 月 16 日

坂田雅道
当院でのパドセブ初期使用経験
第 147 回日本泌尿器科学会鹿児島地方会, 鹿児島, 2023 年 12 月 3 日

東　拓郎, 德留明夫, 穂原　光, 神尾真樹
診断に DWIBS を利用した子宮体癌の一例
第 149 回鹿児島産婦人科学会, 鹿児島, 2023 年 9 月 23 日

穂原　光, 東　拓郎, 德留明夫, 神尾真樹
ペムブロリズマブにより劇症1型糖尿病を発症した再発子宮体癌の一例
第 149 回鹿児島産婦人科学会, 鹿児島, 2023 年 9 月 23 日

田中智規, 西元謙吾, 高木　実, 原口めぐみ, 松崎勉
上咽頭に発生した脊索腫の1例
第 33 回頭頸部外科学会総会, 松山, 2024 年 2 月 1 日

後藤正道, 野元三治, 城ヶ崎泰代, 西元謙吾, 松崎　勉
鼻腔・副鼻腔の呼吸上皮腺腫様過誤腫(REAH)50 例の病理学的解析
第 112 回日本病理学会総会, 下関, 2023 年 4 月 13 日

後藤正道, 北島信一
ハンセン病の中枢神経病変 －2007～2022 年の論文レビュー
第 96 回日本ハンセン病学会総会, 札幌, 2023 年 5 月 18 日

木村菜美子, 中村康典, 大河内孝子, 下田平佳純, 福永莉々亜, 西　恭宏, 中村典史
鹿児島医療センターにおける頭頸部癌放射線治療に対する周術期口腔機能管理の現状
平成 5 年第 20 回日本口腔ケア学会総会・学術大会, 東京, 2023 年 4 月 20 日

大河内孝子, 中村康典, 木村菜美子, 下田平佳純, 福永莉々亜, 西　恭宏
鹿児島医療センターにおける頭頸部癌放射線治療に対する周術期口腔機能管理の現状
平成 5 年第 77 回国立病院総合医学会, 広島, 2023 年 10 月 21 日

中村康典, 大河内孝子, 木村菜美子, 吉村卓也, 手塚征宏, 鈴木　甫, 西　恭宏
鹿児島医療センターにおける心臓弁膜症に対する周術期口腔機能管理
平成 5 年第 68 回（公社）日本口腔外科学会総会・学術集会, 大阪, 2023 年 11 月 11 日

青木恵美, 西原克彦, 佐々木奈津子, 平野慎吾, 山本宗太郎, 松下茂人
2022 年鹿児島医療センター皮膚腫瘍科・皮膚科死亡患者集計
第 193 回日本皮膚科学会鹿児島地方会, 鹿児島, 2023 年 4 月 9 日

西原克彦, 青木恵美, 佐々木奈津子, 山村健太郎, 日高太陽, 平野唯, 吉元秋穂, 年永麻由子, 寺原真咲,
小牟禮大地, 柳瀬桜子, 相良良子, 白石ゆり, 田中清史, 松下茂人
2022 年鹿児島医療センター皮膚腫瘍科・皮膚科　手術集計
第 193 回鹿児島地方会, 鹿児島, 2023 年 4 月 9 日

青木恵美, 山村健太郎, 西原克彦, 平野慎吾, 山本宗太郎, 松下茂人
基底細胞癌のスクリーニングによって明らかになった腫瘍の特徴について
第 66 回日本形成外科学会総会・学術集会, 長崎, 2023 年 4 月 27 日

西原克彦, 青木恵美, 佐々木奈津子, 後藤啓介, 松下茂人
当院で経験した脂漏性角化症から生じた有棘細胞癌の検討
第 122 回日本皮膚科学会総会, 横浜, 2023 年 6 年 1 日

佐々木奈津子, 青木恵美, 山村健太郎, 坂本翔一, 西原克彦, 松下茂人
毛巣洞に対する手術療法についての単施設後ろ向き研究
第 38 回日本皮膚外科学会総会・学術集会, 久留米, 2023 年 7 月 22 日

松下茂人
本邦のメラノーマ診療における手術療法の位置づけと将来展望
第 39 回日本皮膚悪性腫瘍学会学術大会, 名古屋, 2023 年 8 月 4 日

松下茂人
症例提示 1　ディスカッション
第 39 回日本皮膚悪性腫瘍学会学術大会, 名古屋, 2023 年 8 月 4 日

坂本翔一, 青木恵美, 山村健太郎, 西原克彦, 魚住公治, 上山友子, 久保文克, 髙木信介, 松下茂人
頭蓋骨浸潤を呈した有棘細胞癌の 2 例に対する集学的治療経験
第 39 回日本皮膚悪性腫瘍学会学術大会, 名古屋, 2023 年 8 月 5 日

青木恵美, 山村健太郎, 西原克彦, 平野慎吾, 山本宗太郎, 松下茂人
多発性基底細胞癌の診察ポイント
日本皮膚科学会第 406 回福岡地方会, 小倉, 2023 年 9 月 9 日

西原克彦, 青木恵美, 山本宗太郎, 平野愼悟, 佐々木奈津子, 松下茂人
隆起性皮膚線維肉腫における術前画像検査の有用性の検討
第 75 回日本皮膚科学会西部支部学術大会, 沖縄, 2023 年 9 月 17 日

青木恵美, 山村健太郎, 西原克彦, 平野慎吾, 山本宗太郎, 松下茂人
基底細胞癌の診かた　-形成外科医に求められること-
第 121 回九州・沖縄形成外科学会学術集会, 宮崎, 2023 年 10 月 28 日

塗木徳人
心電図から発作性上室頻拍を鑑別する
カテーテルアブレーション関連秋季大会 2023, 福岡, 2023 年 11 月 18 日

富山高至, 田中秀樹
長期経過での多量心嚢液貯留を認めた滲出性収縮性心膜炎の 1 例
第 134 回日本循環器学会九州地方会, 熊本, 2023 年 6 月 24 日

下園　航, 田中秀樹
緊張性気腹による循環不全を合併した十二指腸穿孔性腹膜炎の一例
第 134 回日本循環器学会九州地方会, 熊本, 2023 年 6 月 24 日

松下朋彦, 梅原　正, 恒吉祐成, 上村　豪, 岩本美博, 岩本嘉志, 今村智美, 森園翔一朗, 武田亜矢, 前田光喜, 青木雅也, 永田俊行, 上田和弘
側弯による慢性呼吸不全を有する気胸に対して局麻下胸腔鏡により治療し得た1手術例
第 60 回九州外科学会/第 60 回九州小児外科学会/大59回九州内分泌外科学会, 大分, 2024 年 3 月 8 日

田中大智, 岩本嘉志, 森園翔一朗, 岩本美博, 恒吉祐成, 梅原　正, 武田亜矢, 上村　豪, 青木雅也, 永田俊行, 上田和弘
肺癌術後化学療法（UFT）中に薬剤性皮疹に起因する SCC の上昇を認めた1例
第 60 回九州外科学会/第 60 回九州小児外科学会/大59回九州内分泌外科学会, 大分, 2024 年 3 月 8 日

鳥山陽子, 原口浩一, 諫見圭佑, 大塚眞紀, 山形真一
骨髄移植後に生じたアデノウイルス出血性膀胱炎による疼痛管理に高用量のオピオイドが必要と思われた一例
第 16 回緩和医療薬学会年会, 神戸, 2023 年 5 月 27 日

鳥山陽子，原口浩一，諫見圭佑，大塚眞紀，山形真一
骨髄移植後に生じたアデノウイルス出血性膀胱炎による疼痛管理に高用量のオピオイドが必要と思われた一例
第 76 回国立病院総合医学会，広島, 2023 年 10 月 20 日

諫見圭佑，鳥山陽子，杉尾由希子，今村聖奈，大窪典子，山形真一
三酸化二ヒ素投与後による徐脈性不整脈に対して埋め込み型ペースメーカー対処することで治療継続できた一例
第 76 回国立病院総合医学会，広島, 2023 年 10 月 20 日

山形真一，鈴木寛人，阿部香澄，鶴賀叶女，渡嘉敷崇，津曲恭一
神経筋難病患者に対する薬学ケアの必要性
第 33 回医療薬学会年会，仙台, 2023 年 11 月 4 日

中釜実乃里
こんなところまで血栓像!?　卵円孔を介した危険な下肢静脈由来血栓
第 48 回日本超音波検査学会学術集会(イメージコンテスト)，大阪, 2023 年 6 月 10～11 日

城戸隆宏，上西菜月，岡村優樹，宮下恵美，大迫亮子，日野出勇次，梅橋功征，西方菜穂子
急性胆管炎及び急性胆嚢炎によって形成された門脈血栓症と推測できた 1 症例
2023 年度日臨技九州支部医学検査学会（第 57 回），佐賀, 2023 年 10 月 21 日

樋渡まこ，山口　俊，吉野　歩，高瀬　泉，梅橋功征，西方菜穂子
新型コロナウイルス抗原定量検査の臨床的有用性の検討
2023 年度日臨技九州支部医学検査学会（第 57 回），佐賀, 2023 年 10 月 21 日

赤峯未紀，江藤裕哉，吉野　歩，城ケ崎泰代，後藤正道，野元三治
卵巣原発神経内分泌腫瘍の 1 例
第 62 回日本臨床細胞学会秋期大会，福岡, 2023 年 11 月 4 日

江藤裕哉，赤峯未紀，吉野　歩，城ケ崎泰代，後藤正道，野元三治
胞巣状軟部肉腫の一例
第 62 回日本臨床細胞学会秋期大会，福岡, 2023 年 11 月 5 日

池田光，城戸隆宏，上西菜月，岡村優樹，久保祐子，日野出勇次，梅橋功征，西方菜穂子
胆嚢癌との鑑別に腹部超音波検査が有用であった黄色肉芽腫性胆嚢炎の 1 症例
第 19 回鹿児島医学検査学会，鹿児島, 2024 年 2 月 18 日

日野出勇次
シンポジウムアンケート調査結果報告
第 19 回鹿児島医学検査学会，鹿児島, 2024 年 2 月 18 日

宮川裕司，礒口藍斗，高瀬　泉，吉野　歩，梅橋功征，西方菜穂子
高頻度抗原に対する抗体（抗 Gya）を検出した 1 症例
第 19 回鹿児島医学検査学会，鹿児島, 2024 年 2 月 18 日

久保祐子，岡村優樹，大迫亮子，日野出勇次，梅橋功征，西方菜穂子
高安大動脈炎に合併した Bentall 術後仮性動脈瘤と PVL の観察に苦慮した一症例
第 19 回鹿児島医学検査学会，鹿児島, 2024 年 2 月 18 日

久木野豊，宮島隆一，薗田正浩
経皮的カテーテル心筋焼灼術における被ばく線量の推移
第 31 回日本心血管インターベンション治療学会，福岡, 2023 年 8 月 4 日

松下真優，久木野豊，阿南恵吾，宮島隆一
防護板の使用率及び防護効果の向上に向けた検討
令和5年度九州国立病院機構診療放射線技師会総会及び学術大会，都城, 2023 年 9 月 2 日

堀上英昭，市野凌資，安武翼，木原　諒，阿南恵吾，宮島隆一
COVID-19 クラスター発生時における放射線治療の対応について
令和5年度九州国立病院機構診療放射線技師会総会及び学術大会，都城, 2023 年 9 月 2 日

木原　諒, 山口英明, 宮島隆一, 村山淳一
冠動脈 CT における撮影条件の最適化
令和5年度九州国立病院機構診療放射線技師会総会及び学術大会, 福岡, 2023 年 10 月 7 日

市野凌資
MUS 法を用いた 201TI 心筋血流シンチにおける至適画像処理パラメータの検討
令和5年度九州国立病院機構診療放射線技師会総会及び学術大会, 福岡, 2023 年 10 月 7 日

岩元優樹, 久木野豊, 阿南恵吾, 宮島隆一
ヨード造影剤使用による『Kounis 症候群』を誘発した1例を経験して
第 77 回国立病院総合医学会, 広島, 2023 年 10 月 20 日

山口英明, 岩元優樹, 宮島隆一, 塗木徳人
カテーテルアブレーション術前単純 3D-CT における、3 次元画像解析システムの自動抽出精度と再構成関数の検討
第 18 回 九州放射線医療技術学術大会, 大分, 2023 年 11 月 4 日

溝口将平, 植園航太, 宮之下誠, 佐藤妙子, 蔡　榮鴻, 塗木徳人
遠隔モニタリングで右室リードの脱落に気付いた 1 例
第 18 回九州・沖縄臨床工学会, 久留米, 2023 年 11 月 4 日

日高　優, 溝口将平, 戸田拓弥, 鮫島航己, 植園航太, 倉見谷耕太, 中村充良, 宮久保和久, 淵脇陽一, 宮之下誠
無抗凝固薬での持続的腎代替療法が出血などに与える影響についての検討
第 18 回九州・沖縄臨床工学会, 久留米, 2023 年 11 月 5 日

鮫島航己
五感でつなぐ体外循環技術～視覚編～
第 29 回 JaSECT 九州地方会秋季セミナー, 嬉野, 2023 年 11 月 25 日

戸田拓弥
深夜の call「ECMO が回らなくなった」!?
2023 年度 NHO 九州臨床工学協議会九州支部学術大会, 福岡, 2023 年 9 月 9 日

植園航太
両側からの心房ペースマッピングで対側の最早期を同定し右房からの焼灼で横隔神経麻痺を回避した一例
第 30 回鹿児島県臨床工学会, 鹿児島, 2024 年 1 月 21 日

宮之下誠
人工心肺の最前線
第 30 回鹿児島県臨床工学会, 鹿児島, 2024 年 1 月 21 日

森　菜海, 田中美穂, 酒匂庸子
当院における心不全増悪予防に関する実践報告と今後の課題
第 59 回日本循環器病予防学会学術集会, 鹿児島, 2023 年 6 月 4 日

大迫朋子, 肥後あゆみ, 中川勇樹, 井口麻里
A 病院における DiNQL 活動～導入から 5 年目を迎えての現状と課題～
第 54 回日本看護学会学術集会, 大阪, 2023 年 9 月 29 日

榎谷小春, 池田美由紀, 米丸美希, 花田道代
COVID-19 流行期におけるオンラインシステムを活用した腹膜透析導入患者の入院支援の取り組み
第 29 回日本腹膜透析医学会学術集会, 東京, 2023 年 9 月 30 日

池田美由紀, 榎谷小春, 米丸美希, 花田道代
腹膜透析患者支援につながる ACP の取り組み
第 29 回日本腹膜透析医学会学術集会, 東京, 2023 年 9 月 30 日

森　菜海, 田中美穂, 酒匂庸子
コロナ禍での当院における心不全再増悪予防に関する実践報告と今後の課題
第 77 回国立病院総合医学会, 広島, 2023 年 10 月 20 日

栗脇千春, 山下健一郎, 大塚真紀
COVID－19 流行期における県外移動制限の有用性について
第 77 回国立病院総合医学会, 広島, 2023 年 10 月 20 日

出口喬一
低左心機能に伴う大動脈弁狭窄症による心原性ショックに対して TAVI 及び ECPELLA 管理を行った一例
第 9 回日本 NP 学会学術集会, 北海道, 2023 年 10 月 20 日

伊藤由加, 塗木健介
胆嚢炎疑い患者を診療看護師（NP）が担当しワイル病の診断と治療に繋げることができた一例
第 9 回日本 NP 学会学術集会, 北海道, 2023 年 10 月 20 日

大迫朋子, 松崎　勉, 有元友範, 入江遼太
働き方改革に伴う出退勤打刻システムの導入報告
第 77 回国立病院総合医学会, 広島, 2023 年 10 月 21 日

新坂享子
救急科所属の診療看護師（NP）だからこそ対応できる意思決定支援(パネルディスカッション)
第 9 回日本 NP 学会学術集会, 北海道, 2023 年 10 月 22 日

田原えり奈, 下内広美, 北原こゆき, 福丸美貴, 原田恵子, 中本　恵, 今吉弥生
Driving Surf Protocol 導入後の栄養管理に対する看護師の意識と行動変容～適切な栄養管理を目指して～
第 49 回日本脳卒中学会学術集会, 横浜, 2024 年 3 月 9 日

今田南生人, 根路銘安仁
新人看護師の就業全の楽観性・悲観性と職業キャリア成熟度との関連
第 33 回日本看護学教育学会学術集会, 福岡, 2023 年 8 月 27 日

深野久美, 大野美穂, 山田　巧
「コロナ禍の影響により2年次の老年看護学実習の経験差が生じた看護学生の卒業前の老人のイメージ（SD 調査）」
第 21 回国立病院看護研究学会学術集会, 吹田, 2023 年 12 月 2 日

澁谷幸子, 濱崎友実, 星野睦美, 西園里美, 藤内聖子, 山田　巧, 深野久美
コロナ禍による老年看護学実習経験差に伴う老年観の特徴～「私の老年観」のレポート内容の違い～
第 21 回国立病院看護研究学会学術集会, 吹田, 2023 年 12 月 2 日

星野睦美, 深野久美
コロナ禍による老年看護学学内実習前後での看護学生が認知症高齢者に抱くイメージの変化
第 77 回国立病院総合医学会, 広島, 2023 年 10 月 21 日

筆頭演者が鹿児島医療センターの職員以外

＜国内学会＞

小代 彩, 吉満　誠, 鎌田勇平, 中村大輔, 永野太一, 赤星里佳, 竹下有節, 上野卓也, 島 晃大, 有馬直佑, 林田真衣子, 石塚賢治
結膜原発 MALT リンパ腫の治療成績の後方視的解析
第 85 回日本血液学会学術集会, 東京, 2023 年 10 月 14 日

崔 日承, 吉満 誠, 下川元継, 宇都宮與, 末廣洋子, 日高智徳, 野坂生郷, 佐々木秀法, 頼 晋也, 田村志宜, 大渡五月, 高起 良, 日高道弘, 加藤丈晴, 城 達郎, 森内幸美, 緒方正男, 大塚英一, 鈴島 仁, 伊藤薫樹, 吉田真一郎, 伊藤 旭, 中村大輔, 徳永雅仁, 関根雅明, 坂本祐真, 稲垣 宏, 石田高司, 石塚賢治
高齢者成人 T 細胞白血病リンパ腫に対するモガムリズマブ併用 CHOP-14 療法：多施設共同第 2 相試験
第 85 回日本血液学会学術集会, 東京, 2023 年 10 月 14 日

馬渡誠一, 玉井 努, 最勝寺晶子, 室町香織, 谷山央樹, 豊留亜衣, 伊集院 翔, 坂江 遥, 楢 一晃, 小田耕平, 熊谷公太郎, 森内昭博, 櫻井一宏, 平峯靖也, 井戸章雄
Intermediate stage 肝細胞癌に対する薬物療法の治療成績
第 27 回 日本肝臓学会大会, 神戸, 2023 年 11 月 2 日

藤村 卓, 前川武雄, 伊東孝通, 加藤裕史, 松下茂人, 吉野公二, 藤澤康弘, 神林由美, 橋本 彰, 浅野善英
タキサン系抗がん剤無効皮膚血管肉腫に対するセカンドライン化学療法の検証：多施設共同研究
第 122 回日本皮膚科学会総会, 横浜, 2023 年 6 年 1 日

Shigenari Ishizuka, Yuji Miyamoto, Tomomi Kawakita, Yumi Maeda, Masamichi Goto, Manabu Ato, Masamichi Nagae, Sho Yamasaki
Mycobacterium leprae deactivates a potent PAMP to achieve immune evasion
第 52 回日本免疫学会学術集会, 千葉, 2024 年 1 月 17 日

西 恭宏, 原田佳枝, 中村康典
義歯洗浄剤と超音波洗浄器を併用した洗浄方法とその洗浄温度が微生物除去効果に及ぼす影響.
平成 5 年第 20 回日本口腔ケア学会総会・学術大会, 東京, 2023 年 4 月 21 日

石畑清秀, 渡辺祐奈, 木村菜美子, 大河内孝子, 岐部俊郎, 手塚征宏, 上栗裕平, 椎木彩乃, 芹澤慎生, Farid Ratman Mohammad, 中村典史
片側性不完全唇裂症例に対する Cronin 法による口唇形成術の三次元的治療評価
平成 5 年度第 47 回日本口蓋裂学会総会・学術集会, 東京, 2023 年 5 月 25 日

西 恭宏, 濵野 徹, 有村健二, 中村康典, 西村正宏
口腔機能低下症検査時に行う簡易型体組成計を用いたサルコペニア診断の試み
平成 5 年日本老年歯科医学会第 34 回学術大会, 横浜, 2023 年 6 月 18 日

野元菜美子, 大河内孝子, 椎木彩乃, 芹澤慎生, 上栗裕平, 手塚征宏, 岐部俊郎, 石畑清秀, 中村典史
唇裂患者における腸骨移植を併用した口唇外鼻修正術治療効果についての三次元形態評価
平成 5 年第 68 回（公社）日本口腔外科学会総会・学術集会, 大阪, 2023 年 11 月 10 日

谷本憲哉, 杉尾由希子, 鳥山陽子, 大窪典子, 山形真一
ラスブリカーゼを使用後にメトヘモグロビン血症を発症した 1 例
第 33 回医療薬学会年会, 仙台, 2023 年 11 月 3 日

大井邦治, 宮島隆一, 増井飛沙人, 渋谷 充, 太田一郎, 財前誠, 市川和幸, 池田敏久, 阿南恵吾, 松井謙典, 筒井昭詔
Ｘ線撮影における再撮影の発生状況と要因分析について第 2 報再撮影低減に向けた知識やスキルアップ支援策の提供
第 39 回日本診療放射線技師学術大会, 熊本, 2023 年 9 月 30 日

増井飛沙人, 宮島隆一, 大井邦治, 渋谷 充, 太田一郎, 財前 誠, 市川和幸, 池田敏久, 阿南恵吾, 松井謙典, 筒井昭詔
Ｘ線撮影における再撮影の発生状況と要因分析について第 1 報多施設ディジタル撮影システムにおける検討
第 77 回国立病院総合医学会, 広島, 2023 年 10 月 20 日

大井邦治, 宮島隆一, 増井飛沙人, 渋谷 充, 太田一郎, 財前誠, 市川和幸, 池田敏久, 阿南恵吾, 松井謙典, 筒井昭詔
Ｘ線撮影における再撮影の発生状況と要因分析について第 2 報再撮影低減に向けた知識やスキルアップ支援策の提供
第 77 回国立病院総合医学会, 広島, 2023 年 10 月 20 日

④ 研究会

立石直毅
胸合部仮性肩肱痛による脳梗塞の一例
Abhott Value Summit, 福岡市, 2023 年 10 月 1 日

濵田祐樹, 宮下史生, 西　萌生, 池田め衣, 岡田敬史, 髙口　剛, 松岡秀樹
Pinnacle blue20 と 8Fr Optimo を用いた経上腕アプローチによる CAS の経験
Cerebrovascular Neurologist 研究会, 福岡市, 2023 年 5 月 13 日

二宮由美子
陸上短距離選手の中学生, 過換気発作時の心電図異常
第 34 回九州不整脈研究会, 福岡, 2023 年 11 月 4 日

徳留明夫, 神尾真樹
当科におけるレンバチニブ、ペンブロリゾマブ療法の使用経験からの考察
子宮体癌地域連携セミナーin 鹿児島, 鹿児島, 2023 年 9 月 25 日

西元謙吾
頭頸部アルミノックス治療の経験からの考察
南九州頭頸部アルミノックス治療講演会, Web 開催, 2023 年 7 月 27 日

佐多菜穂子, 杉尾由希子, 大窪典子, 山形真一
入院中薬学ケアにより副作用を軽減した症例について病院-薬局間の薬剤師が連携することで患者満足度向上につながった一例
第 1 回鹿児島県薬剤師フェスタ, 鹿児島, 2023 年 11 月 18 日

西村尚芳, 谷口　潤, 山形真一
薬剤師業務を薬剤助手へタスクシフトするための訓練の効果
第 1 回鹿児島県薬剤師フェスタ, 鹿児島, 2023 年 11 月 18 日

上之園咲, 今村聖奈, 鳥山陽子, 杉尾由希子, 大窪典子, 山形真一
アルミノックス療法の実施環境整備：注文から調製，投与後まで
国立病院薬剤師会宮崎・鹿児島地区薬学研究会, 鹿児島, 2023 年 9 月 30 日

上之園咲, 今村聖奈, 鳥山陽子, 杉尾由希子, 大窪典子, 山形真一
アルミノックス療法の実施環境整備：注文から調製，投与後まで
第 7 回鹿児島県病院薬剤師会学術大会（鹿児島），鹿児島, 2024 年 1 月 27 日

城戸隆宏
急性胆管炎及び急性胆嚢炎によって形成された門脈血栓症
第 329 回鹿児島県超音波医学研究会, Web, 2023 年 5 月 23 日

岡村優樹, 上西菜月, 久保祐子, 日野出勇次, 梅橋功征, 西方菜穂子, 馬場善政
感染性心内膜炎にて僧帽弁大動脈弁間線維骨格仮性動脈瘤を呈した 1 例
国臨協九州支部生理検査部門症例報告会, Web, 2023 年 6 月 28 日

城戸隆宏
膠原病に伴う肺動脈性肺高血圧症の 1 例
第 330 回鹿児島県超音波医学研究会, Web, 2023 年 6 月 28 日

岡村優樹
肝内胆管拡張が疑われた1例
第 331 回鹿児島超音波医学研究会, Web, 2023 年 7 月 25 日

上西菜月
巨大腹腔内腫瘍を認めた一症例
第 333 回鹿児島超音波医学研究会, Web, 2023 年 9 月 26 日

日野出勇次
典型的心アミロイドーシスの 1 症例
鹿児島超音波医学研究会循環器部門定例会, Web, 2023 年 10 月 25 日

日野出勇次
大動脈弁位人工弁 detachment の 1 症例
鹿児島超音波医学研究会秋季大会, Web, 2023 年 11 月 29 日

池田 光, 城戸隆宏, 上西菜月, 岡村優樹, 久保祐子, 日野出勇次, 梅橋功征, 西方菜穂子
黄色肉芽腫性胆嚢炎の 1 症例
第 336 回鹿児島県超音波医学研究会, Web, 2023 年 12 月 5 日

原田美里
心臓浸潤が疑われた悪性リンパ腫の 1 例
第 337 回鹿児島超音波医学研究会, Web, 2024 年 1 月 31 日

日野出勇次
当院で経験した DPM の 2 症例
第 41 回多施設共同心エコーミーティング, Web, 2024 年 2 月 19 日

中釜美乃里
経胸壁心エコー図検査が診断の一助となった左室心筋内に浸潤を来した悪性リンパ腫の一症例
第 338 回鹿児島超音波医学研究会, Web, 2024 年 2 月 27 日

岡村優樹
Wellens 症候群の一例
第 338 回鹿児島超音波医学研究会, Web, 2024 年 2 月 27 日

⑤ 学術講演会

片岡哲郎
当院におけるサピエン3の成績
第 13 回日本径カテーテル心臓弁治療学会学術集会 JTVT2023, 東京, 2023 年 7 月 28 日

福永研吾, 片岡哲郎, 沖野秀人, 野元裕太朗, 髙﨑州亜, 中島 均, 大石 充
当院における狭小弁輪に対する Sapien3 を用いた TAVR の治療成績
第 71 回日本心臓病学会学術集会, 東京, 2023 年 9 月 10 日

福永研吾
虚血性心疾患とその予防
生活習慣病予防教室, 鹿児島, 2023 年 9 月 26 日

立石直毅
心臓血管外科分野における手術部位感染症と創管理
ゴンバテック創傷ケア Web セミナー, Web, 2023 年 5 月 1 日

金城玉洋
低侵襲治療は定型的心臓外科手術を凌駕するのか
日本手術医学会教育委員会主催令和 5 年 第 1 回日本手術医学会教育セミナー, 宮崎, 2023 年 9 月 2 日

金城玉洋
心臓血管外科ハイボリュームセンターにおける「医師の働き方改革」
第 76 回済生会学会令和 5 年度済生会総会ランチョンセミナー, 熊本, 2024 年 1 月 28 日

金城玉洋
職業講演（医師）
宮崎市加納中学校，宮崎, 2023 年 7 月 13 日

岡田敬史
パーキンソン病の運動合併症への対応
第 5 回チェスト！鹿児島, 2023 年 6 月 16 日

松岡秀樹
心原性脳塞栓症とは ？
第 59 回日本循環器病予防学会 市民公開講座，鹿児島, 2023 年 6 月 4 日

松岡秀樹
脳卒中診療 UP to date - 発症予防から後遺症管理まで -
SNS @ Web～Special Edition～，横浜, 2023 年 8 月 1 日

松岡秀樹
鹿児島医療センターにおける脳卒中診療
第 14 回山峰会研究会，宇都宮, 2023 年 10 月 8 日

松岡秀樹
脳梗塞救急治療の現状と課題
社会医療法人恒心会 教育講演会，鹿屋, 2023 年 11 月 10 日

松岡秀樹
鹿児島医療センターにおける脳出血の現状
Experience Sharing Symposium in Kagoshima，鹿児島, 2024 年 2 月 27 日

濵田祐樹
どうする脳梗塞治療 ～今昔エビデンス～
脳卒中トータルケア Web セミナー，鹿児島, 2023 年 4 月 24 日

濵田祐樹
最新の脳卒中診療とてんかん
脳卒中トータルケア Web セミナー，鹿児島, 2023 年 5 月 22 日

濵田祐樹
最新の脳卒中診療とてんかん
脳卒中トータルケア Web セミナー，鹿児島, 2024 年 1 月 15 日

郡山暢之
SDM カスタマイズド鹿児島 New Version
DiaMond Seminar in 鹿児島，鹿児島（WEB, 2023 年 6 月 14 日

郡山暢之
SDM カスタマイズド鹿児島 up to date -経口血糖降下薬を考える-
第 12 回 臨床に「薬だつ」研修会，鹿児島（WEB），2023 年 6 月 30 日

郡山暢之
SDM カスタマイズド鹿児島 up to date -経口血糖降下薬を考える-
SDM カスタマイズド鹿児島 in 北薩，鹿児島（WEB），2023 年 7 月 6 日

郡山暢之
糖尿病患者のフットケアと予防の実際～症例をもとに～
第 28 回糖尿病医療連携体制講習会，鹿児島（ハイブリッド），2023 年 7 月 18 日

郡山暢之
糖尿病患者の足病変 ～病態生理から治療まで～
令和 5 年度糖尿病重症化予防（フットケア）研修，鹿児島, 2023 年 10 月 19 日

森内昭博
糖尿病との関連を含めた肝疾患フォローアップの勘所
第2回鹿児島県内科医会 WEB 講座, WEB, 2023 年 10 月 12 日

田中裕治
大人になっていく心臓病のこどもたち～移行期から成人期への諸問題～
令和 5 年度小児慢性特定疾病児支援研修会，鹿児島, 2024 年 2 月 8 日

中村康典
急性期病院における口腔機能低下症
第 2 回鹿児島口腔ケアフォーラム 講演，鹿児島, 2024 年 2 月 4 日

松下茂人
皮膚がん診療のリアル～患者さん一人ひとりに最適な治療を考える～
ポートアイランド皮膚疾患研究会 2023，神戸, 2023 年 4 月 8 日

松下茂人
基底細胞がん
2023 希少がんセミナーMeet the Expert 国立がん研究センターx 鹿児島医療センター, Web, 2023 年 9 月 8 日

松下茂人
日本人のメラノーマ～患者さん一人ひとりに最適な診療を考える～
近畿若手メラノーマ研究会，大阪, 2024 年 3 月 1 日

青木恵美
もう一歩先の皮膚外科手術 -鼻と口唇
第 122 回日本皮膚科学会総会，横浜, 2023 年 6 月 2 日

青木恵美
手術とインフォームドコンセント
第 39 回日本皮膚悪性腫瘍学会学術大会，名古屋, 2023 年 8 月 4 日

青木恵美
教育講演トリセツ
第 29 回日本形成外科手術手技学会，佐賀, 2024 年 3 月 2 日

鳥山陽子
保険薬局との連携，現状から見える課題と今後に関する話題
第 1 回地域医療連携 Web セミナー，鹿児島, 2023 年 11 月 6 日

鳥山陽子，諫見圭介，山形真一
鹿児島医療センターの院外処方箋に関する調剤変更に関する事前合意プロトコールの運用について
鹿児島市薬剤師会研修会，鹿児島, 2024 年 1 月 24 日

吉野 歩
認定病理技師資格試験 対策講義
国臨協九州支部病理部門研修会，福岡（Web）, 2023 年 6 月 14 日

日野出勇次
左室収縮能の評価と HFrEF
第 13 回 KYUSHU 心血管超音波セミナー，鹿児島, 2023 年 6 月 17 日

山口 俊
血液培養より Gemella morbillorum を検出した心内膜炎の一例
令和 5 年度第 1 回臨床微生物部門 Web 研修会, Web, 2023 年 6 月 24 日

日野出勇次
超音波検査検査士試験対策ゼミ「基礎編」
The Echo Web 第 7 回ソノゼミ, Web, 2023 年 7 月 6 日

波野真伍
血算データの見方・考え方
長崎県臨床検査技師会　令和 5 年度血液検査研究班研修会, Web, 2023 年 7 月 15 日

高瀬　泉
骨髄検査の基礎
熊本県臨床検査技師会　臨床血液部門研修会, Web, 2023 年 7 月 25 日

吉野　歩, 富田大介, 有村郷司
認定病理技師資格試験に関する情報提供
鹿児島県診療検査技師会　第一回病理細胞診部門研修会, 鹿児島, 2023 年 9 月 9 日

波野真伍
貧血精査目的に紹介され凝固第 XIII/13 因子欠乏が判明した一例
第 4 回南九州凝固・線溶セミナー, 鹿児島, 2023 年 9 月 16 日

日野出勇次
超音波検査検査士試験対策ゼミ「基礎編」
The Echo Web 第 13 回ソノゼミ, Web, 2023 年 10 月 5 日

日野出勇次
超音波検査検査士試験対策ゼミ「循環器臨床編」
The Echo Web 第 14 回ソノゼミ, Web, 2023 年 10 月 19 日

日野出勇次
経胸壁心エコー図検査時にリニアプローブが役立った 6 症例
GE Meet The Expert 鹿児島, Web, 2023 年 12 月 8 日

吉野　歩, 富田大介, 有村郷司
ホルムアルデヒドの取り扱い上の注意点と労働安全衛生規則変更に関する情報提供
鹿児島県臨床検査技師会スキルアップ研修会, 鹿児島, 2023 年 12 月 9 日

江藤裕哉
病理システム導入における妥当性確認の進め方～当院での事例を踏まえて～
鹿児島県臨床検査技師会　令和 5 年　第 2 回　病理細胞診部門研修会, 鹿児島, 2024 年 2 月 3 日

岡村優樹
謎多きペースメーカの世界
鹿児島県臨床検査技師会　生理部門研修会, Web, 2024 年 2 月 28 日

日野出勇次
心アミロイドーシスのゲートキーパーとしてエコー室ができること
地域で診る心アミロイドーシスセミナーin 鹿児島, 鹿児島, 2024 年 3 月 18 日

日野出勇次
心アミロイドーシスのゲートキーパーとしてエコー室ができること
地域で診る心アミロイドーシスセミナーin 鹿児島, 鹿児島, 2024 年 3 月 18 日

宮島隆一
X 線透視における被ばく管理
第 79 回日本放射線技術学会総会学術大会専門部会講座放射線防護部会入門編, 横浜, 2023 年 4 月 15 日

宮島隆一
令和 5 年度放射線関連法令における立入検査報告 労働基準監督署の立ち入り検査
令和 5 年度医療職（二）等職場長管理研修放射線分科会, Web, 2023 年 6 月 21 日

阿南恵吾
放射性同位元素等の規制に関する法律に基づく立ち入り検査
令和 5 年度医療職（二）等職場長管理研修放射線分科会, Web, 2023 年 6 月 21 日

宮島隆一
被ばく管理を行っている診療放射線技師の立場から
日本放射線看護学会 第 12 回学術集会 JSRT RNSJ 共同企画, 長崎, 2023 年 9 月 10 日

宮島隆一
診療報酬の取れ漏れ確認
令和 5 年度第 2 回九州国立病院機構診療放射線技師長協議会研修会経営改善研修会, Web, 2023 年 12 月 18 日

森 菜海, 片岡哲郎, 酒匂庸子, 田中美穂, 福迫直美, 村田淳子, 髙﨑州亜, 薗田正浩, 中島 均
当院における心不全再増悪予防に関する実践報告と今後の課題
第 59 回日本循環器病予防学会学術集会, 鹿児島, 2023 年 6 月 3 日

深野久美
鹿児島医療センターにおける附属看護学校の閉校と大学誘致の経緯と課題について
第 77 回国立病院総合医学会, 広島, 2023 年 10 月 21 日

4. 論文

当院所属で筆頭者として発表された論文を掲載します。

CARDIOVASCULAR FLASHLIGHT

https://doi.org/10.1093/eurheartj/ehad207
Online publish-ahead-of-print 8 April 2023

Constrictive pericarditis with massive pericardial effusion

Mari Nakabeppu [1]*, Shun Ijuin [1], and Naoki Tateishi[2]

[1]Department of Cardiovascular Medicine, National Hospital Organisation Kagoshima Medical Center: Kokuritsu Byoin Kiko Kagoshima Iryo Center, 8-1, Shiroyama-cho, Kagoshima-shi, Kagoshima 892-0853, Japan; and [2]Department of Cardiovascular Surgery, National Hospital Organisation Kagoshima Medical Center: Kokuritsu Byoin Kiko Kagoshima Iryo Center, 8-1, Shiroyama-cho, Kagoshima-shi, Kagoshima 892-0853, Japan
*Corresponding author. Tel: +81 992231151, Email: mary.berry.happy@gmail.com

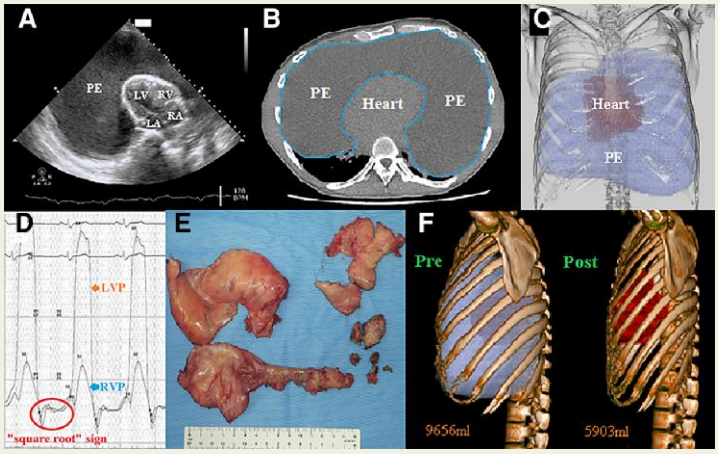

A 27-year-old man was admitted to our hospital for the investigation of pericardial effusion (PE) and ascites. Despite the accumulation of excessive pericardial fluid, vital signs of cardiac tamponade were not observed. He had no prior medical history except for a blunt chest trauma 10 years earlier. Echocardiography showed a tiny heart in extraordinarily retained massive PE (*panel A*, Supplementary data online, *Video S1*). Computed tomography (CT) revealed a distended overfilling pericardial cavity that remarkably compressed his heart and lung (*panels B* and *C*). Magnetic resonance imaging showed a thickened pericardium and a respiratory septal bounce phenomenon (see Supplementary data online, *Video S2*). Heart catheterization followed by a pericardial drainage of gigantic 6500 mL amount of exudative fluid suggested constrictive property of diastolic square root sign in left and right ventricular simultaneous pressure tracings (*panel D*). He was diagnosed with effusive–constrictive pericarditis. Despite the removal of pericardial fluid and the treatment with anti-inflammatory medications, the underlying pericardial constricted property continued to cause symptoms. He underwent a surgical removal of the thickened pericardium uneventfully (*panel E*). Further analysis of the volume of the thoracic cavity utilizing a comprehensive 3D-rendered CT revealed a significantly greater pre-operative volume of 9569 mL compared with the post-operative volume of 5903 mL (*panel F*, Supplementary data online, *Video S3*). This is the first report to suggest that the compensative and elastic ability of both the thoracic and pericardial cavities plays a role in protecting hemodynamics in effusive–constrictive pericarditis.

Supplementary data is available at *European Heart Journal* online.

This report did not receive any funding from government, commercial, or non-profit organizations. The authors have submitted their declaration, which can be found in Supplementary material online. The data underlying this article are available in the article and in its online supplementary material. Supplementary material is available at *European Heart Journal* online.

ESC European Society of Cardiology
European Heart Journal - Case Reports (2024) **8**, 1–2
https://doi.org/10.1093/ehjcr/ytae024

Right heart failure due to compression of right ventricular outflow tract by post-operative aortic pseudoaneurysm

Shun Ijuin [1]*, Yushi Yamashita[2], and Tamahiro Kinjo[2]

[1]Department of Cardiovascular Medicine, National Hospital Organization Kagoshima Medical Center: Kokuritsu Byoin Kiko Kagoshima Iryo Center, 8-1, Shiroyama-cho, Kagoshima-shi, Kagoshima 892-0853, Japan; and [2]Department of Cardiovascular Surgery, National Hospital Organization Kagoshima Medical Center: Kokuritsu Byoin Kiko Kagoshima Iryo Center, 8-1, Shiroyama-cho, Kagoshima-shi, Kagoshima 892-0853, Japan

Received 23 November 2023; revised 15 December 2023; accepted 11 January 2024; online publish-ahead-of-print 25 January 2024

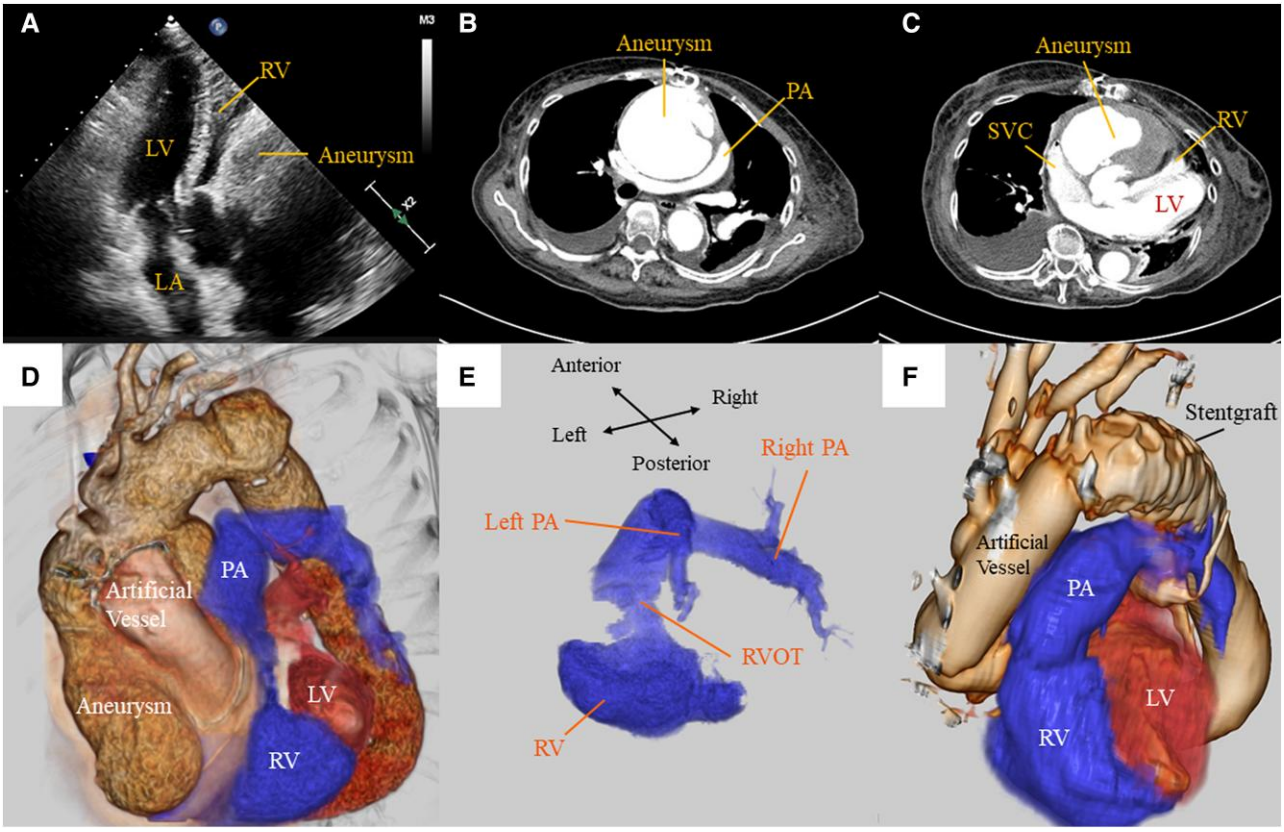

* Corresponding author. Tel: +81 99 223 1151, Email: silver.gray.dragon@gmail.com
Handling Editor: Can Gollmann-Tepeköylü

A 78-year-old man presented with effort dyspnoea and oedema. He had undergone a replacement of ascending aorta for acute aortic dissection 3 years earlier, and no problems have been detected in post-operative computed tomography (CT). Echocardiogram showed a compressed right ventricle from extra-cardiac structures, resulting in right ventricular outflow tract (RVOT) stenosis and subsequent pulmonary hypertension (*Panel A*; Supplementary data online, *Video S1*). Computed tomography revealed a huge aortic pseudoaneurysm originating from peripheral anastomosis of the artificial aortic graft, which compressed the right ventricle as well as the superior vena cava, right atrium, and pulmonary artery (*Panels B* and *C*; Supplementary data online, *Video S2*). Additional reconstructed 3D-rendered CT clearly demonstrated that the RVOT was pinched and constricted by the aortic pseudoaneurysm (*Panels D* and *E*; Supplementary data online, *Video S3*). He was diagnosed with right heart failure due to compression around the RVOT by post-operative aortic pseudoaneurysm. He underwent a redo with a total arch replacement with an open stent graft to release the compression. During surgery, we found bleeding at the anastomosis between the graft and the aorta. We considered that the aortic tissue was fragile and the aortic wall would be dissected one after another by suturing haemostasis, so we added Bentall surgery. Post-operative computed tomography revealed the expanded RVOT (*Panel F*; Supplementary data online, *Video S4*) resulting in a haemodynamic normalization. He was discharged home 77 days after surgery. This is the first case of an aortic pseudoaneurysm that compressed the RVOT and led to a right heart failure.

Supplementary material

Supplementary material is available at *European Heart Journal – Case Reports* online.

Acknowledgements

The authors thank Yuki Iwamoto (radiologist) for technical assistance with re-construction of 3D-rendered CT imaging.

Consent: The authors confirm that written consent for submission and publication of this case report including images and associated text has been obtained from the patient in line with COPE guidance.

Conflict of interest: None declared.

Funding: All authors have declared no support from any organization for the submitted work, no financial relationships with any organizations that might have an interest, and no other relationships or activities that could appear to have influenced the submitted work.

Data availability

The data underlying this article are available in the article and in its online Supplementary material.

Surgical Case Reports

CASE REPORT Open Access

Successful sutureless repair of multiple left ventricular free wall ruptures due to Takotsubo cardiomyopathy: a case report

Hiroto Yasumura[1*], Koji Tao[1], Ryo Imada[1], Yushi Yamashita[1], Naoki Tateishi[1] and Tamahiro Kinjo[1]

Abstract

Background Takotsubo cardiomyopathy (TCM) is a temporary and reversible systolic abnormality of the left ventricular apical area resembling a myocardial infarction. Cardiac rupture due to TCM is a rare but fatal complication. Without cardiac surgery, 94% of patients with left ventricular free wall rupture (LVFWR) due to TCM die. Furthermore, successful surgical cases are rare. We report herein the successful treatment of multiple LVFWRs due to TCM using a sutureless repair.

Case presentation An 80-year-old man quarreled with his daughter and had a sudden onset of chest pain. He was transferred to our hospital in shock. Electrocardiography showed ST elevation and contrast-enhanced computed tomography revealed a bloody pericardial effusion. Emergent coronary angiography showed no significant stenosis. Cardiac arrest ensued because of cardiac tamponade. Emergent surgery was undertaken and three oozing lacerations on the lateral and inferior walls were noted. A sutureless repair was performed using TachoSil® patches. We also applied Surgicel Nu-Knit® absorbable hemostat with Hydrofit® where TachoSil® failed to completely adhere because of hematoma formation and achieved complete hemostasis. We diagnosed the ruptures due to TCM according to the Mayo criteria. The patient was discharged on postoperative day 71.

Conclusions A sutureless repair using TachoSil® patches and Surgicel® with Hydrofit® is a minimally invasive and effective method for the treatment of multiple LVFWRs due to TCM.

Keywords Takotsubo cardiomyopathy, Left ventricular rupture, Sutureless repair

Background

Takotsubo cardiomyopathy (TCM), also known as "broken heart syndrome" or "apical ballooning syndrome", is a temporary and reversible systolic abnormality of the left ventricular apical area resembling a myocardial infarction in the absence of coronary artery disease [1]. Cardiac rupture due to TCM is a rare but fatal complication. Without cardiac surgery, 17 of 18 (94%) patients with left ventricular free wall rupture (LVFWR) due to TCM died [2]. Furthermore, successful surgical reports are rare. The cardiac surgeries for LVFWR generally involve suture or sutureless repair. The former technique includes linear closure, infarctectomy, and closure or patch closure, whereas the latter technique includes repair with a collagen patch, such as TachoSil® (CSL Behring, Pennsylvania, USA) [3]. In the current report, we present a patient with multiple LVFWRs due to TCM that were successfully treated using a sutureless repair.

Case presentation

An 80-year-old man bitterly quarreled with his daughter at night in the summer and had the sudden onset of chest pain while in the shower. He was transferred to

*Correspondence:
Hiroto Yasumura
hiroto1331255@yahoo.co.jp
[1] Department of Cardiovascular Surgery, National Hospital Organization Kagoshima Medical Center, 8-1, Shiroyamacho, Kagoshima, Kagoshima 892-0853, Japan

our hospital. He had been followed by cardiologists for suspected vasospasm angina, non-sustained ventricular tachycardia, and paroxysmal atrial fibrillation. On physical examination the arterial pressure was 70/59 mmHg and the heart rate was 99 beats per minute. The laboratory data showed an elevated troponin I level (2437 pg/mL [reference value, < 26.2 pg/mL]) and an elevated creatine kinase (CK) level (443 U/L [reference value, 59–248 U/L]). Electrocardiography showed ST elevation in leads I, aVL, and V3–V6 (Fig. 1a). Transthoracic echocardiography (TTE) showed that the ventricles were compressed by a substantial pericardial effusion. Contrast-enhanced computed tomography revealed a bloody pericardial effusion and a focal low-density area in the lateral wall covered with a hematoma (Fig. 1b). Emergent coronary angiography showed that there was no significant stenosis (Fig. 1c, d). He had a pulseless electrical activity arrest due to cardiac tamponade shortly after intra-aortic balloon pumping (IABP) was established. Cardiopulmonary resuscitation and pericardiocentesis restored spontaneous circulation. The hemoglobin level of the > 500 mL drainage fluid was 12 g/dL and did not decrease despite the low blood pressure. Therefore, we performed emergent surgery. Four hours after the diagnosis of LVFWR, a median sternotomy was performed and the femoral artery was simultaneously exposed for cardiopulmonary bypass (CPB). The lateral wall of the left ventricle was covered with a viscous hematoma. After removing the hematoma and manually elevating the heart, we noted three oozing lacerations [two on the lateral wall (Fig. 2a) and one on the inferior wall (Fig. 2b)]. An oozing-type LVFWR was diagnosed and a sutureless repair was performed using TachoSil® fibrin sealant patches (9.5 cm × 4.8 cm and 4.8 cm × 4.8 cm; Fig. 2b, c). Surgicel Nu-Knit® absorbable hemostat (Ethicon, New Jersey, USA) with Hydrofit® (Terumo, Tokyo, Japan) were also applied to the areas where TachoSil® failed to completely adhere because of hematoma formation. In so

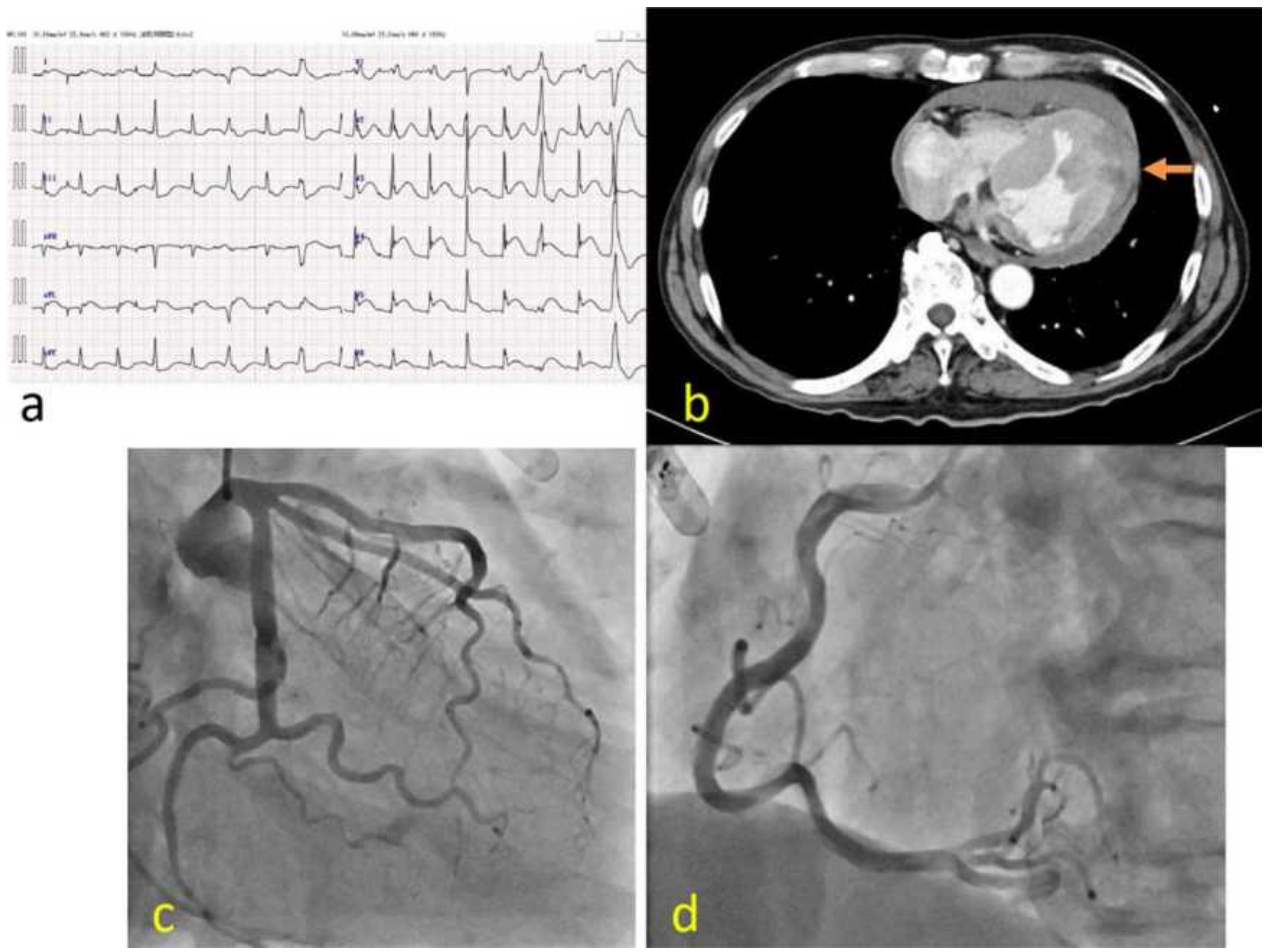

Fig. 1 Findings on admission. **a** Electrocardiography showed ST elevation in leads I, aVL, and V3–V6. **b** A contrast-enhanced computed tomography scan revealed a substantial pericardial effusion and a focal low-density area covered with hematoma in the lateral wall (orange arrow). **c**, **d** Emergent coronary angiography showed that there was no significant stenosis. *LAD* left anterior descending artery

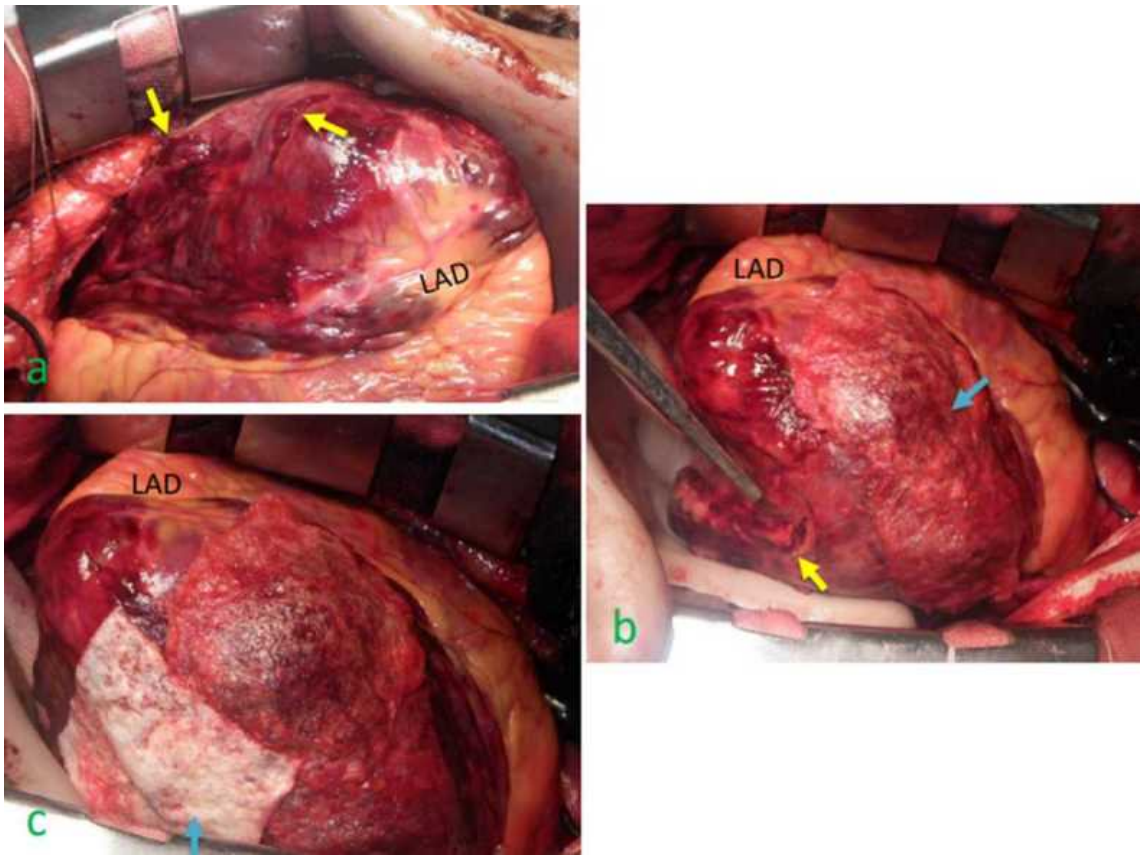

Fig. 2 Intraoperative findings. **a** Manual elevation of the heart enabled us to note two oozing lacerations on the lateral wall (yellow arrows). **b** TachoSil® (blue arrow) was applied to the oozing lacerations surrounded by a hematoma on the lateral wall but did not adhere completely because of a wet scaffold. Surgicel Nu-Knit® absorbable hemostat with Hydrofit® successfully adhered to the lacerations. Another laceration was noted on the inferior wall (yellow arrow). **c** TachoSil® (blue arrow) successfully adhered to the laceration on the inferior wall

doing, complete hemostasis was achieved. Hemodynamic parameter was stable with catecholamines decreasing. He was withdrawn from IABP under dobutamine 1 γ(μg/kg/min) and noradrenaline 0.07 γ on postoperative day (POD) 3 to prevent catheter related blood stream infection and begin rehabilitation. He was withdrawn from the respirator on POD 7. The peak CK level was 3729 U/L. TTE showed no pseudoaneurysm on POD 66. There was also no evidence of cardiomyopathy, cerebrovascular disease, or pheochromocytoma, which met the Mayo Clinic diagnostic criteria for TCM (Table 1) [4]. He was discharged from the hospital on POD 71.

Discussion

TCM is a temporary, reversible, benign disease, which is often triggered by intense physical or emotional stress. In this case, the patient had no physical stress and a bitter quarrel was considered to trigger TCM. The most serious complication of TCM is LVFWR and rupture of the ventricular septum. The etiology of TCM rupture is

Table 1 Mayo Clinic criteria for Takotsubo cardiomyopathy

1.	Transient hypokinesis, akinesis, or dyskinesis of the left ventricular mid segments with or without apical involvement; the regional wall motion abnormalities extend beyond a single epicardial vascular distribution; a stressful trigger is often, but not always present
2.	Absence of obstructive coronary disease or angiographic evidence of acute plaque rupture
3.	New electrocardiographic abnormalities (either ST-segment elevation and/or T-wave inversion) or modest elevation in cardiac troponin
4.	Absence of pheochromocytoma or myocarditis

unrelated to an acute myocardial infarction (AMI) [5]. Emotional stress increases catecholamine release. Direct catecholamine toxicity on the cardiac muscle cells causes contraction band necrosis, inflammatory cell infiltration, and localized fibrosis [6, 7]. One histopathological case report of LVFWR due to TCM described that myocardial injury involved both ischemic and catecholaminergic etiology [8].

Although TCM rupture occurred within an hour after a quarrel in our case, it generally occurs on days 2–5 of hospitalization [2]. Therefore, LVFWR due to TCM is rare, but should be considered in the differential diagnosis of an unexpected pericardial effusion in the emergency room and on the ward. In our case, there was no significant stenosis of the coronary arteries, thus we did not suspect the presence of TCM and did not perform left ventriculography to confirm TCM.

LVFWR is often accompanied with an AMI and is one of the most severe life-threatening mechanical complications. LVFWR develops in up to 2% of patients with an AMI and accounts for 14–26% of deaths after an AMI [9, 10]. By contrast, LVFWR develops in 1.89% of patients with TCM and accounts for 77% of deaths after TCM [2]. The high mortality rate of LVFWR due to TCM may in part be because AMI is under the watchful eyes of a cardiologist. However, TCM is often caused by stress and other non-cardiovascular diseases, and rupture occurs abruptly under the care of non-cardiologists, thus forcing physicians to withdraw or withhold treatment.

The patient presented herein had an excellent outcome because of prompt diagnosis and appropriate surgical repair. Case reports on the successful surgical repair of LVFWR due to TCM are rare. Indeed, we found only four such surgical cases [11–14] in a PubMed search (Table 2). These case reports lacked detailed descriptions about the rupture type and surgery performed. Our case involved oozing-type LVFWRs and a sutureless repair using collagen patches without CPB. The advantage of a sutureless repair includes the avoidance of CPB and systemic heparinization, and avoidance of suturing a fragile myocardium [3]. Therefore, in cases with multiple oozing-type LVFWRs, sutureless repair is feasible and effective.

Sutureless repair may cause postoperative complications, such as re-rupture and pseudoaneurysm. Sutureless repair with TachoSil®/TachoComb® collagen patches (Nycomed, Zurich, Switzerland) is a major emergent treatment option for LVFWR. TachoSil is a medicated sponge coated with human fibrinogen and thrombin and facilitate secondary hemostasis; however, the re-rupture rate after sutureless repair for oozing-type LVFWR due to an AMI was reported to be 12% (4 of 33 cases), occurring on POD 0 in 3 patients and on POD 5 in 1 patient [15]. The re-rupture rate after sutureless repair for a blowout-type LVFWR due to an AMI has been reported to be 0–100% in a limited number of cases [15, 16]. Among patients with re-rupture of an LVFWR, the noteworthy intraoperative findings at the time of initial sutureless surgery with TachoSil®/TachoComb® included wet and unstable scaffold-like oozing of blood from multiple areas of the epicardium, bulging of the infarcted myocardium in the systolic phase, a severely edematous heart, and a large hematoma in the epicardium [15]. In the present case, TachoSil® did not completely adhere to the oozing laceration with a hematoma, but Surgicel® with Hydrofit® sealant successfully adhered to the lacerations. Cases involving the successful use of Hydrofit® sealant for an LVFWR have been recently reported, even for a blowout rupture [17, 18]. Hydrofit® is a viscous diisocyanate prepolymer and has high affinity for wet scaffolds. Water contact initiates the chemical change to form elastomer and adhere rapidly[19]. Surgicel® is an oxidized cellulose polyanhydroglucuronic acid and is

Table 2 Successful surgical case reports of LVFWR due to TCM

Author(s) and year of publication	Age (years)	Gender (F/M)	LVFWR site	Rupture type	CPB(+)	Surgery	Death(+)
Ishida et al. (2005) [11]	67	F	Unknown	Unknown	Unknown	Unknown	–
Zalewska-Adamiec et al. (2016) [12]	74	F	Apex	Blow out	–	Suture on a double-layered Teflon pad	–
Kudaiberdiew et al. (2017) [13]	63	F	Inferior lateral wall	Unknown	+	Resection of LV pseudoaneurysm and pericardial patch repair	–
Al-Tkrit et al. (2020) [14]	77	F	Unknown	Unknown	–	Large patch repair	+
Present case	80	M	Lateral, inferior wall	Multiple oozing	–	Sutureless repair with TachoSil® patch and Surgicel® with Hydrofit®	–

LVFWR left ventricular free wall rupture, *CPB* cardiopulmonary bypass

able to hold or contain water and blood, which facilitates clot formation. Thus, Hydrofit® is usually reinforced with Surgicel® [17]. The use of Hydrofit® sealant and Surgicel® at the wet scaffold leads to effective hemostasis and provides a dry scaffold for adherence of TachoSil®/TachoComb®. Depending on the condition of the epicardium, a multidisciplinary hemostat approach is imperative for an LVFWR.

Conclusions

Sutureless repair using a TachoSil® patch and Surgicel® with Hydrofit® is a minimally invasive and effective method for the treatment of multiple LVFWRs due to TCM.

Abbreviations

TCM	Takotsubo cardiomyopathy
LVFWR	Left ventricular free wall rupture
IABP	Intra-aortic balloon pumping
POD	Postoperative day
AMI	Acute myocardial infarction

Acknowledgements
We would like to thank the cardiologists, Yutaro Nomoto, MD and Kento Tagata, MD, for the preoperative examination and postoperative treatment.

Author contributions
HY wrote the initial draft of the manuscript. KT and TK supervised the writing of the manuscript. HY and KT performed the surgery and HY followed up the patient. All authors participated in the treatment of the patient. All authors read and approved the final manuscript.

Funding
Not applicable.

Availability of data and materials
There are no additional data to disclose.

Declarations

Ethics approval and consent to participate
Not applicable.

Consent for publication
Consent for the publication of this manuscript was obtained from the patient.

Competing interests
The authors declare that they have no competing interests.

Received: 26 December 2023 Accepted: 15 February 2024
Published online: 23 February 2024

References

1. Patankar GR, Choi JW, Schussler JM. Reverse takotsubo cardiomyopathy: two case reports and review of the literature. J Med Case Rep. 2013;7:84.
2. Zalewska-Adamiec M, Bachórzewska-Gajewska H, Dobrzycki S. Cardiac rupture—the most serious complication of takotsubo syndrome: a series of five cases and a systematic review. J Clin Med. 2021;10:1066.
3. Yousef S, Sultan I, VonVille HM, Kahru K, Arnaoutakis GJ. Surgical management for mechanical complications of acute myocardial infarction: a systematic review of long-term outcomes. Ann Cardiothorac Surg. 2022;11:239–51.
4. Prasad A, Lerman A, Rihal CS. Apical ballooning syndrome (tako-tsubo or stress cardiomyopathy): a mimic of acute myocardial infarction. Am Heart J. 2008;155:408–17.
5. Kumar S, Kaushik S, Nautiyal A, Choudhary SK, Kayastha BL, Mostow N, et al. Cardiac rupture in takotsubo cardiomyopathy: a systematic review. Clin Cardiol. 2011;34:672–6.
6. Nef HM, Möllmann H, Kostin S, et al. Tako-Tsubo cardiomyopathy: intraindividual structural analysis in the acute phase and after functional recovery. Eur Heart J. 2007;28:2456–64.
7. Khullar M, Datta BN, Wahi PL, et al. Catecholamine-induced experimental cardiomyopathy—a histopathological, histochemical and ultrastructural study. Indian Heart J. 1989;41:307–13.
8. Indorato F, Akashi YJ, Rossitto C, et al. Takotsubo cardiomyopathy associated with rupture of the left ventricular apex: assessment of histopathological features of a fatal case and literature review. Forensic Sci Med Pathol. 2015;11:577–83.
9. Nishiyama K, Okino S, Andou J, Nakagawa Y, Kimura T, Nobuyoshi M. Coronary angioplasty reduces free wall rupture and improves mortality and morbidity of acute myocardial infarction. J Invasive Cardiol. 2004;16:554–60.
10. Stevenson WG, Linssen GC, Havenith MG, Brugada P, Wellens HJ. The spectrum of death after myocardial infarction: a necropsy study. Am Heart J. 1989;118:1182–8.
11. Ishida T, Yasu T, Arao K, Kawakami M, Saito M. Bedside diagnosis of cardiac rupture by contrast echocardiography. Circulation. 2005;112:e354–5.
12. Zalewska-Adamiec M, Bachórzewska-Gajewska H, Kozuch M, Frank M, Hirnle T, Dobrzycki S. Cardiac rupture in takotsubo cardiomyopathy treated surgically. Postepy Kardiol Interwencyjnej. 2016;12:278–9.
13. Kudaiberdiev T, Akhmedova I, Imanalieva G, Abdildaev I, Jooshev K, Ashimov J, et al. Surgical treatment of left ventricular wall rupture, regarded as a consequence of Takotsubo cardiomyopathy. SAGE Open Med Case Rep. 2017;5:2050313X16689210.
14. Al-Tkrit A, Mekaiel A, Aneeb M, Alawawdeh F, Mangla A. Left ventricular free wall rupture in broken-heart syndrome: a fatal complication. Cureus. 2020;12: e11316.
15. Okamura H, Kimura N, Mieno M, Matsumoto H, Yuri K, Yamaguchi A. Sutureless repair for postinfarction left ventricular free wall rupture. J Thorac Cardiovasc Surg. 2019;158:771–7.
16. Raffa GM, Tarelli G, Patrini D, Settepani F. Sutureless repair for postinfarction cardiac rupture: a simple approach with a tissue-adhering patch. J Thorac Cardiovasc Surg. 2013;145:598–9.
17. Ishii H, Endo H, Tsuchiya H, Inaba Y, Terakawa K, Kubota H. Off-pump hemostasis for left ventricular rupture after myocardial infarction with Hydrofit® and Surgicel®. Gen Thorac Cardiovasc Surg. 2018;66:753–5.
18. Kagaya S, Aida H, Chida Y. Successful repair of a blow-out type left ventricular free wall rupture after acute myocardial infarction using a viscous diisocyanate prepolymer. Kyobu Geka. 2019;72:1061–5.
19. Sonoda H, Ushijima T, Oishi Y, et al. Long term function of hydrofit as hemostatic agent. Jpn Soc Cardiovasc Surg. 2018;47:62–5.

Publisher's Note

doi: 10.2176/jns-nmc.2023-0071

NMC Case Report Journal 10, 273-278, 2023

Alternative Proximal Protection Method during Carotid Artery Stenting Using Combined Transbrachial and Transradial Artery Approaches

Yuki HAMADA,[1] Fumio MIYASHITA,[2] Hideki MATSUOKA,[1] Yuki NISHINAKAMA,[1] Yusuke KAI,[1] Yusuke YAMASHITA,[1] Mei IKEDA,[1] Go TAKAGUCHI,[1] Keisuke MASUDA,[3] Fumikatsu KUBO,[3] and Hiroshi TAKASHIMA[4]

[1]*Department of Strokology, Stroke Center, National Hospital Organization Kagoshima Medical Center, Kagoshima, Kagoshima, Japan*

[2]*Division of Neurology, Kagoshima City Hospital, Kagoshima, Kagoshima, Japan*

[3]*Department of Neurosurgery, Stroke Center, National Hospital Organization Kagoshima Medical Center, Kagoshima, Kagoshima, Japan*

[4]*Department of Neurology and Geriatrics, Kagoshima University Graduate School of Medical and Dental Sciences, Kagoshima, Kagoshima, Japan*

Abstract

Herein, we report a case of carotid artery stenting with proximal flow protection for severe stenosis of the left internal carotid artery using transbrachial and transradial artery approaches. Because an abdominal aortic aneurysm was present, we avoided the transfemoral approach. The procedure was successfully performed with a combination of an 8-Fr balloon guide catheter and microballoon catheter on separate axes. No complications such as pseudoaneurysm, thrombosis, or dissection were observed at the puncture site. The patient was discharged without complications and showed good outcomes at 3 months. This technique may offer a useful alternative for patients with severe stenosis who cannot be treated using a femoral artery approach.

Keywords: carotid artery stenting, proximal protection, transbrachial, transradial, internal carotid artery stenosis

Introduction

The proximal protection (PP) method during carotid artery stenting (CAS) is useful for patients at high risk of distal embolization, such as those with severe internal carotid artery (ICA) stenosis or large amounts of unstable plaque.[1)] The transfemoral approach is commonly used for the PP method during CAS. However, advancing a guide catheter from the femoral artery to the carotid artery is difficult in patients with a tortuous aortic arch, supraaortic dissection, aortic disease, or unfavorable femoral artery occlusion. We report here a case of CAS with an alternative PP method using a balloon guide catheter (BGC) and microballoon catheter (MBC) in combination with transbrachial and transradial approaches to yield favorable outcomes.

Case Report

A 67-year-old man presented to our hospital after severe stenosis of the left ICA was incidentally found during screening carotid ultrasonography performed to investigate mild memory dysfunction. His medical history included hypertension, dyslipidemia, and an abdominal aortic aneurysm 44 mm in diameter (Fig. 1A). The patient was also a current smoker, with a 40-year history of smoking one pack of cigarettes a day. The patient had a history of chronic obstructive pulmonary disease, and preoperative evaluation of spirometry function showed a decreased forced expiratory volume in 1 second of 51%. Magnetic resonance imaging (MRI) demonstrated no abnormalities such as old cerebral infarction or ischemic changes, but magnetic resonance angiography demonstrated a decreased signal from the left intracranial ICA due to severe

Received April 5, 2023; Accepted July 21, 2023

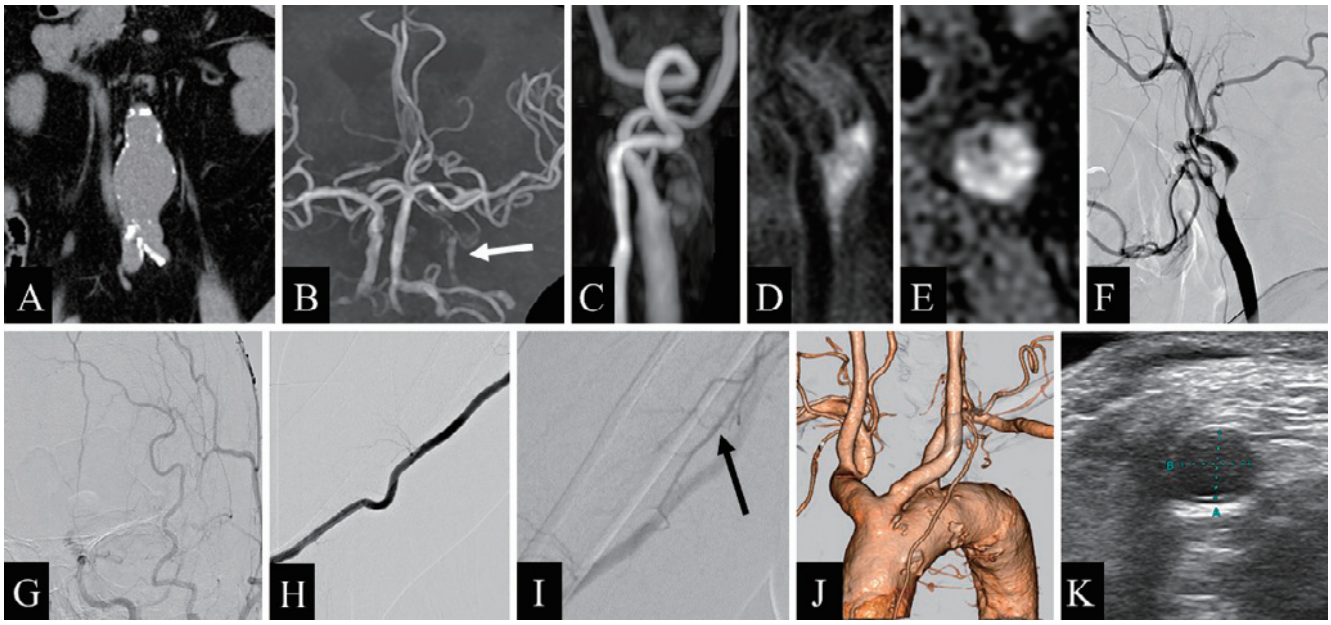

Fig. 1 A) Computed tomography (CT) shows an abdominal aortic aneurysm, 44 mm in diameter. B) Magnetic resonance angiography of the head reveals a decreased signal from the left intracranial internal carotid artery (ICA) due to severe stenosis (white arrow). C) Time-of-flight magnetic resonance imaging demonstrates a high-intensity signal of the common carotid artery (CCA). D) Magnetization-prepared rapid gradient echo imaging shows a high-intensity signal in the CCA. E) T1-weighted black blood imaging reveals a high-intensity signal from the CCA, suggesting a vulnerable plaque. F) Left CCA angiography (lateral view) shows anterograde string-like filling of the ICA beyond the carotid bifurcation. G) Left CCA injection (frontal view) demonstrates prolonged cerebral circulation time in the left cerebral hemisphere. H) Contrast-enhanced CT angiography shows a bovine-type arch of the aorta. I, J) Right brachial angiography demonstrates a well-developed deep brachial artery (black arrow). K) Vascular echocardiography shows that the right brachial artery at the cubital fossa has a vascular diameter of approximately 4.7 mm.

stenosis (Fig. 1B). Carotid ultrasonography revealed a vulnerable plaque at the origin of the left ICA and an increase in peak systolic velocity to 400 cm/s. MRI of the neck plaque demonstrated high-intensity signals on time-of-flight imaging (Fig. 1C), magnetization-prepared rapid gradient echo imaging (Fig. 1D), and T1-weighted black blood imaging (Fig. 1E). On the basis of these findings, we diagnosed a vulnerable plaque with intraplaque hemorrhage. Left carotid angiography revealed anterograde string-like filling of the ICA beyond the carotid bifurcation (Fig. 1F) and showed that the stenosis had prolonged cerebral circulation time in the left cerebral hemisphere (Fig. 1G). A collateral pathway via the ipsilateral posterior communicating artery was also observed. Right brachial angiography showed no prominent coiling or bending of the brachial artery (Fig. 1H) and a well-developed deep brachial artery (Fig. 1I). Contrast-enhanced computed tomography angiography (CTA) revealed a bovine aortic arch (Fig. 1J). Vascular echocardiography showed that the right brachial artery at the cubital fossa had a vascular diameter of approximately 4.7 mm (Fig. 1K). Because of the problem of decreased respiratory function, we considered that carotid endarterectomy and direct carotid artery puncture requiring general anesthesia should be avoided because of the risk of postoperative respiratory complications. To address severe carotid stenosis, CAS was planned after obtaining an informed consent.

Clinical course and procedure

Because of the large amount of plaque and near-occlusion, we considered that CAS using the PP method was desirable to adequately prevent distal embolization during the passage of the stenosis. However, due to the abdominal aortic aneurysm, the transfemoral artery approach was considered a high risk, so we decided to use an upper limb for the approach route. A PP device such as a Mo.Ma (Medtronic, Minneapolis, MN, USA) would have been desirable in this case but was avoided because of the high risk of puncture complications due to the need to puncture the brachial artery with an 8- or 9-Fr sheath. Furthermore, because two types of balloon are required to perform the PP method, we decided to perform CAS using a combined ipsilateral transbrachial and transradial approach wherein the BGC and MBC are guided from the brachial and radial arteries, respectively. An approach using the right and left upper limbs was also considered, but given the possibility of access difficulty due to the bovine-type bifurcation of the left common carotid artery (CCA), a tandem puncture was performed ipsilaterally instead.

The procedure was performed with the patient awake

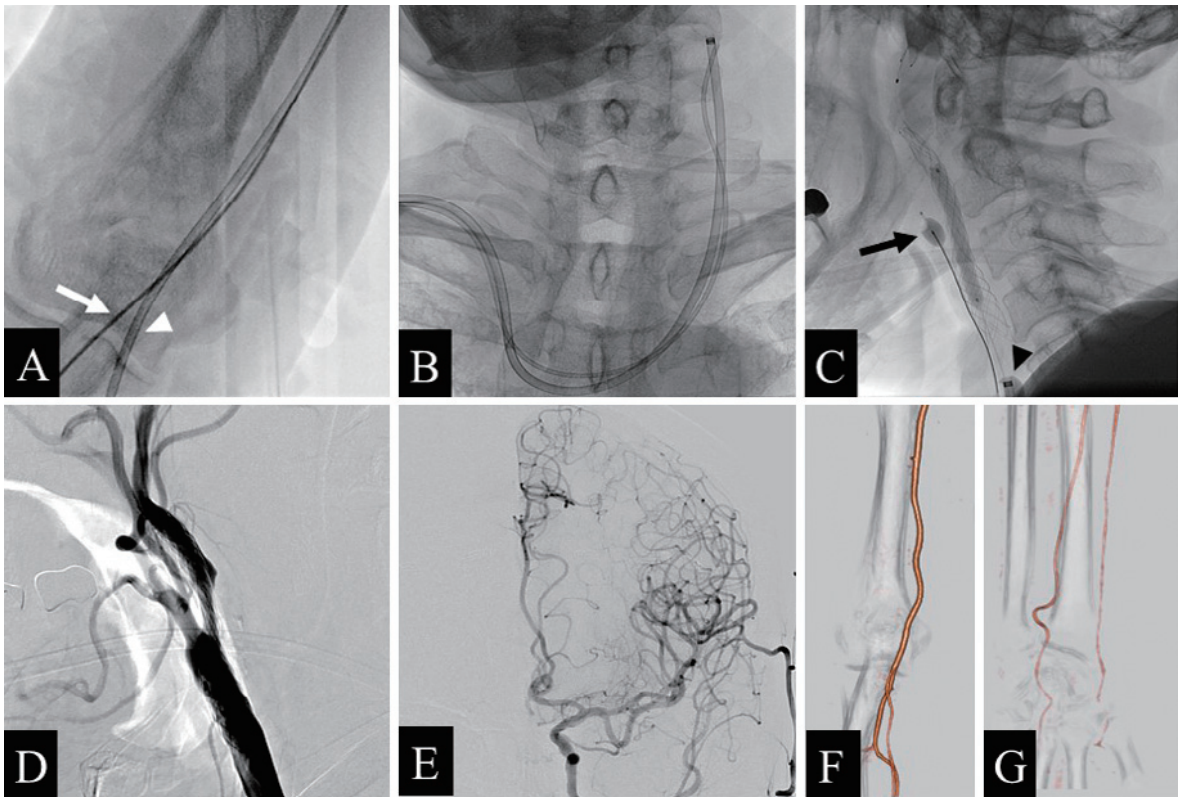

Fig. 2 Angiography during carotid artery stenting. A) An 8-Fr balloon guide catheter (BGC) is navigated from the right brachial artery (white arrowhead), and a 4-Fr catheter is guided from the right radial artery (white arrow). B) BGC and 4-Fr catheter navigated to the left common carotid artery (CCA). C) Fluoroscopic lateral view in which postdilation has been performed after placement of the carotid stent using a flow-reversal system with a microballoon catheter (MBC) (black arrow) and a BGC (black arrowhead). D) Left CCA injection (lateral view) after all procedures were completed. E) Left CCA angiography (frontal view) reveals no contrast-enhanced defect. F, G) Contrast-enhanced computed tomography angiography after 5 days of intervention shows no puncture site complications in the right brachial (F) and radial (G) arteries.

and under minimal sedation. Venipuncture was first performed through the right femoral vein, placing a 3-Fr sheath for arterial blood return. The right brachial artery was punctured with an 18-G needle, and a 0.035-inch-diameter guidewire was inserted into the outer casing to the subclavian artery. An 8-Fr BGC (OPTIMO; Tokai Medical Products, Aichi, Japan) with a dilator (TMP dilator I; Tokai Medical Products) was inserted into the lumen of the BGC and advanced into the right subclavian artery along the guidewire. After systemic heparinization, a 4-Fr sheath was inserted into the right radial artery, and a 4-Fr catheter (JB2 100 cm; Medikit, Tokyo, Japan) was carefully navigated into the left CCA (Fig. 2A, B). When advancing the 4-Fr catheter, no resistance attributable to interference with the BGC was encountered. Then, the 8-Fr BGC was navigated into the left CCA. The subsequent treatment procedure is shown in Fig. 3. A 0.014-inch microguidewire (CHIKAI; Asahi Intecc, Aichi, Japan) was placed deep into the external carotid artery (ECA), and the MBC (Pinnacle blue 20; Tokai Medical Products) was placed at the origin of the ECA along the microguidewire. Then the ECA and CCA were occluded with the BGC and MBC, forming a flow-reversal procedure. At that time, we confirmed the absence of side leakage aside from the gap between the BGC and shaft of the MBC. Using the roadmap technique, the 0.014-inch microguidewire was carefully advanced across the stenotic lesion while applying manual blood suction from the BGC, and dilation was performed using a 2.0 mm × 40 mm balloon catheter (Coyote; Boston Scientific, Natick, MA, USA) at the site of stenosis. The microguidewire was subsequently exchanged for a Spider Rx distal filter protection device (Medtronic/Covidien), which was positioned within the left distal ICA. Because the left superior thyroid artery bifurcated from the left CCA, the procedure with ECA and CCA occlusions was continued. Predilation was performed using a 4.0 mm × 40 mm balloon catheter (Sterling; Boston Scientific) at the site of stenosis. After that, an 8 mm × 30 mm carotid stent (CASPER Rx; MicroVention, Terumo, Tustin, CA, USA) was placed. Postdilation was performed using a 4.5 mm × 40 mm balloon catheter (Sterling; Boston Scientific) at the site of stenosis (Fig. 2C). After the left ECA and CCA balloons were deflated, all procedures were completed. The brachial artery was manually hemostatic for 20 minutes,

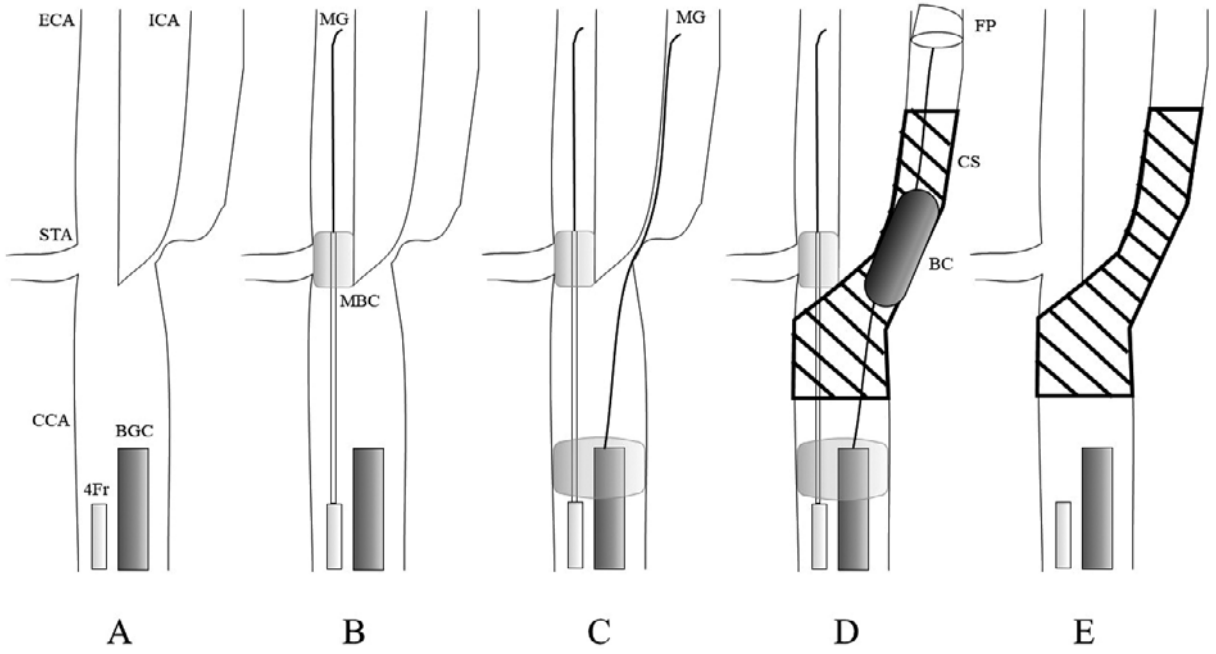

Fig. 3 Schematic illustration of treatment procedures during carotid artery stenting. A) After placement of the balloon guide catheter (BGC) and a 4-Fr catheter. B) The microguidewire (MG) is inserted deep into the external carotid artery (ECA), with the microballoon catheter (MBC) placed at the origin of the ECA alongside the MG. C) The ECA and common carotid artery are occluded with the BGC and MBC, forming a flow-reversed system. The MG is advanced across the stenotic lesion. D) The MG is exchanged for a filter protection (FP) device after angioplasty with the balloon catheter (BC). Predilation and postdilation with BC and placement of a carotid stent (CS) are performed. E) The MBC is deflated and removed first; then, the BGC is deflated. All procedures are completed.

followed by fixation with a hemostatic tape at a pressure of 60 mmHg for 6 hours. The radial artery was fixed with a band for 4 hours to achieve hemostasis. Left CCA injection showed no contrast-enhanced defect (Fig. 2D, E). No perioperative complications were observed, and ultrasonography showed no plaque protrusion. Contrast-enhanced CTA 5 days after CAS showed no abnormalities in the right brachial (Fig. 2F) and radial (Fig. 2G) arteries. Finally, the patient was discharged with a modified Rankin scale score of 0. On follow-up at 3 months after discharge, modified Rankin scale score remained 0. Consent for publishing this report was obtained from the patient.

Discussion

Endovascular treatment via a brachial or radial approach has been increasing in recent years, and CAS is no exception. This case was novel in that CAS was performed using PP method via the brachial and radial arteries. The key points of this case can be divided into PP via transbrachial and transradial artery approaches and points to keep in mind when performing this procedure, along with a discussion of the literature.

PP method via the transbrachial and transradial arteries

In this case, the transfemoral approach was avoided because of the presence of an abdominal aortic aneurysm, and the transfemoral approach is commonly used when CAS is performed using a PP method.[2] Previous studies have shown that CAS using the PP method has a low risk of perioperative cerebral infarction.[1,3] This is achieved using a dedicated PP device such as Mo.Ma or GORE (Gore & Associates, Flagstaff, AZ, USA), but the transbrachial approach is rarely used because of problems with device diameter, stiffness, and arterial bifurcation morphology. As of 2022, the PercuSurge Guardwire (Medtronic) is no longer available, so the Parodi method, which uses the BGC and PercuSurge Guardwire in combination to block the ECA and CCA, cannot be performed.[4] In this method, a PercuSurge Guardwire was placed coaxially in the BGC and implanted in the ECA to create a flow-reversal circuit; however, currently, no device with a balloon can be inserted coaxially when performing CAS. Therefore, we performed CAS using the PP method with the BGC and MBC on separate axes, using both transbrachial and transradial approaches.

Relatively few reports in the literature on CAS have described using a transbrachial or transradial approach with the PP method. Montrsi et al.[5] prospectively reviewed the

outcomes and complications of CAS performed using transbrachial or transradial approaches. They inserted an 8-Fr sheath into the brachial or radial artery and performed 61 CAS procedures under PP method using an 8-Fr Mo.Ma. The mean stenosis rate was 87.8% in the European Carotid Surgery Trial.[6] The brachial artery was used in 31 cases (51%) and the radial artery in 30 cases (49%), and the procedure was completed in 55 cases (90%). Of the six patients for whom the procedure could not be completed, Mo.Ma could not be induced because of anatomical reasons in one patient (1.6%), and the blockade was not tolerated by five patients (8.1%). Complications included pseudoaneurysm of the brachial artery in one case (1.6%) and acute occlusion of the radial artery after surgery in two of 30 cases (6.6%). The present report is rare in that the 8-Fr sheath was inserted not only via a transbrachial approach but also via a transradial approach, and the procedure was performed using Mo.Ma.

Points when performing this procedure

The following is a list of points to be considered in this procedure. First, the diameter of the brachial artery is important. In this procedure, two catheters are navigated from the same upper extremity through the brachial artery. For example, the outer diameter of an 8-Fr BGC is approximately 2.7 mm and that of a 4-Fr catheter is approximately 1.3 mm, so the brachial artery must have an inner diameter of ≥4.0 mm. In this case, the diameter of the brachial artery was measured preoperatively using echocardiography and confirmed as 4.7 mm, and thus, the procedure was deemed feasible. The diameter of the brachial artery is estimated to be approximately 4.5 and 3.5 mm in adult men and women, respectively.[7,8] The order of puncture is also important, and the brachial artery should be punctured first. If the radial artery is punctured first to guide the device, the puncture of the brachial artery may damage the device. To reduce puncture site complications as much as possible, BGC was inserted using a 5-Fr long dilator into the brachial artery without a sheath. Koge et al.[9] reported a case in which a BGC was safely guided into the CCA without the need for a sheath, using a dedicated 6-Fr long dilator in combination with a 9-Fr BGC. However, in the cardiovascular field, bleeding complications at the puncture site were observed in 2.3% of patients using the transbrachial approach,[10] which is higher than the rate of 2.0%[10] seen when using the transfemoral approach. Furthermore, 6-Fr intra-aortic balloon pumping has reportedly shown fewer puncture site complications than 8-Fr IABP.[10] Another report found that the insertion of a sheath with a diameter larger than 8-Fr was associated with pseudoaneurysm as a complication at the puncture site.[11] In other words, the brachial artery approach using an 8-Fr sheath is considered a high risk in Japanese patients who have smaller arterial diameters than Westerners. We used a sheathless technique with an 8-Fr BGC to reduce the size of the puncture site to that of a 6-Fr sheath. However, the risk of puncture site complications in the upper extremities is expected to increase due to ipsilateral radial artery puncture in addition to brachial artery puncture. It might have been better to remove the 4-Fr catheter after dilating the MBC to reduce the risk of upper extremity ischemia. This procedure is indicated only for very specific cases with large brachial arteries and is not recommended for universal use in Japanese patients, who, as already mentioned, have smaller arterial diameters in the upper extremities than Westerners.

The order of hemostasis may also be important. In our case, hemostasis was applied to the brachial artery, which has a large volume of perfusion to the upper limb, followed by hemostasis of the radial artery. However, if hemostasis was applied to the brachial artery while a sheath was inserted into the radial artery, perfusion to the ulnar artery, which is a collateral blood vessel, would be reduced, possibly resulting in further hypoperfusion inhibition. The collateral vessels function in the deep brachial artery[12] when the brachial artery is occluded and in the interosseous artery when the radial and ulnar arteries are occluded. Therefore, evaluating this information preoperatively would be desirable.

Difficulty in guiding the device should also be noted. In particular, in left-sided lesions with a normally shaped aortic arch (e.g., arch type I), the angle of bifurcation of the CCA is so steep that the device may vector toward the ascending aorta and slide off during device advancement. In the present case, the device was easily guided to the left CCA because the aortic arch was the bovine type. However, an MBC could conceivably be guided from the left upper extremity using a Simmons-type guiding catheter.

With the method we applied, the MBC is guided in parallel with the BGC and implanted at the origin of the ECA, rather than coaxially with the BGC. Therefore, when the balloon of the BGC is inflated, a gap exists between the shaft of the MBC and BGC, which may prevent complete blockage of progressive blood flow. In this case, we used a contrast medium to check for residual progressive blood flow after the blood flow was supposed to have been blocked. Fortunately, we confirmed that complete blood flow blockage had been achieved. However, depending on the degree of balloon expansion of the guiding catheter, leakage or damage to the vessel wall may occur. Caution is therefore warranted. Another attractive point is the ease of balloon positioning: the distance between ECA and CCA balloons cannot be changed in Mo.Ma.

This presents a review of the literature. This technique may be useful in CAS for ICA stenosis with severe stenosis where intraoperative distal embolization is a concern, when a conventional transfemoral approach is difficult, and when anatomical access is considered possible.

Conclusion

We have described a case of CAS with the PP method for severe left ICA stenosis using a combination of transbrachial and transradial artery approaches. This method may be effective in cases of severe stenosis with a high risk of distal embolization and anatomical abnormalities preventing the use of the femoral artery approach.

Conflicts of Interest Disclosure

All authors have no conflicts of interest.

References

1) Ansel GM, Hopkins LN, Jaff MR, et al.: Safety and effectiveness of the INVATEC MO.MA proximal cerebral protection device during carotid artery stenting: results from the ARMOUR pivotal trial. *Catheter Cardiovasc Interv* 76: 1-8, 2010
2) Yadav JS, Wholey MH, Kuntz RE, et al.: Protected carotid-artery stenting versus endarterectomy in high-risk patients. *N Engl J Med* 351: 1493-1501, 2004
3) Nikas D, Reith W, Schmidt A, et al.: Prospective, multicenter European study of the GORE flow reversal system for providing neuroprotection during carotid artery stenting. *Catheter Cardiovasc Interv* 80: 1060-1068, 2012
4) Parodi JC, La Mura R, Ferreira LM, et al.: Initial evaluation of carotid angioplasty and stenting with three different cerebral protection devices. *J Vasc Surg* 32: 1127-1136, 2000
5) Montorsi P, Galli S, Ravagnani PM, et al.: Carotid artery stenting with proximal embolic protection via a transradial or transbrachial approach: pushing the boundaries of the technique while maintaining safety and efficacy. *J Endovasc Ther* 23: 549-560, 2016
6) Warlow C: MRC European Carotid Surgery Trial: interim results for symptomatic patients with severe (70-99%) or with mild (0-29%) carotid stenosis. *Lancet* 337: 1235-1243, 1991
7) Dalli E, Segarra L, Ruvira J, et al.: [Brachial artery flow-mediated dilation in healthy men, men with risk factors, and men with acute myocardial infarction. Importance of occlusion-cuff position]. *Rev Esp Cardiol* 55: 928-935, 2002 (Spanish)
8) Holubkov R, Karas RH, Pepine CJ, et al.: Large brachial artery diameter is associated with angiographic coronary disease in women. *Am Heart J* 143: 802-807, 2022
9) Koge J, Nakahara I, Ohta T, et al.: [Carotid artery stenting under proximal balloon protection via the transbrachial approach using a balloon guiding catheter: sheathless method with 9Fr Optimo]. *JNET* 9: 108-114, 2015 (Japanese)
10) Kiemeneij F, Laarman GJ, Odekerken D, Slagboom T, Van Der, Wieken R: A randomized comparison of percutaneous transluminal coronary angioplasty by the radial, brachial and femoral approaches: the access study. *J Am Coll Cardiol* 29: 1269-1275, 1997
11) Webber GW, Jang J, Gustavson S, Olin JW: Contemporary management of postcatheterization pseudoaneurysms. *Circulation* 115: 2666-2674, 2007
12) Mendiz OA, Sampaolesi AH, Londero HF, Fava CM, Lev GA, Valdivieso LR: Initial experience with transradial access for carotid artery stenting. *Vasc Endovascular Surg* 45: 499-503, 2011

Corresponding author: Yuki Hamada, MD.
Department of Strokology, Stroke Center, National Hospital Organization Kagoshima Medical Center, 8-1 Shiroyama, Kagoshima, Kagoshima 892-0853, Japan.
e-mail: sunamushi.elmonkichi@gmail.com

Internal Medicine
The Japanese Society of Internal Medicine
doi: 10.2169/internalmedicine.2704-23
Intern Med 63: 1669-1670, 2024
http://internmed.jp

【 PICTURES IN CLINICAL MEDICINE 】

Eagle Syndrome Induced by the Head Retroflexion

Aiko Masuda[1], Yuki Hamada[1], Hideki Matsuoka[1] and Hiroshi Takashima[2]

Key words: Eagle syndrome, stroke, head position

(Intern Med 63: 1669-1670, 2024)
(DOI: 10.2169/internalmedicine.2704-23)

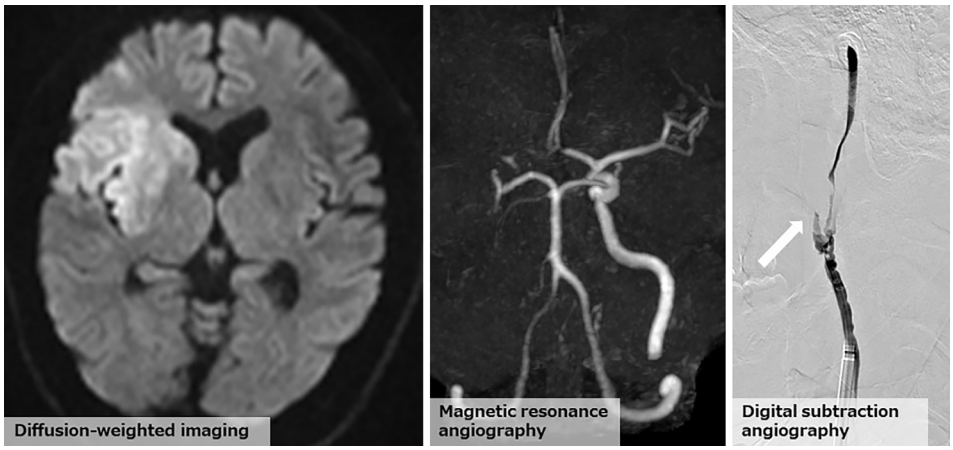

Picture 1.

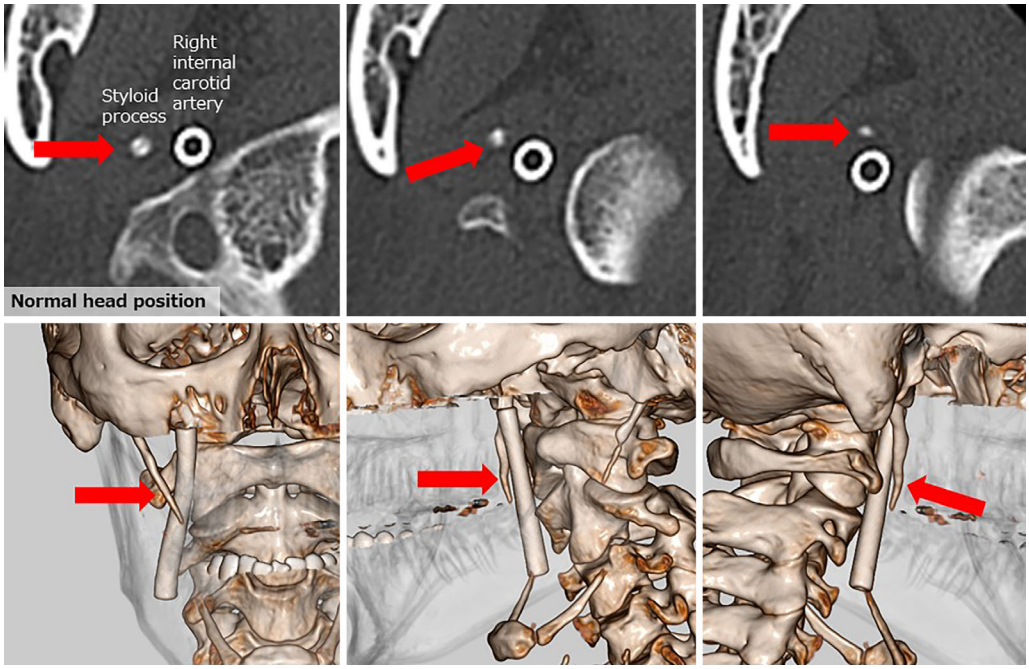

Picture 2.

[1]Department of Strokology, Stroke Center, National Hospital Organization Kagoshima Medical Center, Japan and [2]Department of Neurology and Geriatrics, Kagoshima University Graduate School of Medical and Dental Sciences, Japan
Received: August 2, 2023; Accepted: August 28, 2023; Advance Publication by J-STAGE: October 6, 2023
Correspondence to Dr. Yuki Hamada, sunamushi.elmonkichi@gmail.com

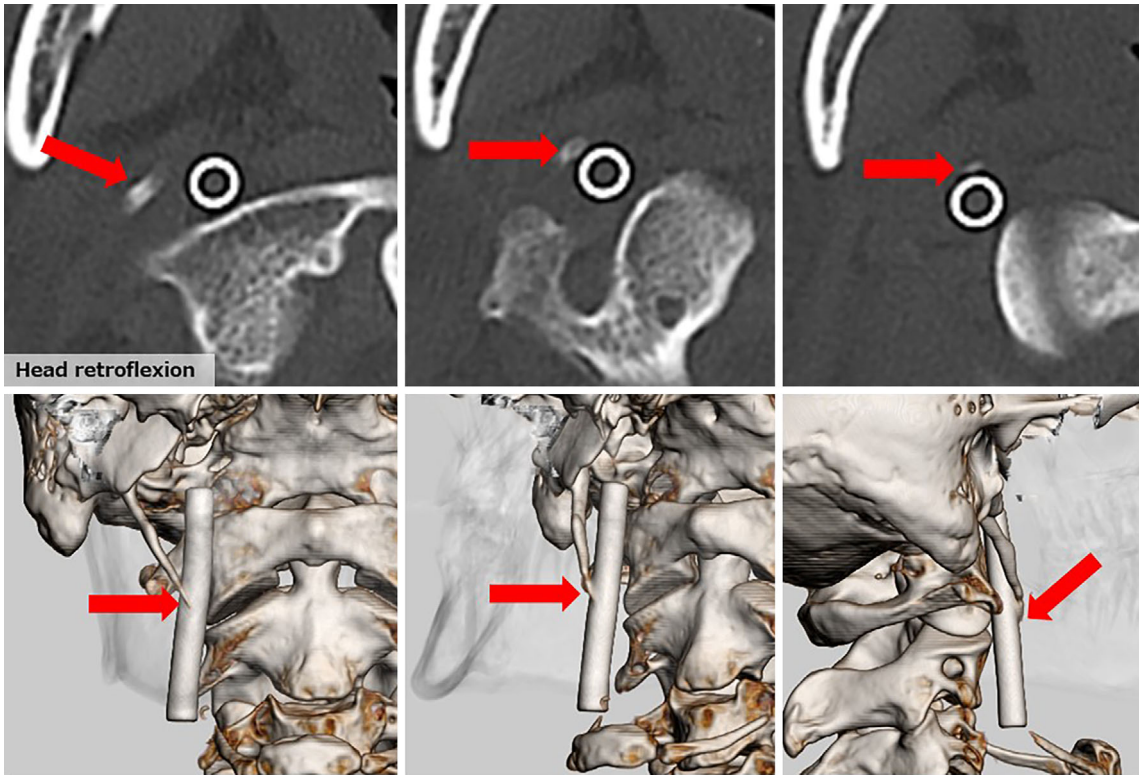

Picture 3.

A 50-year-old man presented with left-sided hemiparesis. He had no smoking history, and his occupation was a desk job. Magnetic resonance imaging demonstrated signal hyperintensity on diffusion-weighted imaging and occlusion of the right internal carotid artery (ICA). Right carotid angiography showed dissection (white arrow) (Picture 1). Mechanical thrombectomy and carotid artery stenting were also performed. Contrast-enhanced computed tomography angiography revealed that the right styloid process (red arrows) and right ICA were not in anatomic contact in the normal head position (Picture 2); however, in the retroflexed position, both were adjoined (Picture 3). Because right buccal pain was induced by the retroflexed position, we diagnosed the patient with Eagle syndrome. Reduced cerebral blood flow has been reported in the forward-bending (1) and right-rotated positions (2). This is a rare case of a prolonged styloid process that caused damage to the right ICA due to head retroflexion.

The authors state that they have no Conflict of Interest (COI).

References

1. Sun J, Zhang C, Liu B, et al. Eagle syndrome with internal carotid artery compression causing recurred syncope. Intern Med **62**: 1067-1071, 2023.
2. Li Z, Hua Y, Yang J, Li J. Ultrasound evaluation of transient ischemic attack caused by styloid process elongation: a case report. Front Neurol **10**: 26, 2019.

Advance Publication

Circulation Journal
doi:10.1253/circj.CJ-23-0409

ORIGINAL ARTICLE

Holter Electrocardiographic Approach to Predicting Outcomes of Pediatric Patients With Long QT Syndrome

Masao Yoshinaga, MD, PhD; Yumiko Ninomiya, MD; Yuji Tanaka, MD, PhD; Megumi Fukuyama, MD, PhD; Koichi Kato, MD, PhD; Seiko Ohno, MD, PhD; Minoru Horie, MD, PhD; Hiromitsu Ogata, PhD

Background: This study was performed to clarify the clinical findings of pediatric patients diagnosed with long QT syndrome (LQTS) through electrocardiographic screening programs and to predict their outcome using Holter electrocardiographic approaches.

Methods and Results: This retrospective study included pediatric patients with a Schwartz score of ≥3.5 who visited the National Hospital Organization Kagoshima Medical Center between April 2005 and March 2019. Resting 12-lead and Holter electrocardiograms were recorded at every visit. The maximum resting QTc and maximum Holter QTc values among all recordings were used for statistical analyses. To test the prognostic value of QTc for the appearance of cardiac events after the first hospital visit, receiver operating characteristic curves were used to calculate the area under the curve (AUC). Among 207 patients, 181 (87%) were diagnosed through screening programs. The prevalence of cardiac events after the first hospital visit was 4% (8/207). Among QTc at diagnosis, maximum resting QTc, and maximum Holter QTc, only maximum Holter QTc value was a predictor (P=0.02) of cardiac events after the hospital visit in multivariate regression analysis. The AUC of the maximum Holter QTc was significantly superior to that of maximum resting QTc.

Conclusions: The maximum Holter QTc value can be used to predict the appearance of symptoms in pediatric patients with LQTS.

Key Words: Children; Holter electrocardiogram; Long QT syndrome; Prognosis; Screening

Long QT syndrome (LQTS) is a genetic disorder characterized by abnormal ventricular myocardial repolarization and prolongation of the QT interval on an electrocardiogram (ECG).[1–3] LQTS-related cardiac events include syncope or life-threatening arrhythmic events, such as aborted cardiac arrest (ACA) or sudden cardiac death (SCD). Since the first description of 4 patients with deafness and a long QT interval in 1957,[4] considerable progress has been made in understanding the genetics, pathogenesis, diagnosis, and treatment of LQTS.[1–3] Substantial improvements in patient outcomes have recently been seen.[5] However, life-threatening arrhythmic events still occur in a certain percentage of patients according to relatively recent reports from both single-center[5,9,13–15,18] and multicenter studies.[6–8,10–12,16,17,19]

A nationwide, school-based ECG screening program for heart disease in 1st, 7th, and 10th graders in Japan was established in 1994, and participation is mandatory. This program has identified children and adolescents with prolonged QT intervals. Many patients are asymptomatic at diagnosis in the program,[20] partly because they may be screened before the appearance of cardiac events. This means that the development of LQTS-related cardiac events could be prevented if careful examinations are performed and follow-up strategies are implemented from the first visit. However, there are no recent reports on all clinical findings and outcomes of patients who have been diagnosed through the ECG screening program.

QTc values on resting 12-lead ECGs are generally used to predict the appearance of LQTS-related cardiac events.[21,22] A longer QTc value is an independent predictor for cardiac events in patients with Type 1 and 2 LQTS (LQT1 and LQT2, respectively).[23] Holter monitoring of the QT interval showed more frequent QT prolongation during the night-time hours than during daytime hours in patients with LQT2 and LQT3.[24] QTc values reached their maximum at night or early in the morning in both pediatric controls and pediatric patients with LQTS.[25] In our

Received June 16, 2023; revised manuscript received September 30, 2023; accepted October 11, 2023; J-STAGE Advance Publication released online December 1, 2023 Time for primary review: 9 days

Department of Pediatrics, National Hospital Organization Kagoshima Medical Center, Kagoshima (M.Y., Y.N., Y.T.); Orange Medical and Welfare Center for Severe Motor and Intellectual Disabilities, Kirishima (M.Y.); Department of Cardiovascular Medicine, Shiga University of Medical Science, Otsu (M.F., K.K., M.H.); Department of Bioscience and Genetics, National Cerebral and Cardiovascular Center, Suita (S.O.); and Graduate School of Kagawa Nutrition University, Sakado (H.O.), Japan

Mailing address: Masao Yoshinaga, MD, PhD, Department of Pediatrics, National Hospital Organization Kagoshima Medical Center, 8-1 Shiroyama-cho, Kagoshima 892-0853, Japan. email: myoshi330@yahoo.co.jp

ISSN-1346-9843

clinical experience, QTc values at night are quite different from those on a routine ECG recorded during daytime hours in the hospital (**Figure 1**). These findings suggest that we should consider the maximum QTc values among repeated Holter ECGs; however, the use of the QTc value on Holter ECGs remains controversial.[18,26]

Therefore, the aims of the present study were to clarify the outcomes of young patients with LQTS in the era of the ECG screening program in a single center where follow-up strategies were unified, and to determine whether QTc values from Holter ECG recordings are applicable and useful for predicting the appearance of cardiac events.

Methods

Study Population

This retrospective study included 207 infants, children, and adolescents who were diagnosed as a high probability of LQTS (i.e., an LQTS [Schwartz] score of ≥3.5) at the National Hospital Organization Kagoshima Medical Center between April 2005 and March 2019 and who were diagnosed before 20 years of age. Kagoshima City has a population of approximately 600,000. In 2005, an outpatient clinic for inherited arrhythmias was established at the National Hospital Organization Kagoshima Medical Center. Children and adolescents who were screened through the screening program in Kagoshima City all attended this center from 2008 to 2013,[19] within the study period. Thereafter, most (but not all) children and adolescents identified through the screening program also attended the center. The end of the study was set to March 2019 to allow for a longer follow-up period for recent patients. Outcomes were finally checked on March 31, 2022.

The study was approved by the Ethics Committee of the National Hospital Organization Kagoshima Medical Center (No. 30-69). The procedures in this study were performed in accordance with the Declaration of Helsinki and the ethical standards of the institutional committee on human experimentation.

Patients who had secondary causes of LQTS or who had congenital heart diseases, epilepsy, and attention deficit hyperactivity disorder were excluded. Patients with Jervell and Lange-Nielsen syndrome were also excluded because this disease has an extremely severe clinical course. LQTS-related cardiac events were defined as syncope, seizure, documented torsade de pointes (TdP), ACA, SCD, and appropriate implantable cardioverter defibrillator (ICD) shock; however, there were no patients with either SCD or ICD shock in the present study. Syncope was defined as a sudden loss of consciousness with spontaneous recovery and excluded all events assessed to be likely vasovagal in nature (e.g., emotional reactions, heat or dehydration, or abrupt postural changes).[5] All patients were primarily followed by a single cardiologist (M.Y.).

Patients were classified by diagnostic events into a screened group or a clinical (not screened) group. The screened group comprised patients who were screened by the program. The clinical group included patients who visited the hospital with LQTS-related cardiac events, those who were diagnosed by a familial study, and those who were diagnosed by chance, namely during the course of examinations for other conditions, such as heart murmur, palpitation, or chest pain.

ECG Recording and Measurement of QT/RR Intervals

The patients and their parents were asked to visit the outpatient clinic at least once a year. A resting 12-lead ECG and a Holter ECG were recorded at each visit in all patients, including infants. A Master 2-step test (if possible) and a treadmill exercise test (if needed) were also performed. Chest radiography, serum biochemistry, and echocardiography were performed at the first visit.

One of the authors (M.Y.) manually measured 3 consecutive QT/RR intervals in lead V5 on resting ECGs using the tangent method. Each QT interval was corrected by the Bazett formula and Fridericia formula (termed QTcB and QTcF, respectively). The mean QTc value of 3 consecutive beats was calculated. After obtaining QTc values from each visit, the maximum QTc value among all repeated resting ECGs was termed the maximum resting QTc and used for analysis.

For measurement of QT intervals on Holter ECGs (SCM-8000 System, V54-11; Fukuda Denshi, Tokyo, Japan), 5 representative periods were selected to exclude selection bias: night-time sleeping, wake up time, and daytime activities in the morning, afternoon, and evening. Each period was arbitrarily defined as 02:00–04:00, 06:00–08:00, 10:00–12:00, 14:00–16:00, and 20:00–22:00 hours, respectively. In each period, ECGs at maximum, mean, and minimum heart rates were chosen. To obtain QTc values near the longest QTc, we tried to find the place where the heart rate increased abruptly from background heart rate (**Figure 1B,C**), or where notched T waves were present, or where the appearance of peak of T waves was late (**Figure 1B**). Three consecutive QT/RR intervals with stable RR intervals in Lead CM5 were manually measured in the same way as resting ECGs. Among all QTc values obtained throughout the day and among all Holter ECGs recorded at each visit, the maximum QTc value on Holter ECGs was termed the maximum Holter QTc and used for analysis.

Follow-up Strategies

All patients were asked to adhere to the following at their first visit:

1. Patients are allowed to swim under the supervision of a person or persons able to perform resuscitation. If the patient has a long QTc value, they should not swim.
2. Patients are able to participate in competitive sports if: they have not experienced syncope during exercise; they do not have findings of worsening of QTc during the treadmill exercise test; there is at least 1 instructor who can perform resuscitation present during the sports activity; and if an automated external defibrillator is available on site.
3. Patients must not take QT-prolonging medications. The patients and their parents were asked to bring a list of any QT-prolonging drugs to give to their doctors at their first hospital. The note was handed to the patient and parents at the first visit.

Medication was started if LQTS-related cardiac events occurred in patents with a diagnosis of LQTS.[14] For asymptomatic patients, medication was recommended based on the longest QTcF value on Holter ECGs during follow-up. The mean difference between the longest Holter QTcF and the resting QTcB on the same day in the same patient was around 50 or 60 ms at the beginning of the study (it finally reached a mean [±SD] of 69±45 ms in this study). If the longest Holter QTcF a patient was around or

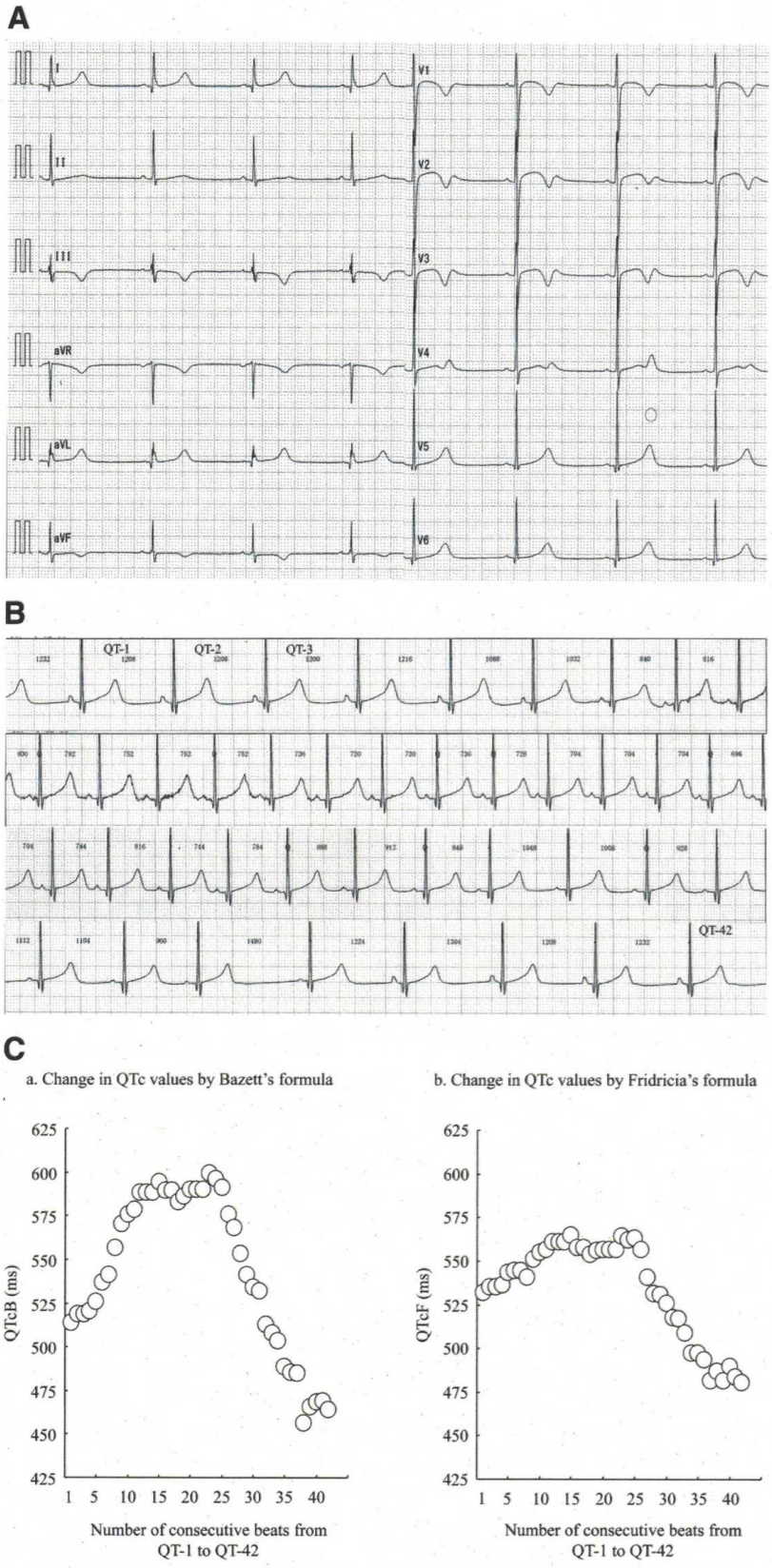

Figure 1. (**A**,**B**) Differences in QTc values between the resting electrocardiogram (ECG) (**A**) and Holter ECG (**B**) in a 12-year-old girl who was screened by an ECG screening program because of a prolonged QT interval. (**A**) Resting ECG on the patient's first hospital visit showed a QT interval of 0.53 s, an RR interval of 1.25 s, and QT intervals corrected by the Bazett formula and Fridericia formula (QTcB and QTcF, respectively) of 0.474 and 0.492, respectively, on the marked beat (○). The Holter recording was started on the same day of the patient's first hospital visit. (**B**) Continuous Holter ECG recording during sleep at 00:52 hours the next day. The QTc value was extremely prolonged during the Holter recording. (**C**) Changes in QTc values in consecutive beats from QT-1 to QT-42 in (**B**) showing changes in QTcB (**Left**) and QTcF (**Right**). Genetic testing using a next-generation sequencer failed to reveal a pathogenic variant.

Table 1. Characteristics of Patients With LQTS Classified by the Appearance of a Cardiac Event After the First Hospital Visit

	Event (–)	Event (+)	P value	Total
No. (%) subjects	199 (96)	8 (4)		207 (100)
Female sex	84 (42)	7 (88)	0.02	91 (44)
No. (%) screened by the program	124 (87)	7 (88)	0.26	181 (87)
At diagnosis				
Age (years)	12.5 [7.7–13.2]	12.8 [8.9–13.2]	0.57	12.5 [7.8–13.2]
Heart rate (beats/min)	75 [67–85]	65 [62–74]	0.047	74 [66–85]
QTcB (resting) (ms)	483 [472–497]	481 [468–490]	0.81	483 [472–497]
Schwartz score	4.5 [4.0–5.0]	6.0 [5.6–6.8]	<0.001	4.5 [4.0–5.0]
Genotype tested	116 (58)	8 (100)	0.02	124 (60)
Genotype determined[A]	36 (31)	5 (63)	0.11	41 (33)
LQT1	13	2		15
LQT2	15	3		18
LQT3	2	0		2
Other	6	0		6
Family history of LQTS	45 (23)	1 (13)	0.69	46 (22)
Family history of SCD	2 (1)	0 (0)	>0.99	2 (1)
Overall cardiac events	2 (1)	8 (100)	<0.001	10 (5)
Cardiac events before visit	2 (1)	2 (25)	0.008	4 (2)
Syncope/seizure	2	8		10
Documented TdP	0	0		0
Aborted cardiac arrest	0	0		0
Therapy				
Oral	46 (23)	8 (100)	<0.001	54 (26)
β-blocker	24	3		27
Na channel blocker	15	1		16
β-blocker and Na channel blocker	7	4		11
ICD/LCSD	0/0	0/0		0/0
Follow-up period (years)	5.7 [3.3–7.8]	10.4 [9.2–10.9]	<0.001	6.0 [3.4–8.2]
QTc values at various times				
QTcF at diagnosis (resting) (ms)	467 [451–479]	472 [457–482]	0.28	468 [452–481]
Maximum QTcB (resting) (ms)	484 [476–499]	499 [476–524]	0.16	486 [477–503]
Maximum QTcF (resting) (ms)	469 [454–486]	487 [473–521]	0.01	471 [456–490]
Maximum QTcB (Holter) (ms)	549 [533–574]	614 [599–631]	<0.001	553 [534–580]
Maximum QTcF (Holter) (ms)	512 [491–532]	582 [548–598]	<0.001	514 [493–540]

Unless indicated otherwise, values are expressed as n (%) or the median [interquartile range]. [A]The percentages were calculated as (number determined)/(number tested)×100. Statistical analyses were performed using the Mann-Whitney test or Fisher's exact probability test. ICD, implantable cardioverter defibrillator; LCSD, left cardiac sympathetic denervation; LQT1, LQT2, LQT3, long QT syndrome types 1, 2, and 3, respectively; LQTS, long QT syndrome; QTcB, QT interval corrected by Bazett's formula; QTcF, QT interval corrected by Fridericia's formula; SCD, sudden cardiac arrest; TdP, torsade de pointes.

more than 530 ms (470+60 ms), medication was recommended because the established criterion for starting medication is a QTcB of ≥470 ms on the resting ECG.[21]

Genetic Testing

Genetic testing was performed for patients whose maximum Holter QTcF was around or greater than 500 ms or whose parents requested genetic testing. Until 2018, Sanger sequencing was performed in Kagoshima Medical Center for potassium voltage-gated channel subfamily Q member 1 (*KCNQ1*), potassium voltage-gated channel subfamily H member 2 (*KCNH2*), sodium voltage-gated channel alpha subunit 5 (*SCN5A*), potassium voltage-gated channel subfamily E regulatory subunit 1 (*KCNE1*), and potassium voltage-gated channel subfamily E regulatory subunit 2 (*KCNE2*). When we failed to detect any pathogenic variants, and after 2018 generally, genetic analyses were performed using HaloPlex HS custom panels (Agilent Technologies, Santa Clara, CA, USA) that included 56 genes related to inherited arrhythmia syndrome and a bench-top next-generation sequencer (MiSeq; Illumina, San Diego, CA, USA). The data obtained were analyzed using SureCall software (Agilent Technologies) in Shiga University of Medical Science.[12] Based on the Clinical Genome Resource (ClinGen),[27] LQTS-related genes were limited to the following: *KCNQ1*, *KCNH2*, *SCN5A*, *KCNE1*, *KCNJ2*, and calcium voltage-gated channel subunit alpha1 C (*CACNA1C*). No patients in this study had calmodulin or triadin gene mutations.

Statistical Analysis

Statistical analyses were performed using statistical software (IBM® SPSS® Statistics v23.0; IBM Japan, Ltd., Tokyo, Japan). Data are expressed as the median and interquartile range (IQR). Statistical analyses were performed using the Mann-Whitney test or Fisher's exact

Table 2. Predictive Factors for the Appearance of Cardiac Events After the First Hospital Visit (Using QTcB Values as Markers of the QT Interval)

Variables	Reference	Univariate regression				Multivariate regression (n=207)		
		n	OR	95% CI	P value	OR	95% CI	P value
Age	Per age	207	1.05	0.85–1.30	0.64			
Female sex[A]	Male	207	9.58	1.16–79.4	0.04	8.72	0.49–156	0.14
Schwartz score	Per point	207	9.13	2.67–31.2	<0.001	6.64	0.74–59.8	0.09
Pathogenic variants	Absent	124	3.70	0.84–16.3	0.08			
Family history of LQTS	Absent	207	0.49	0.06–4.08	0.51			
Clinical group[B]	Screened group	207	0.99	0.12–8.42	>0.99			
Cardiac events before visit	Absent	207	32.8	3.94–273	0.001	1.04	0.009–121	0.99
QTcB at diagnosis	Per QTcB	207	1,799	2.4E-10–1.4E+16	0.62			
Maximum QTcB (resting)	Per maximum QTcB	207	6.0E+7	1.59–2.3E+15	0.04	1.2E-13	1.2E-37–1.3E+11	0.29
Maximum QTcB (Holter)	Per maximum Holter QTcB	207	2.8E+35	1.8E+17–4.5E+53	<0.001	9.3E+28	1.4E+6–6.3E+51	0.01
Follow-up period	Per year	207	1.47	1.16–1.86	0.002	1.29	0.92–1.80	0.14

[A]Sex was dichotomized (boys=1, girls=2). [B]Diagnosis by screening or clinically was dichotomized (screened group=1, clinical group=2). CI, confidence interval; OR, odds ratio. Other abbreviations as in Table 1.

Table 3. Predictive Factors for the Overall Presence of Cardiac Events by Logistic Regression Analysis (Using QTcB Values as Markers of the QT Interval)

Variables	Reference	Univariate regression				Multivariate regression (n=207)		
		n	OR	95% CI	P value	OR	95% CI	P value
Age	Per age	207	1.07	0.88–1.29	0.52			
Female sex[A]	Male sex	207	5.49	1.14–26.5	0.03	3.85	0.62–8.90	0.19
Schwartz score	Per point	207	11.6	3.28–40.7	<0.001	5.08	1.20–21.6	0.03
Pathogenic variants[B]	Absent	124	5.49	1.34–22.5	0.02			
Family history of LQTS	Absent	207	0.38	0.05–3.04	0.36	1.20	0.31–4.67	0.79
Clinical group[C]	Screened group	207	1.80	0.36–8.99	0.47			
Cardiac events before visit	Absent	207	5.3E+10	0.000–	0.999			
QTcB at diagnosis	Per QTcB	207	3.2E+10	0.001–1.1E+18	0.16			
Maximum QTcB (rest)	Per maximum QTcB	207	5.7E+8	45.1–7.3E+15	0.02	0.002	8.1E-19–8-5.7E+12	0.73
Maximum QTcB (Holter)	Per maximum Holter QTcB	207	1.6E+32	7.1E+16–3.4E+47	<0.001	5.0E+26	3.4E+7–7.3E+45	0.006
Follow-up period	Per year	207	1.30	1.07–1.57	0.009	1.04	0.81–1.34	0.77

[A]Sex was dichotomized (boys=1, girls=2). [B]The presence of a pathogenic variant was not used as an independent variable in the multivariate regression analysis because the number of patients who were tested was limited to 124. In the multivariate regression analysis with 124 patients, the presence of a pathogenic variant was not a significant predictor of the overall appearance of cardiac events (data not shown). [C]Diagnosis by screening or clinically was dichotomized (screened group=1, clinical group=2). Other abbreviations as in Tables 1,2.

probability test. To predict the presence or absence of cardiac events, logistic regression analysis was performed using the following as independent variables: age at diagnosis, sex, presence or absence of the pathogenic variant, family history of LQTS, screened or clinical (not screened) diagnosis, cardiac events before the first visit, resting QTc at diagnosis, maximum resting QTc value, maximum Holter QTc value, and follow-up period. To test the prognostic value of QTc for the presence of cardiac events, receiver operating characteristic (ROC) curves were used to calculate the area under the curve (AUC). To determine the cut-off QTc, Youden's index and the distance from the point (0,1) and the ROC plots were used. Two-sided P<0.05 was considered statistically significant.

Results

The characteristics of patients classified by the presence or absence of cardiac events after the hospital visit are presented in **Table 1**. The mean age and mean QTc values at diagnosis did not differ between the 2 groups; however, maximum resting QTcF, maximum Holter QTcB, and maximum Holter QTcF were significantly longer in the group with than without cardiac events after the first hospital visit (P=0.01, P<0.001, and P<0.001, respectively). In addition, the median Schwartz score was higher in the group with than without cardiac events (P<0.001), primarily because the Schwartz score awards 1 or 2 points for the presence of cardiac events (**Supplementary Table 1**). The

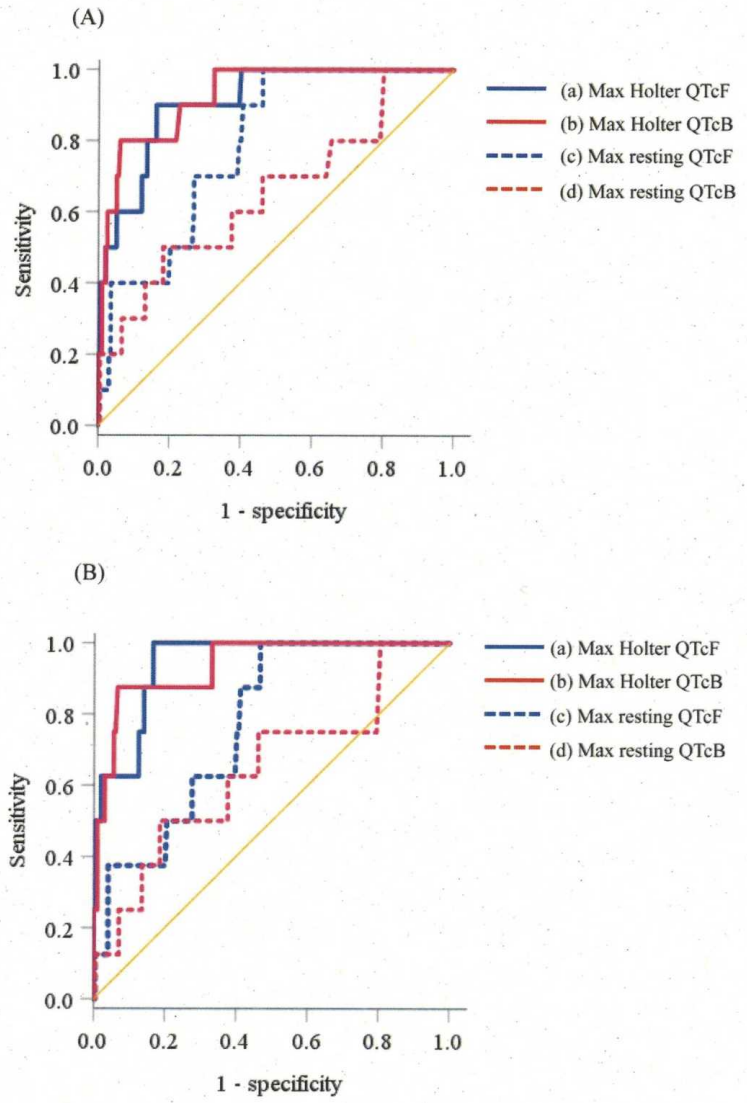

Figure 2. Receiver operating characteristic curves of 4 QTc values for predicting (**A**) the appearance of cardiac events after the first hospital visit and (**B**) the presence of overall cardiac events. Lines represent the maximum (Max) Holter QT interval corrected by the Fridericia formula (QTcF; a), Max Holter QT interval corrected by the Bazett formula (QTcB; b), Max resting QTcF (c), and Max resting QTcB (d). (**A**) The areas under the curve (AUCs) and 95% confidence intervals (CIs) for (a), (b), (c), and (d) were 0.942 (0.888–0.996), 0.938 (0.858–1.017), 0.770 (0.635–0.905), and 0.646 (0.426–0.866), respectively. P values for differences in AUCs were as follows: P=0.86 for (a) vs. (b); P=0.009 for (a) vs. (c); P=0.003 for (a) vs. (d); P=0.01 for (b) vs. (c); P=0.002 for (b) vs. (d); and P=0.049 for (c) vs. (d). (**B**) The AUCs and 95% CIs for (a), (b), (c), and (d) were 0.910 (0.829–0.990), 0.928 (0.856–0.999), 0.790 (0.675–0.905), and 0.653 (0.455–0.851), respectively. P values for differences in AUCs were as follows: P=0.52 for (a) vs. (b); P=0.06 for (a) vs. (c); P=0.003 for (a) vs. (d); P=0.01 for (b) vs. (c); P=0.001 for (b) vs. (d); and P=0.02 for (c) vs. (d).

prevalence of cardiac events before the first hospital visit was also higher in the group with than without cardiac events (P=0.008; **Table 1**).

Of the 207 patients, 181 (87%) were diagnosed through the screening program (**Supplementary Table 2**). Of the 26 patients in the clinical group, 1 was diagnosed by the presence of cardiac events, 8 were diagnosed by a familial study, and 17 were diagnosed by chance. The mean age of patients was lower in the clinical than screened group (P<0.001). The risk for the appearance of cardiac events after the first hospital visit did not differ between the 2 groups (**Supplementary Table 2**).

The diagnostic yield of genetic testing was low (33%; **Table 1**), even though patients who underwent such testing were analyzed using next-generation sequencers. The prevalence of the overall presence of cardiac events was significantly higher in patients with than without pathogenic variants (7/41 [17.1%] vs. 3/83 [3.6%], respectively; P=0.01).

Predictive factors for the appearance of cardiac events after the first hospital visit were determined using QTcB values as markers of the QT interval (**Table 2**). Univariate regression analysis showed that female sex, Schwartz score, cardiac events before the first hospital visit, maximum resting QTc value, maximum Holter QTc values, and the follow-up period were significant predictors of the appearance of cardiac events. Multivariate regression analysis showed that longer maximum Holter QTc was the sole predictive factor among all variables (P=0.01). When QTcF values were used instead of QTcB values, the predictor in the multivariate logistic regression analysis was the same (**Supplementary Table 3**).

Predictive factors for the overall presence of cardiac events were determined using QTcB values as markers of the QT interval (**Table 3**). Univariate regression analysis showed that female sex, Schwartz score, the presence of pathogenic variants, maximum resting QTcB, maximum Holter QTcB, and follow-up period were significant predictors of the appearance of cardiac events. Multivariate

Table 4. Statistical Analysis for Cut-Off Values to Predict the Appearance of Cardiac Events After the First Hospital Visit

Cut-off (ms)	Sensitivity	Specificity	PPV	NPV	Youden's index	Distance
a. Maximum resting QTcB value						
≥470	1.000	0.176	0.047	1.000	1.176	0.824
≥480	0.750	0.317	0.042	0.969	1.067	0.728
≥490	0.625	0.628	0.063	0.977	1.253	0.528*
≥500	0.500	0.759	0.077	0.974	1.259*	0.555
≥510	0.375	0.819	0.077	0.970	1.194	0.651
≥520	0.250	0.915	0.105	0.968	1.165	0.755
≥530	0.125	0.930	0.067	0.964	1.055	0.878
b. Maximum resting QTcF value						
≥450	1.000	0.181	0.047	1.000	1.181	0.819
≥460	1.000	0.322	0.056	1.000	1.322	0.678
≥470	1.000	0.518	0.077	1.000	1.518*	0.482
≥480	0.625	0.698	0.077	0.979	1.323	0.481*
≥490	0.500	0.779	0.083	0.975	1.279	0.547
≥500	0.375	0.879	0.111	0.972	1.254	0.637
≥510	0.375	0.920	0.158	0.973	1.295	0.630
c. Maximum Holter QTcB value						
≥550	1.000	0.508	0.075	1.000	1.508	0.492
≥560	1.000	0.618	0.095	1.000	1.618	0.382
≥570	0.875	0.724	0.113	0.993	1.599	0.303
≥580	0.875	0.799	0.149	0.994	1.674	0.237
≥590	0.875	0.879	0.226	0.994	1.754*	0.174*
≥600	0.750	0.945	0.353	0.989	1.695	0.256
≥610	0.500	0.980	0.500	0.980	1.480	0.500
d. Maximum Holter QTcF value						
≥510	1.000	0.467	0.070	1.000	1.467	0.533
≥520	1.000	0.613	0.094	1.000	1.613	0.387
≥530	1.000	0.739	0.133	1.000	1.739	0.261
≥540	1.000	0.814	0.178	1.000	1.814*	0.186*
≥550	0.750	0.859	0.176	0.988	1.609	0.287
≥560	0.625	0.925	0.250	0.984	1.550	0.383
≥570	0.625	0.970	0.455	0.985	1.595	0.376

*Best values of Youden's index and the distance in each QTc values. Youden's index denotes (sensitivity+specificity−1); the largest value is the best value. Distance denotes the shortest distance between the point (0,1) and the receiver operating characteristic (ROC) plot, that minimizes $([1-\text{sensitivity}]^2+[1-\text{specificity}]^2)^{0.5}$; the smallest value is the best value. NPV, negative predictive value; PPV, positive predictive value. Other abbreviations as in Table 1.

regression analysis showed that a longer maximum Holter QTcB and Schwarz score were independent predictors of the appearance of cardiac events. When QTcF values were used instead of QTcB values, the predictors in the multivariate logistic regression analysis were the same (**Supplementary Table 4**).

To determine which QTc value more effectively predicted the appearance of cardiac events, ROC curves were created for maximum Holter QTcB and maximum Holter QTcF values. For this analysis, the maximum resting QTc values were also included (**Figure 2**) because Holter ECGs were not routinely tested. The ROC curves to predict the appearance of cardiac events after the visit to the National Hospital Organization Kagoshima Medical Center are shown in **Figure 2A**. The AUCs of the maximum Holter QTc values were significantly superior to those of the maximum resting QTc values. The ROC curves to predict the overall presence of cardiac events are shown in **Figure 2B**. The AUCs of the maximum Holter QTc values were superior to those of the maximum resting QTc values, except between the maximum Holter QTcF and the maximum resting QTcF (P=0.055).

The best cut-off values for maximum resting QTcB, maximum resting QTcF, maximum Holter QTcB, and maximum Holter QTcF to predict the appearance of events after the first hospital visit as assessed by Youden's index and by the shortest distance (in parentheses) were ≥500 (≥490), ≥470 (≥480), ≥590 (≥590), and ≥540 (≥540) ms, respectively (**Table 4**). The sensitivity of the best cut-offs values for maximum resting QTcB, maximum resting QTcF, maximum Holter QTcB, and maximum Holter QTcF by Youden's index and by the shortest distance (in parentheses) was 0.500 (0.625), 1.000 (0.625), 0.875 (0.875), and 1.000 (1.000), respectively. The best cut-off values for the overall presence of cardiac events were the same as those for the appearance of events after the first hospital visit (**Supplementary Table 5**).

Discussion

The present study showed that the prevalence of cardiac events after the first hospital visit was 4%. Multiple logistic regression analysis revealed that the maximum Holter QTc value was the sole predictor of the appearance of cardiac events after the first hospital visit (P=0.02). Using the maximum Holter QTc value is appropriate to predict the appearance of symptoms in pediatric patients with LQTS.

Risk of Cardiac Events After the First Hospital Visit

Relatively recent reports have shown that the risk for LQTS-related cardiac events is high at about or more than a few dozen percent.[6-14,16-18] A possible reason for the high risk in these studies may be that the data included cardiac events before the first hospital visit in areas where the screening program was not present. Rohatgi et al reported that 27.4% of patients of their entire cohort were symptomatic at the first visit and that the risk of the appearance of cardiac events after this visit in the symptomatic patients was 25.2% (42/166 patients), compared with a risk of 1.8% (8/440 patients) for patients without symptoms at their first visit (P<0.001).[5] In the present study, the prevalence of cardiac events after the first hospital visit was 50% (2/4) in previously symptomatic patients and 3.0% (6/203) in asymptomatic patients (P=0.008).These data suggest that if patients begin follow-up while asymptomatic, as in the era of ECG screening programs, if they are given enough information about strategies such as sophisticated preventive procedures[15] or precision medicine,[28] and if information is sufficiently conveyed to patients and their families, we would be able to decrease the risk for cardiac events to a reasonably low level. We should then consider using QTc values based on Holter recordings to predict the appearance of cardiac events after the first hospital visit.

QTc Values on Holter ECG Recordings

QTc values on resting 12-lead ECGs are generally used to predict the appearance of LQTS-related cardiac events.[21] QTc values on Holter recordings are well known to be quite longer than those on resting 12-lead ECGs.[23-25,29] Holter recordings provide around 100,000 QT/RR pairs per day. Therefore, automated or semiautomated measurements of QT intervals have been adopted to differentiate the data of patients with LQTS from those of normal or control individuals.[18,23,29,30] However, data obtained by automated QT measurement do not seem to be applicable for clinical use because QT intervals at higher or lower heart rates[18,24] or too-long or too-short QT intervals[24] are automatically discarded by the software. In our experience, automatic measurement of too-long or too-short QTc values must be extensively checked, particularly when the isoelectronic baseline fluctuates or biphasic T waves, low-voltage T waves, and artifacts are present. In addition, many studies used 1 Holter recording per patient to evaluate the QTc values of patients with LQTS. We should use the longest QTc values among repeated Holter ECGs, as for repeated resting 12-lead ECGs.[21] Therefore, in the present study we: (1) manually measured Holter recordings;[24] (2) chose 5 representative periods in a day and obtained 3 ECGs (maximum, average, and minimum heart rates) from each period; and (3) recorded Holter ECGs at every patient's visit. Finally, we used the maximum Holter QTc value throughout the day and among repeated Holter recordings.

Of the 3 QTc values (i.e., resting QTc at diagnosis, maximum resting QTc, and maximum Holter QTc), the maximum Holter QTc value obtained using our methodology was the sole predictor of the appearance of cardiac events after the first hospital visit (**Table 2**; **Supplementary Table 3**). The maximum Holter QTc was one of the independent predictors of the overall presence of cardiac events (**Table 3**; **Supplementary Table 4**). We believe that the maximum QTc on Holter ECGs should be considered for the prediction of cardiac events in patients with LQTS; however, no reports have addressed the maximum Holter QTc values among repeated recordings of Holter ECGs. Future studies should be performed to validate the present data to determine whether the maximum Holter QTc is independently predictive of the appearance of new cardiac symptoms for all symptomatic patients at diagnosis or for all patients with pathogenic variants. The cut-off values in this study should also be validated.

Genetic Testing

The yield of genetic testing in the present study (33%) was much lower than in previous studies (around 70%[12] or 80%[31]). The genetically determined prevalence of LQTS is at least 1 in 2,534 among apparently healthy live births (i.e., in the general population).[32] The probability of diagnosing LQTS through ECGs in the general population is 1 in 988 among 7th graders (aged 12 years) according to the criteria of the HRS/EHRA/APHRS expert consensus statement.[20] Therefore, the estimated yield of genetic testing in the general population with ECG-determined LQTS is 39% (988 divided by 2,534). In a large study involving 44,596 otherwise healthy infants in Italy, the prevalence of disease-causing variants in infants with a QTcB of >470ms was 43% (12/28 infants).[32] These data suggest that the yield of genetic testing in patients from the general population who were diagnosed through an ECG is around 40%.

Study Limitations

This study had 3 main limitations. First, many patients were asymptomatic at their first visit and more than half did not have pathogenic variants, although one of the aims of this study was to clarify the outcome of those patients. The statistical analysis of a resting QTc of ≥470ms, which is the recommended value at which medication should be started,[21] revealed that the sensitivity was 100% but the specificity was 17.6% (**Table 4**). Additional studies are needed for patients in areas where proactive cardiogenetic counseling programs[2] or school-based ECG screening programs[19,20] exist. Second, the number of patients with cardiac events after the first hospital visit was also very small (8/207 patients [4%]). This may be an advantage of the screening program but a disadvantage for statistical robustness. An increase in the number of patients with cardiac events after the visit is not desired; however, a large number of patients with symptoms should be obtained. Finally, a gene-specific statistical analysis revealed that the maximum Holter QTc value was not a significant predictor of the appearance of cardiac events in patients with LQT1 or LQT2 (**Supplementary Table 5**), probably because of a small number of patients with pathogenic mutations and those with cardiac events. Further studies are also needed to investigate this issue after increasing the number of patients with each pathogenic mutation and those with cardiac events.

Conclusions

The present study showed that the prevalence of cardiac events after the first hospital visit was 4%. Multivariate logistic regression analysis revealed that the maximum Holter QTc was the sole predictive factor for the appearance of cardiac events after the first hospital visit. These data indicate that the maximum Holter QTc should be considered when predicting the appearance of cardiac events, although the data should be validated in areas where there are no screening programs.

Acknowledgment

The authors thank Angela Morben, DVM, ELS, from Edanz (https://jp.edanz.com/ac) for editing a draft of this manuscript.

Sources of Funding

This work was supported, in part, by Health and Labour Sciences Research Grants from the Japanese Ministry of Health, Labour and Welfare (Comprehensive Research on Cardiovascular Diseases; H22-032, H26-002, H29-055, 21FC1004).

Disclosures

The authors declare that there is no conflict of interest.

IRB Information

This study was approved by the Ethics Committee of the National Hospital Organization Kagoshima Medical Center (No. 30-69).

References

1. Schwartz PJ, Crotti L, Insolia R. Long QT syndrome: From genetics to management. *Circ Arrhythm Electrophysiol* 2012; **5:** 868–877.
2. Schwartz PJ, Ackerman MJ, Antzelevitch C, Bezzina CR, Borggrefe M, Cuneo BF, et al. Inherited cardiac arrhythmias. *Nat Rev Dis Primers* 2020; **6:** 58.
3. Wilde AAM, Amin AS, Postema PG. Diagnosis, management and therapeutic strategies for congenital long QT syndrome. *Heart* 2022; **108:** 332–338.
4. Jervell A, Lange-Nielsen F. Congenital deaf-mutism, functional heart disease with prolongation of the Q-T interval and sudden death. *Am Heart J* 1957; **54:** 59–68.
5. Rohatgi RK, Sugrue A, Bos JM, Cannon BC, Asirvatham SJ, Moir C, et al. Contemporary outcomes in patients with long QT syndrome. *J Am Coll Cardiol* 2017; **70:** 453–462.
6. Ozawa J, Ohno S, Hisamatsu T, Itoh H, Makiyama T, Suzuki H, et al. Pediatric cohort with long QT syndrome: *KCNH2* mutation carriers present late onset but severe symptoms. *Circ J* 2016; **80:** 696–702.
7. Mazzanti A, Maragna R, Vacanti G, Monteforte N, Bloise R, Marino M, et al. Interplay between genetic substrate, QTc duration, and arrhythmia risk in patients with long QT syndrome. *J Am Coll Cardiol* 2018; **71:** 1663–1671.
8. Kutyifa V, Daimee UA, McNitt S, Polonsky B, Lowenstein C, Cutter K, et al. Clinical aspects of the three major genetic forms of long QT syndrome (LQT1, LQT2, LQT3). *Ann Noninvasive Electrocardiol* 2018; **23:** e12537.
9. Kwok SY, Liu AP, Chan CY, Lun KS, Fung JL, Mak CC, et al. Clinical and genetic profile of congenital long QT syndrome in Hong Kong: A 20-year experience in paediatrics. *Hong Kong Med J* 2018; **24:** 561–570.
10. Lahrouchi N, Tadros R, Crotti L, Mizusawa Y, Postema PG, Beekman L, et al. Transethnic genome-wide association study provides insights in the genetic architecture and heritability of long QT syndrome. *Circulation* 2020; **142:** 324–338.
11. Younis A, Aktas MK, Rosero S, Kutyifa V, Polonsky B, McNitt S, et al. Outcome by sex in patients with long QT syndrome with an implantable cardioverter defibrillator. *J Am Heart Assoc* 2020; **9:** e016398.
12. Ohno S, Ozawa J, Fukuyama M, Makiyama T, Horie M. An NGS-based genotyping in LQTS; minor genes are no longer minor. *J Hum Genet* 2020; **65:** 1083–1091.
13. Tse G, Lee S, Zhou J, Liu T, Wong ICK, Mak C, et al. Territory-wide Chinese cohort of long QT syndrome: Random survival forest and Cox analyses. *Front Cardiovasc Med* 2021; **8:** 608592.
14. Ergül Y, Tunca Şahin G, Kafalı HC, Öztürk E, Özgür S, Haydin S, et al. Clinical and genetic characteristics and course of congenital long QT syndrome in children: A nine-year single-center experience. *Anatol J Cardiol* 2021; **25:** 250–257.
15. Tobert KE, Bos JM, Garmany R, Ackerman MJ. Return-to-play for athletes with long QT syndrome or genetic heart diseases predisposing to sudden death. *J Am Coll Cardiol* 2021; **78:** 594–604.
16. Goldenberg I, Bos JM, Yoruk A, Chen AY, Lopes C, Huang DT, et al. Risk prediction in women with congenital long QT syndrome. *J Am Heart Assoc* 2021; **10:** e021088.
17. Mazzanti A, Trancuccio A, Kukavica D, Pagan E, Wang M, Mohsin M, et al. Independent validation and clinical implications of the risk prediction model for long QT syndrome (1-2-3-LQTS-Risk). *Europace* 2022; **24:** 614–619.
18. Waddell-Smith KE, Chaptynova AA, Li J, Crawford JR, Hinds H, Skinner JR. Holter recordings at initial assessment for long QT syndrome: Relationship to genotype status and cardiac events. *J Cardiovasc Dev Dis* 2022; **9:** 164.
19. Fukuyama M, Horie M, Aoki H, Ozawa J, Kato K, Sawayama Y, et al. School-based routine screenings of electrocardiograms for the diagnosis of long QT syndrome. *Europace* 2022; **24:** 1496–1503.
20. Yoshinaga M, Kucho Y, Nishibatake M, Ogata H, Nomura Y. Probability of diagnosing long QT syndrome in children and adolescents according to the criteria of the HRS/EHRA/APHRS expert consensus statement. *Eur Heart J* 2016; **37:** 2490–2497.
21. Priori SG, Wilde AA, Horie M, Cho Y, Behr ER, Berul C, et al. Executive summary: HRS/EHRA/APHRS expert consensus statement on the diagnosis and management of patients with inherited primary arrhythmia syndromes. *Europace* 2013; **15:** 1389–1406.
22. Zeppenfeld K, Tfelt-Hansen J, de Riva M, Winkel BG, Behr ER, Blom NA, et al. 2022 ESC guidelines for the management of patients with ventricular arrhythmias and the prevention of sudden cardiac death. *Eur Heart J* 2022; **43:** 3997–4126.
23. Priori SG, Schwartz PJ, Napolitano C, Bloise R, Ronchetti E, Grillo M, et al. Risk stratification in the long-QT syndrome. *N Engl J Med* 2003; **348:** 1866–1874.
24. Page A, Aktas MK, Soyata T, Zareba W, Couderc JP. "QT clock" to improve detection of QT prolongation in long QT syndrome patients. *Heart Rhythm* 2016; **13:** 190–198.
25. Ogawa Y, Tanaka T, Kido S. Maximum QTc on Holter electrocardiography in children. *Pediatr Int* 2018; **60:** 507–512.
26. Tamr Agha MK, Fakhri G, Ahmed M, El Sedawy O, Abi Saleh B, Bitar F, et al. QTc interval on 24-hour holter monitor: To trust or not to trust? *Ann Noninvasive Electrocardiol* 2022; **27:** e12899.
27. Adler A, Novelli V, Amin AS, Abiusi E, Care M, Nannenberg EA, et al. An international, multicentered, evidence-based reappraisal of genes reported to cause congenital long QT syndrome. *Circulation* 2020; **141:** 418–428.
28. Gnecchi M, Sala L, Schwartz PJ. Precision medicine and cardiac channelopathies: When dreams meet reality. *Eur Heart J* 2021; **42:** 1661–1675.
29. Viitasalo M, Oikarinen L, Väänänen H, Swan H, Piippo K, Kontula K, et al. Differentiation between LQT1 and LQT2-patients and unaffected subjects using 24-hour electrocardiographic recordings. *Am J Cardiol* 2002; **89:** 679–685.
30. Follansbee CW, Beerman L, Arora G. Automated QT analysis on Holter monitors in pediatric patients can differentiate long QT syndrome from controls. *Pacing Clin Electrophysiol* 2018; **41:** 50–56.
31. Taggart NW, Haglund CM, Tester DJ, Ackerman MJ. Diagnostic miscues in congenital long-QT syndrome. *Circulation* 2007; **115:** 2613–2620.
32. Schwartz PJ, Stramba-Badiale M, Crotti L, Pedrazzini M, Besana A, Bosi G, et al. Prevalence of the congenital long-QT syndrome. *Circulation* 2009; **120:** 1761–1767.

Supplementary Files

Please find supplementary file(s);
https://doi.org/10.1253/circj.CJ-23-0409

Endocrine Journal 2023, 70 (7), 745-753

CASE REPORT WITH REVIEW OF LITERATURE

Food-dependent Cushing's syndrome due to unilateral adrenocortical adenoma with cortisol secretion without ACTH elevation detected in peripheral blood by the CRH test: a case report

Miwa Makino[1),2)], Nobuyuki Koriyama[1)], Nami Kojima[1),2)], Takuya Tobo[1),2)] and Yoshihiko Nishio[2)]

[1)] *Department of Diabetes and Endocrine Medicine, National Hospital Organization Kagoshima Medical Center, Kagoshima 892-0853, Japan*

[2)] *Department of Diabetes and Endocrine Medicine, Kagoshima University Graduate School of Medicine and Dental Sciences, Kagoshima University, Kagoshima 890-8520, Japan*

Abstract. We report an extremely rare case of a 61-year old woman with food-dependent Cushing's syndrome (FDC) due to unilateral adrenocortical adenoma (UAA) with cortisol (CORT) secretion without ACTH elevation detected in peripheral blood by the CRH test. She was on oral medications for hypertension and depression, and presented weight gain, general fatigue, muscle weakness, and hypokalemia. Despite the fact that the diurnal variation of ACTH was always suppressed, a diurnal variation in CORT was observed, in the form of low levels in the early morning and high levels in the afternoon. An increase in CORT was shown in a 75 g-oral glucose tolerance test (OGTT) and in a mixed meal tolerance test, but no change in CORT levels was seen in intravenous glucose tolerance tests. Elevated CORT levels were observed in response to intravenous injection of CRH, although ACTH levels were always below the measured sensitivity. Laparoscopic left adrenalectomy was performed, which resulted in postoperative improvement in potassium and ACTH levels and disappearance of the CORT secretory response in the OGTT. Clear expression of glucose-dependent insulinotropic polypeptide receptor (GIPR), CRH and CRH receptor 2 (CRHR2) were confirmed in the surgically-resected UAA specimen by molecular and immunohistochemical analyses, suggesting the involvement of not only GIPR, but also CRH and CRHR2 in FDC.

Key words: Food-dependent Cushing's syndrome, Glucose-dependent insulinotropic polypeptide, CRH, CRH receptor 2

PRIMARY CUSHING'S SYNDROME results from chronic hypercortisolemic exposure of glucocorticoid and mineralocorticoid receptors due to ACTH-independent cortisol (CORT) overproduction associated with adrenocortical tumors, bilateral macronodular adrenal hyperplasia (BMAH) or primary pigmented nodular adrenal dysplasia [1]. Ectopic expression and orthotopic activation of various G protein-coupled hormone receptors (GPCRs), especially in BMAH and unilateral adrenocortical adenoma (UAA), have also been shown to produce cortisol [1, 2]. Since the 1987 report by Hamet *et al.* [3] of food-dependent Cushing's syndrome (FDC) due to ectopic expression of the glucose-dependent insulinotropic polypeptide (GIP) receptor (GIPR), normally

Submitted Dec. 1, 2022; Accepted Mar. 27, 2023 as EJ22-0622
Released online in J-STAGE as advance publication Apr. 15, 2023
Correspondence to: Nobuyuki Koriyama, Department of Diabetes and Endocrine Medicine, National Hospital Organization Kagoshima Medical Center, 8-1 Shiroyama-cho, Kagoshima 892-0853, Japan.
E-mail: koriyama.nobuyuki.wm@mail.hosp.go.jp
Abbreviations: UAA, Unilateral adrenocortical adenoma; CORT, Cortisol; OGTT, 75 g-oral glucose tolerance test; GIPR, Glucose-dependent insulinotropic polypeptide receptor; CRHR, CRH receptor; BMAH, Bilateral macronodular adrenal hyperplasia; GPCRs, G protein-coupled hormone receptors; FDC, Food-dependent Cushing's syndrome; GIP, Glucose-dependent insulinotropic polypeptide; GIPR, GIP receptor; HPA, Hypothalamus-pituitary-adrenal; AAs, Adrenocortical adenomas; HbA1c, Glycosylated hemoglobin; DHEA-S, Dehydroepiandrosterone sulphate; CT, Computed tomography; MRI, Magnetic resonance imaging; MMTT, Mixed meal tolerance test; IVGTT, Intravenous glucose tolerance test; *CRH*, CRH gene; *CRHR1*, CRHR1 gene; *CRHR2*, CRHR2 gene; *GIPR*, GIPR gene; *GLP-1R*, GLP-1R gene; *GHPDH*, Glyceraldehyde-3-phosphate dehydrogenase gene; PA, Patient's resected adrenocortical adenoma tissue blocks; CA, Non-functioning adrenocortical adenoma tissue blocks; RT-PCR, Real-time polymerase chain reaction; ΔC_T value, Average C_T values; GAPDH, Glyceraldehyde-3-phosphate dehydrogenase

expressed in pancreatic β cells, adipocytes, osteoblasts, *etc.*, there have been a total of 38 reported cases of FDC, with 25 cases of BMAH and 13 cases of UAA [4-22], although their exact prevalence is still unknown.

CRH is a major regulator of the hypothalamus-pituitary-adrenal (HPA) axis, and is released from the hypothalamus in response to stress, causing the anterior pituitary to secrete ACTH into the blood. It exerts its effects on many peripheral tissues as an important mediator of autonomic, behavioral and immune responses [23]. CRH exerts its effects in most tissues by binding to the CRH receptor (CRHR), a member of the seven-transmembrane GPCR superfamily, which induces a change in receptor structure and activation of heterotrimeric G proteins, followed by an increase in cyclic AMP (cAMP) levels *via* activation of adenylate cyclase [24]. Two types of CRHRs have been cloned, CRHR1 and CRHR2 [24], and mRNAs encoding them have been reported to be overexpressed 6-fold in adrenocortical adenomas (AAs) and 10- to 60-fold in CORT-producing AAs [23].

Here, we report a rare case of a 61-year old woman with FDC due to UAA with CORT secretion without ACTH elevation detected in peripheral blood by the CRH test.

Case Presentation

The patient was a 61-year-old woman with no special medical or family history. At the age of 51 years, she was diagnosed with hypertension and was started on antihypertensive medication. She had also been depressed since that time. At the age of 57 years, she began to notice weight gain, fatigue and muscle weakness. She was referred to our cardiology department with the chief complaint of respiratory distress at the age of 61 years. Although there was no evidence of ischemic heart disease, arrhythmia or congestive heart failure, she was noted to have treatment-resistant hypertension (148/84 mmHg) and hypokalemia (2.9 mmol/L), and a 25 mm-sized tumor was observed in the left adrenal gland on CT, which led her to our department for endocrinological examination. At the time of her first visit to our department, she was receiving spironolactone 75 mg, nifedipine 80 mg, bisoprolol fumarate 5 mg, ethyl icosapentate 1,800 mg, mosapride citrate 15 mg, duloxetine hydrochloride 60 mg, etizolam 0.5 mg, triazolam 0.25 mg and mirtazapine 15 mg daily for the treatment of hypertension and depression, and lorazepam 0.5 mg was used as required during episodes of increased anxiety.

The patient was 156.3 cm tall, weighed 70.3 kg, had a body mass index of 28.8 kg/m^2, body temperature of 36.1°C, blood pressure of 148/84 mmHg, and pulse rate of 88 beats/min with regular rhythm. She showed no cognitive dysfunctions, and had no pigmentation of the skin and oral mucosa. Her cardiopulmonary examination was normal. She had no abnormal abdominal and neurological findings or skeletal abnormalities. She had exaggerated facial roundness, central obesity, a dorsocervical fat pad, and multiple subcutaneous hemorrhages on both upper and lower extremities. There were no reddish-purple striae or edema in her lower legs bilaterally. She was a non-drinker and non-smoker. Suspecting Cushing's syndrome, we performed laboratory tests and imaging studies to confirm the diagnosis and identify the cause. Her serum levels of potassium, total protein and albumin were inappropriately low (Table 1). Serum lactate dehydrogenase, low density lipoprotein-cholesterol, triglycerides, sodium and glycosylated hemoglobin (HbA1c) levels were all elevated (Table 1). ACTH levels were suppressed to <1.5 pg/mL throughout the day. Dehydroepiandrosterone sulphate (DHEA-S) was in the low normal range (47 μg/dL) and urinary CORT was elevated (124 μg/day) (Table 1). Dexamethasone 1 mg did not suppress serum CORT levels to <5 μg/dL (Table 1). On the other hand, her fasting serum CORT level at 8:00 a.m. was as low as 3.84 μg/mL, but increased during the day to 19.9 μg/mL at 16:00 and 14.0 μg/mL at 23:00. In addition, elevated CORT levels (from 4.6 to 16.2 μg/dL) were observed in response to intravenous injection of 100 μg of human CRH, although ACTH levels were always below measurement sensitivity (<1.5 pg/mL) (Table 2). Both computed tomography (CT) and magnetic resonance imaging (MRI) displayed a tumor 25 mm in size, presumed to be an adenoma, on the left adrenal gland. No tumor was found in the right adrenal gland (Fig. 1A, B). A circular shaped area of highly abnormal tracer uptake was seen at the site of the left adrenal tumor, with diminished tracer accumulation in the right adrenal gland on ^{131}iodine (I)-adosterol scintigraphy (Fig. 1C). Blood glucose levels on a 75 g-oral glucose tolerance test (OGTT) were maintained above 200 mg/dL from 30 min to 120 min after loading, indicating a diabetic-type blood glucose transition (Fig. 2A). Blood glucose transition in the mixed meal tolerance test (MMTT) and intravenous glucose tolerance test (IVGTT) peaked at 30 min after the glucose load (≥200 mg/dL) and decreased thereafter, but showed a tendency to rise again 120 min after the load only in the MMTT (Fig. 2A). In addition, insulin changes in OGTT and MMTT peaked at 30 min after loading (≥100 mg/dL), decreased thereafter, and showed a tendency to rise again after 120 min (Fig. 2B). On the other hand, the peak value of insulin in the IVGTT was <30 μU/mL (Fig. 2B). Furthermore, an increase in

Table 1 Laboratory findings

Peripheral blood		WBC	5,020/μL	
		Neu	62.1%	
		Lym	28.1%	
		Baso	0.6%	
		Eosin	0.8%	
		Mono	8.4%	
Biochemistry		AST	39 IU/L	
		ALT	22 IU/L	
		LDH	273 IU/L	[124–222]
		ALP	116 IU/L	
		γ-GTP	82 IU/L	[9–32]
		Alb	3.72 g/dL	[4.10–5.10]
		Na	147 mmol/L	[138–145]
		K	3.3 mmol/L	[3.6–4.8]
		Cl	109 mmol/L	
		Ca	9 mg/dL	
		IP	3.5 mg/dL	
		LDL-C	161 mg/dL	[65–163]
		HDL-C	68 mg/dL	
		TG	326 mg/dL	[30–117]
		BUN	9.1 mg/dL	
		Cr	0.82 mg/dL	
		eGFR	54 mL/min/1.73m^2	[60<]
		UA	6.9 mg/dL	
		FBG	105 mg/dL	
		HbA_{1c}	6.5%	[4.9–6.0]
Endocrinology		DHEA-S	47 μg/dL	
		U-CORT	124 μg/day	[11.2–80.3]
		U-MN	0.04 μg/mg·Cr	
		U-NMN	0.55 μg/mg·Cr	
	(After 1 mg DST)	ACTH	<1.5 pg/mL	
		CORT	6.11 μg/dL	[<5.0]
	(After 8 mg DST)	ACTH	<1.5 pg/mL	
		CORT	4.40 μg/dL	
	(Daily fluctuation)	ACTH (06:00)	<1.5 pg/mL	[7.2–63.3]
		ACTH (16:00)	<1.5 ng/mL	
		ACTH (23:00)	<1.5 pg/mL	
		CORT (06:00)	3.8 μg/dL	[7.1–19.6]
		CORT (16:00)	19.9 μg/dL	
		CORT (23:00)	14.0 μg/dL	

The reference ranges are shown in square brackets. WBC, white blood cells; Neu, neutrophils; Lym, lymphocytes; Baso, basophils; Eosin, eosinophils; Mono, monocytes; AST, aspartate aminotransferase; ALT, alanine aminotransferase; LDH, lactate dehydrogenase; ALP, alkaline phosphatase; γ-GTP, γ-glutamyltransferase; Alb, albumin; Na, sodium; K, potassium; Cl, chloride; Ca, calcium; IP, inorganic phosphorus; LDL-C, low-density lipoprotein-cholesterol; HDL-C, high-density lipoprotein-C; TG, triglycerides; BUN, blood urea nitrogen; Cr, creatinine; eGFR, estimated glomerular filtration rate; UA, uric acid; FBG, fasting blood glucose; HbA_{1c}, glycosylated hemoglobin; ACTH, adrenocorticotropic hormone; CORT, cortisol; DHEA-S, dehydroepiandrosterone sulphate; U-CORT, urinary-cortisol; U-MN, urinary-metanephrine; U-NMN, urinary-normetanephrine; DST, dexamethasone suppression test.

Table 2 CRH test results

	0	30	60	90	min
ACTH	<1.5	<1.5	<1.5	<1.5	pg/mL
CORT	4.6	12.2	16.2	11.2	μg/dL

100 μg of human CRH was injected intravenously. CRH, corticotropin-releasing hormone; ACTH, adrenocorticotropic hormone; CORT, cortisol.

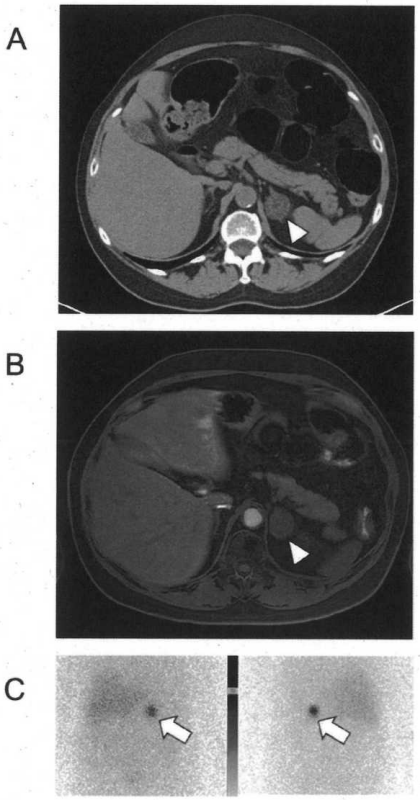

Fig. 1 Imaging for the adrenocortical adenoma

The arrowheads highlight an approximately 25 mm tumor in the left adrenal gland on computed tomography (A) and magnetic resonance imaging (B). The arrow indicates high accumulation in the left adrenal gland tumor on ^{131}iodine (I)-adosterol scintigraphy (C), while accumulation in the right adrenal gland was suppressed and unclear.

CORT was shown in the OGTT and MMTT, but no change in CORT was seen in the IVGTT (Fig. 2C). A diagnosis of FDC was made based on the fact that CORT secretion was only observed when nutrients were administered orally *via* the gastrointestinal tract, and not following their intravenous administration.

Since the patient desired resection of the AA on her left adrenal gland, laparoscopic left adrenalectomy was performed. The size of the resected tumor was 26 × 25 × 20 mm, and the pathological diagnosis was benign adrenocortical adenoma. Postoperatively, her serum K

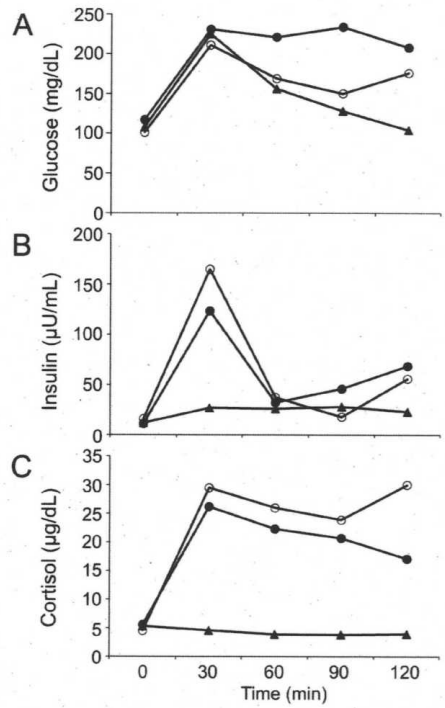

Fig. 2 Changes in blood glucose, insulin and cortisol levels in the OGTT, MMTT and IVGTT

A shows changes in blood glucose levels, B shows changes in insulin levels, and C shows changes in cortisol levels. The closed circles, open circles and closed triangles represent the OGTT, MMTT and IVGTT, respectively. OGTT, 75 g-oral glucose tolerance test; MMTT, mixed meal tolerance test; IVGTT, intravenous glucose tolerance test.

levels improved compared to those before surgery. Furthermore, at 8 months postoperatively, her morning fasting ACTH level had recovered from less than measurement sensitivity to 7.4 pg/mL. The CORT secretory response in the OGTT also disappeared (Table 3).

RT-PCR

In order to identify the expression of the CRH gene (*CRH*), CRHR1 gene (*CRHR1*), CRHR2 gene (*CRHR2*), GIPR gene (*GIPR*) and GLP-1R gene (*GLP-1R*), total RNA extraction from both, the patient's resected adrenocortical adenoma tissue blocks (patient's adenoma, PA) and non-functioning adrenocortical adenoma tissue blocks removed from a 54-year-old woman (control adenoma, CA) (Biovit, Detroit, USA), was performed. Next, we performed real-time polymerase chain reaction (RT-PCR) testing for the glyceraldehyde-3-phosphate dehydrogenase gene (*GHPDH*), *CRH*, *CRHR1*, *CRHR2*, *GIPR* and *GLP-1R* according to the manufacturers' instructions. Differences in the average C_T values (ΔC_T

Table 3 OGTT after tumor resection

	0	30	60	90	120	min
Glucose	115 (101)	212 (212)	154 (168)	199 (150)	196 (176)	mg/dL
Insulin	7.2 (16.0)	194.1 (165)	26.7 (27.0)	100.1 (17.9)	90.3 (56.0)	μU/mL
ACTH	21.4 (0.00)	21.1 (0.00)	20.9 (0.00)	17.2 (0.00)	16.4 (0.00)	pg/mL
CORT	8.53 (4.54)	8.78 (29.5)	6.97 (26.0)	6.24 (23.9)	5.62 (30.0)	μg/dL

OGTT, 75 g-oral glucose tolerance test; ACTH, adrenocorticotropic hormone; CORT, cortisol. The numbers in brackets indicate the respective preoperative values.

Table 4 Average ΔC_T values and fold changes in *CRH*, *CRHR1*, *CRHR2*, *GIPR* and *GLP-1R* by RT-PCR

Sample Name	*CRH*		*CRHR1*		*CRHR2*		*GIPR*		*GLP-1R*	
	Average ΔC_T	Fold Change	Average ΔC_T	Fold Change	Average ΔC_T	Fold Change	Average ΔC_T	Fold Change	Average ΔC_T	Fold Change
PA	15.5	2.08	UD		15.5	7.26	2.8	258.03	15.9	8.75
CA	16.6		UD		18.4		10.8		19.1	

PA, the patient's resected adrenocortical adenoma tissue blocks; CA, non-functioning adrenocortical adenoma tissue blocks (control); *CRH*, corticotropin-releasing hormone gene; *CRHR1*, CRH receptor 1 gene; *CRHR2*, CRH receptor 2 gene; GIPR, Glucose-dependent insulinotropic polypeptide receptor gene; *GLP-1R*, glucagon-like peptide-1 receptor gene; RT-PCR, real-time polymerase chain reaction; C_T, threshold cycle; Average ΔC_T, Average C_T of *CRH*, *CRHR1*, *CRHR2*, *GIPR or GLP-1R*—Average C_T of *GAPDH* (glyceraldehyde-3-phosphate dehydrogenase gene); Fold Change, gene expression ratio of each gene in PA relative to CA (control sample). These were calculated by $\Delta\Delta C_T$ power of 2. $\Delta\Delta C_T$ value, Average ΔC_T of PA—Average ΔC_T of control sample. Technical replicates; 2.

value) for *CRH*, *CRHR2*, *GIPR* and *GLP-1R* were 15.5, 15.5, 2.8 and 15.9, respectively in PA, although *CRHR1* was not detected (Table 4). Fold-changes in PA for *CRH*, *CRHR2*, *GIPR* and *GLP-1R* were 2.08, 7.26, 258.03 and 8.75, respectively (Table 4). These tests were conducted by the Technical Support Center of DNA Chip Research Institute, Inc., Tokyo, Japan.

Western Blotting

Western blotting was performed using CRH/CRF rabbit polyclonal antibody (LSBio, Seattle, Washington, USA), CRHR2/CRF2 Receptor rabbit polyclonal antibody (LSBio), GLP-1R rabbit polyclonal antibody (Novus Biologicals, Littleton, Colorado, USA), GIPR rabbit polyclonal antibody (GeneTex Inc., Irvine, California, USA) and anti-GAPDH mouse monoclonal antibody (Bio-Rad Laboratories Inc., Hercules, California, USA) to identify the protein expression of CRH, CRHR2, GIPR and GLP-1R in PA and CA tissue. Bands were detected near 25–37 kDa (CRH) and near 50 kDa (CRHR2) in both the PA and CA tissues. Further, a band around 25 kDa (CRHR2) was identified in PA tissue, but not in CA tissue. In addition, the bands presumed to be GIPR and GLP-1R around 50 kDa showed stronger signals in PA than in CA. All of these immunoreaction procedures and evaluations were performed by GenoStaff Co., Ltd., Tokyo, Japan (Fig. 3).

Immunohistochemical Staining

Immunohistochemical staining was performed on a 4% paraformaldehyde phosphate buffer solution-fixed tissue block from the resected PA. Coloration of both the vessels and the entire tissue was confirmed to be GIPR-positive (Fig. 4). Pathological processing and evaluation was performed by GenoStaff Co., Ltd.

Discussion

Although the exact prevalence of FDC is unknown, a total of 38 cases have been reported worldwide [4-22]. GIPR is reportedly not expressed in normal adrenocortical tissue [7], although its ectopic expression has been shown to be a cause of FDC. Our patient had several characteristic physical findings of Cushing's syndrome, such as full exaggerated facial roundness and central obesity, and, although there was no evidence of neutropenia, she manifested hypokalemia, hyperglycemia and dyslipidemia (Table 1). In addition, 24-h urinary CORT was elevated and CORT levels were not suppressed by either 1 mg and 8 mg dexamethasone (Table 1), a left adrenal adenoma was observed on CT and MRI (Fig. 1A, B), and strong accumulation of ^{131}I-adosterol in the same tumor and suppressed uptake on the non-tumor side were also observed (Fig. 1C). Hence, a diagnosis of Cushing's syndrome due to UAA was made. Furthermore, despite

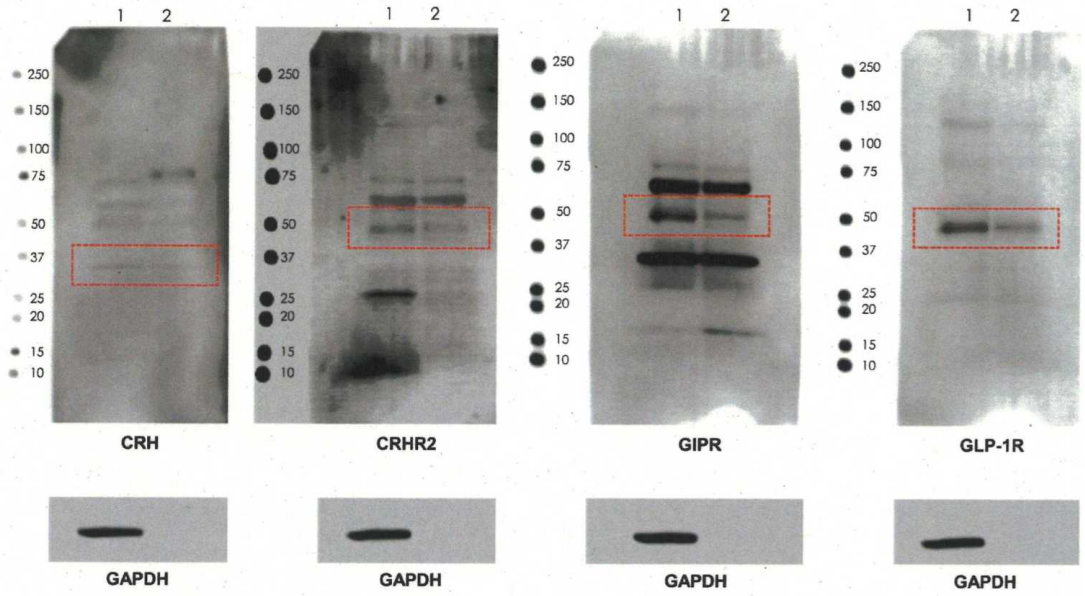

Fig. 3 Western blotting analysis

CRH, corticotropin-releasing hormone; CRHR2, CRH receptor 2; GIPR, glucose-dependent insulinotropic polypeptide receptor; GLP-1R, glucagon-like peptide-1 receptor; GAPDH, glyceraldehyde-3-phosphate dehydrogenase. Lane 1 indicates the patient's resected adrenocortical adenoma tissue, and lane 2 indicates non-functioning adrenocortical adenoma tissue from another patient (control). Lane 2 showed no expression of GAPDH. The parts surrounded by the red dashed lines indicate bands detected around 25–37 kDa, 50 kDa, 50 kDa and 50 kDa in the left adrenal gland tissue, which were considered to correspond to CRH, CRHR2, GIPR and GLP-1R, respectively.

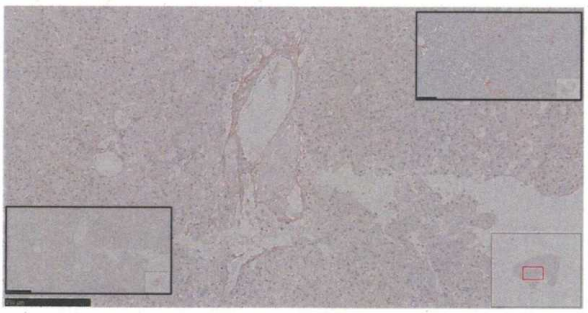

Fig. 4 Immunohistochemical staining of GIPR in the patient's resected adrenocortical adenoma

The lower left inset shows a negative control using normal rabbit immunoglobulin. The upper right inset shows a positive control of human pancreatic tissue stained using rabbit polyclonal anti-human GIPR antibodies. The inset at the lower right shows a weakly magnified photo of the patient's resected adrenocortical adenoma. GIPR, glucose-dependent insulinotropic polypeptide receptor.

the fact that the diurnal variation of ACTH was always suppressed, a diurnal variation in CORT was observed, which was characterized by a low level at 6:00 and high levels at 16:00 and 23:00 (Table 1). Reznik Y *et al.* reported that plasma GIP concentrations are usually maximal after meal intake, at around 200 pmol/L, and are very low, at approximately 20 pmol/L, during fasting [5], and this low GIP level, coupled with suppression of ACTH, might be responsible for the specific finding of low early morning CORT levels. Since the findings in our patient were consistent with the characteristics of FDC, OGTT, MMTT and IVGTT were performed. Since CORT secretion was stimulated only by OGTT and MMTT (Fig. 2), the involvement of incretin was inferred, which was the basis for the diagnosis of FDC in this case.

FDC has been recognized in BMAH, which is presumably due to the acquisition of mutations during adrenal embryogenesis, as well as in UAA, presumably due to the expansion of single-cell clones that abnormally express GIPR [6]. The ectopic expression of GIPR in UAA has been suggested as being due to somatic mutations in the DNA segments that regulate their expression, and might also be related to abnormal mRNA splicing [9]. On the other hand, since GIP has been shown to stimulate DNA synthesis in tumor cells, it has been speculated that GIPR might also be involved in tumor cell development [9]. In a previous study, a somatic mutation in p. Ser45Cys of β-catenin/CTNNB1, a mediator in the WNT signaling pathway, was identified in one of the UAAs expressing the GIP receptor, which might contribute to tumor cell development [22]. Both

the PA and CA showed expression of the GIPR gene and protein. However, the expression was clearly increased in PA compared to CA (Table 2 and Fig. 3). In PA, GLP-1R gene and protein expression was also elevated compared to in the CA (Table 2 and Fig. 3). Chabre O *et al.* reported that adrenal tumors stimulated to secrete CORT by any type of food intake *in vivo* were also stimulated by GIP, but not by GLP-1, *in vitro* [9]. GLP-1 has been shown to have no effect on cortisol production at concentrations of up to 10^7 pmol/L [19], while total GLP-1 concentrations in normal subjects are only elevated up to 40 pmol/L after dietary intake [23]. Furthermore, in immunohistochemical staining, the entire PA was stained GIPR-positive (Fig. 4). Thus, in our case, overexpression of GIPR in the UAA was also considered to be the cause of FDC. However, a limitation of our study is that we did not examine GPCRs other than GIPR, GLP-1R and CRHR, nor did we search for genes involved in tumor growth.

In this case, the CRH test showed CORT secretion without ACTH elevation in peripheral blood (Table 2). In previous reports, cases in which either both ACTH and CORT were non-responsive [4, 6] or both these hormones were responsive [13, 14] to CRH administration have been observed, but this is the first report of a CORT response without an ACTH response in peripheral blood. It has been reported that the expression of mRNA encoding CRHR1 and CRHR2 is very high in tissue specimens rich in adrenocortical cells, with 6-fold overexpression in AA and 10- to 60-fold overexpression in CORT-producing AA [24], which supports the observations in our case. Although CRHR1 gene expression was not observed in both the PA and CA, CRHR2 gene and protein expression was observed in both, with stronger expression in PA compared to CA (Table 2 and Fig. 3). The expression of CRHR2 is surprising, since the expression of CRHR1, which is supposed to be highly expressed in the anterior pituitary, is instead expected [25]. Splice variants called α, β, and γ have been identified in CRHR2, which are speculated to contribute to its diversity in binding efficiency or affinity with CRH and CRH-related agonists, and to its ability to acquire multiple signaling pathway activation capabilities [26]. We speculate that a splice variant of CRHR2 might have triggered cortisol overproduction, mediated by the action of CRH, for which it has a low affinity, in our case. A truncated form of CRHR2α (CRHR2α-tr) has been identified in rat amygdala. CRHR2α-tr is a truncated CRHR (approximately 26 kDa) consisting of 236 amino acids, including the first three transmembrane domains and part of the fourth transmembrane domain of CRHR2α, and has been reported to bind to CRH with low affinity, but not to other ligands [27]. As seen in Fig. 3, in our case, a strong band was observed at around 26 kDa in the PA tissue, but not in CA tissue. We speculate that this protein, which suggests a truncated splicing variant of CRHR2, might have been involved in expression of the CRH effect. Furthermore, complex formation and functional interactions between different receptors have recently been reported in G protein-coupled receptors (adenosine A1 receptor and type-1 metabotropic glutamate receptor) [28]. Hence, we speculated that the CRHR2-tr-mediated signal might functionally share or amplify the cortisol-producing signal of GIPR, which could be the reason for the cortisol secretory response to the CRH stimulation test in this case. On the other hand, ectopic ACTH production in adrenocortical cells in Cushing's syndrome has been reported in a few BMAH and UAA cases [1, 29, 30], and expression of propiomelanocortin mRNA and ACTH in BMAH has also been confirmed [31]. ACTH gradients in adrenal venous sampling have also been demonstrated in two patients with BMAH [31]. These reports led us to speculate that, in the present case, CRH might have stimulated cortisol secretion *via* paracrine secretion of ACTH locally in the AA. A limitation of our study is that we did not examine the expression of ACTH or urocortin, which are known ligands for CRHR2 [32], in PA, nor did we examine stimulation-secretion linkage *in vitro* (*e.g.*, batch incubation or perfusion experiments) or perform adrenal venous sampling. Furthermore, we consider it a limitation that we did not measure ACTH by other highly sensitive assays or bioassays.

The finding of CRH gene expression in PA and CA is interesting. In humans, cortisol has been reported to stimulate placental CRH [33]. It is possible that a positive feedback system by CORT also exists in UAA, which might be involved in the overproduction of CORT. Furthermore, we speculated that autocrine-paracrine mechanisms in the UAA might be involved in the overproduction of CORT and tumor growth. Further studies on this topic are required in the future.

In conclusion, we report an extremely rare case of FDC due to UAA with CORT secretion without ACTH elevation detected in peripheral blood by the CRH test, in which clear expression of GIPR, CRH and CRHR2 were confirmed in the surgically-resected UAA specimen by molecular and immunohistochemical analysis. In addition, we found a relative increase in mRNA expression of these receptors in the PA compared to CA, suggesting the involvement of not only GIPR, but also CRH and CRHR2 in FDC.

Acknowledgements

We wish to thank GenoStaff Co., Ltd., Tokyo, Japan,

for the Western blotting and immunohistochemical staining, and the Technical Support Center of DNA Chip Research Institute, Inc., Tokyo, Japan, for gene expression analysis by RT-PCR. We also thank the patient for her permission to publish this manuscript. Furthermore, we thank Forte Science Communications for their medical editing services.

Disclosures

Ethics approval and consent to participate

Performance of RT-PCR, Western blotting and immunohistochemical examinations on the excised tissue were approved by the clinical ethics review committee of Kagoshima Medical Center (Authorization number 21012, September 2, 2021). The patient gave written informed consent for evaluation of the tissue.

Consent for publication

Written informed consent was obtained from the patient for publication of this case report and any accompanying images.

Conflicts of interest

The authors declare no conflict of interest associated with this manuscript.

Contributions

M.M., N. Kori., N. Koji. and T.T. attended to the patient; M.M. and N. Kori. wrote the manuscript; Y.N. gave conceptual advice. N. Kori. supervised management of the case and contributed to writing and editing the manuscript. All authors have read and approved the final manuscript.

References

1. El Ghorayeb N, Bourdeau I, Lacroix A (2015) Multiple aberrant hormone receptors in Cushing's syndrome. *Eur J Endocrinol* 173: M45–M60.
2. Lacroix A, Ndiaye N, Tremblay J, Hamet P (2001) Ectopic and abnormal hormone receptors in adrenal Cushing's syndrome. *Endocr Rev* 22: 75–110.
3. Hamet P, Larochelle P, Franks DJ, Cartier P, Bolte E (1987) Cushing syndrome with food-dependent periodic hormonogenesis. *Clin Invest Med* 10: 530–533.
4. Lacroix A, Bolte E, Tremblay J, Dupre J, Poitras P, *et al.* (1992) Gastric inhibitory polypeptide-dependent cortisol hypersecretion–a new cause of Cushing's syndrome. *N Engl J Med* 327: 974–980.
5. Reznik Y, Allali-Zerah V, Chayvialle JA, Leroyer R, Leymarie P, *et al.* (1992) Food-dependent Cushing's syndrome mediated by aberrant adrenal sensitivity to gastric inhibitory polypeptide. *N Engl J Med* 327: 981–986.
6. De Herder WW, Hofland LJ, Usdin TB, de Jong FH, Uitterlinden P, *et al.* (1996) Food-dependent Cushing's syndrome resulting from abundant expression of gastric inhibitory polypeptide receptors in adrenal adenoma cells. *J Clin Endocrinol Metab* 81: 3168–3172.
7. Lebrethon MC, Avallet O, Reznik Y, Archambeaud F, Combes J, *et al.* (1998) Food-dependent Cushing's syndrome: characterization and functional role of gastric inhibitory polypeptide receptor in the adrenals of three patients. *J Clin Endocrinol Metab* 83: 4514–4519.
8. N'Diaye N, Tremblay J, Hamet P, De Herder WW, Lacroix A (1998) Adrenocortical overexpression of gastric inhibitory polypeptide receptor underlies food-dependent Cushing's syndrome. *J Clin Endocrinol Metab* 83: 2781–2785.
9. Chabre O, Liakos P, Vivier J, Chaffanjon P, Labat-Moleur F, *et al.* (1998) Cushing's syndrome due to a gastric inhibitory polypeptide-dependent adrenal adenoma: insights into hormonal control of adrenocortical tumorigenesis. *J Clin Endocrinol Metab* 83: 3134–3143.
10. Luton JP, Bertherat J, Kuhn J, Bertagna X (1998) Aberrant expression of the GIP (gastric inhibitory polypeptide) receptor in an adrenal cortical adenoma responsible for a case of food-dependent Cushing's syndrome. *Bull Acad Natl Med* 182: 1839–1850 (In French).
11. N'Diaye N, Hamet P, Tremblay J, Boutin JM, Gaboury L, *et al.* (1999) Asynchronous development of bilateral nodular adrenal hyperplasia in gastric inhibitory polypeptide-dependent Cushing's syndrome. *J Clin Endocrinol Metab* 84: 2616–2622.
12. Pralong FP, Gomez F, Guillou L, Mosimann F, Franscella S, *et al.* (1999) Food-dependent Cushing's syndrome: possible involvement of leptin in cortisol hypersecretion. *J Clin Endocrinol Metab* 84: 3817–3822.
13. Croughs RJ, Zelissen PM, van Vroonhoven TJ, Hofland LJ, N'Diaye N, *et al.* (2000) GIP-dependent adrenal Cushing's syndrome with incomplete suppression of ACTH. *Clin Endocrinol (Oxf)* 52: 235–240.
14. Tsagarakis S, Tsigos C, Vassiliou V, Tsiotra P, Pratsinis H, *et al.* (2001) Food-dependent androgen and cortisol secretion by a gastric inhibitory polypeptide-receptor expressive adrenocortical adenoma leading to hirsutism and subclinical Cushing's syndrome: *in vivo* and *in vitro* studies. *J Clin Endocrinol Metab* 86: 583–589.
15. Gerl H, Rohde W, Biering H, Schulz N, Lochs H (2000) Food-dependent Cushing's syndrome of long standing with mild clinical features. *Dtsch Med Wochenschr* 125: 1565–1568 (In German).
16. Noordam C, Hermus ARMM, Pesman G, N'Diaye N, Sweep CGJ, *et al.* (2002) An adolescent with food-dependent Cushing's syndrome secondary to ectopic

expression of GIP receptor in unilateral adrenal adenoma. *J Pediatr Endocrinol Metab* 15: 853–860.

17. Groussin L, Perlemoine K, Contesse V, Lefebvre H, Tabarin A, *et al.* (2002) The ectopic expression of the gastric inhibitory polypeptide receptor is frequent in adrenocorticotropin-independent bilateral macronodular adrenal hyperplasia, but rare in unilateral tumors. *J Clin Endocrinol Metab* 87: 1980–1985.
18. Bourdeau I, Antonini SR, Lacroix A, Kirschner LS, Matyakhina L, *et al.* (2004) Gene array analysis of macronodular adrenal hyperplasia confirms clinical heterogeneity and identifies several candidate genes as molecular mediators. *Oncogene* 23: 1575–1585.
19. Bertherat J, Contesse V, Louiset E, Barrande G, Duparc C, *et al.* (2005) *In vivo* and *in vitro* screening for illegitimate receptors in adrenocorticotropin-independent macronodular adrenal hyperplasia causing Cushing's syndrome: identification of two cases of gonadotropin/gastric inhibitory polypeptide-dependent hypercortisolism. *J Clin Endocrinol Metab* 90: 1302–1310.
20. Preumont V, Mermejo LM, Damoiseaux P, Lacroix A, Maiter D (2011) Transient efficacy of octreotide and pasireotide (SOM230) treatment in GIP-dependent Cushing's syndrome. *Horm Metab Res* 43: 287–291.
21. Ito K, Yoshii T, Shinmoto H, Kanbara T, Sumitomo M, *et al.* (2013) Laparoscopic enucleation of macronodules in a patient with ACTH-independent macronodular adrenal hyperplasia 7 years after unilateral adrenalectomy: consideration of operative procedure. *Urol Int* 90: 253–258.
22. Lecoq AL, Stratakis CA, Viengchareun S, Chaligné R, Tosca L, *et al.* (2017) Adrenal GIPR expression and chromosome 19q13 microduplications in GIP-dependent Cushing's syndrome. *JCI Insight* 2: e92184.
23. Vollmer K, Holst JJ, Baller B, Ellrichmann M, Nauck MA, *et al.* (2008) Predictors of incretin concentrations in subjects with normal, impaired, and diabetic glucose tolerance. *Diabetes* 57: 678–687.
24. Willenberg HS, Haase M, Papewalis C, Schott M, Scherbaum WA, *et al.* (2005) Corticotropin-releasing hormone receptor expression on normal and tumorous human adrenocortical cells. *Neuroendocrinology* 82: 274–281.
25. Wong ML, Licinio J, Pasternak KI, Gold PW (1994) Localization of corticotropin-releasing hormone receptor mRNA in adult rat brain by *in situ* hybridization histochemistry. *Endocrinology* 135: 2275–2278.
26. Grammatopoulos DK, Chrousos GP (2002) Functional characteristics of CRH receptors and potential clinical applications of CRH-receptor antagonists. *Trends Endocrinol Metab* 13: 436–444.
27. Miyata I, Shiota C, Ikeda Y, Oshida Y, Chaki S, *et al.* (1999) Cloning and characterization of a short variant of the corticotropin-releasing factor receptor subtype from rat amygdala. *Biochem Biophys Res Commun* 256: 692–696.
28. Kamikubo Y, Tabata T, Sakairi H, Hashimoto Y, Sakurai T (2015) Complex formation and functional interaction between adenosine A1 receptor and type-1 metabotropic glutamate receptor. *J Pharmacol Sci* 128: 125–130.
29. El Ghorayeb N, Bourdeau I, Lacroix A (2017) Pathophysiology and genetic landscape of adrenocortical tumors and hyperplasias. In: Levine A (ed) Adrenal disorders: physiology, pathophysiology and treatment. Humana Press, Totowa, USA: 147–171.
30. Mazzuco TL, Thomas M, Martinie M, Cherradi N, Sturm N, *et al.* (2007) Cellular and molecular abnormalities of a macronodular adrenal hyperplasia causing beta-blocker-sensitive Cushing's syndrome. *Arq Bras Endocrinol Metabol* 51: 1452–1462.
31. Louiset E, Duparc C, Young J, Renouf S, Tetsi Nomigni M, *et al.* (2013) Intraadrenal corticotropin in bilateral macronodular adrenal hyperplasia. *N Engl J Med* 369: 2115–2125.
32. Hashimoto K, Makino S, Asaba K, Nishiyama M (2001) Physiological roles of corticotropin-releasing hormone receptor type 2. *Endocr J* 48: 1–9.
33. Robinson BG, Emanuel RL, Frim DM, Majzoub JA (1988) Glucocorticoid stimulates expression of corticotropin-releasing hormone gene in human placenta. *Proc Natl Acad Sci U S A* 85: 5244–5248.

Internal Medicine
The Japanese Society of Internal Medicine
doi: 10.2169/internalmedicine.1496-22
Intern Med 62: 3373-3379, 2023
http://internmed.jp

【 CASE REPORT 】

A Rare Case of Painless Destructive Thyroiditis Resulting in Thyroid Storm

Miwa Makino[1,2], Nobuyuki Koriyama[1], Nami Kojima[1,2] and Yoshihiko Nishio[2]

Abstract:
Thyroid storm is a life-threatening clinical condition that is usually triggered by untreated or interrupted treatment of Graves' disease, leading to the sudden onset of severe thyrotoxicosis, which requires an immediate diagnosis and treatment based on diagnostic criteria. Cases of thyroid storm caused by painless/painless subacute thyroiditis are very rare. We herein report an 85-year-old man with features of severe thyrotoxicosis caused by painless/painless subacute thyroiditis who had no uptake of $^{99m}TcO_4$ and was negative for thyroid-stimulating hormone receptor antibodies. In thyroid storm patients in whom the findings are inconsistent with Graves' disease, careful follow-up and management are necessary, assuming the possibility of painless or painless subacute thyroiditis.

Key words: thyroid storm, painless thyroiditis, thyrotoxicosis

(Intern Med 62: 3373-3379, 2023)
(DOI: 10.2169/internalmedicine.1496-22)

Introduction

Thyroid storm is a life-threatening situation caused by high thyroid hormone levels and physical stress, leading to multiple organ failure. A high fever, circulatory failure, impaired consciousness, diarrhea, jaundice, and other symptoms are common in thyroid storm. The treatment includes antithyroid medication, inorganic iodine, and corticosteroids. Although most cases are caused by poorly controlled Graves' disease, other causes, such as thyroid-stimulating hormone (TSH)-producing tumors and destructive thyroiditis (due to immune checkpoint inhibitors, amiodarone, or lithium therapy), have also been reported (1, 2).

Painless thyroiditis is usually characterized by mild to moderate thyrotoxicosis, moderate goiter, a low radioiodine uptake, and negativity for TSH receptor antibodies. Histologically, the thyroid gland shows lymphocytic infiltration, sometimes with germinal centers, focal Hürthle cell changes, and/or focal hyperplasia of the thyroid epithelium surrounding the areas of lymphocytic infiltration (3). Painless thyroiditis is an autoimmune-mediated inflammation of the thyroid gland, with release of thyroid hormones resulting in transient hyperthyroidism, lasting about two months before recovery, and usually does not require treatment. Subsequently, a period of hypothyroidism often ensues, before recovery of the thyroid function. The timing of the transition to permanent hypothyroidism can be early or late, ranging from many years to decades later (4).

Subacute thyroiditis tends to present with pain in the anterior neck followed by upper respiratory tract infection or sore throat and is postulated as being caused by viral infection. Inflammatory symptoms, such as nodular or diffuse enlargement of the goiter with spontaneous pain, tenderness and a fever, are also seen, as are symptoms of thyrotoxicosis, such as palpitations (5). Echography shows an indistinct hypoechoic area with reduced blood flow signals, in line with the induration, enlargement or pain, and in about 60% of cases, enlarged lymph nodes around the thyroid gland are reported (6) It is rare in children and the elderly (7), and most cases heal within a few months, although about 20% relapse during recovery (8, 9), and 15% develop permanent hypothyroidism (9).

We herein report a rare case of a patient who developed thyroid storm secondary to painless destructive thyroiditis.

[1]Department of Diabetes and Endocrinology, National Hospital Organization, Kagoshima Medical Center, Japan and [2]Department of Diabetes and Endocrine Medicine, National Hospital Organization Kagoshima Medical Center, Japan
Received: December 23, 2022; Accepted: February 23, 2023; Advance Publication by J-STAGE: April 7, 2023
Correspondence to Dr. Nobuyuki Koriyama, koriyama.nobuyuki.wm@mail.hosp.go.jp

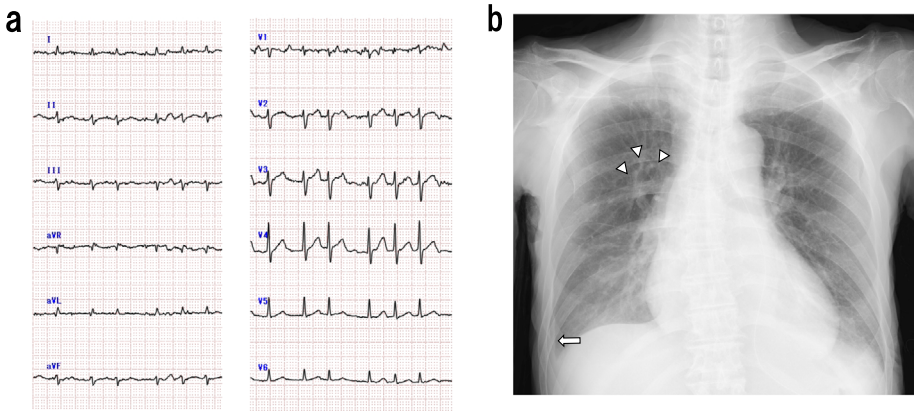

Figure 1. Electrocardiography and chest radiography findings. a) Electrocardiography showed tachycardic atrial fibrillation. b) Posteroanterior chest radiography. The arrowheads indicate peribronchial cuffing, and the arrow indicates pleural thickening-like findings.

Case Report

An 85-year-old Japanese man (163.0 cm tall, weighing 50.7 kg, body mass index 19.1 kg/m^2) with atrial fibrillation and Lewy body dementia presented to the emergency department of another hospital with a fever and palpitations (Day 0). The fever and palpitations did not improve despite the use of antipyretics, and the patient was admitted to the hospital six days later with congestive heart failure.

Laboratory tests after admission revealed thyrotoxicosis with TSH <0.007 μIU/mL [normal value (NV): 0.61-4.23] and free T4 >7.77 ng/dL (NV: 0.76-1.65). Fifteen milligrams of thiamazole was started on Day 10 but was discontinued because of TSH receptor antibody (TRAb) negativity. On the same day, he developed psychiatric symptoms, watery diarrhea, and a high fever of 40.6°C. Due to suspicion of thyroid storm, the patient was urgently transferred to our hospital and admitted to our department.

A physical examination on admission showed an impaired consciousness (Glasgow Coma Scale score: E3V2M5), fever of 38-40°C, blood pressure of 85/53 mmHg, peripheral oxygen saturation on pulse oximetry (SpO_2) of 97.0% under 1 L/min oxygen via a nasal cannula, and tachycardia with arrhythmia (136 beats/min). There was no cervical swelling, and no vascular murmur was noted. Coarse crackles were present in both lung fields, and intestinal peristalsis was increased. An electrocardiogram showed tachycardic atrial fibrillation (132/min) with no ST-T changes (Fig. 1a). Chest X-ray demonstrated congestion in the lung fields bilaterally, along with pleural effusion and peribronchial cuffing, with a cardiothoracic ratio of 59.7% (Fig. 1b). An ultrasound examination of the thyroid gland showed no glandular enlargement (estimated thyroid volume approximately 17 g) and no hypervascularization. The thyroid parenchyma showed heterogeneous echogenicity, with a hypoechoic area 14 mm in size in the left lobe (Fig. 2).

The laboratory findings at the time of admission showed an increased leukocyte count [white blood cells (WBCs)] with leftward nuclear migration, elevated C-reactive protein (CRP) levels, mild anemia, and coagulation abnormalities [WBCs 21,820/μL, neutrophils 201,000/μL lymphocytes 1,100/μL, CRP level 4.89 mg/dL, hemoglobin (Hb) level 10.1 g/dL, prothrombin time-international normalized ratio (PT-INR) 2.09, fibrinogen degradation product level 6.32 μg/mL, and D-dimer (D-D) level 1.72 μg/mL] (Table). In addition, elevated alkaline phosphatase (ALP), γ-glutamyltransferase (γ-GTP), direct bilirubin (D-Bil), adrenocorticotropic hormone (ACTH), cortisol (CORT), and brain natriuretic peptide (BNP) values (ALP 172 U/L, γ-GTP 131 U/L, D-Bil 0.58 mg/dL, ACTH 211 pg/mL, CORT 20.2 μg/dL and BNP 497.5 pg/dL) and a decrease in the estimated glomerular filtration rate (eGFR) and albumin (Alb) level (eGFR 40.7 mL/min/1.73 m^2 and Alb 2.42 g/dL) were observed (Table).

The results of endocrinological tests were as follows: TSH: 0.028 μIU/mL; free T4: 5.27 ng/dL; and free T3: 14.32 pg/mL (NV: 2.48-4.14). Since the patient's laboratory test findings met the diagnostic criteria of thyrotoxicosis, and given that he had relevant symptoms, such as central nervous system effects, a fever, tachycardia, cardiovascular dysfunction, and watery diarrhea, thyroid storm was diagnosed as the probable cause of his condition (2, 3).

The patient was subsequently admitted to the intensive care unit for intensive monitoring. Oxygen was administered via a nasal cannula at 4-5 L/min on day 1, with maintenance of SpO_2 at 94-96%; after day 2, similar SpO_2 levels were maintained by an oxygen flow of 1-2 L/min via nasal cannula. He was cooled and managed with a continuous infusion of landiolol (3 γ), 5 mg propranolol, hydrocortisone (100 mg ×8 h), 30 mg thiamazole, and 200 mg iodide administered orally via a gastric tube. With this treatment, his level of consciousness improved to E4V4M5 the next day, and his thyroid hormone levels improved relatively quickly to free T4 of 1.85 ng/dL and free T3 of 5.5 pg/mL on the 6th day from the start of treatment. Since the patient's heart rate remained under control from the second day of starting treatment, the dose of propranolol was increased to 7.5 mg,

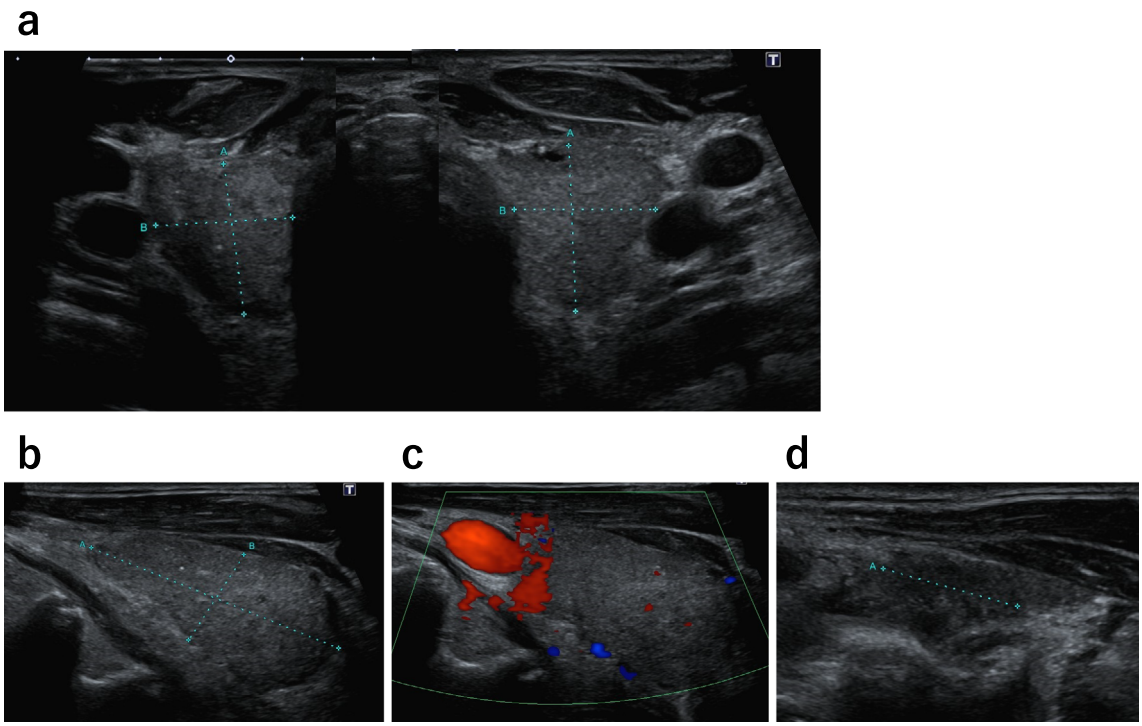

Figure 2. **Thyroid ultrasound. a) The thyroid gland showed no enlargement and presented heterogeneous parenchyma. b) Right thyroid lobe in a sagittal view (41×21×19 mm). c) Thyroid doppler ultrasound showed no hypervascularization. d) Sagittal view of the left thyroid lobe (42×23×17 mm) showed the presence of a 14-mm hypoechoic area. The estimated thyroid volume was approximately 17 g.**

and landiolol was reduced to 2 γ following the advice of the cardiologist. Landiolol was further reduced to 1 γ on the 4th day and discontinued on the 5th day. Subsequently, propranolol was reduced to 5 mg on the 13th day, and to 2.5 mg on the 23rd day.

Since the patient's thyroglobulin levels were elevated [537 ng/mL (NV: ≤33.7)] with the various thyroid antibody titers remaining within normal limits [anti-thyroglobulin antibody: 11.1 IU/mL (NV: <28.0); anti-thyroid peroxidase antibody: 4.7 IU/mL (NV: <16.0); TRAb (3rd): 0.7 IU/L (NV: <2.0), and thyroid-stimulating antibody (TSAb): 104% (NV: ≤120)], the possibility of transient thyrotoxicosis caused by thyroid follicular cell destruction was considered. In addition, although the patient received daily doses of rivaroxaban 10 mg, azosemide 30 mg, donepezil 5 mg, levodopa 200 mg/benserazide hydrochloride 50 mg, ramelteon 8 mg, lemborexant 5 mg, and 1.5 mg of clonazepam prior to the onset of thyroid storm, induction of thyroiditis by these drugs was ruled out.

Since there were several criteria that were inconsistent with Graves' disease, such as rapid improvement of the thyroid hormone levels and TRAb or TSAb negativity, scintigraphy was performed to identify the cause of the thyrotoxicosis. Scintigraphy of the thyroid gland showed a radioactive $^{99m}TcO_4$ uptake of 0% (TSH value 0.813 μIU/mL following a 50-mg dose of inorganic iodine administration on day 12), confirming the diagnosis of thyrotoxicosis due to destructive thyroiditis (Fig. 3). The patient's thyroid hormone levels normalized after 10 days without recurrence after tapering of hydrocortisone, thiamazole, and iodide. However, because of a further reduction in the thyroid hormone levels and a TSH value of 11.9 μIU/mL on Day 26, levothyroxine replacement therapy was started. The patient's level of consciousness did not improve beyond the Glasgow Coma Scale (GCS) score of E4V4M5 on day 2 of admission, probably due in part to Lewy body dementia, and he had difficulty with oral intake. However, his body weight increased by about 2 kg. On day 54, the patient was transferred back to the referring hospital to continue levothyroxine supplementation (Fig. 4).

Discussion

We suspected that physiological stress resulting from infectious disease had increased the ACTH levels via stimulation by inflammatory cytokines, such as Interleukin-6, leading to increased cortisol secretion, so we ruled out concomitant adrenal insufficiency.

Our patient had thyrotoxicosis with central nervous system symptoms, a fever over 38°C, tachycardia over 130/min, heart failure symptoms, and watery diarrhea, which led us to definitively diagnose him with thyroid storm (10). An evaluation using the Burch-Wartofsky point scale (11) also revealed a total score of 75 points, indicating a strong possibility of thyroid storm. However, the low total GCS score of 10 points in this patient only improved to 13 points despite

Table. Laboratory Findings on Admission.

Peripheral blood	WBC	21,820 /μL	(3,300-8,600)
	NEUT (Neut)	20.1 (92.0) $\times10^3$/μL (%)	[1.50-7.50 (42.0-74.0)]
	LYMPH (Lymph)	1.1 (5.0) $\times10^3$/μL (%)	[1.00-4.00 (18.0-50.0)]
	RBC	330 $\times10^4$/μL	(435-555)
	Hb	10.1 g/dL	(13.7-16.8)
	MCV	86.1 fL	
	MCH	30.6 pg	
	MCHC	35.6 g/dL	(31.7-35.3)
	HCT	28.4 %	(40.7-50.1)
	PLT	22.4 $\times10^4$/μL	
Coagulation profile	PT	34 %	(82.7-117.7)
	PT-INR	2.09	(0.98-1.08)
	APTT	30.3 s	
	Fib	390 mg/dL	
	FDP	6.32 μg/mL	(<5)
	D-dimer	1.72 μg/mL	(<1)
Biochemistry	AST	33 U/L	
	ALT	15 U/L	
	LDH	221 U/L	
	ALP	172 U/L	(38-113)
	γ-GTP	131 U/L	(13-64)
	T-Bil	0.94 mg/dL	
	D-Bil	0.58 mg/dL	(0.00-0.30)
	CK	124 U/L	
	TP	5.39 g/dL	(6.60-8.10)
	Alb	2.42 g/dL	(4.10-5.10)
	BUN	29.7 mg/dL	(8.0-20.0)
	CRE	1.3 mg/dL	(0.65-1.07)
	eGFR	40.7 mL/min/1.73 m^2	(60<)
	FPG	104 mg/dL	
	CRP	4.89 mg/dL	(0.00-0.14)
	Na	138 mmol/L	
	K	3.9 mmol/L	
	Cl	102 mmol/L	
Urinalysis	Protein	(-)	
	WBC	(-)	
	Occult blood	(-)	
Others	ACTH	211 pg/mL	(7.2-63.3)
	CORT	20.2 μg/dL	(7.1-19.6)
	BNP	497.5 pg/mL	(0.0-18.4)
	SARS-CoV-2 PCR	(-)	

The reference ranges of data showing abnormal values are shown in brackets. WBC: white blood cell, NEUT: neutrophil (absolute value), Neut: neutrophil (percentage), LYMPH: lymphocyte (absolute value), Lymph: lymphocyte (percentage), RBC: red blood cell, Hb: hemoglobin, MCV: mean corpuscular volume, MCH: mean corpuscular hemoglobin, MCHC: mean corpuscular hemoglobin concentration, HCT: hematocrit, PLT: platelets, PT: prothrombin time, PT-INR: prothrombin time-international normalized ratio, APTT: activated partial thromboplastin time, Fib: fibrinogen, FDP: fibrin/fibrinogen degradation products, AST: aspartate aminotransferase, ALT: alanine aminotransferase, LDH: lactate dehydrogenase, ALP: alkaline phosphatase, γ-GTP: γ-glutamyltransferase, ChE: cholinesterase, T-Bil: total bilirubin, D-Bil: direct bilirubin, CK: creatine kinase, TP: total protein, Alb: albumin, Na: sodium, K: potassium, Cl: chloride, BUN: blood urea nitrogen, CRE: creatinine, UA: uric acid, eGFR: estimated glomerular filtration rate, FPG: fasting blood glucose, CRP: C-reactive protein, ACTH: adrenocorticotropic hormone, CORT: cortisol, BNP: brain natriuretic peptide, SARS-CoV-2: severe acute respiratory syndrome coronavirus 2

a rapid recovery of his other symptoms, suggesting the difficulty in making judgments regarding central nervous system symptoms in cases complicated by dementia.

In the present case, although thyroid storm was definitively diagnosed by two different sets of criteria, the clinical picture was confounded by the absence of multiorgan failure (12) and limited improvement in neurological symptoms with treatment. Thyroid storm is a very rare condition with

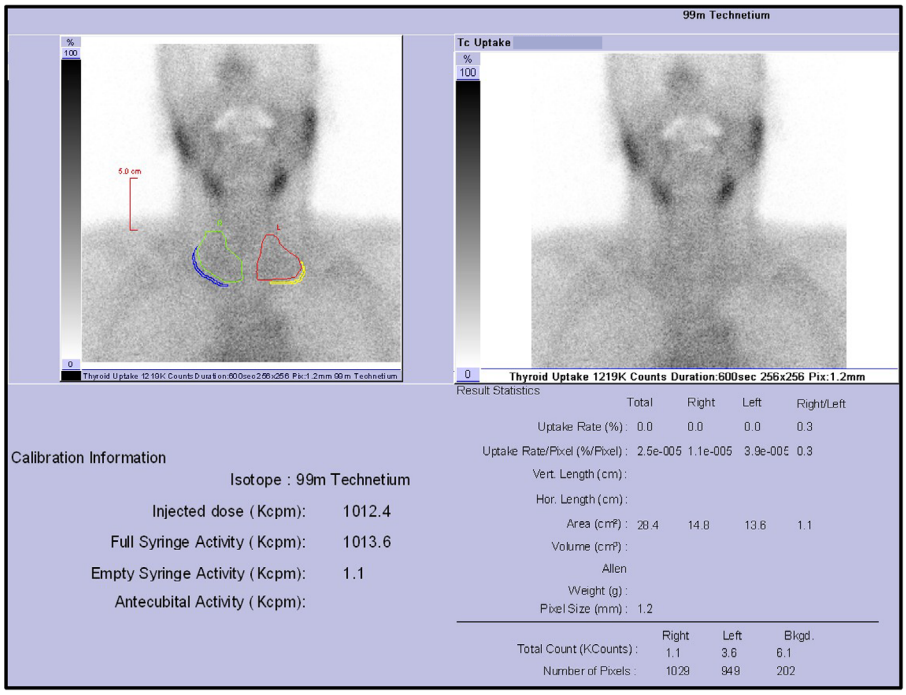

Figure 3. **Thyroid static imaging with $^{99m}TcO_4$ showed a decreased uptake in the thyroid gland (0%).**

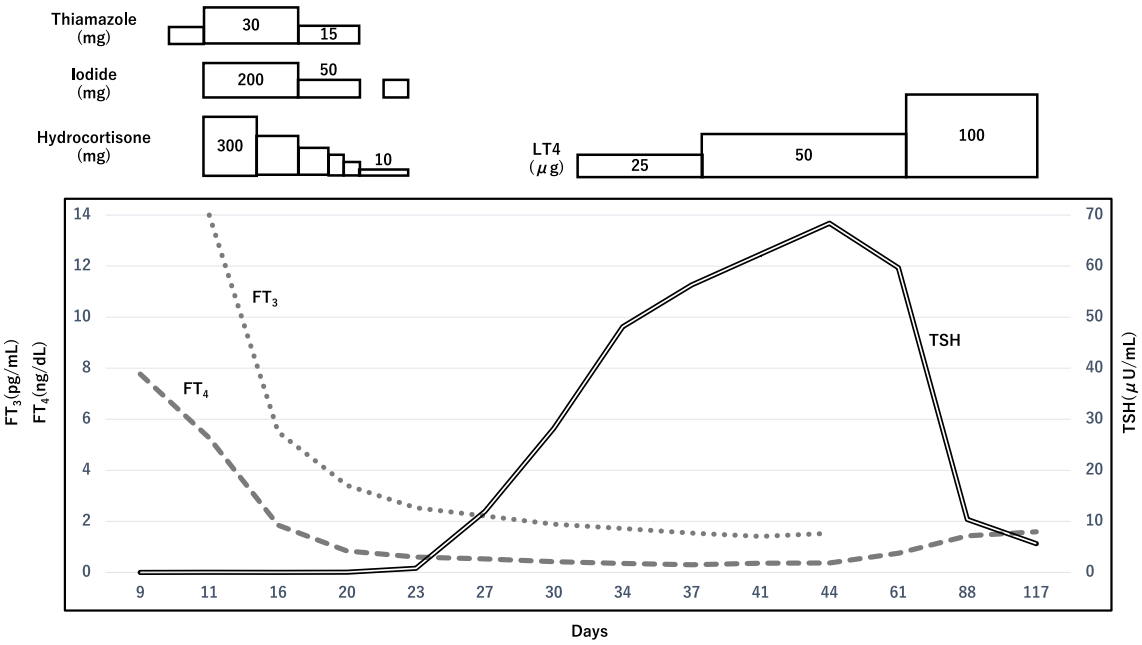

Figure 4. **The patient's clinical course. Treatment for thyroid storm that was presumed to be caused by Grave's disease was commenced after the patient's admission to the hospital. Subsequently, the patient's thyroid hormone levels improved relatively quickly and normalized without recurrence after tapering of hydrocortisone, thiamazole, and iodide. Thereafter, the further reduction of hormone levels continued, and levothyroxine replacement therapy was started on Day 29.**

an annual incidence of just two cases per million people in Japan (10). It consists of severe hyperthyroidism with physiologic decompensation of one or more organ systems and carries a relatively high mortality rate (about 10%) (10, 13, 14). Graves' disease is the most common causative disease (about 98%), in which withdrawal of antithyroid therapy might trigger thyroid storm (10). In contrast, since destructive thyroiditis typically causes only mild to moderate thyrotoxicosis, it only rarely causes thyroid storm. In a nationwide survey conducted in Japan in 2012, only 5

cases of destructive thyroiditis were reported among 356 with thyroid storm (10), although there have been reports of subacute thyroiditis (15-19) and drug (immune checkpoint inhibitors, amiodarone, or lithium)-induced destructive thyroiditis leading to thyroid storm (1, 2).

A literature search revealed only one previous report of painless thyroiditis causing thyroid storm (20), indicating that it is extremely rare. The reason why thyroid storm due to subacute thyroiditis is reported more frequently than that due to painless thyroiditis is because subacute thyroiditis produces a strong inflammatory response, which might lead to thyroid storm due to the production of inflammatory cytokines and their effect on thyroid hormone metabolism (13). Furthermore, it has been reported that subacute thyroiditis is significantly more prone to causing hypoalbuminemia than painless thyroiditis (21), and the state of physical wasting due to intense inflammation might be a contributing factor. It is interesting that the case reported by Harada et al. was confirmed at pathological autopsy to be advanced chronic thyroiditis, possibly atrophic thyroiditis (20), and that the laboratory findings and course of the disease were very similar to those of our case.

In the present case, we were unable to identify any obvious risk factors for the development of thyroid storm. Given the elevated WBC and neutrophil counts and CRP level at the time of admission (Table), and the fact that the risk factors for Graves' disease leading to thyroid storm include infection and stress, in addition to those related to treatment and examinations, we speculate that some infection might have been involved in this case. A thyroid storm might occur in an elderly person with physiological impairment following the induction of thyrotoxicosis by painless thyroiditis and when the patient is under some kind of stress or infection. The mortality rate has been reported to be significantly higher in older patients with thyroid crisis than in younger patients (14). It is speculated that the low frequency of typical symptoms and the coexistence of nonspecific signs and symptoms caused by other diseases and aging might delay the diagnosis and treatment in this patient group (22), so they require more careful attention than others.

In cases of thyroid storm due to destructive thyroiditis, antithyroid drugs and inorganic iodine are ineffective and should not be administered. However, in the present case, it took five days for the TSH receptor antibody status to be known. In medical institutions where a real-time definitive diagnosis is as difficult as in our hospital, we believe that the high mortality rate of thyroid storm and the infrequency of the causative disease should not deter the prompt initiation of treatment (including the administration of antithyroid drugs and inorganic iodine) as in thyroid storm due to Graves' disease. However, if Graves' disease is ruled out, antithyroid drugs and inorganic iodine, which are ineffective for thyrotoxicosis due to destructive thyroiditis, should be promptly and rapidly discontinued, since high doses of antithyroid drugs can cause adverse drug reactions, such as liver dysfunction and agranulocytosis, which require careful monitoring.

In the present case, the diagnosis of destructive thyroiditis was made with an emphasis on the radioactive $^{99m}TcO_4$ uptake of 0%, but its diagnostic accuracy is limited by the fact that the result was obtained after a large dose of inorganic iodine had been administered.

Thyrotoxicosis varies in severity, and its course is usually not protracted and might not require treatment. However, about 10% of patients with painless thyroiditis have recurrent episodes, and several authors have reported troublesome and recurrent cases requiring total thyroidectomy or radioactive iodine therapy. In our case, however, since a hypoechoic area was identified in the left lobe of the thyroid gland on ultrasound (Fig. 2d) and his CRP level was elevated (4.89 mg/dL) (Table), the possibility of painless subacute thyroiditis, which Neupane et al. reported as a cause of an unknown fever (23), could not be excluded.

Recently, cases of painless subacute thyroiditis have been reported in relation to COVID-19 infection (24). However, there have been no reports of painless subacute thyroiditis leading to thyroid storm, and if painless subacute thyroiditis was indeed the cause of the destructive thyroiditis in our case, this would make it the first such report. A limitation of this report is that we were unable to confirm the histological findings in the thyroid gland.

Conclusion

We herein report a rare case of thyroid storm presumably due to painless thyroiditis or painless subacute thyroiditis. The triggers for this patient's thyroid storm were not clear. Thyroid storm is a highly fatal condition that should be diagnosed and treated promptly using diagnostic criteria. While Graves' disease is the most common cause of thyroid storms, in cases with contradictory findings, the possibility of destructive thyroiditis, such as painless thyroiditis or painless subacute thyroiditis, should also be considered.

Written, informed consent was obtained from the patient and his family for publication of this case report and all accompanying images.

The authors state that they have no Conflict of Interest (COI).

Acknowledgement

The authors wish to thank the patient and his family for their permission to publish this manuscript.

References

1. McMillen B, Dhillon MS, Yong-Yow S. A rare case of thyroid storm. BMJ Case Rep **2016**: bcr2016214603, 2016.
2. Raza MA, Jain A, Mumtaz M, et al. Thyroid storm in a patient on chronic amiodarone treatment. Cureus **14**: e24164, 2022.
3. Mizukami Y, Michigishi T, Hashimoto T, et al. Silent thyroiditis: a histologic and immunohistochemical study. Hum Pathol **19**: 423-

431, 1988.
4. Akamizu T, Amino N. Hashimoto's Thyroiditis. In: Endotext [Internet]. Feingold KR, Anawalt B, Blackman MR, et al., Eds. MDText.com, South Dartmouth, 2017 Jul 17 [cited 2023 Feb 10]. Available from: https://www.ncbi.nlm.nih.gov/books/NBK285557/
5. Hennessey Jv. Subacute Thyroiditis. In: Endotext [Internet]. Feingold KR, Anawalt B, Blackman MR, et al., Eds. MDText.com, South Dartmouth, 2018 Jun 12 [cited 2023 Feb 10]. Available from: https://www.ncbi.nlm.nih.gov/books/NBK279084/
6. Frates MC, Marqusee E, Benson CB, et al. Subacute granulomatous (de Quervain) thyroiditis: grayscale and color Doppler sonographic characteristics. J Ultrasound Med **32**: 505-511, 2013.
7. Nishihara E, Ohye H, Amino N, et al. Clinical characteristics of 852 patients with subacute thyroiditis before treatment. Intern Med **47**: 725-729, 2008.
8. Mizukoshi T, Noguchi S, Murakami T, et al. Evaluation of recurrence in 36 subacute thyroiditis patients managed with prednisolone. Intern Med **40**: 292-295, 2001.
9. Fatourechi V, Aniszewski JP, Fatourechi GZ, et al. Clinical features and outcome of subacute thyroiditis in an incidence cohort: Olmsted County, Minnesota, study. J Clin Endocrinol Metab **88**: 2100-2105, 2003.
10. Akamizu T, Satoh T, Isozaki O, et al.; Japan Thyroid Association. Diagnostic criteria, clinical features, and incidence of thyroid storm based on nationwide surveys. Thyroid **22**: 661-679, 2012.
11. Burch HB, Wartofsky L. Life-threatening thyrotoxicosis. Thyroid storm. Endocrinol Metab Clin North Am **22**: 263-277, 1993.
12. Angell TE, Lechner MG, Nguyen CT, et al. Clinical features and hospital outcomes in thyroid storm: a retrospective cohort study. J Clin Endocrinol Metab **100**: 451-459, 2015.
13. Akamizu T. Thyroid storm: a Japanese perspective. Thyroid **28**: 32-40, 2018.
14. Ono Y, Ono S, Yasunaga H, et al. Factors associated with mortality of thyroid storm: analysis using a national inpatient database in Japan. Medicine (Baltimore) **95**: e2848, 2016.
15. Sherman SI, Simonson L, Ladenson PW. Clinical and socioeconomic predispositions to complicated thyrotoxicosis: a predictable and preventable syndrome? Am J Med **101**: 192-198, 1996.
16. Swinburne JL, Kreisman SH. A rare case of subacute thyroiditis causing thyroid storm. Thyroid **17**: 73-76, 2007.
17. Salih AM, Kakamad FH, Rawezh QS, et al. Subacute thyroiditis causing thyrotoxic crisis; a case report with literature review. Int J Surg Case Rep **33**: 112-114, 2017.
18. Gaballa S, Hlaing KM, Bos N, et al. A rare case of subacute painful thyroiditis causing thyroid storm and a successful trial of propylthiouracil. Cureus **29**: e9461, 2020.
19. Newman K, Walthall L. A case of thyroid storm caused by thyroiditis. J Investig Med High Impact Case Rep **10**: 23247096221129468, 2022.
20. Harada Y, Handa M, Koyama K, et al. Atypical case of thyroid storm revealed by autopsy. Int J Case Rep Short Rev **3**: 49-52, 2017.
21. Yanai H, Hakoshima M, Katsuyama H. Differences in clinical and laboratory findings among Graves' disease, painless thyroiditis and subacute thyroiditis patients with hyperthyroidism. J Endocrinol Metab **9**: 37-42, 2019.
22. Goichot B, Caron P, Landron F, et al. Clinical presentation of hyperthyroidism in a large representative sample of outpatients in France: relationships with age, aetiology and hormonal parameters. Clin Endocrinol (Oxf) **84**: 445-451, 2016.
23. Neupane B, Karki S, Tirthani E, et al. A case of painless subacute thyroiditis presenting as fever of unknown origin. Cureus **14**: e24949, 2022.
24. Dolkar T, Jitidhar F, Patel MJ, et al. Painless subacute thyroiditis in a patient with acute COVID-19 infection: a transient event. Cureus **14**: e26924, 2022.

Received: 6 July 2023 | Revised: 6 September 2023 | Accepted: 13 September 2023

DOI: 10.1111/cup.14539

CASE STUDY

JOURNAL OF CUTANEOUS PATHOLOGY WILEY

Apocrine carcinoma with marked sebocyte-like cytological features: A report of two cases

Natsuko Sasaki-Saito MD, PhD[1,2] | Keisuke Goto MD[1,3,4,5,6,7,8,9,10] | Megumi Aoki MD[1] | Katsuhiko Nishihara MD[1] | Tsubasa Hiraki MD, PhD[3] | Shusuke Yoshikawa MD[11] | Shigeto Matsushita MD, PhD[1]

[1]Department of Dermato-Oncology/Dermatology, National Hospital Organization Kagoshima Medical Center, Kagoshima, Japan

[2]Department of Dermatology, University of Occupational and Environmental Health, Kitakyushu, Japan

[3]Department of Diagnostic Pathology, Shizuoka Cancer Center Hospital, Sunto, Japan

[4]Department of Pathology, Tokyo Metropolitan Cancer and Infectious Disease Center Komagome Hospital, Tokyo, Japan

[5]Department of Pathology, Itabashi Central Clinical Laboratory, Tokyo, Japan

[6]Department of Anatomic Pathology, Tokyo Medical University, Tokyo, Japan

[7]Department of Diagnostic Pathology, Chutoen General Medical Center, Kakegawa, Japan

[8]Department of Diagnostic Pathology and Cytology, Osaka International Cancer Institute, Osaka, Japan

[9]Department of Diagnostic Pathology, Osaka National Hospital, Osaka, Japan

[10]Department of Dermatology, Hyogo Cancer Center, Akashi, Japan

[11]Department of Dermatology, Shizuoka Cancer Center Hospital, Sunto, Japan

Correspondence
Keisuke Goto, Department of Dermato-Oncology/Dermatology, National Hospital Organization Kagoshima Medical Center, Kagoshima, Japan.
Email: goto.keisuke@icloud.com

Funding information
Japan Society for the Promotion of Science, KAKENHI, Grant/Award Number: JP22K06994

Abstract

Apocrine carcinoma cases with sebaceous differentiation have not been reported and can be misdiagnosed as sebaceous carcinoma. We present two cases of apocrine carcinoma with marked sebocyte-like cytological features. Tumors were observed in the left axilla of a 68-year-old man (Case 1) and the right axilla of a 72-year-old man (Case 2). Both patients presented with multiple lymph node metastases. Histopathology revealed densely distributed solid nests of tumor cells containing foamy cytoplasm and enlarged round nuclei with prominent nucleoli. The tumor cells diffusely expressed adipophilin, PRAME (cytoplasmic pattern), androgen receptor, BerEP4, and GCDFP15 but did not express p63 in both cases. *PIK3CA* E726K and H1047R mutations were detected in Cases 1 and 2, respectively. Tumor location in the axilla, the presence of eosinophilic granular cytoplasm, prominent nucleoli, and *PIK3CA* mutations, immunoreactivity for BerEP4 and GCDFP15, and lack of p63 immunoexpression findings matched apocrine carcinoma characteristics, but not sebaceous carcinoma. Thus, apocrine carcinoma can demonstrate intracytoplasmic lipid accumulation and rarely exhibit sebocyte-like cytological features. Apocrine carcinoma should be distinguished from sebaceous carcinoma due to the former's higher metastatic potential and lack of association with Muir–Torre syndrome.

KEYWORDS
adipophilin, apocrine carcinoma, *PIK3CA*, sebaceous carcinoma, sebaceous differentiation

1 | INTRODUCTION

From the perspective of tumor cell differentiation, cutaneous appendageal tumors can be classified into those with apocrine, eccrine, follicular, or sebaceous differentiation, each of which includes several benign and malignant tumor types.[1] Most tumors usually present with one type of cellular differentiation; however, several cases of cutaneous appendageal tumors with biphenotypic or multilineage differentiation have been reported. For instance, there have been case reports previously of sebaceoma with apocrine differentiation[2–4] and sebaceous carcinoma with apocrine differentiation.[2,5–8] Follicular or apocrine/eccrine tumors often show sebaceous differentiation. For example, trichoblastoma, basal cell carcinoma, apocrine mixed tumor, poroma, porocarcinoma, microcystic adnexal carcinoma, and adenoid cystic carcinoma can exhibit sebaceous differentiation.[9–14] Generally, it is considered that adnexal tumors with apocrine, follicular, or sebaceous differentiation can show another cell differentiation of the folliculo-sebaceous-apocrine unit. However, there have been no reports of apocrine carcinoma with sebaceous differentiation.

Herein, we bridge this gap and present two cases of apocrine carcinoma with sebocyte-like cytological features.

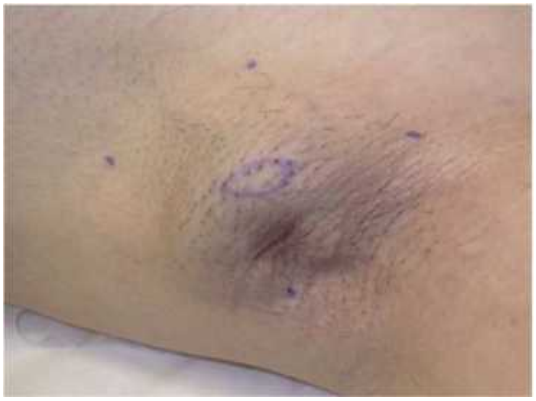

FIGURE 1 Clinical findings of Case 1. A 7.5 × 5.0 cm subcutaneous mass was seen in the patient's left axilla before chemotherapy.

2 | CASE REPORTS

The study has been approved by the research ethics committees of KMC (Ref: 2023-1) and SCCH (Ref: T2023-16).

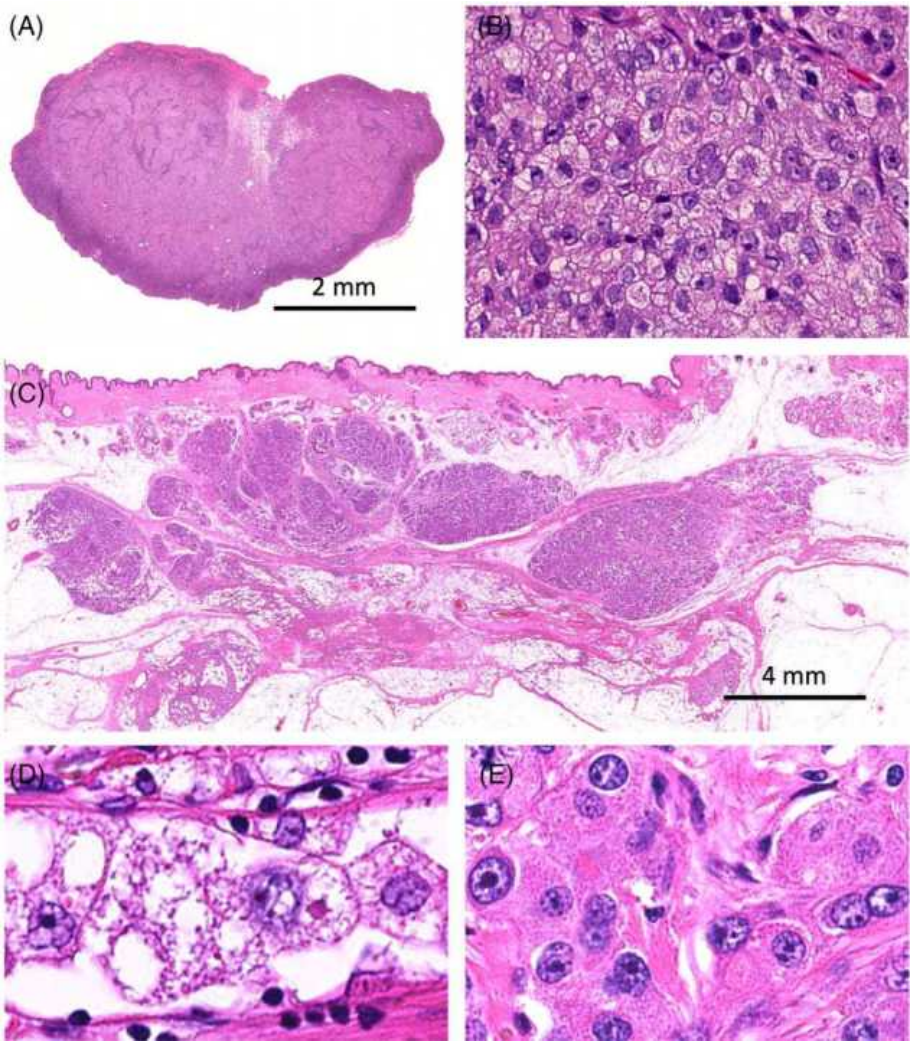

FIGURE 2 Histopathologic findings of Case 1. (A) Whole biopsy section before chemotherapy (H&E stain, ×20). (B) Vacuolated or foamy cytoplasm in the tumor cells (H&E stain, ×600). (C) Excised specimen section after chemotherapy (H&E stain, ×10). (D) Vacuolated tumor cells with degeneration due to chemotherapy (H&E stain, ×1000). (E) Eosinophilic granular cytoplasm of the tumor cells, which can often be seen in typical apocrine carcinoma (H&E stain, ×1000).

2.1 | Case 1

A 68-year-old man presented with a subcutaneous tumor (7.5 × 5.0 cm) in the left axilla (Figure 1). The tumor had grown gradually and irregularly for 2 years. Positron emission tomography–computed tomography revealed multiple lymph node metastases with a maximum diameter of 45 mm. After a diagnosis of apocrine carcinoma was made by evaluating the biopsy sample, dose-dense therapy with doxorubicin and cyclophosphamide and other chemotherapies (carboplatin, paclitaxel, and pembrolizumab) were administered as neoadjuvant therapies. The tumor decreased in size (partial response) and was excised. Lymph node dissection revealed multiple metastases to the axillary and cervical lymph nodes.

Tumor biopsy revealed fragmented tumor tissue composed of solid tumor nests without glandular structures (Figure 2A). Numerous tumor cells harbored foamy cytoplasm (Figure 2B). The tumor excision revealed a subcutaneous multinodular tumor with a central fibrosing scar (Figure 2C). No glandular formation was seen. The tumor cells had sebocyte-like bubbly cytoplasm (Figure 2D) or eosinophilic granular cytoplasm (Figure 2E). Both tumor cell types had prominent nucleoli (Figure 2D,E). Cytoplasmic degeneration due to chemotherapy was observed in most of the tumor cells (Figure 2D).

Immunohistochemically, the tumor cells were diffusely positive for adipophilin (Figure 3A,B) and PRAME (Figure 3C,D) in the cytoplasm. Androgen receptor, BerEP4 (Figure 3E), and GCDFP15 were strongly and diffusely expressed. No p63+ tumor cells were observed (Figure 3F). Estrogen receptor and progesterone receptor were completely negative for the tumor cells.

Panel sequencing using FoundationOne® CDx (Foundation Medicine, Inc.) revealed *PIK3CA* E726K mutation and *CDK12* deletion in exons 11–13.

2.2 | Case 2

The patient was a 72-year-old man with a 14 × 8 mm skin tumor on his right axilla. He had been aware of the tumor for 1 year. Surgical excision of the primary tumor and dissection of the regional lymph nodes were performed. Recurrence in the cervical lymph nodes was confirmed 6 years after surgery; however, no recurrence had been confirmed for 7 years since the first recurrence.

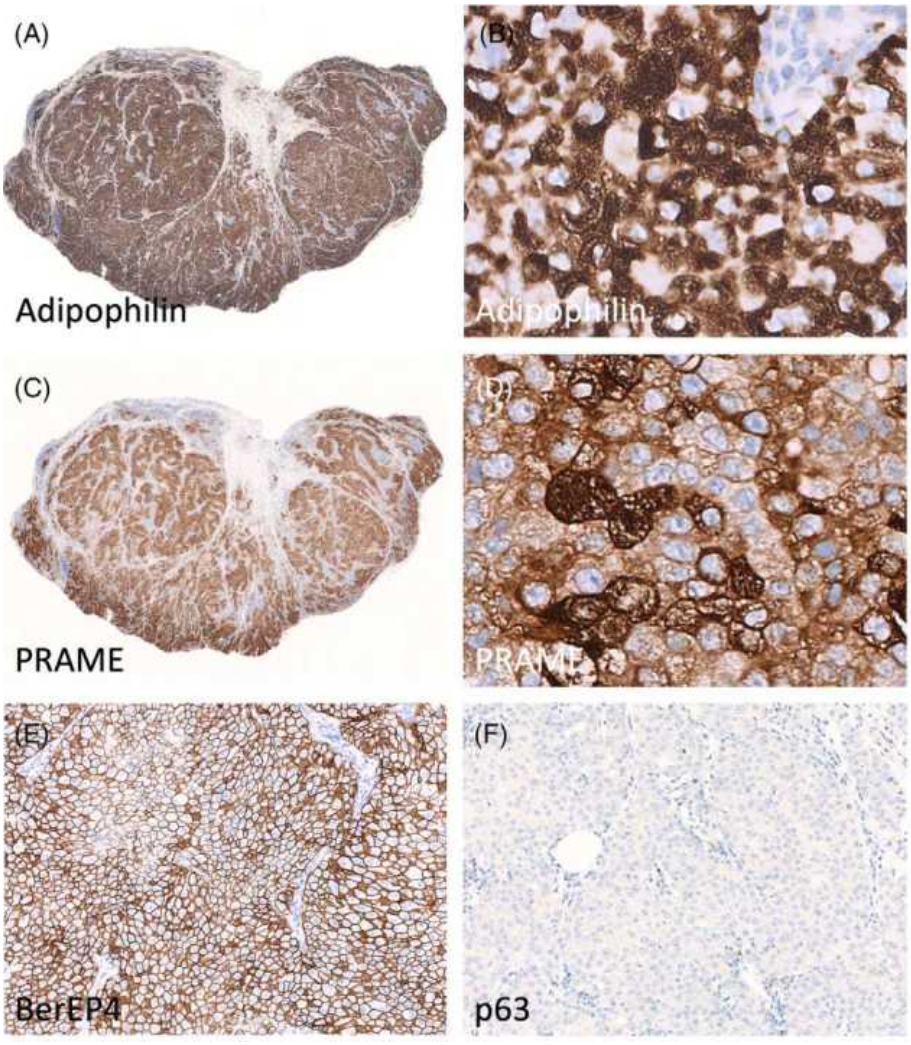

FIGURE 3 Immunohistochemical findings of Case 1. (A) Diffuse expression of adipophilin (adipophilin immunostain, ×20). (B) Cytoplasmic adipophilin expression with vacuolated pattern (adipophilin immunostain, ×600). (C) Diffuse expression of PRAME (PRAME immunostain, ×20). (D) Cytoplasmic PRAME expression with vacuolated pattern (PRAME immunostain, ×600). (E) Diffuse and strong expression of BerEP4 (BerEP4 immunostain, ×200). (F) Lack of p63 expression (p63 immunostain, ×200).

Histopathology revealed a relatively well-circumscribed tumor with no fibrous capsules in the dermis and superficial subcutis (Figure 4A). The tumor was composed of solid tumor nests, over half of which contained tumor cells with foamy cytoplasm (Figure 4B). The remaining nests were composed of tumor cells with eosinophilic granular cytoplasm (Figure 4C). Glandular formations with apocrine snouts were also frequently observed. Both tumor cell types harbored prominent nucleoli. The tumor nests were compactly distributed with little stromal component in the tumor area.

Diffuse immunoexpression of adipophilin (Figure 5A) and PRAME (Figure 5B) was observed in the cytoplasm of most tumor cells. Androgen receptor (Figure 5C), BerEP4 (Figure 5D), and GCDFP15 (Figure 5E) were diffusely positive in the tumor cells, but p63 was completely negative (Figure 5F). Estrogen receptor and progesterone receptor were completely negative for the tumor cells. The *PIK3CA* H1047R mutation was detected by panel sequencing in the tumor in Case 2.

3 | DISCUSSION

This is a report of two cases describing an apocrine carcinoma with sebocyte-like (sebocytoid) cytological features. Both patients in this study presented with sebocyte-like cytological features across a broad area of the tumors rather than in the focal area; thus, their histopathology resembled that of sebaceous carcinoma. Apocrine carcinoma was diagnosed based on the location of the axilla, presence of lymph node metastases, focal but definitive eosinophilic granular cytoplasm of the tumor cells, prominent and large nucleoli, immunoreactivity for BerEP4, negativity for p63, and *PIK3CA* mutation.

Apocrine carcinoma is an exclusionary diagnostic concept of a malignant tumor with apocrine and eccrine differentiation, which manifests unequivocal signs of apocrine secretion.[1] To make a definitive diagnosis of apocrine carcinoma, no association with any preexisting well-defined benign sweat gland tumors nor specific glandular origin (ciliary glands/Moll glands, ceruminous glands, or anogenital

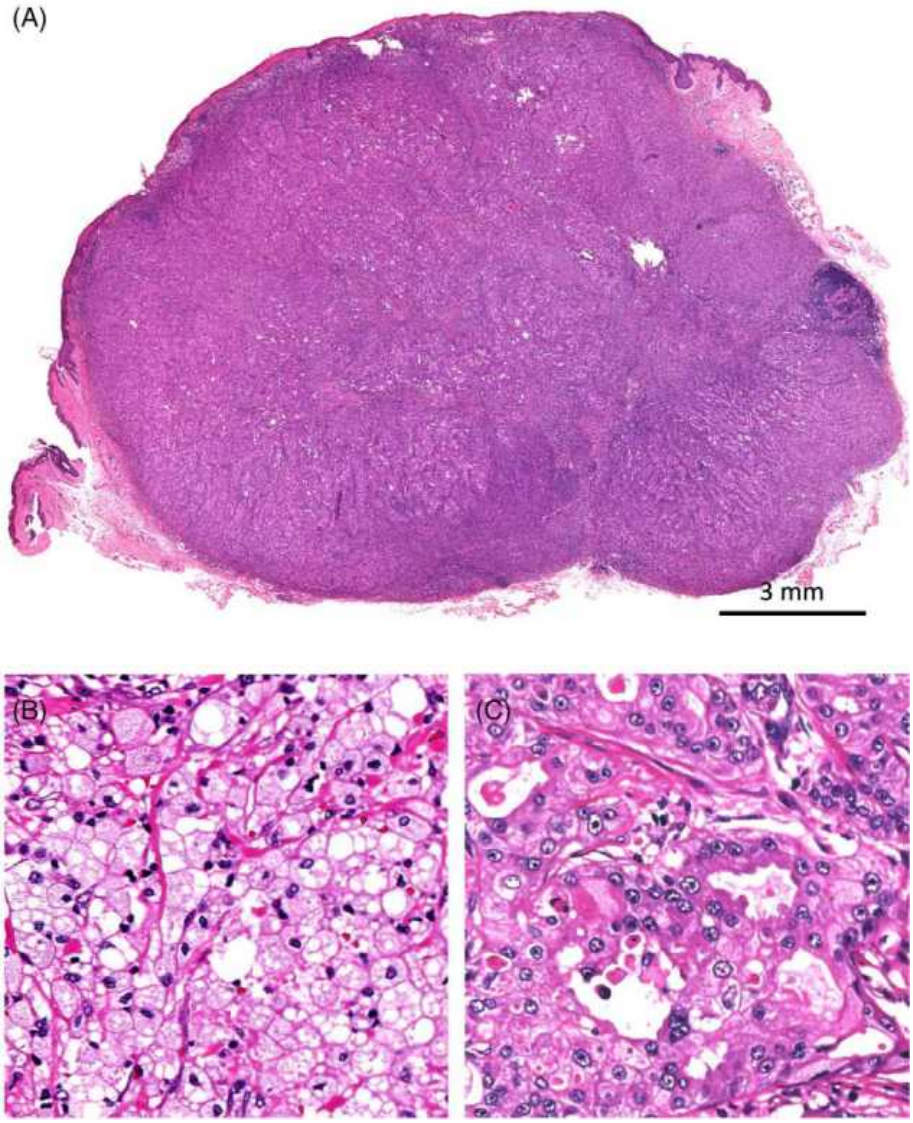

FIGURE 4 Histopathologic findings of Case 2. (A) Excised specimen section for the primary tumor (H&E stain, ×10). (B) The tumor cells with sebocyte-like cytological change (H&E stain, ×200). (C) Glandular tumor cells with apocrine snouts (H&E stain, ×400).

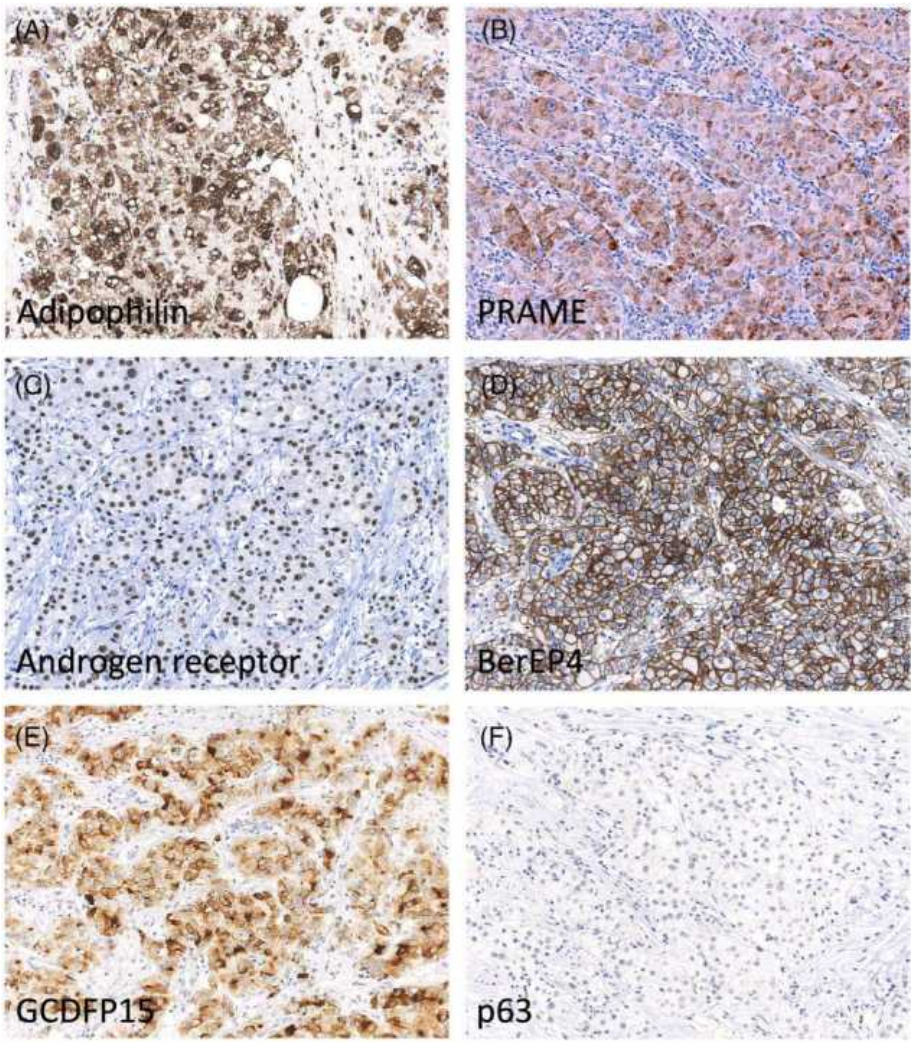

FIGURE 5 Immunohistochemical findings of Case 2. (A) Diffuse immunoexpression of adipophilin (adipophilin immunostain, ×200). (B) Diffuse cytoplasmic immunoexpression of PRAME (PRAME immunostain, ×200). (C) Diffuse positivity for androgen receptor (androgen receptor immunostain, ×200). (D) Diffuse membranous expression of BerEP4 (BerEP4 immunostain, ×200). (E) GCDFP15 immunoexpression was seen in all tumor cells (GCDFP15 immunostain, ×200). (F) Complete negativity of p63 nuclear expression (p63 immunostain, ×200).

mammary-like glands) must be confirmed.[1] However, the tumor type typically favors the site of the axilla and presents with frequent *PIK3CA* mutations.[15] Histopathologically, apocrine carcinoma can demonstrate various structural growth patterns, including glandular, cribriform, solid, and infiltrative patterns; however, the condition does not usually show other appendageal differentiation. Cytopathologically, cytoplasmic zymogen granules and large nucleoli can be observed. The two cases in this study presented all of the above characteristics.

A few studies have reported that cutaneous or mammary apocrine carcinomas exhibit adipophilin immunoreactivity,[16,17] although there have been no reports of apocrine carcinomas morphologically showing sebaceous differentiation. In addition, salivary duct carcinoma, which is a close relative of apocrine carcinoma, and lung adenocarcinoma with apocrine-like features can also show an immunoexpression of adipophilin.[18,19] Therefore, it should be considered that apocrine carcinomas and their relatives can exhibit intracytoplasmic lipid accumulation.

Moreover, various melanocytic tumors occasionally show intracytoplasmic lipid accumulation and sebocyte-like cytological features. Cytological features can be observed in banal melanocytic nevi, dysplastic nevi, BAP1-inactivated melanocytic tumors, blue nevi, and melanomas.[20–25]

Such findings in apocrine carcinomas and melanocytic tumors may be due to intracytoplasmic lipid accumulation or lipidization; however, not as a result of the differentiation toward sebocytes. Immunohistochemically, the tumor cells in the present cases of apocrine carcinoma were not similar to sebocytes because the tumor cells were positive for BerEP4 and negative for p63.[26–28] Melanocytic tumors, as in the above cases, also preserve melanocytic differentiation but do not show sebocytic differentiation. Thus, labeling the condition as apocrine carcinomas with sebocyte-like cytological features would be more appropriate than apocrine carcinomas with sebaceous differentiation. The label for sebocytoid apocrine carcinoma would also be acceptable; however, seboapocrine carcinoma or seboapocrine lesion, which may be terminologically confused with sebocytoid apocrine carcinoma, have been used in previous studies of sebaceous carcinoma or sebaceoma with apocrine differentiation.[2,6]

Sebaceous carcinoma is a significant and unique differential diagnosis for apocrine carcinoma with sebocyte-like cytological features. However, apocrine carcinoma demonstrates a higher rate of lymph node or distant metastasis than sebaceous carcinoma and is not associated with Muir–Torre syndrome, unlike sebaceous carcinoma.[15,29] Thus, it would be significant to distinguish apocrine carcinoma from

sebaceous carcinoma. Clinically, apocrine carcinoma is usually observed in the axilla of elderly men,[15] and sebaceous carcinoma shows a slight predominance in women and is rarely located in the axilla.[15,29] Cytoplasmic zymogen granules and prominent large nucleoli, which are characteristic of apocrine carcinoma, are not observed in sebaceous carcinoma. While both tumors express the epithelial membrane antigen, androgen receptor, and adipophilin,[15,26,27] sebaceous carcinoma is definitely positive for p63 but usually negative for BerEP4, unlike apocrine carcinoma.[15,26,28] In addition, *PIK3CA* mutations, which are frequently confirmed in apocrine carcinoma,[15] are not observed in sebaceous carcinoma,[30] although genetic sequencing for *PIK3CA* is not consistently necessary for the differential diagnosis.

Here, we presented two cases of apocrine carcinoma with sebocyte-like cytological features. The study showed that apocrine carcinomas can potentially exhibit intracytoplasmic lipid accumulation and rarely resemble sebaceous carcinomas. All the findings, including the tumor site of the axilla, presence of the eosinophilic granular cytoplasm and prominent nucleoli, positivity for BerEP4, negativity for p63, and *PIK3CA* mutations, correspond with apocrine carcinoma and not sebaceous carcinoma. It is clinically significant to distinguish apocrine carcinoma from sebaceous carcinoma because of the higher metastatic potential and lack of association with Muir–Torre syndrome seen in apocrine carcinoma.

ACKNOWLEDGMENTS

This work was partly supported by Japan Society for the Promotion of Science, KAKENHI (Grant Number JP22K06994; Keisuke Goto).

CONFLICT OF INTEREST STATEMENT

The authors have disclosed that they have no significant relationships with, or financial interest in, any commercial companies pertaining to this study.

DATA AVAILABILITY STATEMENT

The data that support the findings of this study are available on request from the corresponding author. The data are not publicly available due to privacy or ethical restrictions.

ETHICS STATEMENT

The study has been approved by the research ethics committees of the National Hospital Organization Kagoshima Medical Center (Ref: 2023-1) and Shizuoka Cancer Center Hospital (Ref: T2023-16).

ORCID

Natsuko Sasaki-Saito https://orcid.org/0000-0001-6122-8429
Keisuke Goto https://orcid.org/0000-0002-4165-1809
Katsuhiko Nishihara https://orcid.org/0000-0002-3801-4278
Shigeto Matsushita https://orcid.org/0000-0003-2001-5341

REFERENCES

1. Massi D, Cree IA, Elder DE, Kazakov DV, Scolyer RA. Appendageal tumours. In: Elder DE, Massi D, Scolyer RA, Willemze R, eds. *WHO Classification of Skin Tumours*. IARC Press; 2018:153-222.
2. Kazakov DV, Calonje E, Rütten A, Glatz K, Michal M. Cutaneous sebaceous neoplasms with a focal glandular pattern (seboapocrine lesions): a clinicopathological study of three cases. *Am J Dermatopathol*. 2007;29(4):359-364. doi:10.1097/DAD.0b013e31806f6a4d
3. Tanahashi J, Kashima K, Daa T, et al. A case of sebaceoma with extensive apocrine differentiation. *Am J Dermatopathol*. 2008;30(4):408-411. doi:10.1097/DAD.0b013e31817d2a4a
4. Misago N, Narisawa Y. Ripple/carcinoid pattern sebaceoma with apocrine differentiation. *Am J Dermatopathol*. 2011;33(1):94-97. doi:10.1097/DAD.0b013e3181ddf50c
5. Misago N, Narisawa Y. Sebaceous carcinoma with apocrine differentiation. *Am J Dermatopathol*. 2001;23(1):50-57. doi:10.1097/00000372-200102000-000009
6. Ishida M, Okabe H. Sebaceous carcinoma with apocrine differentiation (seboapocrine carcinoma). *Pathol Int*. 2012;62(6):438-440. doi:10.1111/j.1440-1827.2012.02820.x
7. Afroz N, Zaidi N, Rizvi SA. Sebaceous carcinoma with apocrine differentiation: a rare entity with aggressive behavior. *Indian J Pathol Microbiol*. 2013;56(4):408-410. doi:10.4103/0377-4929.125354
8. Pinheiro JAF, Lopes JMPB. Periocular sebaceous carcinoma with apocrine differentiation: a case report and review of the literature. *Int J Surg Pathol*. 2019;27(4):432-436. doi:10.1177/1066896918816806
9. Misago N, Mihara I, Ansai SI, Narisawa Y. Sebaceous and related neoplasms with sebaceous differentiation: a clinicopathologic study of 30 cases. *Am J Dermatopathol*. 2002;24(4):294-304. doi:10.1097/00000372-200208000-00002
10. Misago N, Suse T, Uemura T, Narisawa Y. Basal cell carcinoma with sebaceous differentiation. *Am J Dermatopathol*. 2004;26(4):298-303. doi:10.1097/00000372-200408000-00006
11. Kazakov DV, Belousova IE, Bisceglia M, et al. Apocrine mixed tumor of the skin ("mixed tumor of the folliculosebaceous-apocrine complex"). Spectrum of differentiations and metaplastic changes in the epithelial, myoepithelial, and stromal components based on a histopathologic study of 244 cases. *J Am Acad Dermatol*. 2007;57(3):467-483. doi:10.1016/j.jaad.2007.02.029
12. Kazakov DV, Kutzner H, Spagnolo DV, et al. Sebaceous differentiation in poroid neoplasms: report of 11 cases, including a case of metaplastic carcinoma associated with apocrine poroma (sarcomatoid apocrine porocarcinoma). *Am J Dermatopathol*. 2008;30(1):21-26. doi:10.1097/DAD.0b013e31815f2ae3
13. Fernandez-Flores A, Llamas-Velasco M, Saus C, Patel A, Rütten A. Microcystic adnexal carcinoma with sebaceous differentiation: three cases. *J Cutan Pathol*. 2018;45(4):290-295. doi:10.1111/cup.13109
14. Ooms KDW, Chiosea S, Lamarre E, Shah AA. Sebaceous differentiation as another feature of metatypical adenoid cystic carcinoma: a case report and letter to the editor. *Am J Surg Pathol*. 2023;47(1):145-146. doi:10.1097/PAS.0000000000001993
15. Goto K, Kukita Y, Honma K, et al. Signet-ring cell/histiocytoid carcinoma of the axilla: a clinicopathological and genetic analysis of 11 cases, review of the literature, and comparison with potentially related tumours. *Histopathology*. 2021;79(6):926-939. doi:10.1111/his.14436
16. Moritani S, Ichihara S, Hasegawa M, et al. Intracytoplasmic lipid accumulation in apocrine carcinoma of the breast evaluated with adipophilin immunoreactivity: a possible link between apocrine carcinoma and lipid-rich carcinoma. *Am J Surg Pathol*. 2011;35(6):861-867. doi:10.1097/PAS.0b013e31821a7f3e
17. Piris A, Peng Y, Boussahmain C, Essary LR, Gudewicz TM, Hoang MP. Cutaneous and mammary apocrine carcinomas have different immunoprofiles. *Hum Pathol*. 2014;45(2):320-326. doi:10.1016/j.humpath.2013.09.007
18. Hirai H, Tada Y, Nakaguro M, et al. The clinicopathological significance of the adipophilin and fatty acid synthase expression in salivary duct carcinoma. *Virchows Arch*. 2020;477(2):291-299. doi:10.1007/s00428-020-02777-w

19. Fujimoto M, Yoshizawa A, Sumiyoshi S, et al. Adipophilin expression in lung adenocarcinoma is associated with apocrine-like features and poor clinical prognosis: an immunohistochemical study of 328 cases. *Histopathology*. 2017;70(2):232-241. doi:10.1111/his.13048
20. Vazmitel M, Michal M, Mukensnabl P, Kazakov DV. Melanoma associated with a dysplastic nevus: report of two cases with unusual sebocyte-like melanocytes in the nevus part of the lesion. *Am J Dermatopathol*. 2007;29(6):566-567. doi:10.1097/DAD.0b013e31815400db
21. Kacerovska D, Michal M, Kazakov DV. Sebocyte-like melanocytes in desmoplastic blue nevus. *Am J Dermatopathol*. 2008;30(5):509-510. doi:10.1097/DAD.0b013e31817d4cab
22. Kazlouskaya V, Guo Y, Maia-Cohen S, Mones J. Clear-cell melanocytic lesions with balloon-cell and sebocyte-like melanocytes: a unifying concept. *Am J Dermatopathol*. 2014;36(5):380-386. doi:10.1097/DAD.0b013e31829fdcd7
23. Marušić Z, Buljan M, Busam KJ. Histomorphologic spectrum of BAP1 negative melanocytic neoplasms in a family with *BAP1*-associated cancer susceptibility syndrome. *J Cutan Pathol*. 2015;42(6):406-412. doi:10.1111/cup.12493
24. Molina-Ruiz AM, Ortiz-reina S, Carranza C, Kutzner H, Requena L. Sebocyte-like cell primary cutaneous melanoma: a rare cytologic variant of malignant melanoma. *Am J Dermatopathol*. 2015;37(11):862-865. doi:10.1097/DAD.0000000000000275
25. Resnik KS. Sebocyte-like melanocytes—additional relevant (and behind the scenes) historical information. *Am J Dermatopathol*. 2017;39(3):233-236. doi:10.1097/DAD.0000000000000628
26. Ansai SI, Takeichi H, Arase S, Kawana S, Kimura T. Sebaceous carcinoma: an immunohistochemical reappraisal. *Am J Dermatopathol*. 2011;33(6):579-587. doi:10.1097/DAD.0b013e31820a2027
27. Plaza JA, Mackinnon A, Carrillo L, Prieto VG, Sangueza M, Suster S. Role of immunohistochemistry in the diagnosis of sebaceous carcinoma: a clinicopathologic and immunohistochemical study. *Am J Dermatopathol*. 2015;37(11):809-821. doi:10.1097/0000000000000255
28. Boecker W, Reusch M, Mielke V, et al. Spatial analysis of p63, K5 and K7 defines two groups of progenitor cells that differentially contribute to the maintenance of normal sebaceous glands, extraocular sebaceous carcinoma and benign sebaceous tumors. *J Dermatol*. 2019;46(3):249-258. doi:10.1111/1346-8138.14765
29. Kyllo RL, Brady KL, Hurst EA. Sebaceous carcinoma: review of the literature. *Dermatol Surg*. 2015;41(1):1-15. doi:10.1097/DSS.0000000000000152
30. North JP, Golovato J, Vaske CJ, et al. Cell of origin and mutation pattern define three clinically distinct classes of sebaceous carcinoma. *Nat Commun*. 2018;9(1):1894. doi:10.1038/s41467-018-04008-y

How to cite this article: Sasaki-Saito N, Goto K, Aoki M, et al. Apocrine carcinoma with marked sebocyte-like cytological features: A report of two cases. *J Cutan Pathol*. 2024;51(2):92-98. doi:10.1111/cup.14539

International Journal of
Molecular Sciences

MDPI

Article

Inhibitory Effects of Simvastatin on IL-33-Induced MCP-1 via the Suppression of the JNK Pathway in Human Vascular Endothelial Cells

Katsuyuki Umebashi, Masayoshi Yamamoto, Akinori Tokito, Ku Sudou, Yoko Takenoshita and Michihisa Jougasaki *

Institute for Clinical Research, National Hospital Organization Kagoshima Medical Center, Kagoshima 892-0853, Japan; umebashi.katsuyuki.gc@mail.hosp.go.jp (K.U.); yamamoto.masayoshi.bc@mail.hosp.go.jp (M.Y.); tokininn@hotmail.com (A.T.); pd3z8uos@okayama-u.ac.jp (K.S.); takenoshita.yoko.cj@mail.hosp.go.jp (Y.T.)
* Correspondence: jogasaki.michihisa.kb@mail.hosp.go.jp; Tel.: +81-99-223-1151

Abstract: An alarmin, interleukin (IL)-33 is a danger signal that causes inflammation, inducing chemotactic proteins such as monocyte chemoattractant protein (MCP)-1 in various cells. As statins have pleiotropic actions including anti-inflammatory properties, we investigated the effects of simvastatin on IL-33-induced MCP-1 expression in human umbilical vein endothelial cells (HUVECs). HUVECs were stimulated with IL-33 in the presence or absence of simvastatin. Gene expression and protein secretion of MCP-1, phosphorylation of mitogen-activated protein kinase (MAPK), nuclear translocation of phosphorylated c-Jun, and human monocyte migration were investigated. Immunocytochemical staining and Western immunoblot analysis revealed that IL-33 augmented MCP-1 protein expression in HUVECs. Real-time reverse transcription–polymerase chain reaction (RT-PCR) and enzyme-linked immunosorbent assay (ELISA) showed that IL-33 significantly increased MCP-1 mRNA and protein secretion, which were suppressed by c-jun N-terminal kinase (JNK) inhibitor SP600125 and p38 MAPK inhibitor SB203580. Simvastatin inhibited IL-33-induced MCP-1 mRNA, protein secretion, phosphorylation of JNK and c-Jun. Additionally, the IL-33-induced nuclear translocation of phosphorylated c-Jun and THP-1 monocyte migration were also blocked by simvastatin. This study demonstrated that IL-33 induces MCP-1 expression via the JNK and p38 MAPK pathways in HUVECs, and that simvastatin inhibits MCP-1 production by selectively suppressing JNK. Simvastatin may inhibit the progression of IL-33-induced inflammation via suppressing JNK to prevent MCP-1 production.

Keywords: interleukin-33; monocyte chemoattractant protein-1; cell migration; mitogen-activated protein kinase; cytokine; statins

Citation: Umebashi, K.; Yamamoto, M.; Tokito, A.; Sudou, K.; Takenoshita, Y.; Jougasaki, M. Inhibitory Effects of Simvastatin on IL-33-Induced MCP-1 via the Suppression of the JNK Pathway in Human Vascular Endothelial Cells. *Int. J. Mol. Sci.* **2023**, *24*, 13015. https://doi.org/10.3390/ijms241613015

Academic Editor: Jeffrey L. Platt

Received: 8 August 2023
Revised: 17 August 2023
Accepted: 18 August 2023
Published: 21 August 2023

1. Introduction

Interleukin (IL)-33, originally identified as a nuclear factor in postcapillary high endothelial venules, is a ligand for the orphan IL-1 family receptor suppression of tumorigenicity (ST) 2 [1]. As a cytokine, IL-33 is released from various cells in response to tissue damage or mechanical strain to alert the immune system [2,3]. IL-33 acts as a danger signal with potent inflammatory properties, and therefore it is called an "alarmin". IL-33 binds to its transmembrane receptor ST2 on the inflammatory cells, inducing Th2-associated cytokines and chemokines [1,4]. The signal transduction system induced by IL-33 includes nuclear factor-kappa B (NFκB) and mitogen-activated protein kinases (MAPKs), such as extracellular signal-regulated kinase (ERK)1/2, p38 MAPK, and c-jun N-terminal kinase (JNK) [1,5]. We recently reported that IL-33 increased the gene and protein expressions of chemokines, such as growth-regulated oncogene (GRO)-α and IL-8 in human vascular endothelial cells [6,7]. Using an antibody array assay, we also showed that IL-33 enhanced

monocyte chemoattractant protein (MCP)-1 expression in human vascular endothelial cells [7]. Monocyte chemoattractant protein (MCP)-1, also called C-C motif chemokine ligand (CCL) 2, is a key member of the CC chemokine family that is involved in the pathophysiology of inflammatory diseases, and the findings that MCP-1 is a downstream molecule of IL-33 are supported by several other investigations [8–15]. Besides the property of migrating monocytes into the site of inflammation, MCP-1 also promotes migration of cancer cells [16–20]. In addition, accumulating evidence has demonstrated that IL-33 also promotes migration of normal cells [21–23] as well as cancer cells [24–26]. Hu et al. revealed that IL-33 and its receptor ST2 were co-expressed in decidual stromal cells, and IL-33 promoted migration of decidual stromal cells by upregulating MCP-1 via the ERK1/2 signaling pathway [27]. However, the precise role of MCP-1 on IL-33-mediated cell migration remains undefined.

Statins, 3-hydroxy-3-methylglutaryl CoA (HMG-CoA) reductase inhibitors, have been established as a primary and secondary prevention of cardiovascular events by lowering low-density lipoprotein cholesterol [28]. In addition to the cholesterol-lowering effect, statins have pleiotropic actions, including attenuation of vascular inflammation, improved endothelial cell function, stabilization of atherosclerotic plaque, decreased vascular smooth muscle cell migration and proliferation, and inhibition of platelet aggregation [29,30]. We previously reported that simvastatin suppressed IL-6-induced monocyte chemotaxis and MCP-1 expression in human vascular endothelial cells [31]. Likewise, simvastatin caused an inhibition of C-reactive protein-mediated MCP-1 secretion and migration in human primary monocytes [32]. In addition, simvastatin inhibited MCP-1 synthesis in peripheral blood mononuclear cells exposed to lipopolysaccharide and in human endothelial cells exposed to IL-1β [33]. However, the specific mechanisms by which statins suppress MCP-1 and cell migration are not fully understood.

In the present study, we hypothesized that statins could suppress IL-33-induced monocyte chemotaxis through inhibiting MCP-1 expression. Thus, this study was designed to investigate the effects of simvastatin on IL-33-induced monocyte chemotaxis and MCP-1 expression in human umbilical vein endothelial cells (HUVECs), specifically focusing on the signal transduction system of MAPK pathways.

2. Results

2.1. Immunocytochemical Staining for MCP-1

Immunocytochemical staining showed faint positive immunoreactivities for MCP-1 in untreated HUVECs, and the intensity of immunoreactivity for MCP-1 in HUVECs was enhanced by the treatment with 10^{-9} mol/L of IL-33 for 24 h (Figure 1A). In addition, the cells treated with normal IgG, instead of the primary antibody against MCP-1, demonstrated no immunoreactivity for MCP-1. Semiquantitative analysis showed a significant increase in the intensity of immunoreactivity for MCP-1 in IL-33-stimulated cells compared with the untreated cells (Figure 1B).

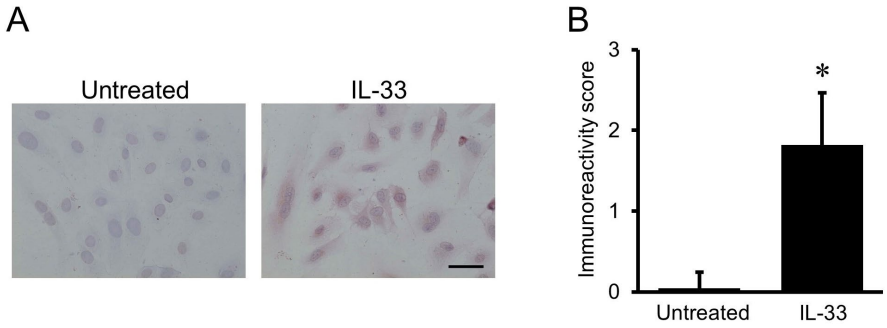

Figure 1. Interleukin (IL)-33-stimulated monocyte chemoattractant protein (MCP)-1 protein expression in human umbilical vein endothelial cells (HUVECs). (**A**) Representative immunocytochemical

staining showing the localization of MCP-1 in HUVECs with or without exposure to 10^{-9} mol/L of IL-33 for 24 h. Intensity of immunoreactivity for MCP-1 was increased in HUVECs treated with IL-33 compared with the untreated cells. Original magnification: ×400. Scale bar = 50 µm. (**B**) Semiquantitative analysis of staining intensity of immunoreactivity for MCP-1. * $p < 0.05$ vs. untreated cells.

2.2. Western Immunoblot Analysis for MCP-1

Immunocytochemical findings were supported by Western immunoblot analysis of the cell lysates using anti-MCP-1 antibody (Figure 2A). As shown in Figure 2B, treatment with 10^{-9} mol/L of IL-33 resulted in a significant increase in MCP-1 protein expression in HUVECs.

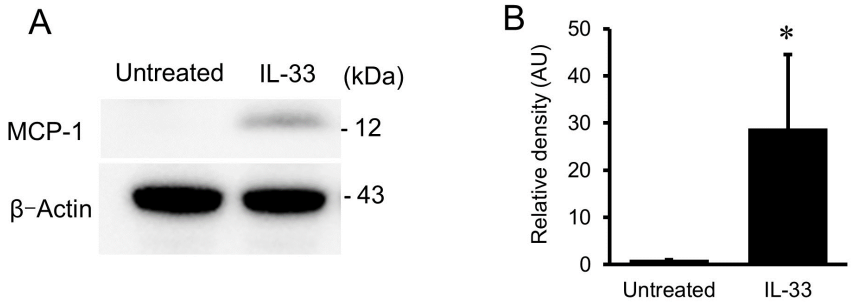

Figure 2. (**A**) Western immunoblot analysis of the whole-cell lysates using anti-MCP-1 antibody in HUVECs with or without exposure to 10^{-9} mol/L of IL-33 for 24 h. (**B**) Bars represent densitometric data of each expression signal after normalization to β-actin and relative to the untreated cells. MCP-1 protein expression was increased in HUVECs treated with IL-33 compared with the untreated cells. * $p < 0.05$ vs. untreated cells.

2.3. IL-33-Induced Gene Expression and Protein Secretion of MCP-1 in HUVECs

Real-time reverse transcription–polymerase chain reaction (RT-PCR) demonstrated that treatment with IL-33 (10^{-12} to 10^{-8} mol/L) resulted in an increase in MCP-1 mRNA in a dose-dependent manner with a statistical significance at 10^{-9} and 10^{-8} mol/L of IL-33 (Figure 3A). As shown in Figure 3B, IL-33 at the dose of 10^{-9} mol/L significantly increased MCP-1 mRNA between 4 and 24 h, peaking at 8 h after stimulation with IL-33. An enzyme-linked immunosorbent assay (ELISA) showed that IL-33 increased MCP-1 protein secretion from HUVECs in a dose-dependent manner with a significant increase at the doses over 10^{-11} mol/L (Figure 3C), and in a time-dependent manner with a significant increase between 8 and 24 h of IL-33 treatment (Figure 3D).

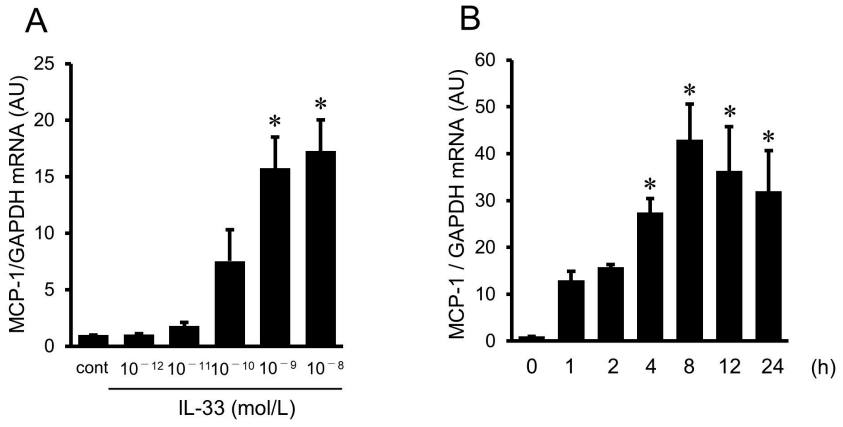

Figure 3. *Cont.*

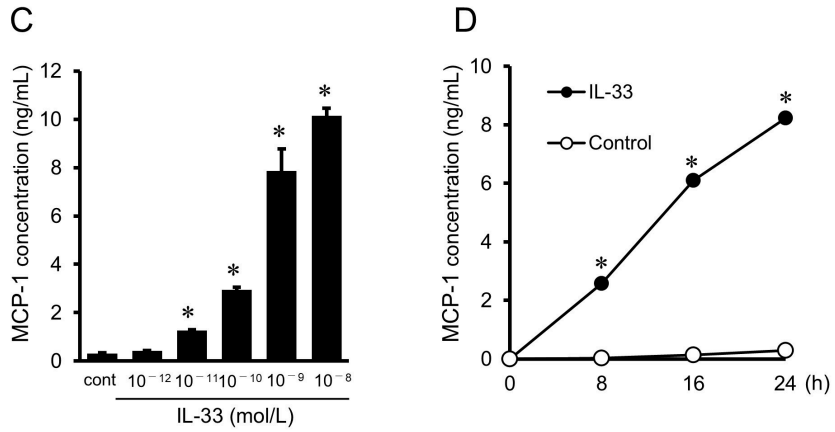

Figure 3. IL-33-stimulated gene expression and protein secretion of MCP-1 in HUVECs. (**A**) MCP-1 mRNA expression in HUVECs after treatment with the indicated concentrations of IL-33 for 8 h (n = 3), as evaluated by real-time reverse transcription–polymerase chain reaction (RT-PCR). (**B**) Time course of MCP-1 mRNA after treatment with 10^{-9} mol/L of IL-33 (n = 3), as evaluated by real-time RT-PCR. Bars represent MCP-1 mRNA after normalization to glyceraldehyde-3-phosphate dehydrogenase (GAPDH) mRNA and relative to the untreated control (cont) in (**A**) and 0 h in (**B**). (**C**) MCP-1 concentrations in the supernatant after treatment with the indicated concentrations of IL-33 for 24 h (n = 6), as analyzed by enzyme-linked immunosorbent assay (ELISA). Bars represent MCP-1 protein secretion per 10^5 cells. (**D**) Time course of MCP-1 concentrations in the supernatant after treatment with 10^{-9} mol/L of IL-33 (closed circles, n = 6), as analyzed by ELISA. Spontaneous secretion of MCP-1 without IL-33 treatment is shown in open circles (n = 6), as analyzed by ELISA. * $p < 0.05$ vs. cont in (**A**,**C**), vs. 0 h in (**B**), and vs. each control at the same time in (**D**).

2.4. IL-33-Induced Phosphorylation of JNK, p38 MAPK, and ERK1/2 in HUVECs

HUVECs were exposed to IL-33 for different time periods (5–120 min), and their protein extracts were examined by Western immunoblot analysis. IL-33 induced the phosphorylation of JNK (Figure 4A), peaking at 30 min and declining at 60 min. In addition, IL-33 induced the phosphorylation of p38 MAPK (Figure 4B) and ERK1/2 (Figure 4C), peaking between 15 min and 30 min and declining at 60 min.

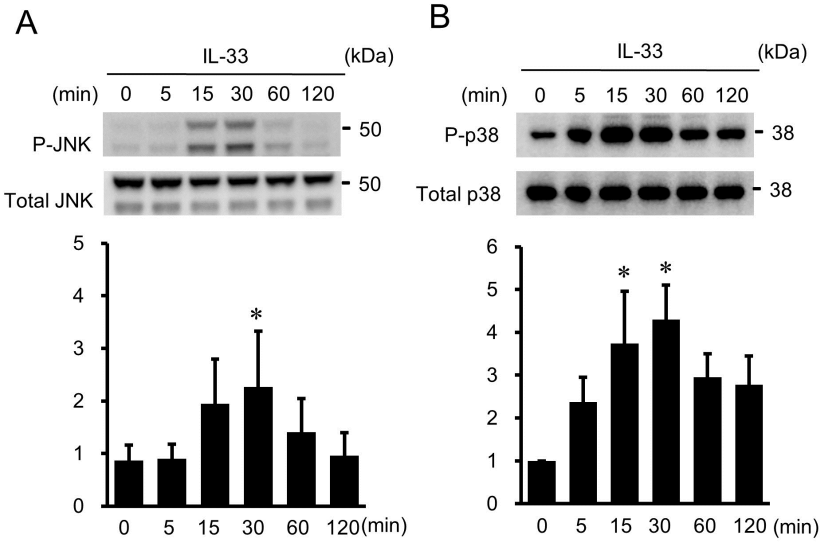

Figure 4. *Cont.*

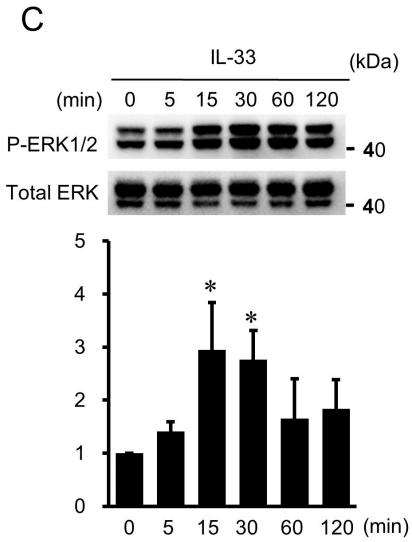

Figure 4. IL-33-activated mitogen-activated protein kinase (MAPK) pathway in HUVECs. (**A**–**C**) Western immunoblot analysis showed that IL-33 stimulated the phosphorylation of c-jun N-terminal kinase (JNK) (**A**), p38 MAPK (**B**), and extracellular signal-regulated kinase (ERK) 1/2 (**C**). HUVECs were treated with 10^{-9} mol/L of IL-33 for 5, 15, 30, 60, and 120 min. Bars represent results from densitometric analyses of each phosphorylation signal after normalization to total protein and relative to the untreated control (0 min). Blots are representative of three independent experiments. * $p < 0.05$ vs. 0 min.

2.5. Effects of Pharmacological Inhibitors of MAPK Signaling Pathways on Gene Expression and Protein Secretion of MCP-1 in HUVECs

Involvement of the MAPK pathway in the IL-33-induced gene expression and protein secretion of MCP-1 was examined using pharmacological inhibitors of MAPK, such as SP600125 (JNK inhibitor), SB203580 (p38 MAPK inhibitor), and PD98059 (ERK1/2 inhibitor). HUVECs were pretreated with these pharmacological inhibitors for 2 h, followed by stimulation with IL-33 (10^{-9} mol/L) for 8 h to measure MCP-1 mRNA expression, and for 24 h to examine MCP-1 protein secretion from HUVECs. Real-time RT-PCR demonstrated that the IL-33-induced increase in MCP-1 mRNA expression was significantly suppressed by the pretreatment with SP600125 and SB203580 in HUVECs (Figure 5A). As shown in Figure 5B, the IL-33-induced increase in MCP-1 protein secretion from HUVECs was also significantly attenuated by the pretreatment with SP600125 and SB203580. In contrast, PD98059 had no effect on the IL-33-induced upregulation of gene expression or protein secretion of MCP-1 in HUVECs.

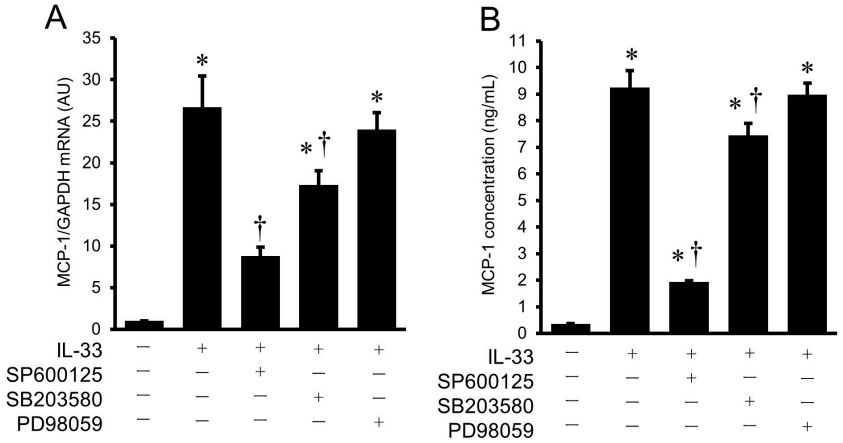

Figure 5. Effects of pharmacological inhibitors of MAPK pathway on IL-33-induced gene expression and protein secretion of MCP-1 in HUVECs. (**A**,**B**) HUVECs were pre-incubated with SP600125 (30 μmol/L),

SB203580 (10 μmol/L), and PD98059 (30 μmol/L) for 2 h, followed by stimulation with IL-33 (10^{-9} mol/L) for 8 h ((**A**), MCP-1 mRNA) or with IL-33 (10^{-9} mol/L) for 24 h ((**B**), MCP-1 secretion). MCP-1 mRNA was evaluated by real-time RT-PCR ((**A**), $n = 3$), and MCP-1 concentration was examined by ELISA ((**B**), $n = 6$). * $p < 0.05$ vs. untreated control. † $p < 0.05$ vs. IL-33.

2.6. Effects of Simvastatin on Cell Viability

MTT assay was used to examine cytotoxicity of various doses of simvastatin to the cultured HUVECs. No significant changes in cell viability were observed in HUVECs treated with simvastatin at a dose of less than 10 μmol/L (Figure 6). However, 100 μmol/L of simvastatin significantly decreased cell viability, and therefore this dose was not used in the present study.

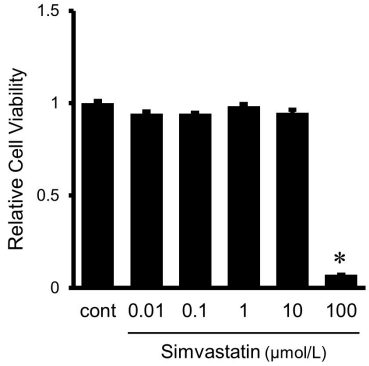

Figure 6. Effects of simvastatin on cell viability. HUVECs were treated with different concentrations of simvastatin for 24 h. Cell viability was measured by MTT assay. The results are expressed as percentage of the untreated control, and each value represents five independent experiments ($n = 5$). * $p < 0.05$ vs. untreated control (cont).

2.7. Effects of Simvastatin on IL-33-Induced Gene Expression and Protein Secretion of MCP-1 in HUVECs

To investigate the effects of simvastatin on IL-33-induced gene expression and protein secretion of MCP-1, HUVECs were pretreated with various concentrations of simvastatin (0.1, 1, 10 μmol/L), followed by stimulation with IL-33 (10^{-9} mol/L) for 8 h to examine MCP-1 mRNA expression, and for 24 h to measure MCP-1 protein secretion from HUVECs. The IL-33-induced increase in MCP-1 mRNA expression was significantly inhibited by 10 μmol/L of simvastatin (Figure 7A). As shown in Figure 7B, the IL-33-induced MCP-1 protein secretion from HUVECs for 24 h was also significantly suppressed by 10 μmol/L of simvastatin.

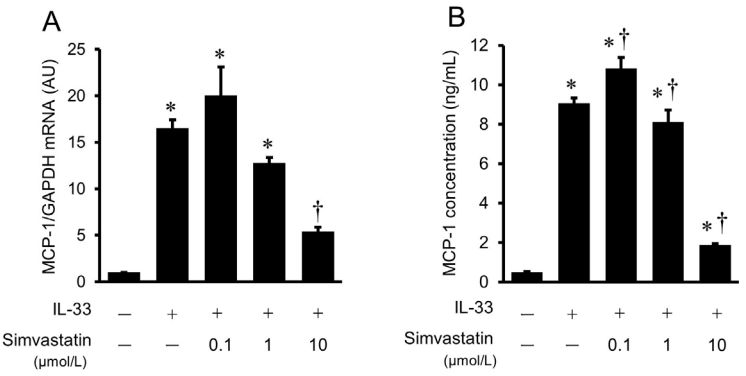

Figure 7. Effects of simvastatin on gene expression and protein secretion MCP-1 in HUVECs. IL-33-induced MCP-1 gene expression (**A**) and MCP-1 protein secretion (**B**) were suppressed by simvastatin.

HUVECs were treated with IL-33 (10^{-9} mol/L) for 8 h (**A**) or 24 h (**B**) with or without pretreatment with simvastatin (0.1 to 10 μmol/L). Bars represent MCP-1 mRNA after normalization to GAPDH mRNA and relative to the untreated control in (**A**). Bars represent MCP-1 protein secretion per 10^5 cells in (**B**). * $p < 0.05$ vs. untreated control. † $p < 0.05$ vs. IL-33.

2.8. Effects of Simvastatin on IL-33-Stimulated Phosphorylation of JNK and p38 MAPK in HUVECs

To evaluate whether simvastatin suppresses JNK and p38 MAPK activity, the phosphorylation of JNK and p38 MAPK was examined by Western immunoblot analysis. HUVECs were pretreated with various concentrations of simvastatin and then incubated with IL-33 (10^{-9} mol/L) for 15 min. IL-33-stimulated JNK phosphorylation was significantly inhibited by simvastatin at the dose of 10 μmol/L (Figure 8A). However, simvastatin had no effect on the phosphorylation of p38 MAPK (Figure 8B).

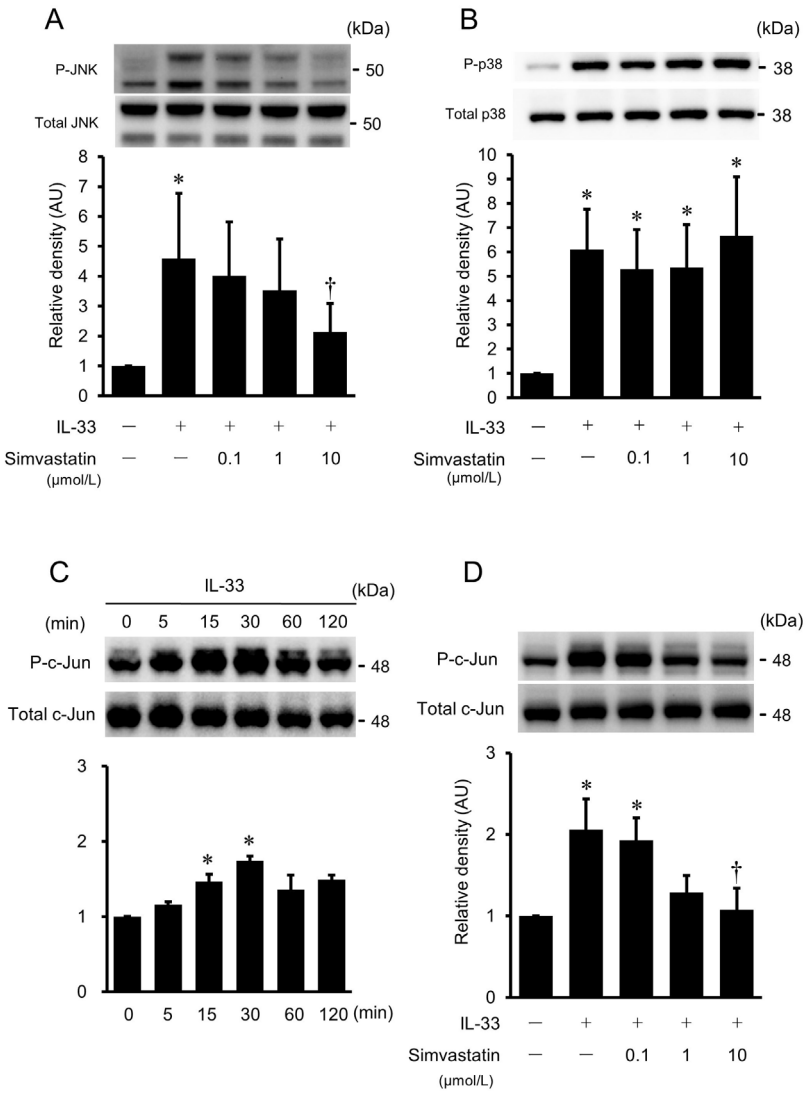

Figure 8. Effects of simvastatin on IL-33-induced phosphorylation of JNK, p38 MAPK, and c-Jun. (**A**,**B**) Simvastatin dose-dependently suppressed phosphorylation of JNK (**A**) but did not inhibit phosphorylation of p38 MAPK (**B**). HUVECs were pretreated with simvastatin and then incubated with IL-33 (10^{-9} mol/L) for 15 min. Bars represent results from densitometric analyses of each phosphorylation signal after normalization to total protein and relative to the untreated control. Blots

are representative of three independent experiments. * $p < 0.05$ vs. untreated control. † $p < 0.05$ vs. IL-33. (**C**) Time course of IL-33-induced phosphorylation of c-Jun as evaluated by Western immunoblot analysis. HUVECs were treated with IL-33 (10^{-9} mol/L) for the indicated time periods. Bars represent results from densitometric analyses of each phosphorylation signal after normalization to total protein and relative to the untreated control (0 min). Blots are representative of three independent experiments. * $p < 0.05$ vs. 0 min. † $p < 0.05$ vs. IL-33. (**D**) Simvastatin dose-dependently suppressed phosphorylation of c-Jun. HUVECs were pretreated with simvastatin and then incubated with IL-33 (10^{-9} mol/L) for 30 min. Bars represent results from densitometric analyses of each phosphorylation signal after normalization to total protein and relative to the untreated control. Blots are representative of three independent experiments. * $p < 0.05$ vs. untreated control. † $p < 0.05$ vs. IL-33.

2.9. Effects of Simvastatin on IL-33-Stimulated Phosphorylation of c-Jun in HUVECs

To determine the downstream signaling pathway of JNK, phosphorylation of c-Jun was assessed by Western immunoblot analysis. IL-33 induced the phosphorylation of c-Jun, peaking at 30 min and declining at 120 min (Figure 8C). The effects of simvastatin on the phosphorylation of c-Jun were examined by the pretreatment of HUVECs with various concentrations of simvastatin, followed by stimulation with IL-33 (10^{-9} mol/L) for 30 min. IL-33-stimulated c-Jun phosphorylation was significantly suppressed by the addition of simvastatin at the dose of 10 μmol/L (Figure 8D).

2.10. Immunofluorescence Staining

HUVECs were pre-incubated with simvastatin followed by incubation with IL-33 for 30 min, and immunofluorescence staining was performed to examine whether simvastatin affects the translocation of c-Jun to the nucleus by inhibiting IL-33-induced c-Jun phosphorylation. The immunofluorescence signal of phospho-c-Jun was localized in the nuclei of HUVECs after incubation with IL-33 for 30 min compared with the untreated control cells (Figure 9A). The phospho-c-Jun activation by IL-33 was inhibited by simvastatin at the dose of 10 μmol/L. The addition of mevalonate reversed the phosphorylation. The percentage of phospho-c-Jun-positive cell nuclei was significantly increased by IL-33 stimulation, and simvastatin treatment reduced the number of phospho-c-Jun-positive cells, which was reversed by the addition of mevalonate (Figure 9B).

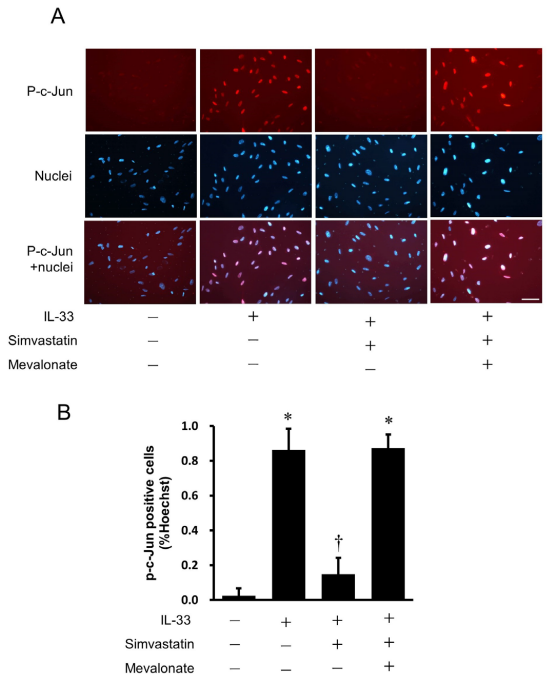

Figure 9. Effects of simvastatin on IL-33-induced translocation of phospho-c-Jun to the nucleus as determined by immunofluorescence staining. HUVECs were pretreated with simvastatin (10 μmol/L)

or simvastatin plus mevalonate (100 μmol/L), followed by additional incubation with IL-33 (10^{-9} mol/L) for 30 min. (**A**) Representative immunofluorescence images showing the localization of phospho-c-Jun in HUVECs. Red staining indicates the specific Alexa staining for phospho-c-Jun, and blue staining indicates the nuclei (Hoechst 33342). Original magnification: ×400. Scale bar = 50 μm. (**B**) Percentages of phospho-c-Jun-positive cells relative to total cell numbers. * $p < 0.05$ vs. untreated control. † $p < 0.05$ vs. IL-33.

2.11. Simvastatin Reduces THP-1 Monocyte Chemotaxis Enhanced by IL-33-Induced MCP-1

The culture medium from IL-33-treated HUVECs increased migration of THP-1 cells compared with that from the untreated cells. Pre-incubation of the culture medium with goat anti-human MCP-1 polyclonal antibody inhibited IL-33-enhanced THP-1 migration; however, goat IgG had no effect on THP-1 monocyte migration, indicating that IL-33-induced THP-1 monocyte migration was, at least in part, due to the chemotactic actions of MCP-1 (Figure 10). Pretreatment of HUVECs with simvastatin at a concentration of 10 μmol/L suppressed IL-33-enhanced THP-1 monocyte migration, and the addition of mevalonate reversed the THP-1 monocyte migration (Figure 10).

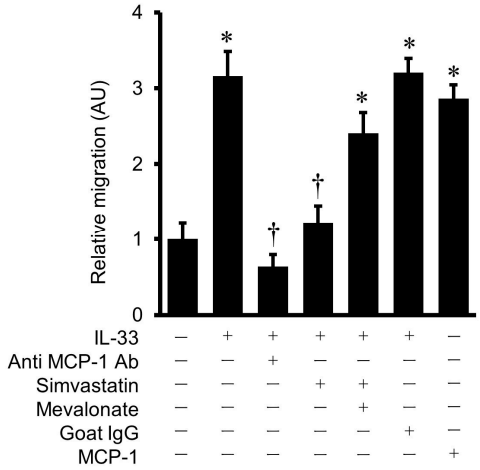

Figure 10. Effects of simvastatin on THP-1 monocyte migration as determined by chemotaxis assay. Relative migration indicates the ratio of migrating THP-1 cells towards the culture medium from HUVECs treated with various reagents relative to those from the untreated cells. THP-1 monocyte chemotaxis was promoted in response to the culture medium treated with 10^{-9} mol/L of IL-33. Pre-incubation of the culture medium with polyclonal anti-MCP-1 antibody (80 μg/mL), but not with goat IgG, resulted in an inhibition of chemotaxis. Simvastatin (10 μmol/L) inhibited IL-33-induced THP-1 monocyte chemotaxis, which was reversed by the addition of mevalonate. Recombinant human MCP-1 (100 nmol/L) served as a positive control. Bars represent mean ± SD of three independent experiments. * $p < 0.05$ vs. untreated control. † $p < 0.05$ vs. IL-33.

3. Discussion

Chemokines are small-molecule inflammatory proteins that are divided into four canonical subclasses according to the position of N-terminal cysteine residues: C, CC, CXC, and CX3C chemokines [34]. MCP-1, also known as CCL2, plays a central role in the pathogenesis of several different disease processes, including vascular permeability and attraction of immune cells during metastasis, various neurological disorders, autoimmune disease, obesity, and atherosclerosis [35]. We previously reported that IL-33 enhanced MCP-1 protein expression in HUVECs by the method of antibody array assay [7]. Previous studies also demonstrated that IL-33 increased MCP-1 expression in various cells, including human and mouse mast cells [8,10,12,14], human corneal epithelial cells [11], human vascular endothelial cells [9,15], and human cancer cells [13,26]. In the present study, immunocytochemical examination and Western immunoblot assay revealed that IL-33

increased MCP-1 protein expression in HUVECs. In addition, real-time PCR and ELISA demonstrated that IL-33 increased gene expression and protein secretion of MCP-1 in a dose- and time-dependent manner in HUVECs. The biological roles of IL-33-induced MCP-1 upregulation in various cells need further investigation.

Extracellular IL-33 binds transmembrane receptor ST2 and causes ST2-dependent signaling pathways including MAPK pathways, such as ERK1/2, p38 MAPK, and JNK. Signal transduction pathways involved in IL-33-induced MCP-1 activation were investigated by previous studies. Yagami et al. demonstrated that the IL-33-mediated synthesis of MCP-1 were dramatically and dose-dependently reduced by the addition of p38 MAPK inhibitor SB202190 but not by ERK inhibitor PD98059, indicating that p38 MAPK is required for the IL-33-mediated increase in MCP-1 in human vascular endothelial cells [15]. Another study showed that p38 MAPK inhibition with SB203580 suppressed IL-33-induced MCP-1 secretion without inhibiting MCP-1 gene expression in human skin mast cells, suggesting post-transcriptional involvement [10]. IL-33-induced MCP-1 gene expression was significantly inhibited by either MEK inhibitor U0126 or p38 MAPK inhibitor SB203580, suggesting that both ERK1/2 and p38 MAPK pathways are involved in the IL-33-induced upregulation of MCP-1 in bone marrow-derived mast cells [14]. In the present study, upregulation of MCP-1 mRNA and protein secretion induced by IL-33 in HUVECs was significantly suppressed by p38 MAPK inhibitor SB203580 and JNK inhibitor SP600124, suggesting that IL-33-induced MCP-1 upregulation involves both p38 MAPK and JNK pathways in HUVECs. These findings were supported by the previous investigation that stimulation of human mast cells with IL-33 significantly increased MCP-1 secretion via p38 MAPK and JNK pathways, with a higher concentration of JNK inhibitor required to inhibit MCP-1 release in human mast cells [8]. Further studies are required to explore the role of the MAPK pathways in the biological actions of IL-33 in various types of cells.

Cell migration is essential for proper immune response, wound repair, and tissue homeostasis, while aberrant cell migration is found in various pathological conditions [36]. MCP-1 plays an important role in migration of not only monocytes/macrophages but also cancer cells. MCP-1 induces cancer cell abscission, migration, and invasion in both autocrine and paracrine manners, playing a pivotal role in tumor metastasis [19,20]. In addition to the cell-migrating properties of MCP-1, accumulating evidence has revealed that IL-33 also promotes migration of various cells. IL-33 increased the migration of human endothelial cells, playing an important role in angiogenesis [21] and lymphangiogenesis [22]. IL-33 also stimulated the migration and invasion of human gastric cancer cells [24], human lung cancer cells [25], and human esophageal cancer cells [26]. Lin et al. demonstrated that IL-33 enhanced cell migration and invasion via inducing the epithelial-to-mesenchymal transition by JNK activation in human glioma cells [37]. Tjota et al. [38] demonstrated that IL-33 promoted the expression of multiple chemokines including MCP-1 and that exogenous recombinant IL-33 migrated monocytes to the lung interstitium. The significant roles of IL-33-induced MCP-1 were examined by other investigations. Hu et al. reported that IL-33 and its receptor ST2 were co-expressed in decidual stromal cells, and IL-33 stimulated the activation of NFκB and ERK1/2 to increase the expression of MCP-1, thereby promoting the migration and invasion of decidual stromal cells [27]. IL-33 promoted cancer cell migration and invasion via inducing epithelial-to-mesenchymal transition by the activation of MCP-1 in esophageal squamous cell carcinoma [26]. Although these findings raise the possibility that IL-33 might promote cell migration via activating MCP-1 in various cells, the precise roles of MCP-1 on IL-33-promoted normal or cancer cell migration remain undefined. In the current study, we confirmed that IL-33 promoted THP-1 migration, which was significantly suppressed by anti-MCP-1 antibody, suggesting that MCP-1 induced by IL-33 plays an important role in the migration of monocytes. Taken together, these results suggest that IL-33 is involved in the pathophysiology of cell migration due to upregulation of MCP-1 in vascular endothelial cells.

Statins, HMG-CoA reductase inhibitors, are cholesterol-lowering drugs that are widely prescribed in the treatment of cardiovascular diseases. Statins exert numerous pleiotropic

effects including anti-inflammatory actions [30]. Indeed, we have already demonstrated that simvastatin reduces IL-6-induced monocyte chemotaxis and MCP-1 expression in human vascular endothelial cells by inhibiting the Janus kinase-signal transducers and activators of transcription (JAK-STAT) pathway [31]. The effects of statins on IL-33-mediated inflammation have been reported in the literature. Montecucco et al. demonstrated that simvastatin inhibited C-reactive protein-induced MCP-1 secretion and monocyte migration through the inhibition of the ERK1/2 signaling pathway [32]. Romano et al. reported that simvastatin also caused a dose-dependent inhibition of MCP-1 production in peripheral blood mononuclear cells exposed to lipopolysaccharide and in human endothelial cells exposed to IL-1β [33]. The present study revealed that simvastatin suppressed MCP-1 gene expression and protein secretion induced by IL-33 in HUVECs. Furthermore, it is interesting that simvastatin only suppressed the IL-33-mediated phospho-JNK pathway but not the p38 MAPK pathway. In addition, simvastatin suppressed the phosphorylation of c-Jun and its translocation to the nucleus in HUVECs in the present study. These findings suggest that simvastatin may act as a JNK inhibitor in the treatment of inflammation.

The simvastatin concentrations used in the present study are higher than the therapeutic plasma concentrations of simvastatin in clinical situations with humans. The present study demonstrated that 10 μmol/L of simvastatin inhibited the gene expression and protein secretion of MCP-1 as well as the phosphorylation of JNK and c-Jun in HUVECs. In pharmacokinetic studies, Lilja et al. [39] reported that the maximal plasma concentrations of simvastatin in human subjects receiving 40 mg of simvastatin daily were almost 5–30 ng/mL (0.01–0.07 μmol/L). However, previous in vitro studies have also reported that simvastatin is used with similar concentrations as those of the current study in monocytes, osteoblasts, and vascular endothelial cells [31,40,41]. In addition, the duration of exposure to statins in HUVECs should be considered in the in vitro cell culture experiments. Despite low levels of simvastatin in plasma, cells are constantly exposed to simvastatin and may be accumulated intracellularly. As the time of exposure of cells to simvastatin is very short, usually only for an hour, any significant inhibition of the MCP-1 gene and protein expression induced by IL-33 might require higher concentrations of simvastatin in the in vitro experiments. The clinical relevance of simvastatin concentrations in the in vitro studies needs further investigation.

4. Materials and Methods

4.1. Regents

Recombinant human IL-33 was purchased from Pepro Tech (Rocky Hill, NJ, USA). The mouse monoclonal anti-human MCP-1 antibody was from Santa Cruz Biotechnology (Heidelberg, Germany). The rabbit polyclonal antibodies for JNK, phospho-JNK (Thr183/Tyr185), p38, phospho-p38 (Thr180/Tyr182), ERK1/2, phospho-ERK1/2 (p42/44 MAPK), c-Jun, and phospho-c-Jun (Ser73) were obtained from Cell Signaling Technology (Beverly, MA, USA). SP600125 (JNK inhibitor) was purchased from BIOMOL (Plymouth Meeting, PA, USA). Simvastatin, PD98059 (ERK1/2 inhibitor), and SB203580 (p38 MAPK inhibitor) were purchased from FUJIFILM Wako Pure Chemical (Osaka, Japan). Mevalonate was obtained from Sigma (St Louis, MO, USA).

4.2. Cell Culture of HUVECs

HUVECs were purchased from Kurabo (Osaka, Japan) and seeded in plastic plates precoated with type I collagen (Asahi Techno Glass, Nagoya, Japan) and were maintained in endothelial cell growth medium (Promo cell, Heidelberg, Germany) supplemented with 0.5 μg/mL fungizone, 0.25 μg/mL amphotericin B, 100 μg/mL streptomycin, and 100 U/mL penicillin (Life Technologies, Carlsbad, CA, USA).

4.3. Immunocytochemical Staining

HUVECs incubated on a Biocoat slide glass (BD Biosciences, San Jose, CA, USA) were fixed with 4% buffered paraformaldehyde (FUJIFILM Wako Pure Chemical, Osaka, Japan)

for 20 min. The indirect immunoperoxidase method was used for the immunocytochemical analysis as described previously [42]. The primary antibody against MCP-1 was used at 100-fold dilution. The specificity of the staining was confirmed by substitution of the normal mouse IgG for the primary antibody. The intensity of staining was semiquantitatively evaluated by two independent examiners. Grades for the staining intensity ranged from 0 to 3, with 0 indicating no staining; 1, weak staining; 2, moderate staining; and 3, strong staining.

4.4. Western Immunoblot Analysis

Western immunoblot analysis was performed as described previously with some modifications [42,43]. In brief, HUVECs were lysed with ice-cold cell lysis buffer together with phenylmethylsulphonyl fluoride and protease inhibitor cocktail. The harvested cells were resuspended in sodium dodecyl sulfate sample buffer and dithiothreitol, sonicated, and boiled for 5 min. They were separated by 4–12% NuPAGE Bis-Tris gels (Life Technologies, Carlsbad, CA, USA) and transferred to a polyvinylidene difluoride membrane by electroblotting for 2 h. The membrane was soaked in 5% nonfat dry milk blocking buffer. The membrane was then incubated with the primary antibody overnight at 4 °C at concentrations as suggested by the manufacturer, followed by incubation with horseradish peroxidase-conjugated secondary antibody (Cell Signaling Technology, Beverly, MA, USA) for 1 h. The protein bands were visualized by ECL prime (GE Healthcare, Buckinghamshire, UK), and the intensities of the blots were analyzed by a ChemiDoc Touch Imaging System (Bio-Rad, Hercules, CA, USA).

4.5. Total RNA Extraction and Real-Time RT-PCR

A Pure Link RNA Mini kit (Invitrogen, Carlsbad, CA, USA) was used for the extraction of total RNA from HUVECs, and cDNA was synthesized with a Superscript VILO cDNA Synthesis kit (Invitrogen, Carlsbad, CA, USA). Real-time PCR was performed using Power SYBR Green PCR Master Mix (Applied Biosystems, Warrington, UK) on a CFX connect thermal cycler (Bio-Rad, Hercules, CA, USA). The value of each cDNA was calculated using the ΔΔCq method and normalized to the value of the housekeeping gene glyceraldehyde-3-phosphate dehydrogenase (GAPDH).

Oligonucleotide PCR primers targeting MCP-1 mRNA were designed according to a previous report [44], and the specificity of the primers was confirmed by BLAST search and melting curve analysis. The primer sequences are shown in Table 1.

Table 1. Primers and amplicons of real-time RT-PCR.

Gene Name	Primer Sequences (Forward/Reverse)	Position (nt)	Amplicon Size (bp)
MCP-1	F: 5′-CATAGCAGCCACCTTCATTCC-3′ R: 5′-TCTCCTTGGCCACAATGGTC-3′	109–129 274–293	185
GAPDH	F: 5′-GCACCGTCAAGGCTGAGAAC-3′ R: 5′-TGGTGAAGACGCCAGTGGA-3′	361–380 498–516	138

The reaction conditions were as follows: activation step at 95 °C for 10 min, followed by 40 cycles of denaturation at 95 °C for 15 s and annealing/extension at 60 °C for 1 min.

4.6. Enzyme-Linked Immunosorbent Assay (ELISA)

Concentrations of MCP-1 in the culture medium were determined by using a human MCP-1 ELISA kit (R&D Systems, Minneapolis, MN, USA) according to the manufacturer's protocol. The optical densities of samples and standards were measured spectrophotometrically with an iMark microplate reader (BIORAD, Hercules, CA, USA). MCP-1 concentrations were determined by comparison of the optical density results with the standard curve.

4.7. Cell Viability

Cell viability was determined based on the MTT assay (Roche, Mannheim, Germany). HUVECs were treated with 0.01, 0.1, 1, 10, or 100 μmol/L simvastatin for 24 h, after which 0.5 mg/mL MTT solution was added to the culture medium, and then incubated for 4 h. After adding dimethyl sulfoxide to the cells, the absorbance at 570 nm was measured with an iMark microplate reader (BIORAD, Hercules, CA, USA). The survival rates of the simvastatin-treated cells were compared with those of the control untreated cells.

4.8. Immunofluorescence Staining

HUVECs plated on a BioCoat slide glass (BD biosciences, San Jose, CA, USA) were fixed with 4% paraformaldehyde and permeabilized with 0.1% Triton X-100. They were blocked with normal horse serum for 30 min and incubated with the rabbit phospho-c-Jun antibody at 800-fold dilution overnight. Then, they were washed and incubated with anti-rabbit IgG-Alexa (Cell Signaling Technology, Beverly, MA, USA) at 250-fold dilution for 1 h, and the nuclei were counterstained with Hoechst 33342 (Invitrogen, Carlsbad, CA, USA) for 5 min. Images were analyzed by fluorescence microscope (Olympus, Tokyo, Japan). The percentage of phospho-c-Jun-positive cell nuclei was evaluated in five fields of each slide.

4.9. Chemotaxis Assay

A microchemotaxis chamber with polyvinylpyrrolidone-free polycarbonate filter (5 μm pore size) was used for the chemotaxis assay. THP-1 monocytic cells (8×10^6 cells/mL) were plated in the upper wells of ChemoTx microplates (Neuro Probe Inc. Gaithersburg, MD, USA). The culture medium derived from untreated or IL-33-treated cells was added to the lower wells. The number of THP-1 cells migrated to the lower chamber was counted by a hemocytometer. The culture medium from the untreated cells supplemented with recombinant human MCP-1 at 100 nmol/L (PeproTech, Rocky Hill, NT, USA) served as a positive control. Normal goat IgG (R&D Systems, Minneapolis, MN, USA) was used as a negative control. To evaluate MCP-1 specific chemotaxis, anti-human MCP-1 polyclonal antibody (R&D Systems, Minneapolis, MN, USA) was added at 80 μg/mL to neutralize the secreted MCP-1.

4.10. Statistical Analysis

Data are shown as mean ± SD. Each data point represents the average of three to six independent experiments. Statistical significance of the data was assessed by one-way ANOVA with the Tukey–Kramer's post hoc test. p value < 0.05 was considered statistically significant.

5. Conclusions

In conclusion, the present study demonstrated that IL-33 induces gene expression and protein secretion of MCP-1 through the activation of the JNK and p38 MAPK pathways in human vascular endothelial cells. Furthermore, simvastatin suppressed MCP-1 production by selectively inhibiting the JNK pathway. We speculate that the increase in local and circulating IL-33 levels in patients with inflammatory disease would stimulate the vascular endothelial cells to enhance MCP-1 production via the JNK and p38 MAPK pathways. Simvastatin could reduce IL-33-mediated MCP-1 production by inhibiting the JNK pathway and suppressing the recruitment of monocytes into the inflammatory lesions. These findings indicate that simvastatin may be potentially utilized as a novel therapeutic strategy for IL-33-associated inflammation.

Author Contributions: M.J. supervised and conceived the project. K.U. and M.J. designed experiments and wrote the manuscript. K.U., M.Y., A.T., K.S. and Y.T. performed experiments and interpreted data. K.U., K.S. and Y.T. contributed reagents/analytic tools. M.J. edited the manuscript. All authors have read and agreed to the published version of the manuscript.

Funding: This research was funded by a grant from National Hospital Organization Collaborative Clinical Research.

Institutional Review Board Statement: Not applicable. This study did not involve human participants or animals.

Informed Consent Statement: Not applicable. This study did not involve humans.

Data Availability Statement: The data that support the findings of this study are available from the authors upon reasonable request.

Acknowledgments: We thank Reiko Saino for secretarial work.

Conflicts of Interest: The authors declare no conflict of interest.

References

1. Schmitz, J.; Owyang, A.; Oldham, E.; Song, Y.; Murphy, E.; McClanahan, T.K.; Zurawski, G.; Moshrefi, M.; Qin, J.; Li, X.; et al. IL-33, an interleukin-1-like cytokine that signals via the IL-1 receptor-related protein ST2 and induces T helper type 2-associated cytokines. *Immunity* **2005**, *23*, 479–490. [CrossRef] [PubMed]
2. Kakkar, R.; Hei, H.; Dobner, S.; Lee, R.T. Interleukin 33 as a mechanically responsive cytokine secreted by living cells. *J. Biol. Chem.* **2012**, *287*, 6941–6948. [CrossRef] [PubMed]
3. Miller, A.M. Role of IL-33 in inflammation and disease. *J. Inflamm.* **2011**, *8*, 22. [CrossRef] [PubMed]
4. Villarreal, D.O.; Weiner, D.B. Interleukin 33: A switch-hitting cytokine. *Curr. Opin. Immunol.* **2014**, *28*, 102–106. [CrossRef] [PubMed]
5. Weber, A.; Wasiliew, P.; Kracht, M. Interleukin-1 (IL-1) pathway. *Sci Signal* **2010**, *3*, cm1. [CrossRef] [PubMed]
6. Umebashi, K.; Tokito, A.; Yamamoto, M.; Jougasaki, M. Interleukin-33 induces interleukin-8 expression via JNK/c-Jun/AP-1 pathway in human umbilical vein endothelial cells. *PLoS ONE* **2018**, *13*, e0191659. [CrossRef] [PubMed]
7. Yamamoto, M.; Umebashi, K.; Tokito, A.; Imamura, J.; Jougasaki, M. Interleukin-33 induces growth-regulated oncogene-alpha expression and secretion in human umbilical vein endothelial cells. *Am. J. Physiol. Regul. Integr. Comp. Physiol.* **2017**, *313*, R272–R279. [CrossRef] [PubMed]
8. Bawazeer, M.A.; Theoharides, T.C. IL-33 stimulates human mast cell release of CCL5 and CCL2 via MAPK and NF-kappaB, inhibited by methoxyluteolin. *Eur. J. Pharmacol.* **2019**, *865*, 172760. [CrossRef]
9. Demyanets, S.; Konya, V.; Kastl, S.P.; Kaun, C.; Rauscher, S.; Niessner, A.; Pentz, R.; Pfaffenberger, S.; Rychli, K.; Lemberger, C.E.; et al. Interleukin-33 induces expression of adhesion molecules and inflammatory activation in human endothelial cells and in human atherosclerotic plaques. *Arterioscler. Thromb. Vasc. Biol.* **2011**, *31*, 2080–2089. [CrossRef]
10. Franke, K.; Wang, Z.; Zuberbier, T.; Babina, M. Cytokines stimulated by IL-33 in human skin mast cells: Involvement of NF-κB and p38 at distinct levels and potent co-operation with FcεRI and MRGPRX2. *Int. J. Mol. Sci.* **2021**, *22*, 3580. [CrossRef]
11. Lin, J.; Zhao, G.Q.; Wang, Q.; Xu, Q.; Che, C.Y.; Hu, L.T.; Jiang, N.; Wang, Q.; Zhang, L.L. Regulation of interleukin 33/ST2 signaling of human corneal epithelium in allergic diseases. *Int. J. Ophthalmol.* **2013**, *6*, 23–29.
12. Moulin, D.; Donzé, O.; Talabot-Ayer, D.; Mézin, F.; Palmer, G.; Gabay, C. Interleukin (IL)-33 induces the release of pro-inflammatory mediators by mast cells. *Cytokine* **2007**, *40*, 216–225. [CrossRef] [PubMed]
13. O'Donnell, C.; Mahmoud, A.; Keane, J.; Murphy, C.; White, D.; Carey, S.; O'Riordain, M.; Bennett, M.W.; Brint, E.; Houston, A. An antitumorigenic role for the IL-33 receptor, ST2L, in colon cancer. *Br. J. Cancer* **2016**, *114*, 37–43. [CrossRef] [PubMed]
14. Ohto-Ozaki, H.; Hayakawa, M.; Kamoshita, N.; Maruyama, T.; Tominaga, S.I.; Ohmori, T. Induction of IκBζ augments cytokine and chemokine production by IL-33 in mast cells. *J. Immunol.* **2020**, *204*, 2033–2042. [CrossRef] [PubMed]
15. Yagami, A.; Orihara, K.; Morita, H.; Futamura, K.; Hashimoto, N.; Matsumoto, K.; Saito, H.; Matsuda, A. IL-33 mediates inflammatory responses in human lung tissue cells. *J. Immunol.* **2010**, *185*, 5743–5750. [CrossRef] [PubMed]
16. Fang, W.B.; Jokar, I.; Zou, A.; Lambert, D.; Dendukuri, P.; Cheng, N. CCL2/CCR2 chemokine signaling coordinates survival and motility of breast cancer cells through Smad3 protein- and p42/44 mitogen-activated protein kinase (MAPK)-dependent mechanisms. *J. Biol. Chem.* **2012**, *287*, 36593–36608. [CrossRef] [PubMed]
17. Liu, J.F.; Chen, P.C.; Chang, T.M.; Hou, C.H. Monocyte Chemoattractant Protein-1 promotes cancer cell migration via c-Raf/MAPK/AP-1 pathway and MMP-9 production in osteosarcoma. *J. Exp. Clin. Cancer Res.* **2020**, *39*, 254. [CrossRef] [PubMed]
18. Loberg, R.D.; Day, L.L.; Harwood, J.; Ying, C.; St John, L.N.; Giles, R.; Neeley, C.K.; Pienta, K.J. CCL2 is a potent regulator of prostate cancer cell migration and proliferation. *Neoplasia* **2006**, *8*, 578–586. [CrossRef]
19. Xu, M.; Wang, Y.; Xia, R.; Wei, Y.; Wei, X. Role of the CCL2-CCR2 signalling axis in cancer: Mechanisms and therapeutic targeting. *Cell Prolif.* **2021**, *54*, e13115. [CrossRef]
20. Zhang, J.; Lu, Y.; Pienta, K.J. Multiple roles of chemokine (C-C motif) ligand 2 in promoting prostate cancer growth. *J. Natl. Cancer Inst.* **2010**, *102*, 522–528. [CrossRef]

21. Choi, Y.S.; Choi, H.J.; Min, J.K.; Pyun, B.J.; Maeng, Y.S.; Park, H.; Kim, J.; Kim, Y.M.; Kwon, Y.G. Interleukin-33 induces angiogenesis and vascular permeability through ST2/TRAF6-mediated endothelial nitric oxide production. *Blood* **2009**, *114*, 3117–3126. [CrossRef] [PubMed]
22. Han, L.; Zhang, M.; Liang, X.; Jia, X.; Jia, J.; Zhao, M.; Fan, Y. Interleukin-33 promotes inflammation-induced lymphangiogenesis via ST2/TRAF6-mediated Akt/eNOS/NO signalling pathway. *Sci. Rep.* **2017**, *7*, 10602. [CrossRef] [PubMed]
23. Toyama, S.; Moniaga, C.S.; Nakae, S.; Kurosawa, M.; Ogawa, H.; Tominaga, M.; Takamori, K. Regulatory T cells exhibit interleukin-33-dependent migratory behavior during skin barrier disruption. *Int. J. Mol. Sci.* **2021**, *22*, 7443. [CrossRef] [PubMed]
24. Huang, N.; Cui, X.; Li, W.; Zhang, C.; Liu, L.; Li, J. IL-33/ST2 promotes the malignant progression of gastric cancer via the MAPK pathway. *Mol. Med. Rep.* **2021**, *23*, 361. [CrossRef] [PubMed]
25. Yang, Z.; Gao, X.; Wang, J.; Xu, L.; Zheng, Y.; Xu, Y. Interleukin-33 enhanced the migration and invasiveness of human lung cancer cells. *OncoTargets Ther.* **2018**, *11*, 843–849. [CrossRef] [PubMed]
26. Yue, Y.; Lian, J.; Wang, T.; Luo, C.; Yuan, Y.; Qin, G.; Zhang, B.; Zhang, Y. Interleukin-33-nuclear factor-κB-CCL2 signaling pathway promotes progression of esophageal squamous cell carcinoma by directing regulatory T cells. *Cancer Sci.* **2020**, *111*, 795–806. [CrossRef] [PubMed]
27. Hu, W.T.; Li, M.Q.; Liu, W.; Jin, L.P.; Li, D.J.; Zhu, X.Y. IL-33 enhances proliferation and invasiveness of decidual stromal cells by up-regulation of CCL2/CCR2 via NF-κB and ERK1/2 signaling. *Mol. Hum. Reprod.* **2014**, *20*, 358–372. [CrossRef]
28. Grundy, S.M.; Stone, N.J.; Bailey, A.L.; Beam, C.; Birtcher, K.K.; Blumenthal, R.S.; Braun, L.T.; de Ferranti, S.; Faiella-Tommasino, J.; Forman, D.E.; et al. 2018 AHA/ACC/AACVPR/AAPA/ABC/ACPM/ADA/AGS/APhA/ASPC/NLA/PCNA Guideline on the Management of Blood Cholesterol: Executive Summary: A Report of the American College of Cardiology/American Heart Association Task Force on Clinical Practice Guidelines. *J. Am. Coll. Cardiol.* **2019**, *73*, 3168–3209. [CrossRef]
29. Sadowitz, B.; Maier, K.G.; Gahtan, V. Basic science review: Statin therapy—Part I: The pleiotropic effects of statins in cardiovascular disease. *Vasc. Endovasc. Surg.* **2010**, *44*, 241–251. [CrossRef]
30. Takemoto, M.; Liao, J.K. Pleiotropic effects of 3-hydroxy-3-methylglutaryl coenzyme a reductase inhibitors. *Arterioscler. Thromb. Vasc. Biol.* **2001**, *21*, 1712–1719. [CrossRef]
31. Jougasaki, M.; Ichiki, T.; Takenoshita, Y.; Setoguchi, M. Statins suppress interleukin-6-induced monocyte chemo-attractant protein-1 by inhibiting Janus kinase/signal transducers and activators of transcription pathways in human vascular endothelial cells. *Br. J. Pharmacol.* **2010**, *159*, 1294–1303. [CrossRef] [PubMed]
32. Montecucco, F.; Burger, F.; Pelli, G.; Poku, N.K.; Berlier, C.; Steffens, S.; Mach, F. Statins inhibit C-reactive protein-induced chemokine secretion, ICAM-1 upregulation and chemotaxis in adherent human monocytes. *Rheumatology* **2009**, *48*, 233–242. [CrossRef] [PubMed]
33. Romano, M.; Diomede, L.; Sironi, M.; Massimiliano, L.; Sottocorno, M.; Polentarutti, N.; Guglielmotti, A.; Albani, D.; Bruno, A.; Fruscella, P.; et al. Inhibition of monocyte chemotactic protein-1 synthesis by statins. *Lab. Investig.* **2000**, *80*, 1095–1100. [CrossRef] [PubMed]
34. Van der Vorst, E.P.; Doring, Y.; Weber, C. Chemokines and their receptors in Atherosclerosis. *J. Mol. Med.* **2015**, *93*, 963–971. [CrossRef] [PubMed]
35. O'Connor, T.; Borsig, L.; Heikenwalder, M. CCL2-CCR2 signaling in disease pathogenesis. *Endocr. Metab. Immune Disord. Drug Targets* **2015**, *15*, 105–118. [CrossRef] [PubMed]
36. Trepat, X.; Chen, Z.; Jacobson, K. Cell migration. *Compr. Physiol.* **2012**, *2*, 2369–2392.
37. Lin, L.; Li, Y.; Liu, M.; Li, Q.; Liu, Q.; Li, R. The Interleukin-33/ST2 axis promotes glioma mesenchymal transition, stemness and TMZ resistance via JNK activation. *Aging* **2020**, *12*, 1685–1703. [CrossRef]
38. Tjota, M.Y.; Camacho, D.F.; Turnquist, H.R.; Sperling, A.I. IL-33 drives monocyte recruitment to lung interstitium through chemokine upregulation. *Immunohorizons* **2017**, *1*, 101–108. [CrossRef]
39. Lilja, J.J.; Neuvonen, M.; Neuvonen, P.J. Effects of regular consumption of grapefruit juice on the pharmacokinetics of simvastatin. *Br. J. Clin. Pharmacol.* **2004**, *58*, 56–60. [CrossRef]
40. Thunyakitpisal, P.D.; Chaisuparat, R. Simvastatin, an HMG-CoA reductase inhibitor, reduced the expression of matrix metalloproteinase-9 (Gelatinase B) in osteoblastic cells and HT1080 fibrosarcoma cells. *J. Pharmacol. Sci.* **2004**, *94*, 403–409. [CrossRef]
41. Han, K.H.; Ryu, J.; Hong, K.H.; Ko, J.; Pak, Y.K.; Kim, J.B.; Park, S.W.; Kim, J.J. HMG-CoA reductase inhibition reduces monocyte CC chemokine receptor 2 expression and monocyte chemoattractant protein-1-mediated monocyte recruitment in vivo. *Circulation* **2005**, *111*, 1439–1447. [CrossRef]
42. Ichiki, T.; Jougasaki, M.; Setoguchi, M.; Imamura, J.; Nakashima, H.; Matsuoka, T.; Sonoda, M.; Nakamura, K.; Minagoe, S.; Tei, C. Cardiotrophin-1 stimulates intercellular adhesion molecule-1 and monocyte chemoattractant protein-1 in human aortic endothelial cells. *Am. J. Physiol. Heart Circ. Physiol.* **2008**, *294*, H750–H763. [CrossRef]

43. Tokito, A.; Jougasaki, M.; Ichiki, T.; Hamasaki, S. Cardiotrophin-1 induces matrix metalloproteinase-1 in human aortic endothelial cells. *PLoS ONE* **2013**, *8*, e68801. [CrossRef]
44. Benedetti, F.; Davinelli, S.; Krishnan, S.; Gallo, R.C.; Scapagnini, G.; Zella, D.; Curreli, S. Sulfur compounds block MCP-1 production by Mycoplasma fermentans-infected macrophages through NF-κB inhibition. *J. Transl. Med.* **2014**, *12*, 145. [CrossRef]

International Journal of
Molecular Sciences

MDPI

Article

Autocrine Regulation of Interleukin-6 via the Activation of STAT3 and Akt in Cardiac Myxoma Cells

Michihisa Jougasaki *, Yoko Takenoshita, Katsuyuki Umebashi, Masayoshi Yamamoto, Ku Sudou, Hitoshi Nakashima, Masahiro Sonoda and Tamahiro Kinjo

Institute for Clinical Research, NHO Kagoshima Medical Center, Kagoshima 892-0853, Japan; takenoshita.yoko.cj@mail.hosp.go.jp (Y.T.); umebashi.katsuyuki.gc@mail.hosp.go.jp (K.U.); yamamoto.masayoshi.bc@mail.hosp.go.jp (M.Y.); pd3z8uos@okayama-u.ac.jp (K.S.); nakashima.hitoshi.mc@mail.hosp.go.jp (H.N.); sonoda.masahiro.by@mail.hosp.go.jp (M.S.); kinjo.tamahiro.tr@mail.hosp.go.jp (T.K.)

* Correspondence: jogasaki.michihisa.kb@mail.hosp.go.jp; Tel.: +81-99-223-1151

Abstract: Plasma concentrations of a pleiotropic cytokine, interleukin (IL)-6, are increased in patients with cardiac myxoma. We investigated the regulation of IL-6 in cardiac myxoma. Immunohistochemical staining and reverse transcription-polymerase chain reaction (RT-PCR) revealed that IL-6 and its receptors, IL-6 receptor (IL-6R) and gp130, co-existed in the myxoma cells. Myxoma cells were cultured, and an antibody array assay showed that a conditioned medium derived from the cultured myxoma cells contained increased amounts of IL-6. Signal transducer and activator of transcription (STAT) 3 and Akt were constitutively phosphorylated in the myxoma cells. An enzyme-linked immunosorbent assay (ELISA) showed that the myxoma cells spontaneously secreted IL-6 into the culture medium. Real-time PCR revealed that stimulation with IL-6 + soluble IL-6R (sIL6R) significantly increased IL-6 mRNA in the myxoma cells. Pharmacological inhibitors of STAT3 and Akt inhibited the IL-6 + sIL-6R-induced gene expression of IL-6 and the spontaneous secretion of IL-6. In addition, IL-6 + sIL-6R-induced translocation of phosphorylated STAT3 to the nucleus was also blocked by STAT3 inhibitors. This study has demonstrated that IL-6 increases its own production via STAT3 and Akt pathways in cardiac myxoma cells. Autocrine regulation of IL-6 may play an important role in the pathophysiology of patients with cardiac myxoma.

Keywords: myxoma; interleukin-6; autocrine; STAT3; Akt

Citation: Jougasaki, M.; Takenoshita, Y.; Umebashi, K.; Yamamoto, M.; Sudou, K.; Nakashima, H.; Sonoda, M.; Kinjo, T. Autocrine Regulation of Interleukin-6 via the Activation of STAT3 and Akt in Cardiac Myxoma Cells. *Int. J. Mol. Sci.* **2024**, *25*, 2232. https://doi.org/10.3390/ijms25042232

Academic Editor: Apostolos Zaravinos

Received: 19 January 2024
Revised: 8 February 2024
Accepted: 9 February 2024
Published: 13 February 2024

1. Introduction

Interleukin (IL)-6 is a multifunctional cytokine that plays important roles in immune regulation, inflammation, metabolism, and tissue regeneration [1,2]. In IL-6 classic signaling, IL-6 binds to IL-6-transmembrane receptor (IL-6R) and subsequent recruitment of the transmembrane gp130, activating the intracellular signal transduction system, including Janus kinase (JAK)-signal transducer and activator of transcription (STAT) 3, phosphatidylinositol-3-kinase (PI3K)/Akt, and mitogen-activated protein kinase [3]. A soluble form of IL-6R (sIL-6R) is released from the cell surface by proteolysis or by IL-6 mRNA alternative splicing. The cells lacking transmembrane IL-6R are not responsive to IL-6; however, they respond to IL-6 in the presence of sIL-6R. Thus, the IL-6 + sIL-6R complex binds to transmembrane gp130 on the cells that do not express transmembrane IL-6R, and this process is known as IL-6 trans-signaling [4]. Nowadays, sIL-6R is considered as an agonist molecule, allowing IL-6 to have an effect on the cells lacking IL-6R but ubiquitously expressing transmembrane gp130 [5]. In addition, IL-6 is produced by a variety of cells, such as T cells, B cells, monocytes-macrophages, fibroblasts, epidermal keratinocytes, endothelial cells, mesangial cells, and tumor cells, including cardiac myxoma cells in the human body [6].

Cardiac myxoma is the most common primary tumor of the heart [7]. The clinical presentation of cardiac myxoma typically involves triad of intracardiac obstruction, embolization, and constitutional symptoms [8]. Accumulating evidence has revealed that cardiac myxomas spontaneously produce IL-6 [9–17], which is associated with the constitutional symptoms in patients with cardiac myxoma. Immunohistochemical studies in patients with cardiac myxoma demonstrated that 70 to 80% of tumors showed immunohistochemical expression of IL-6 [18,19]. Increased gene expression of IL-6 was also found in the cardiac myxoma tissue by using the method of reverse transcription-polymerase chain reaction (RT-PCR) [17] and in situ hybridization [13]. A positive correlation between plasma levels of IL-6 and tumor size was observed in patients with cardiac myxoma [16,20,21]. Specifically, Endo et al. showed that patients with constitutional symptoms had significantly larger tumors than those without constitutional signs, suggesting that the production of IL-6 increased in proportion to tumor size [22]. In contrast, other investigators reported that peripheral monocytes contributed to the elevated production of IL-6 in patients with cardiac myxoma [23]. The regulation of IL-6 in patients with cardiac myxoma has not been clarified yet.

In the present study, we hypothesized that IL-6 was produced in an autocrine and paracrine manner through the activation of STAT3 and Akt signaling pathways in the cardiac myxoma cells. Therefore, this study was designed to investigate the production and secretion of IL-6 in the cardiac myxoma cells, specifically focusing on the signal transduction system of STAT3 and Akt pathways.

2. Results

2.1. Patient Profile

A 70-year-old woman presented with transient dizziness due to ischemic cerebral infarctions. Laboratory tests showed a leukocyte count of 9370 cells/mL, C-reactive protein of 0.48 mg/dL, and IL-6 of 3.29 pg/mL. Echocardiographic examination in search of possible embolic sources for cerebral infarction showed a large mass in the left atrium. Cardiac surgery was performed and ellipsoidal $50 \times 80 \times 55$ mm^3 smooth and glossy tumor adherent to the interatrial septum was resected from the heart. Histological examination revealed that the polygonal, spindle-shaped or stellate cells which had oval nuclei and eosinophilic cytoplasm, exhibiting cords or nests, were surrounded by mucoid matrix (HE staining in Figure 1). The nuclei of the tumor cells were without pleomorphism or mitosis, and the tumor was diagnosed as cardiac myxoma. The study protocol was approved by the institutional review board, and informed consent was given by the patient.

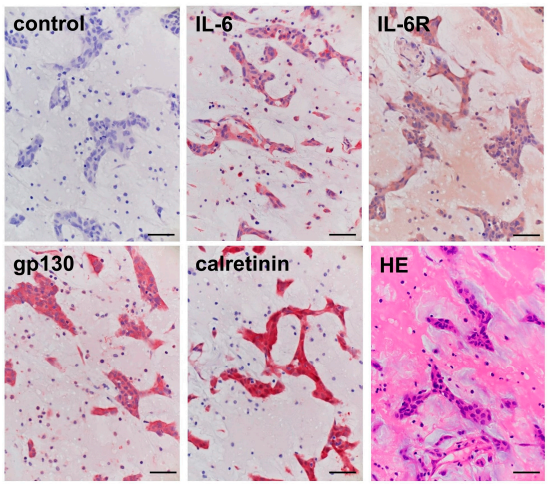

Figure 1. Immunohistochemical staining and hematoxylin-eosin (HE) staining in the cardiac myxoma tissue. Representative immunocytochemical staining showing the localization of IL-6 and its receptor complexes, IL-6R and gp130, and calretinin, together with additional HE staining in the cardiac myxoma tissue. Normal IgG served as a negative control. Original magnification; ×400. Scale bar = 50 μm.

2.2. Immunohistochemical Staining in the Cardiac Myxoma Tissue

Immunohistochemical staining revealed positive immunoreactivities for IL-6, IL-6R, and gp130 in the polygonal, spindle-shaped, or stellate cells of cardiac myxoma (Figure 1). In addition, these myxoma cells showed a strong expression of calretinin. No immunoreactivities were detected in the myxoma tissue when treated with normal IgG instead of the respective primary antibodies.

2.3. Immunocytochemical Staining in the Cardiac Myxoma Cells

Immunocytochemical staining showed positive immunoreactivities for IL-6, IL-6R, and gp130 in the cultured myxoma cells (Figure 2). Immunoreactivities for calretinin was also positive in the myxoma cells. The cells treated with normal IgG instead of the respective primary antibodies demonstrated no immunoreactivities.

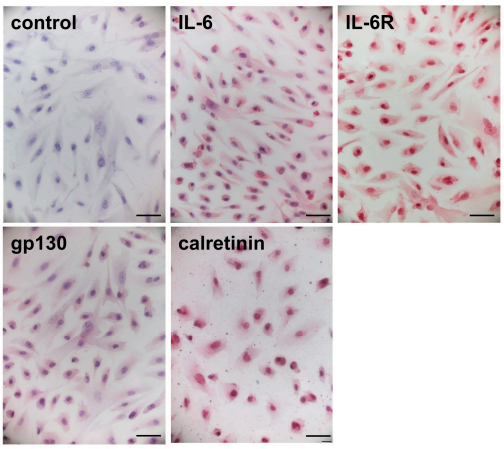

Figure 2. Immunocytochemical staining in the cultured cardiac myxoma cells. Representative immunocytochemical staining showing the localization of IL-6 and its receptor complexes, IL-6R and gp130, and calretinin in the cultured myxoma cells. Normal IgG served as a negative control. Original magnification; ×400. Scale bar = 50 μm.

2.4. Gene Expression of IL-6 and Its Receptor Complexes in the Cardiac Myxoma Cells

To investigate the gene expressions of IL-6, and its receptor complexes, IL-6R and gp130 in the cardiac myxoma cells, total RNA was extracted from the cultured myxoma cells, examined by using RT-PCR, and the results were compared with those in the cultured human umbilical vein endothelial cells (HUVECs). RT-PCR with specific primers demonstrated that both myxoma cells and HUVECs yielded positive products for IL-6, and its receptor complexes, IL-6R and gp130 (Figure 3). However, gene expression of calretinin was detected only in the myxoma cells, but not in the cultured HUVECs.

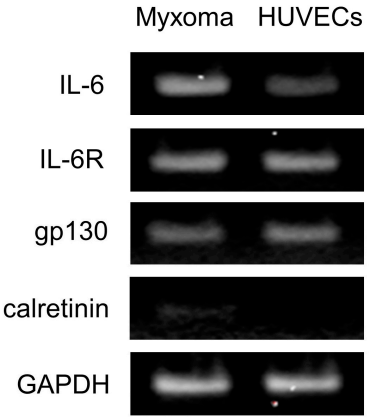

Figure 3. Gene expression of IL-6, IL-6R, gp130, and calretinin in the cardiac myxoma cells. Total RNA was isolated from the cultured cardiac myxoma cells and human umbilical endothelial cells

(HUVECs). Reverse transcription-polymerase chain reaction (RT-PCR) was performed using specific primer pairs for IL-6, IL-6R, gp130, calretinin, and glyceraldehyde-3-phosphate dehydrogenase (GAPDH). PCR reaction was performed using 40 cycles and the PCR products of 149, 124, 107, 118 and 138 bp corresponded to the IL-6, IL-6R, gp130, calretinin, and GAPDH transcripts, respectively.

2.5. Antibody Array Assay

The antibody array assay was used to investigate the protein secreted from the cultured myxoma cells. The culture supernatant of myxoma cells incubated for 7 days were analyzed using a dot blot array. IL-6 was markedly increased in the supernatant of the myxoma cells compared with control culture media (Figure 4). In addition to IL-6, monocyte chemoattractant protein (MCP)-1, granulocyte-macrophage colony-stimulating factor (GM-CSF), and platelet-derived growth factor (PDGF)-BB were also increased in the supernatant of the cultured myxoma cells.

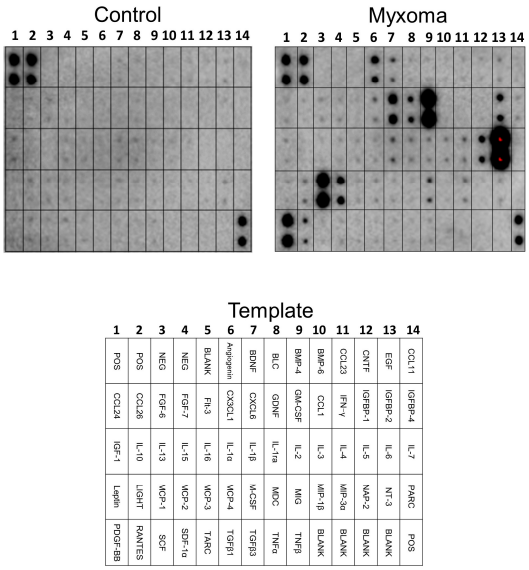

Figure 4. Screening of secreted proteins in the supernatant of the cultured cardiac myxoma cells using antibody array. The culture supernatant of the myxoma cells contained significant amounts of IL-6, monocyte chemoattractant protein (MCP)-1, granulocyte-macrophage colony-stimulating factor (GM-CSF), and platelet-derived growth factor (PDGF)-BB compared with control medium without incubation. POS, positive control; NEG, negative control. For other abbreviations, see RayBio C-Series Human Cytokine Antibody Array C1000 (AAH-CYT-6).

2.6. Culture Supernatant of the Myxoma Cells Induced STAT3 Phosphorylation in HUVECs

We next examined whether the culture supernatant derived from the myxoma cells have transferrable biologic properties to stimulate STAT3 phosphorylation in cultured HUVECs. The myxoma cells were incubated for 7 days, and the supernatant was added to HUVECs, incubated for 30 min, and subjected to Western immunoblot analysis. Culture supernatant derived from the myxoma cells caused activation of STAT3, which was attenuated by the addition of anti-IL-6 antibody, but not by control IgG (Figure 5), suggesting that STAT3 activating properties in the culture supernatant were due, at least in part, to the biological activity of transferable IL-6.

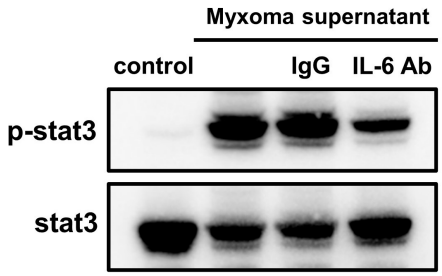

Figure 5. STAT3 phosphorylation induced by the culture supernatant of the cardiac myxoma cells. The culture supernatant derived from the cardiac myxoma cells incubated for 7 days was added to HUVECs and were incubated for 30 min in the presence and absence of anti-IL-6 antibody. Total protein extracts were examined by Western immunoblot analysis.

2.7. Constitutive Phosphorylation of STAT3 and Akt in the Cardiac Myxoma Cells

To determine the phosphorylation status of STAT3 and Akt, the cultured myxoma cells were washed with phosphate-buffered saline, incubated in fresh medium, and left untreated for 24 h. As shown in Figure 6, Western immunoblot analysis demonstrated that STAT3 and Akt were constitutively phosphorylated according to time within 24 h. STAT3 was gradually phosphorylated from 16 to 24 h, although total STAT3 protein was unchanged for 24 h. Phosphorylation of Akt occurred from 4 to 24 h, which was earlier than STAT3 phosphorylation. Similarly, the total Akt protein was not changed for 24 h. On the other hand, STAT1 was not phosphorylated for 24 h.

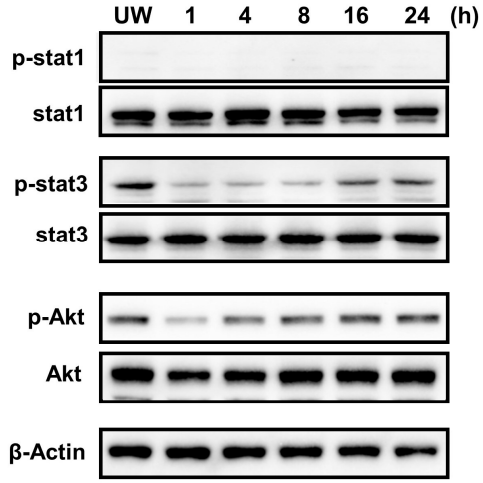

Figure 6. Constitutive phosphorylation of STAT3 and Akt in the cultured cardiac myxoma cells. Cultured cardiac myxoma cells were either unwashed (UW) or washed with phosphate-buffered saline, incubated in fresh culture medium, and left untreated for 1, 4, 8, 16, and 24 h. Total protein extracts were examined by Western immunoblot analysis.

2.8. Secretion of IL-6 from the Cardiac Myxoma Cells

To further examine whether cultured myxoma cells actually secrete IL-6 to the culture medium, the cells were washed with phosphate-buffered saline and incubated in the fresh medium. The supernatant was collected at 8, 16, and 24 h, and the concentration of IL-6 was measured by ELISA. The results were compared with those of HUVECs. Cultured myxoma cells spontaneously secreted considerable amounts of IL-6 into the culture medium from 8 to 24 h (Figure 7A). The addition of antibody against IL-6R or gp130 reduced the secretion of IL-6 from the myxoma cells (Figure 7B). To elucidate the signal transduction pathways accounting for the secretion of IL-6, pharmacological inhibitors were used to interfere with STAT3 and Akt pathways. As shown in Figure 7C, the secretion of IL-6 from the myxoma cells was significantly inhibited by the treatment with AG490 (JAK2 inhibitor, 100 μmol/L),

piceatannol (STAT1/3 inhibitor, 100 μmol/L), LLL12 (STAT3 inhibitor, 10 μmol/L), and Ly294002 (PI3K/Akt inhibitor, 30 μmol/L) (Figure 7C).

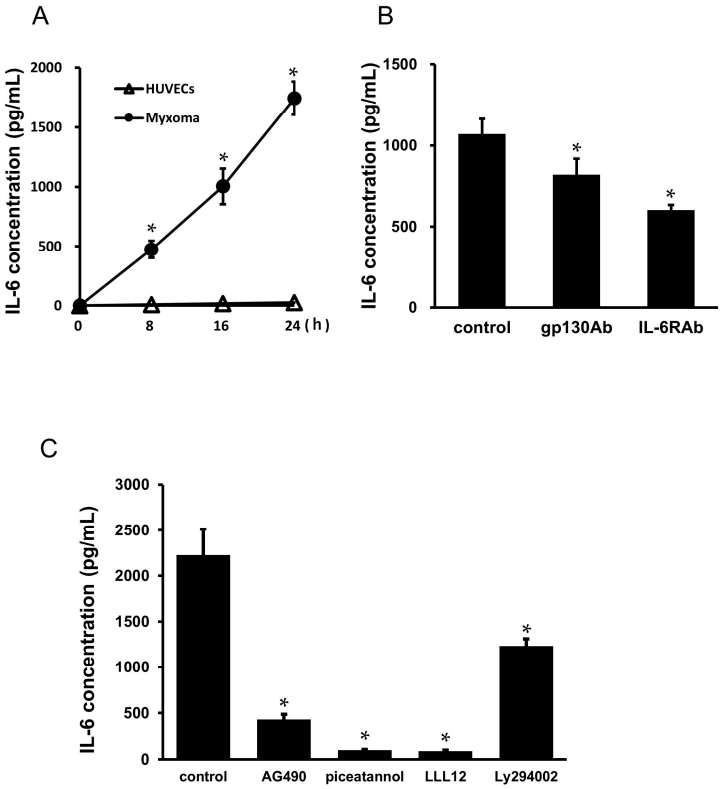

Figure 7. Spontaneous secretion of IL-6 from the cultured cardiac myxoma cells: (**A**) the cultured myxoma cells were washed and incubated in fresh medium. Culture supernatant was collected at 8, 16, and 24 h, measured by ELISA (closed circle), and compared with those of HUVECs (open triangle). IL-6 protein secretion increased in a time-dependent manner. * $p < 0.05$ vs. IL-6 levels in HUVECs at the indicated time; (**B**) the myxoma cells were incubated in fresh medium in the presence or absence of antibody against gp130 or IL-6R. Addition of antibody against gp130 or IL-6R reduced spontaneous secretion of IL-6. * $p < 0.05$ vs. spontaneous IL-6 secretion (control); and (**C**) effects of pharmacological inhibitors of STAT3 and Akt on spontaneous secretion of IL-6 from the cultured myxoma cells. The myxoma cells were pretreated with AG490 (100 μmol/L), piceatannol (100 μmol/L), LLL12 (10 μmol/L), and Ly294002 (30 μmol/L), and IL-6 protein secretion was examined by ELISA ($n = 6$). * $p < 0.05$ vs. IL-6 secretion without any pretreatment (control).

2.9. Effects of STAT3 siRNA Transfection on the Secretion of IL-6 from the Cardiac Myxoma Cells

To further confirm the role of STAT3 in the secretion of IL-6, we transfected antibody-free myxoma cells with STAT3 siRNA. The efficacy of the transfection of siRNA is shown in Figure 8A. Transfection of STAT3 for 48 h reduced STAT3 expression by 56%. Transfection of STAT3 significantly attenuated spontaneous IL-6 secretion from the myxoma cells compared with control-scrambled siRNA transfection (Figure 8B).

2.10. Effects of IL-6 + sIL-6R on the Gene Expression of IL-6 in the Cardiac Myxoma Cells

Real-time PCR demonstrated that treatment with IL-6 + sIL-6R resulted in an increase in IL-6 mRNA in a time-dependent manner with a statistical significance at 4 to 24 h (Figure 9A). To examine whether signaling pathways, such as STAT3 and Akt, were involved in the IL-6 + sIL-6R-induced IL-6 autoregulation, the cultured myxoma cells were pre-treated with pharmacological inhibitors of STAT3 and Akt for 2 h, followed by stimulation with IL-6 + sIL-6R for 4 h to measure IL-6 mRNA in the myxoma cells. Real-time PCR demonstrated that IL-6 + sIL-6R-induced increase in IL-6 mRNA was significantly suppressed by the pretreatment with JAK-STAT inhibitors, such as AG490, piceatannol,

and LLL12 in the myxoma cells (Figure 9B). Akt inhibitor, Ly294002 also decreased IL-6 + sIL-6R-induced increase in IL-6 mRNA as well.

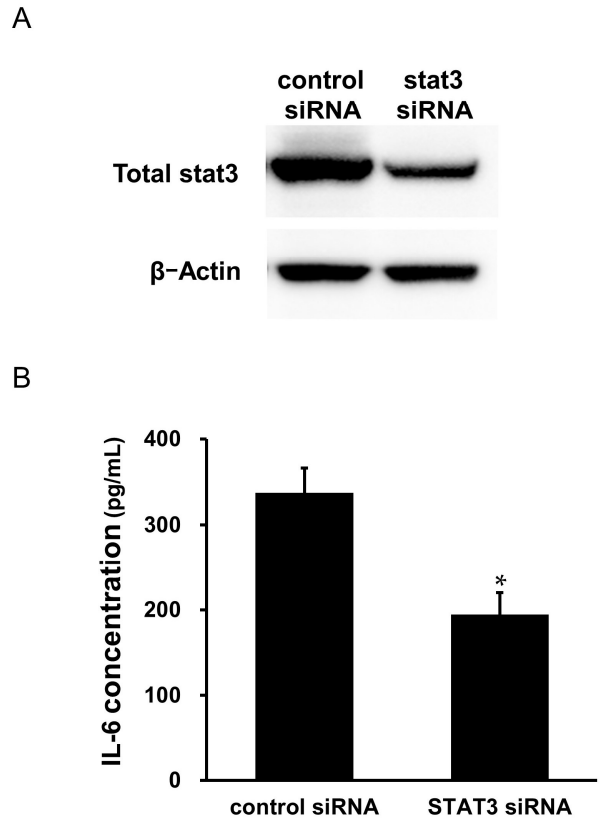

Figure 8. Effects of STAT3 siRNA on the spontaneous secretion of IL-6 from the cardiac myxoma cells. Antibody-free cardiac myxoma cells were transfected with control scrambled siRNA or STAT3 siRNA (100 nmol/L) for 48 h and kept untreated for 24 h: (**A**) cell lysates were evaluated for knock-down of STAT3 by Western immunoblot analysis. β-Actin was used for loading control; and (**B**) IL-6 concentration in the supernatant as measured by ELISA (n = 6). Bars represent IL-6 protein secretion per 10^5 cells (n = 6). * $p < 0.05$ vs. scrambled control siRNA.

2.11. Effects of IL-6 + sIL-6R on the Phosphorylation of STAT3 and Akt in the Cardiac Myxoma Cells

The cultured myxoma cells were exposed to IL-6 + sIL-6R for different time periods (5 to 120 min), and their protein extracts were examined by Western immunoblot analysis. IL-6 + sIL-6R stimulated the phosphorylation of STAT3, peaking at 15 to 30 min, and declined thereafter (Figure 10A). On the other hand, IL-6 + sIL-6R induced phosphorylation of Akt at 5 to 15 min and declined at 30 min (Figure 10B).

2.12. Immunofluorescence Staining

To examine whether inhibition of JAK-STAT pathway affects the translocation of phosphorylated STAT3 to the nucleus, the cultured myxoma cells were pretreated with AG490 followed by incubation with IL-6 + sIL-6R for 30 min. The immunofluorescence signal of phosphorylated STAT3 located in the nuclei of the myxoma cells after incubation with IL-6 + sIL-6R for 30 min was compared with the untreated control cells (Figure 11). The translocation of phosphorylated STAT3 to the nucleus induced by IL-6 + sIL-6R was inhibited by AG490 at the dose of 100 μmol/L.

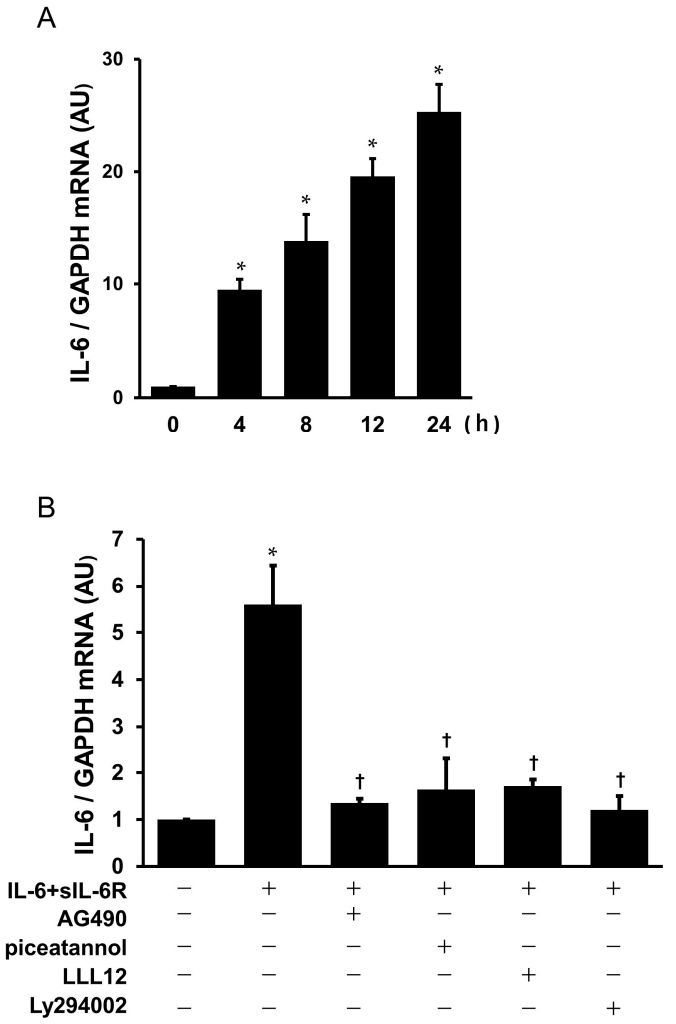

Figure 9. IL-6 + sIL-6R-stimulated IL-6 gene expression in the cardiac myxoma cells: (**A**) time course of IL-6 mRNA after treatment with IL-6 (1 nmol/L) + sIL-6R (1 nmol/L), as evaluated by real-time PCR. Bars represent IL-6 mRNA after normalization to GAPDH mRNA and relative to 0 h (n = 3). * $p < 0.05$ vs. 0 h; and (**B**) effects of pharmacological inhibitors of STAT3 and Akt on IL-6 + sIL-6R-stimulated IL-6 mRNA in the cultured myxoma cells. The myxoma cells were preincubated with AG490 (100 μmol/L), piceatannol (100 μmol/L), LLL12 (10 μmol/L), and Ly294002 (30 μmol/L). * $p < 0.05$ vs. the untreated control. † $p < 0.05$ vs. IL-6 + sIL-6R.

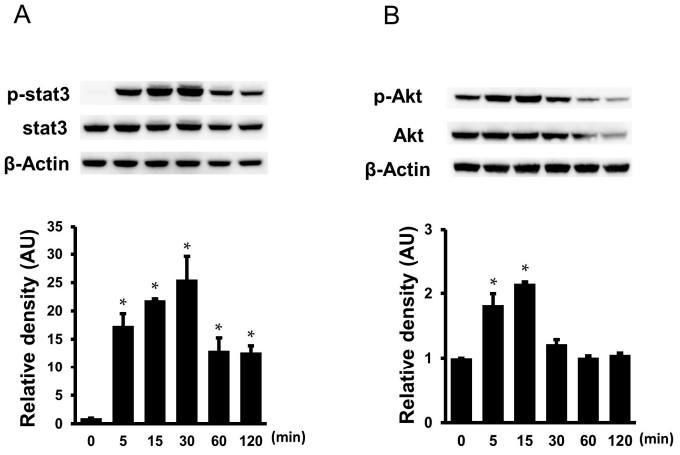

Figure 10. Phosphorylation of STAT3 (**A**); and Akt (**B**) in the cardiac myxoma cells treated with IL-6 (1 nmol/L) + sIL-6R (1 nmol/L). Cultured myxoma cells were treated with IL-6 + sIL-6R for 5, 15, 30,

60, and 120 min. Bars represent densitometric data of each expression signal after normalization to respective total protein and relative to the untreated cells (n = 3). * $p < 0.05$ vs. 0 min.

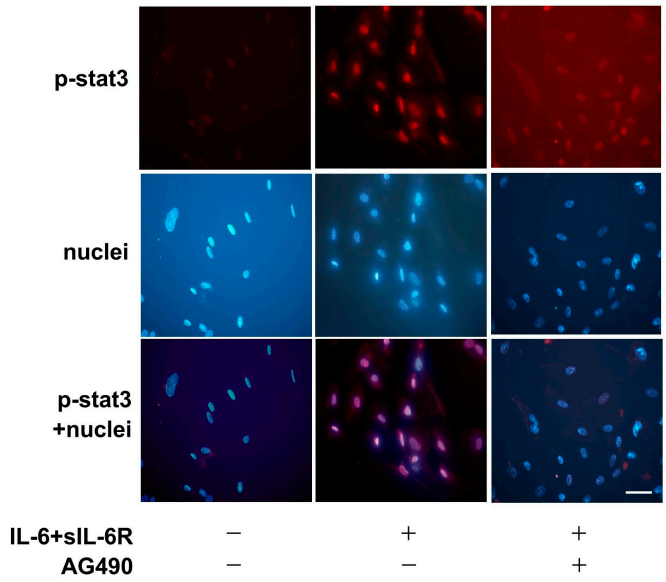

Figure 11. Immunofluorescence staining showing the effects of pharmacological inhibitor of STAT3 on IL-6 + sIL-6R-induced translocation of phosphorylated STAT3 to the nucleus in the cardiac myxoma cells. The cells were pretreated with AG490 (100 μmol/L) followed by additional incubation with IL-6 (1 nmol/L) + sIL-6R (1 nmol/L) for 30 min. Red staining indicates the specific Alexa staining for phosphorylated STAT3, and blue staining indicates the nuclei (Hoechst 33342). Original magnification; ×400. Scale bar = 50 μm.

3. Discussion

The present study demonstrated that human cardiac myxoma cells express IL-6 and its receptor complexes, IL-6R and gp130. Immunohistochemical staining in the excised cardiac myxoma tissue as well as immunocytochemical staining in the cultured cardiac myxoma cells demonstrated that IL-6 and its receptor complexes, such as IL-6R and gp130, were co-localized in the cardiac myxoma cells. In addition, the RT-PCR study showed the expressions of IL-6 mRNA, IL-6R mRNA, and gp130 mRNA in the myxoma cells, together with calretinin mRNA. Calretinin is a calcium-binding protein principally expressed in neurons [24]. Nowadays, calretinin is considered as a reliable marker for cardiac myxoma [25–27], and, therefore, we used the protein and gene expression of calretinin as a validation analysis for the myxoma cells. The presence of ligand and receptors of IL-6 in the myxoma cells supports the idea that both the classic and trans-signaling pathway are involved in the signal transduction system of IL-6 in the human cardiac myxoma cells. It is difficult to measure IL-6 protein levels in the presence of exogenously added IL-6. Therefore, we analyzed the gene expression of IL-6 mRNA to investigate the role of IL-6 on the myxoma cells. In the present study, myxoma cells were treated with exogenous IL-6 + sIL-6R, and mRNA was isolated and analyzed by real-time PCR. Thus, we analyzed trans-signaling by using IL-6 + sIL-6R for activation of IL-6 mRNA and found that IL-6 trans-signaling caused autocrine activation of IL-6 gene expression through STAT3 and PI3K/Akt pathways in the myxoma cells.

The clinical characteristics of cardiac myxoma include intracardiac obstruction, embolization, and constitutional symptoms such as malaise, fever, anorexia, arthralgia, and weight loss [8]. Since the initial study by Hirano et al. [9], accumulating evidence has demonstrated that cardiac myxomas constitutively produce considerable amounts of IL-6 [10–17], explaining the underlying pathophysiology of inflammatory and immune features of constitutional symptoms observed in these patients with cardiac myxoma. Pre-

vious studies reported that plasma levels of IL-6 were positively correlated with tumor size in patients with cardiac myxoma [16,20–22,28]. Mendoza et al., showing the significant correlation between serum IL-6 concentration and primary tumor size, has demonstrated that the overproduction of IL-6 by cardiac myxoma is responsible for the immunological abnormalities and constitutional symptoms seen in patients with cardiac myxoma [20]. Endo et al. analyzed constitutional signs in 204 patients with cardiac myxoma, in whom 90 cases were with constitutional signs, 92 without constitutional signs, with 22 classified as undetermined [22]. The authors demonstrated that patients with constitutional signs had significantly larger tumors than those without constitutional signs, suggesting that the production of IL-6 increases in proportion to tumor size, and that constitutional signs result when IL-6 concentrations exceed a certain threshold [22]. More precise analyses of the relationship between constitutional symptoms and plasma IL-6 concentrations are warranted.

In the present study, the cardiac myxoma cells constitutively produced and secreted considerable amounts of IL-6. IL-6 concentrations in the supernatant of myxoma cells increased in a time-dependent manner. As for the source of IL-6 in patients with cardiac myxoma, the present cell culture study, together with other previous studies [9,10,14,29,30], directly demonstrated that IL-6 was produced and secreted from the cardiac myxoma cells in vitro. Therefore, it seems likely that circulating IL-6 in patients with cardiac myxoma is derived from the neoplastic myxoma cells. On the other hand, Garcia-Zubiri et al. demonstrated the contribution of peripheral monocytes to the increased IL-6 serum levels in a patient with cardiac myxoma [23]. The authors presented a 69-year-old patient with cardiac myxoma, in which 74.4% of peripheral blood monocytes produced IL-6, and the percentage of monocytes producing IL-6 was significantly decreased at one month after surgical resection of the cardiac myxoma [23]. Morishima et al. reported a rare case of IL-6-producing cardiac myxoma resembling multicentric Castleman's disease with lymphadenopathy and abnormal plasma cell infiltration in bone marrow [31]. In addition, other investigators reported that IL-6 secreted by the cardiac myxoma caused the mediastinal lymphadenopathy, and resection of the myxoma tissue resulted in resolution of mediastinal lymphadenopathy together with a reduction in IL-6 levels to normal levels [32,33]. In the present study, Figure 5 showed that secreted IL-6 in the supernatant was biologically transferable and caused STAT3 activation in vascular endothelial cells that were adjacent to myxoma cells in the body. Therefore, it seems possible that IL-6 produced by the neoplastic myxoma cells provokes the activation of monocytes–macrophages to secrete additional IL-6, causing mediastinal lymphadenopathy and multicentric Castleman's disease in patients with cardiac myxoma. Likewise, normal cardiac myocytes might also be influenced by IL-6 secreted from the neoplastic cardiac myxoma cells and might cause ventricular hypertrophy in a patient with cardiac myxoma [34]. Further studies are needed to address these issues.

Since the initial study by Hirano et al. [9], several groups of investigators have isolated and cultured the cardiac myxoma cells, and secreted molecules, including IL-6, in the supernatant have been investigated [10,14,29,30,35]. Besides IL-6, Sakamoto et al. reported that the culture supernatant of cardiac myxoma cells contained significant amounts of IL-8, growth-regulated oncogene (GRO)-α, endothelin (ET)-1, big ET-1, and vascular endothelia growth factor (VEGF) [14,29,30,35]. The present antibody array assay analysis demonstrated that, in addition to IL-6, the culture supernatant of myxoma cells incubated for 7 days included considerable amounts of molecules such as MCP-1, GM-CSF, and PDGF-BB. These findings were supported by findings in previous investigations indicating that these bioactive molecules were expressed in the cardiac myxomas [16,36,37]. Zhang et al. demonstrated in an immunohistochemical analysis of 17 cardiac myxoma tissues that MCP-1 was found in the cytoplasm of the myxoma cells, and that the proportions of MCP-1-positive myxoma cells were significantly correlated with an increased micro-vessel count [37], suggesting the role of MCP-1 in angiogenesis associated with tumor growth. We and other investigators reported that IL-6 induced MCP-1 in human vascular endothelial cells [38,39] and peripheral mononuclear cells [40], suggesting the possibility that IL-6

secreted from the cardiac myxoma cells stimulates MCP-1 production in the myxoma cells or various other cells around. On the other hand, stimulation of vascular smooth muscle cells with MCP-1 resulted in a concentration- and time-dependent secretion of IL-6 [41]. In addition, by using immunohistochemical staining procedures, Gaumann et al. showed that PDGF-BB was present in the cardiac myxoma cells [36]. PDGF-BB increased the expression of IL-6 in cultures of osteoblasts from fetal rat calvariae [42]. Soeparwata et al. reported that one patient out of four patients with cardiac myxoma, in whom plasma GM-CSF concentrations were measured, showed an increased level of GM-CSF [16]. IL-6 is a potent inducer of GM-CSF expression by post-transcriptional stabilization of the GM-CSF mRNA [43], and GM-CSF significantly increased Il-6 secretion via extracellular signal-regulated kinase (ERK)1/2 pathway in macrophages [44]. As mentioned above, cardiac myxoma cells produce significant amounts of IL-8, GRO-α, ET-1, and VEGF, in addition to IL-6 in vitro. The present study added MCP-1, PDGF-BB, and GM-CSF as new members to the secreted substances of the cardiac myxoma cells. These biologically active molecules have pleiotropic properties. Although the precise causative and functional roles of these factors in the cardiac myxoma cells remain unknown, IL-6 and these substances have an important role in inflammation, tumor growth, angiogenesis, and tumor cell migration in the cardiac myxomas. Crosstalk among these molecules in the cardiac myxoma cells is intriguing, and further studies are required to elucidate the role of bioactive molecules secreted from the cardiac myxoma cells.

In the present study, stimulation with IL-6 + sIL-6R resulted in an increase in IL-6 mRNA, and pharmacological inhibitors against JAK/STAT3 and PI3L/Akt inhibited the IL-6 + sIL-6R-induced activation of IL-6 mRNA in the myxoma cells. Likewise, Franchimont et al. demonstrated that IL-6 + sIL-6R induced IL-6 mRNA in rat osteoblastic cells at the transcriptional levels, enhancing IL-6 rates of transcription and promoter activity [45]. The present study also demonstrated that STAT3 was constitutively phosphorylated together with spontaneous secretion of IL-6 in the cultured myxoma cells. Constitutive STAT3 phosphorylation, in association with IL-6 secretion, has been demonstrated in previous investigations [46–49]. Huang et al. showed that the lung adenocarcinoma cells spontaneously secreted IL-6 and possessed constitutively activated STAT3, and that inhibitors of JAK2/STAT3 and PI3-K/Akt pathways downregulated IL-6 secretion in these cells [46]. Schuringa et al. reported that the autocrine and paracrine secretion of IL-6 caused the constitutive activation of STAT3 in acute myelogenous leukemia cells [47]. A small GTPase, Rac1, stimulated STAT3 activation through the induction of an autocrine IL-6 feedback loop that leads to the activation of the JAK/STAT pathway [50]. Hirano reported an amplification mechanism for the production of IL-6 and various other cytokines and chemokines through a synergistic interaction between STAT3 and nuclear factor kappa B (NF-κB) and advocated "IL-6 amplifier (IL-6 Amp)" [51]. IL-6 might exert its biological actions as an autocrine and/or paracrine factor in the cardiac myxoma cells in a similar fashion as other human tumor cells [46–48,52]. Further studies are needed for the precise role of the production of IL-6 in patients with cardiac myxoma.

4. Materials and Methods

4.1. Reagent

Recombinant IL-6 and sIL-6R were purchased from Pepro Tech (Rocky Hill, NJ, USA). The monoclonal antibodies against IL-6, gp130, and β-actin were from Santa Cruz Biotechnology (Heidelberg, Germany). The polyclonal antibodies against STAT1, phospho-STAT1 (Tyr701), STAT3, phospho-STAT3 (Tyr705), Akt, phospho-Akt (Ser473) were obtained from Cell Signaling Technology (Beverly, MA, USA). The polyclonal antibodies against IL-6R and calretinin were purchased from GeneTex (Irvine, CA, USA). AG490 (JAK2 inhibitor), piceatannol (STAT1/3 inhibitor), and LY294002 (PI3K/Akt inhibitor) were purchased from FUJIFILM Wako Pure Chemical (Osaka, Japan). LLL12 was from BioVision (Milpitas, CA, USA). The reagents of siRNA were obtained from Santa Cruz Biotechnology (Heidelberg, Germany).

4.2. Culture of Cardiac Myxoma Cells

Cardiac myxoma tissue obtained by surgery was minced into small pieces, and dissected tissues were treated with collagenase and trypsin before being dissociated and plated in plastic plates precoated with type I collagen (Asahi Techno Glass, Nagoya, Japan). The cells were maintained in culture media containing TIL Media I (IBL, Fujioka, Japan)/Medium 199 (Thermo Fisher Scientific, Waltham, MA, USA) (1:1) supplemented with 10% fetal bovine serum (Life Technologies, Carlsbad, CA, USA), 0.5 mg/mL fungizone, 0.25 mg/mL amphotericin B, 100 mg/mL streptomycin, and 100 U/mL penicillin (Life Technologies, Carlsbad, CA, USA). The cells were incubated at 37 °C in a humidified incubator with 5% CO_2.

4.3. Culture of Human Umbilical Vein Endothelial Cells (HUVECs)

HUVECs were purchased from Kurabo (Osaka, Japan), and seeded in plastic plates precoated with type I collagen (Asahi Techno Glass, Nagoya, Japan). The cells were maintained in an endothelial cell growth medium (Promo cell, Heidelberg, Germany) supplemented with 0.5 mg/mL fungizone, 0.25 mg/mL amphotericin B, 100 mg/mL streptomycin, 100 U/mL penicillin (Life Technologies, Carlsbad, CA, USA). The cells were kept at 37 °C in a humidified incubator with 5% CO_2.

4.4. Immunohistochemical Staining in the Cardiac Myxoma Tissue

The expression and distribution of IL-6 and its receptors, IL-6R and gp130, as well as calretinin in the cardiac myxoma tissue were analyzed by immunohistochemical staining. Cardiac myxoma tissue was fixed with 10% buffered formaldehyde (FUJIFILM Wako Pure Chemical, Osaka, Japan), and embedded in paraffin. Four-μm sections of paraffin-embedded tissue were immunohistochemically stained based on the procedure described in the previous study [53]. The primary antibodies against IL-6, IL-6R, gp130, and calretinin were used at 50-fold dilution. The specificity of the immunostaining was confirmed by substitution of the normal IgG for the primary antibody. Images were taken under microscope at ×400 magnification, and expressions of immunostaining in myxoma were analyzed by microscope (Olympus, Tokyo, Japan).

4.5. Immunocytochemical Staining in the Cardiac Myxoma Cells

Myxoma cells plated on a Biocoat slide glass (BD Biosciences, San Jose, CA, USA) were fixed with 1% buffered paraformaldehyde (FUJIFILM Wako Pure Chemical, Osaka, Japan) for 20 min. The indirect immunoperoxidase method was used for the immunocytochemical analysis, as described previously [53]. The primary antibodies against IL-6, IL-6R, gp130, and calretinin were used at a 50-fold dilution. The specificity of the immunostaining was confirmed by substitution of the normal IgG for the primary antibody. Images were taken under microscope at ×400 magnification, and expression of immunostaining in the myxoma cells were analyzed by microscope (Olympus, Tokyo, Japan).

4.6. Antibody Array Assay

To identify the protein secreted by the myxoma cells, we used the antibody array of RayBio C-Series Human Cytokine Antibody Array C1000 (AAH-CYT-6) (RayBiotech, Norcross, GA, USA). The culture supernatant of the myxoma cells, incubated for 7 days, was applied to each membrane array, and the expression levels of the proteins were analyzed according to the manufacturer's instructions.

4.7. Western Immunoblot Analysis

The cultured myxoma cells were lysed in an ice-cold cell lysis buffer with a protease inhibitor cocktail. Protein samples resuspended in a sodium dodecyl sulfate buffer and dithiothreitol were separated by 4–12% NuPAGE Bis-Tris gels (Life Technologies, Carlsbad, CA, USA). They were transferred to a polyvinylidene difluoride membrane by electroblotting for 7 min using a Trans-Blot Turbo (Bio-Rad, Hercules, CA, USA). The membrane was

incubated with the primary antibody overnight at 4 °C at concentrations recommended by the manufacturer. Subsequently, the membrane was incubated with horseradish peroxidase-conjugated secondary antibody (Cell Signaling Technology, Beverly, MA, USA) for 1 h. The blots were detected using ECL prime (GE Healthcare, Buckinghamshire, UK), and analyzed by a ChemiDoc Touch Imaging System (Bio-Rad, Hercules, CA, USA).

4.8. RT-PCR

Total RNA was extracted from the cultured cardiac myxoma cells and HUVECs using a Pure Link RNA Mini kit (Invitrogen, Carlsbad, CA USA). cDNA was synthesized with a Superscript VILO cDNA Synthesis kit (Invitrogen, Carlsbad, CA USA). PCR was performed by using the primer pairs described in Table 1. The specificity of the primers was confirmed by a BLAST search and melting curve analysis. Amplification was performed for 40 cycles with a CFX connect thermal cycler (Bio-Rad, Hercules, CA, USA). The housekeeping gene GAPDH was used as a positive internal control for the PCR action. The PCR products were electrophoretically size-fractionated on an agarose gel, stained with ethidium bromide to visualize DNA bands, and analyzed to determine the presence of the gene.

Table 1. Primers of RT-PCR.

Gene Name	Sequence5′-3′	Accession Number
IL-6	(Forward) ACRCACCTCTTCAGAACGAATTG (Reverse) CCATCTTTGGAAGGTTCAGGTTG	NM_000600.3
IL-6R	(Forward) CACGCCTTGGACAGAATCC (Reverse) GCTTGTCGCATTTGCAGAATC	NM_181359
gp130	(Forward) TCAAATCCCTACTCCTTCACTTAC (Reverse) TGGTGAGGAAAATAAACAAGGC	NM_175767
Calretinin	(Forward) TGCCTGTCCAGGAAAACTTC (Reverse) TCATGCTCGTCAATGTAGCC	NM_001740.4
GAPDH	(Forward) GCACCGTCAAGGCTGAGAAC (Reverse) TGGTGAAGACGCCAGTGGA	NM_002046

4.9. Real-Time PCR

Semi-quantitative real-time-PCR was performed using Power SYBR Green PCR Master Mix (Applied Biosystems, Warrington, UK) on a CFX connect thermal cycler (Bio-Rad, Hercules, CA, USA). The value of each cDNA was calculated using the ΔΔCq method and normalized to the value of GAPDH.

4.10. Transfection with Small Interfering RNA (siRNA)

Transfection with siRNA was performed according to the manufacturer's protocol (Santa Cruz Biotechnology, Santa Cruz, CA, USA). Transfection complexes were prepared using the siRNA reagent, transfection medium, and STAT3 siRNA, and delivered to cell monolayers with a 100 nmol/L final concentration of siRNA duplexes. A scrambled control siRNA was used as a negative control.

4.11. Enzyme-Linked Immunosorbent Assay (ELISA)

Concentrations of IL-6 in the culture medium were determined using a human IL-6 ELISA kit (R&D Systems, Minneapolis, MN, USA) according to the manufacturer's protocol. Concentrations of IL-6 were determined by comparison of the optical density results with the standard curve.

4.12. Immunofluorescence Staining

The cardiac myxoma cells plated on a BioCoat slide glass (BD biosciences, San Jose, CA, USA) were stimulated with IL-6 + sIL-6R in the presence or absence of AG490 for 30 min. The cells were incubated with the antibody against phospho-STAT3 at 50-fold dilution

overnight. They were incubated with anti-rabbit IgG-Alexa (Cell Signaling Technology, Beverly, MA, USA) at 250-fold dilution for 1 h, and the nuclei were counterstained with Hoechst 33342 (Invitrogen, Carlsbad, CA, USA) for 5 min. The stained cells were analyzed by fluorescence microscope (Olympus, Tokyo, Japan).

4.13. Statistical Analysis

Results of the quantitative studies are expressed as mean ± SEM. Each data point represents the average of three to six independent experiments. A one-way ANOVA test was used to make comparisons among three or more groups and Tukey–Kramer's post hoc test was used to identify differences between two groups. p value < 0.05 was considered statistically significant.

5. Conclusions

In conclusion, the present study demonstrated that IL-6 increases its own production and secretion via the activation of STAT3 and Akt pathways in cardiac myxoma cells. Autocrine regulation of IL-6 may play an important role in the pathophysiology of patients with cardiac myxoma.

Author Contributions: M.J. supervised and conceived the project. M.J., Y.T. and K.U. designed the experiments. H.N., M.S. and T.K. performed data curation. Y.T., K.U., M.Y. and K.S. performed the experiments. M.J., Y.T., K.U., M.Y., K.S., H.N., M.S. and T.K. interpreted data. Y.T., K.U. and K.S. contributed reagents/analytic tools. M.J. wrote the manuscript with help from Y.T. All authors have read and agreed to the published version of the manuscript.

Funding: The present study was supported by a grant from NHO Collaborative Clinical Research.

Institutional Review Board Statement: The study was conducted in accordance with the Declaration of Helsinki and approved by the Ethics Committee of NHO Kagoshima Medical Center for studies involving humans.

Informed Consent Statement: Informed consent was obtained from the subject involved in the study.

Data Availability Statement: The data that support the findings of this study are available from the authors upon reasonable request.

Acknowledgments: We thank Reiko Saino for the secretarial work.

Conflicts of Interest: The authors declare no conflicts of interest.

References

1. Ishihara, K.; Hirano, T. IL-6 in autoimmune disease and chronic inflammatory proliferative disease. *Cytokine Growth Factor. Rev.* **2002**, *13*, 357–368. [CrossRef]
2. Kang, S.; Tanaka, T.; Narazaki, M.; Kishimoto, T. Targeting Interleukin-6 Signaling in Clinic. *Immunity* **2019**, *50*, 1007–1023. [CrossRef] [PubMed]
3. Heinrich, P.C.; Behrmann, I.; Haan, S.; Hermanns, H.M.; Müller-Newen, G.; Schaper, F. Principles of interleukin (IL)-6-type cytokine signalling and its regulation. *Biochem. J.* **2003**, *374*, 1–20. [CrossRef] [PubMed]
4. Rose-John, S. IL-6 trans-signaling via the soluble IL-6 receptor: Importance for the pro-inflammatory activities of IL-6. *Int. J. Biol. Sci.* **2012**, *8*, 1237–1247. [CrossRef]
5. Campbell, I.L.; Erta, M.; Lim, S.L.; Frausto, R.; May, U.; Rose-John, S.; Scheller, J.; Hidalgo, J. Trans-signaling is a dominant mechanism for the pathogenic actions of interleukin-6 in the brain. *J. Neurosci.* **2014**, *34*, 2503–2513. [CrossRef] [PubMed]
6. Naka, T.; Nishimoto, N.; Kishimoto, T. The paradigm of IL-6: From basic science to medicine. *Arthritis Res.* **2002**, *4* (Suppl. S3), S233–S242. [CrossRef] [PubMed]
7. Pinede, L.; Duhaut, P.; Loire, R. Clinical presentation of left atrial cardiac myxoma. A series of 112 consecutive cases. *Medicine* **2001**, *80*, 159–172. [CrossRef]
8. Islam, A. Cardiac myxomas: A narrative review. *World J. Cardiol.* **2022**, *14*, 206–219. [CrossRef]
9. Hirano, T.; Taga, T.; Yasukawa, K.; Nakajima, K.; Nakano, N.; Takatsuki, F.; Shimizu, M.; Murashima, A.; Tsunasawa, S.; Sakiyama, F.; et al. Human B-cell differentiation factor defined by an anti-peptide antibody and its possible role in autoantibody production. *Proc. Natl. Acad. Sci. USA* **1987**, *84*, 228–231. [CrossRef]
10. Jourdan, M.; Bataille, R.; Seguin, J.; Zhang, X.G.; Chaptal, P.A.; Klein, B. Constitutive production of interleukin-6 and immunologic features in cardiac myxomas. *Arthritis Rheum.* **1990**, *33*, 398–402. [CrossRef]

11. Saji, T.; Yanagawa, E.; Matsuura, H.; Yamamoto, S.; Ishikita, T.; Matsuo, N.; Yoshirwara, K.; Takanashi, Y. Increased serum interleukin-6 in cardiac myxoma. *Am. Heart J.* **1991**, *122*, 579–580. [CrossRef]
12. Wiedermann, C.J.; Reinisch, N.; Fischer-Colbrie, R.; Vollmar, A.M.; Herold, M.; Knapp, E. Proinflammatory cytokines in cardiac myxomas. *J. Intern. Med.* **1992**, *232*, 263–265. [CrossRef]
13. Seino, Y.; Ikeda, U.; Shimada, K. Increased expression of interleukin 6 mRNA in cardiac myxomas. *Br. Heart J.* **1993**, *69*, 565–567. [CrossRef]
14. Sakamoto, H.; Sakamaki, T.; Wada, A.; Nakajima, T.; Kanda, T.; Murata, K. Dexamethasone inhibits production of interleukin-6 by cultured cardiac myxoma cells. *Am. Heart J.* **1994**, *127*, 704–705. [CrossRef]
15. Kanda, T.; Sakamaki, T.; Murata, K. A cardiac myxoma with interleukin-6 production and cerebral metastasis. *Int. J. Cardiol.* **1994**, *45*, 144–146. [CrossRef]
16. Soeparwata, R.; Poeml, P.; Schmid, C.; Neuhof, H.; Scheld, H.H. Interleukin-6 plasma levels and tumor size in cardiac myxoma. *J. Thorac. Cardiovasc. Surg.* **1996**, *112*, 1675–1677. [CrossRef]
17. Parissis, J.T.; Mentzikof, D.; Georgopoulou, M.; Gikopoulos, M.; Kanapitsas, A.; Merkouris, K.; Kefalas, C. Correlation of interleukin-6 gene expression to immunologic features in patients with cardiac myxomas. *J. Interferon Cytokine Res.* **1996**, *16*, 589–593. [CrossRef]
18. Acebo, E.; Val-Bernal, J.F.; Gómez-Román, J.J.; Revuelta, J.M. Clinicopathologic study and DNA analysis of 37 cardiac myxomas: A 28-year experience. *Chest* **2003**, *123*, 1379–1385. [CrossRef]
19. Kanda, T.; Umeyama, S.; Sasaki, A.; Nakazato, Y.; Morishita, Y.; Imai, S.; Suzuki, T.; Murata, K. Interleukin-6 and cardiac myxoma. *Am. J. Cardiol.* **1994**, *74*, 965–967. [CrossRef]
20. Mendoza, C.E.; Rosado, M.F.; Bernal, L. The role of interleukin-6 in cases of cardiac myxoma. Clinical features, immunologic abnormalities, and a possible role in recurrence. *Tex. Heart Inst. J.* **2001**, *28*, 3–7.
21. Yokomuro, H.; Yoshihara, K.; Watanabe, Y.; Shiono, N.; Koyama, N.; Takanashi, Y. The variations in the immunologic features and interleukin-6 levels for the surgical treatment of cardiac myxomas. *Surg. Today* **2007**, *37*, 750–753. [CrossRef]
22. Endo, A.; Ohtahara, A.; Kinugawa, T.; Ogino, K.; Hisatome, I.; Shigemasa, C. Characteristics of cardiac myxoma with constitutional signs: A multicenter study in Japan. *Clin. Cardiol.* **2002**, *25*, 367–370. [CrossRef]
23. García-Zubiri, C.; Citores, M.J.; Yebra-Bango, M. Contribution of monocytes to overproduction of interleukin-6 in a case of cardiac myxoma. *Am. J. Med. Sci.* **2009**, *338*, 336–337. [CrossRef]
24. Rogers, J.H. Calretinin: A gene for a novel calcium-binding protein expressed principally in neurons. *J. Cell Biol.* **1987**, *105*, 1343–1353. [CrossRef]
25. Orlandi, A.; Ciucci, A.; Ferlosio, A.; Genta, R.; Spagnoli, L.G.; Gabbiani, G. Cardiac myxoma cells exhibit embryonic endocardial stem cell features. *J. Pathol.* **2006**, *209*, 231–239. [CrossRef]
26. Skamrov, A.V.; Nechaenko, M.A.; Goryunova, L.E.; Feoktistova, E.S.; Khaspekov, G.L.; Kovalevsky, D.A.; Vinnitsky, L.I.; Sheremeteva, G.F.; Beabealashvilli, R. Gene expression analysis to identify mRNA markers of cardiac myxoma. *J. Mol. Cell. Cardiol.* **2004**, *37*, 717–733. [CrossRef]
27. Terracciano, L.M.; Mhawech, P.; Suess, K.; D'Armiento, M.; Lehmann, F.S.; Jundt, G.; Moch, H.; Sauter, G.; Mihatsch, M.J. Calretinin as a marker for cardiac myxoma. Diagnostic and histogenetic considerations. *Am. J. Clin. Pathol.* **2000**, *114*, 754–759. [CrossRef]
28. Yuan, S.M.; Lin, H.Z. Interleukin-6 in Patients with Cardiac Myxoma. *J. Coll. Physicians Surg. Pak.* **2020**, *30*, 849–852.
29. Sakamoto, H.; Sakamaki, T.; Kanda, T.; Hirao, Y.; Ohyama, Y.; Ogishi, K.; Negishi, M.; Masuda, H.; Sumino, H.; Sawada, Y.; et al. Immunosuppressive drugs inhibit the production of interleukin-6 and interleukin-8 in cultured cardiac myxoma cells. *Res. Commun. Mol. Pathol. Pharmacol.* **1997**, *97*, 60–66.
30. Sakamoto, H.; Sakamaki, T.; Sumino, H.; Sawada, Y.; Sato, H.; Sato, M.; Fujita, K.; Kanda, T.; Tamura, J.; Kurabayashi, M. Production of endothelin-1 and big endothelin-1 by human cardiac myxoma cells—Implications of the origin of myxomas. *Circ. J.* **2004**, *68*, 1230–1232. [CrossRef]
31. Morishima, A.; Marui, A.; Shimamoto, T.; Saji, Y.; Nishina, T.; Komeda, M. A case of interleukin-6-producing cardiac myxoma resembling multicentric Castleman's disease. *J. Thorac. Cardiovasc. Surg.* **2009**, *138*, 499–501. [CrossRef]
32. Kuroki, S.; Naitoh, K.; Katoh, O.; Yamada, H.; Itoh, T. Increased interleukin-6 activity in cardiac myxoma with mediastinal lymphadenopathy. *Intern. Med.* **1992**, *31*, 1207–1209. [CrossRef]
33. Takizawa, T.; Sumino, H.; Kanda, T.; Kobayashi, I.; Nagai, R.; Ichikawa, S. An interleukin-6-producing cardiac myxoma associated with mediastinal lymphadenopathy. *Cardiology* **1999**, *92*, 275–277. [CrossRef]
34. Kanda, T.; Nakajima, T.; Sakamoto, H.; Suzuki, T.; Murata, K. An interleukin-6 secreting myxoma in a hypertrophic left ventricle. *Chest* **1994**, *105*, 962–963. [CrossRef]
35. Sakamoto, H.; Sakamaki, T.; Kanda, T.; Tsuchiya, Y.; Sato, M.; Sato, H.; Oyama, Y.; Sawada, Y.; Tamura, J.; Nagai, R.; et al. Vascular endothelial growth factor is an autocrine growth factor for cardiac myxoma cells. *Circ. J.* **2004**, *68*, 488–493. [CrossRef]
36. Gaumann, A.; Strubel, G.; Bode-Lesniewska, B.; Schmidtmann, I.; Kriegsmann, J.; Kirkpatrick, C.J. The role of tumor vascularisation in benign and malignant cardiovascular neoplasms: A comparison of cardiac myxoma and sarcomas of the pulmonary artery. *Oncol. Rep.* **2008**, *20*, 309–318. [CrossRef]
37. Zhang, T.; Koide, N.; Wada, Y.; Tsukioka, K.; Takayama, K.; Kono, T.; Kitahara, H.; Amano, J. Significance of monocyte chemotactic protein-1 and thymidine phosphorylase in angiogenesis of human cardiac myxoma. *Circ. J.* **2003**, *67*, 54–60. [CrossRef]

38. Jougasaki, M.; Ichiki, T.; Takenoshita, Y.; Setoguchi, M. Statins suppress interleukin-6-induced monocyte chemo-attractant protein-1 by inhibiting Janus kinase/signal transducers and activators of transcription pathways in human vascular endothelial cells. *Br. J. Pharmacol.* **2010**, *159*, 1294–1303. [CrossRef]
39. Zegeye, M.M.; Lindkvist, M.; Fälker, K.; Kumawat, A.K.; Paramel, G.; Grenegård, M.; Sirsjö, A.; Ljungberg, L.U. Activation of the JAK/STAT3 and PI3K/AKT pathways are crucial for IL-6 trans-signaling-mediated pro-inflammatory response in human vascular endothelial cells. *Cell Commun. Signal* **2018**, *16*, 55. [CrossRef]
40. Biswas, P.; Delfanti, F.; Bernasconi, S.; Mengozzi, M.; Cota, M.; Polentarutti, N.; Mantovani, A.; Lazzarin, A.; Sozzani, S.; Poli, G. Interleukin-6 induces monocyte chemotactic protein-1 in peripheral blood mononuclear cells and in the U937 cell line. *Blood* **1998**, *91*, 258–265. [CrossRef]
41. Viedt, C.; Vogel, J.; Athanasiou, T.; Shen, W.; Orth, S.R.; Kübler, W.; Kreuzer, J. Monocyte chemoattractant protein-1 induces proliferation and interleukin-6 production in human smooth muscle cells by differential activation of nuclear factor-kappaB and activator protein-1. *Arterioscler. Thromb. Vasc. Biol.* **2002**, *22*, 914–920. [CrossRef]
42. Franchimont, N.; Durant, D.; Rydziel, S.; Canalis, E. Platelet-derived growth factor induces interleukin-6 transcription in osteoblasts through the activator protein-1 complex and activating transcription factor-2. *J. Biol. Chem.* **1999**, *274*, 6783–6789. [CrossRef]
43. Griffin, J.D.; Cannistra, S.A.; Sullivan, R.; Demetri, G.D.; Ernst, T.J.; Kanakura, Y. The biology of GM-CSF: Regulation of production and interaction with its receptor. *Int. J. Cell Cloning* **1990**, *8* (Suppl. S1), 35–44; discussion 44–45. [CrossRef]
44. Farzam-Kia, N.; Moratalla, A.C.; Lemaître, F.; Levert, A.; Da Cal, S.; Margarido, C.; Carpentier Solorio, Y.; Arbour, N. GM-CSF distinctly impacts human monocytes and macrophages via ERK1/2-dependent pathways. *Immunol. Lett.* **2023**, *261*, 47–55. [CrossRef] [PubMed]
45. Franchimont, N.; Rydziel, S.; Canalis, E. Interleukin 6 is autoregulated by transcriptional mechanisms in cultures of rat osteoblastic cells. *J. Clin. Investig.* **1997**, *100*, 1797–1803. [CrossRef]
46. Huang, W.L.; Yeh, H.H.; Lin, C.C.; Lai, W.W.; Chang, J.Y.; Chang, W.T.; Su, W.C. Signal transducer and activator of transcription 3 activation up-regulates interleukin-6 autocrine production: A biochemical and genetic study of established cancer cell lines and clinical isolated human cancer cells. *Mol. Cancer* **2010**, *9*, 309. [CrossRef] [PubMed]
47. Schuringa, J.J.; Wierenga, A.T.; Kruijer, W.; Vellenga, E. Constitutive Stat3, Tyr705, and Ser727 phosphorylation in acute myeloid leukemia cells caused by the autocrine secretion of interleukin-6. *Blood* **2000**, *95*, 3765–3770. [CrossRef]
48. Yeh, H.H.; Lai, W.W.; Chen, H.H.; Liu, H.S.; Su, W.C. Autocrine IL-6-induced Stat3 activation contributes to the pathogenesis of lung adenocarcinoma and malignant pleural effusion. *Oncogene* **2006**, *25*, 4300–4309. [CrossRef] [PubMed]
49. Yoon, S.; Woo, S.U.; Kang, J.H.; Kim, K.; Kwon, M.H.; Park, S.; Shin, H.J.; Gwak, H.S.; Chwae, Y.J. STAT3 transcriptional factor activated by reactive oxygen species induces IL6 in starvation-induced autophagy of cancer cells. *Autophagy* **2010**, *6*, 1125–1138. [CrossRef]
50. Faruqi, T.R.; Gomez, D.; Bustelo, X.R.; Bar-Sagi, D.; Reich, N.C. Rac1 mediates STAT3 activation by autocrine IL-6. *Proc. Natl. Acad. Sci. USA* **2001**, *98*, 9014–9019. [CrossRef]
51. Hirano, T. IL-6 in inflammation, autoimmunity and cancer. *Int. Immunol.* **2021**, *33*, 127–148. [CrossRef] [PubMed]
52. Kang, H.S.; Lee, B.S.; Yang, Y.; Park, C.W.; Ha, H.J.; Pyun, K.H.; Choi, I. Roles of protein phosphatase 1 and 2A in an IL-6-mediated autocrine growth loop of human myeloma cells. *Cell. Immunol.* **1996**, *168*, 174–183. [CrossRef] [PubMed]
53. Ichiki, T.; Jougasaki, M.; Setoguchi, M.; Imamura, J.; Nakashima, H.; Matsuoka, T.; Sonoda, M.; Nakamura, K.; Minagoe, S.; Tei, C. Cardiotrophin-1 stimulates intercellular adhesion molecule-1 and monocyte chemoattractant protein-1 in human aortic endothelial cells. *Am. J. Physiol. Heart Circ. Physiol.* **2008**, *294*, H750–H763. [CrossRef] [PubMed]

International Journal of
Molecular Sciences

MDPI

Article

Inhibitory Effects of Eicosapentaenoic Acid on Vascular Endothelial Growth Factor-Induced Monocyte Chemoattractant Protein-1, Interleukin-6, and Interleukin-8 in Human Vascular Endothelial Cells

Yoko Takenoshita †, Akinori Tokito † and Michihisa Jougasaki *

Institute for Clinical Research, NHO Kagoshima Medical Center, Kagoshima 892-0853, Japan; takenoshita.yoko.cj@mail.hosp.go.jp (Y.T.); tokininn@hotmail.com (A.T.)
* Correspondence: jogasaki.michihisa.kb@mail.hosp.go.jp; Tel.: +81-99-223-1151
† These authors contributed equally to this work.

Abstract: Vascular endothelial growth factor (VEGF) induces monocyte chemoattractant protein-1 (MCP-1) and plays an important role in vascular inflammation and atherosclerosis. We investigated the mechanisms of VEGF-induced MCP-1 expression and the effects of eicosapentaenoic acid (EPA) in human umbilical vein endothelial cells (HUVECs). Real-time reverse transcription polymerase chain reaction (RT-PCR) and enzyme-linked immunosorbent assay (ELISA) demonstrated that VEGF enhanced MCP-1 gene expression and protein secretion in HUVECs. Western immunoblot analysis revealed that VEGF induced the phosphorylation of p38 mitogen-activated protein kinase (MAPK) and inhibitor of nuclear factor (NF)-κB (IκB). Treatment with pharmacological inhibitors of p38 MAPK (SB203580) or NF-κB (BAY11-7085) significantly suppressed VEGF-induced MCP-1 in HUVECs. EPA inhibited VEGF-induced MCP-1 mRNA, protein secretion, phosphorylation of p38 MAPK, and the translocation of phospho-p65 to the nucleus. Additionally, VEGF also stimulated gene expressions of *interleukin (IL)-6* and *IL-8*, which were suppressed by SB203580, BAY11-7085, and EPA. The present study has demonstrated that VEGF-induced activation of MCP-1, IL-6, and IL-8 involves the p38 MAPK and NF-κB signaling pathways and that EPA inhibits VEGF-induced MCP-1, IL-6, and IL-8 via suppressing these signaling pathways. This study supports EPA as a beneficial anti-inflammatory and anti-atherogenic drug to reduce the VEGF-induced activation of proinflammatory cytokine and chemokines.

Keywords: eicosapentaenoic acid; vascular endothelial growth factor; monocyte chemoattractant protein-1; mitogen-activated protein kinase; nuclear factor-kappa B; vascular endothelial cells

Citation: Takenoshita, Y.; Tokito, A.; Jougasaki, M. Inhibitory Effects of Eicosapentaenoic Acid on Vascular Endothelial Growth Factor-Induced Monocyte Chemoattractant Protein-1, Interleukin-6, and Interleukin-8 in Human Vascular Endothelial Cells. *Int. J. Mol. Sci.* **2024**, *25*, 2749. https://doi.org/10.3390/ijms25052749

Academic Editor: Saverio Francesco Retta

Received: 26 January 2024
Revised: 23 February 2024
Accepted: 25 February 2024
Published: 27 February 2024

1. Introduction

Atherosclerosis is recognized as a chronic inflammatory disease of the vessel wall [1]. Neo-angiogenesis is deeply involved in plaque instability and causes consequent plaque rupture. Vascular endothelial growth factor (VEGF), which plays an important role in angiogenesis, causing cell proliferation, apoptosis inhibition, increased vascular permeability, vasodilatation, and recruitment of inflammatory cells to the injury site [2–4], is involved in the development of atherosclerosis and furthers cardiovascular diseases [5]. The VEGF signal transduction system involves the phosphoinositide-3-kinase (PI3K)/Akt, p38 mitogen-activated protein kinase (MAPK), and extracellular signal-regulated kinase (ERK) 1/2, and nuclear factor-kappa B (NF-κB) pathways [3,6]. On the other hand, monocyte chemoattractant protein (MCP)-1, also called CC-motif ligand (CCL) 2, is a member of the CC chemokine family and promotes cell migration and infiltration of inflammatory cells like monocytes/macrophages [7]. Accumulating evidence has revealed that VEGF induces MCP-1 in human and bovine vascular endothelial cells [6,8], and MCP-1 induces

VEGF in an opposite fashion [9,10], delineating a positive feedback loop between VEGF and MCP-1. In addition, interleukin (IL)-6, a multi-functional proinflammatory cytokine, and IL-8, another chemokine known as CXCL8, are both involved in the pathophysiology of inflammation and atherosclerosis [11–13]. However, the precise relationship between these interleukins and VEGF in the pathophysiology of vascular inflammation and atherosclerosis still remains unclarified.

Although statins are prescribed worldwide for atherosclerotic cardiovascular disease, high triglyceride levels may persist in some patients despite statin therapy. Several triglyceride-lowering drugs are available, including fibrates, niacin, and omega-3 polyunsaturated fatty acids, of which prescription omega-3 polyunsaturated fatty acids have the best tolerability and safety profile [14,15]. Eicosapentaenoic acid (EPA) is a long-chain omega-3 polyunsaturated fatty acid that is mainly obtained from marine blue fish. EPA reduces both pro-inflammatory cytokines and chemokines and has been recently used as a drug for hyperlipidemia, preventing atherosclerotic cardiovascular lesions [16]. Matsumoto et al. showed that the administration of EPA suppressed the development of atherosclerotic lesions in a mouse model of hyperlipidemia [17]. The authors also demonstrated that EPA treatment attenuated TNF-α-induced up-regulation of MCP-1 in HUVECs [17]. In addition, Koto et al. reported that EPA treatment resulted in a significant inhibition of MCP-1 in tissue necrosis factor (TNF)-α-stimulated murine vascular endothelial cells and that of VEGF in lipopolysaccharide (LPS)-stimulated murine macrophages [18].

The present study was designed to investigate the signaling pathways involved in the VEGF-induced activation of MCP-1, IL-6, and IL-8 in human umbilical vein endothelial cells (HUVECs). We also elucidated the effects of EPA on the VEGF-induced expressions of MCP-1, IL-6, and IL-8 in HUVECs.

2. Results

2.1. VEGF-Induced Gene Expression and Protein Secretion of MCP-1 in HUVECs

Real-time reverse transcription polymerase chain reaction (RT-PCR) showed that VEGF significantly enhanced *MCP-1* mRNA expression in HUVECs at 1 to 4 h, peaking at 4 h after stimulating with VEGF and declined at 8 h (Figure 1A). HUVECs treated with VEGF for 4 h expressed *MCP-1* mRNA, with a significant increase at doses of 5 to 20 ng/mL (Figure 1B). Enzyme-linked immunosorbent assay (ELISA) demonstrated that VEGF stimulated the secretion of the MCP-1 protein from HUVECs, peaking at 24 h compared with untreated control (Figure 1C). The MCP-1 protein secretion that was stimulated by treatment with VEGF for 24 h was significantly increased at doses of 5 to 20 ng/mL of VEGF in HUVECs (Figure 1D).

2.2. VEGF-Induced Phosphorylation of p38 MAPK and IκB in HUVECs

HUVECs were stimulated by VEGF for different time periods (5–120 min), and the protein extracts were examined by Western immunoblot analysis. VEGF phosphorylated p38 MAPK and inhibitor of NF-κB (IκB), peaking at 5 to 15 min and declining at 60 min (Figure 2A). In addition, VEGF phosphorylated the signaling pathways of p38 MAPK and IκB in a dose-dependent manner (Figure 2B).

2.3. Effects of Pharmacological Inhibitors of the p38 MAPK and NF-κB Signaling Pathways on VEGF-Induced Gene Expression and Protein Secretion of MCP-1 in HUVECs

To examine whether the p38 MAPK and NF-κB signaling pathways are involved in the VEGF-induced gene expression and protein secretion of MCP-1, SB203580 (p38 MAPK inhibitor) and Bay11-7085 (NF-κB inhibitor) were used, followed by stimulation with VEGF. As shown in Figure 3A, the VEGF-induced gene expression of *MCP-1* was significantly inhibited by pretreatment with SB203580 and Bay11-7085. Similarly, the pharmacological inhibitors SB203580 and Bay11-7085 suppressed the VEGF-induced protein secretion of MCP-1 from HUVECs (Figure 3B).

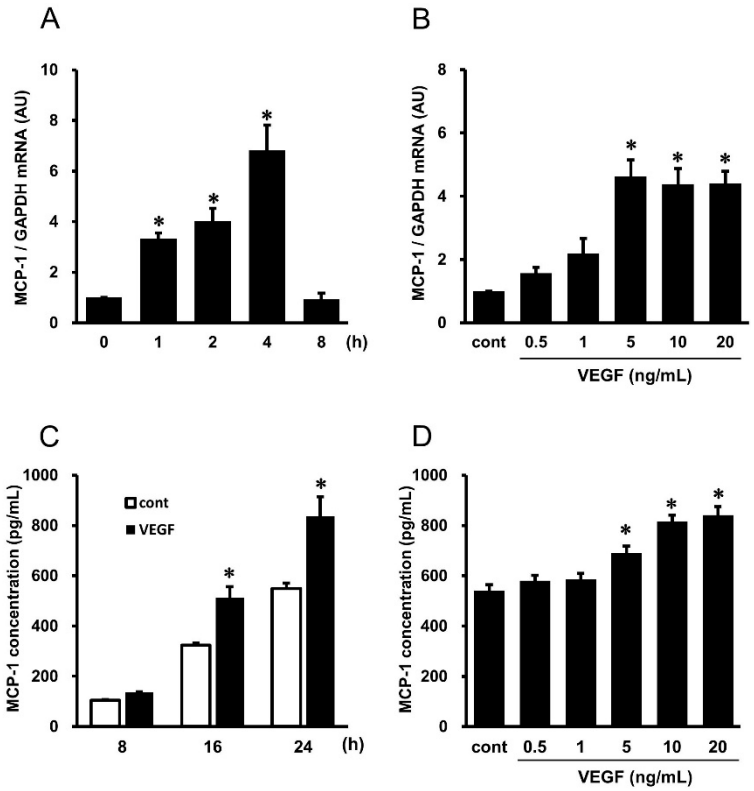

Figure 1. Vascular endothelial growth factor (VEGF)-stimulated gene expression and protein secretion of monocyte chemoattractant protein (MCP)-1 in human umbilical vein endothelial cells (HUVECs). (**A**) Time course of *MCP-1* mRNA expression after treatment with 10 ng/mL of VEGF (n = 3), as evaluated by real-time reverse transcription polymerase chain reaction (RT-PCR). (**B**) *MCP-1* mRNA expression in HUVECs after treatment with the indicated concentrations of VEGF for 4 h (n = 3), as evaluated by real-time RT-PCR. Bars represent *MCP-1* mRNA after normalization to *glyceraldehyde-3-phosphate dehydrogenase* (*GAPDH*) mRNA and relative to 0 h in (**A**) and untreated control (cont) in (**B**). (**C**) Time course of MCP-1 concentrations in the culture supernatant after treatment with 10 ng/mL of VEGF (closed bars, n = 6), as analyzed by ELISA. The control, secretion of MCP-1 without VEGF treatment, is shown in open bars (n = 6), as analyzed by ELISA. (**D**) MCP-1 concentrations in the culture supernatant after treatment with the indicated concentrations of VEGF for 24 h (n = 6), as analyzed by ELISA. * $p < 0.05$ vs. 0 h in (**A**), vs. untreated control (cont) in (**B**,**D**), and vs. each control at the same time in (**C**).

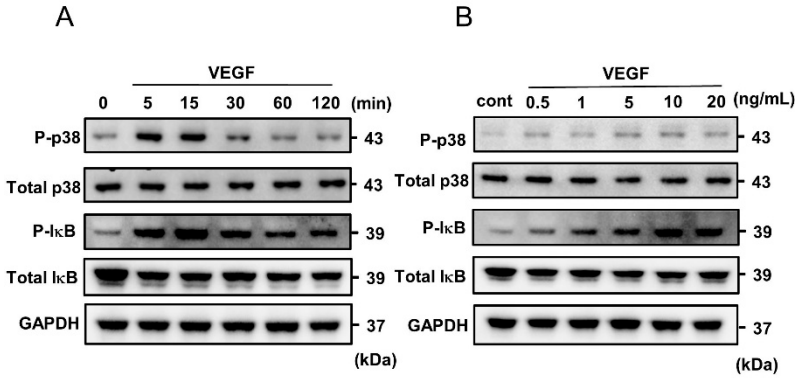

Figure 2. Western immunoblot analysis showing VEGF-stimulated phosphorylation of p38 mitogen-activated protein kinase (MAPK) and inhibitor of nuclear factor (NF)-kappa B (IκB) in HUVECs. (**A**) HUVECs were treated with 10 ng/mL of VEGF for 5, 15, 30, 60, and 120 min. (**B**) HUVECs were treated with different concentrations of VEGF (0.5, 1, 5, 10, and 20 ng/mL) for 5 min.

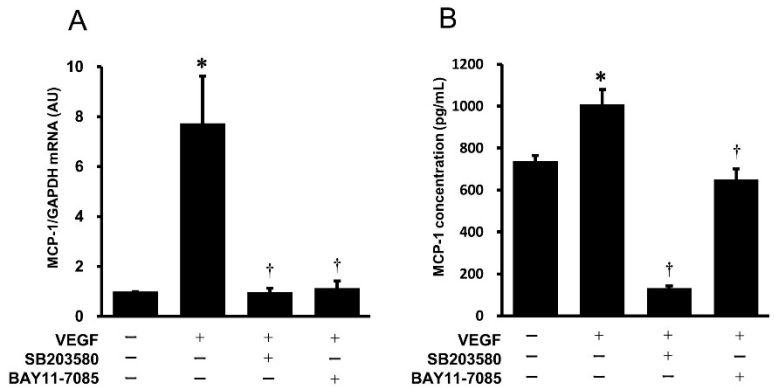

Figure 3. Effects of pharmacological inhibitors of the p38 MAPK and NF-κB pathways on VEGF-induced gene expression (**A**) and protein secretion (**B**) of MCP-1 in HUVECs. HUVECs were preincubated with SB203580 (10 μmol/L) and BAY11-7085 (10 μmol/L) for 2 h, followed by stimulation with VEGF (10 ng/mL) for 4 h to examine *MCP-1* mRNA (**A**) or for 24 h to measure MCP-1 protein concentration (**B**). *MCP-1* mRNA was evaluated by real-time RT-PCR ((**A**), $n = 3$), and MCP-1 concentration was examined by ELISA ((**B**), $n = 6$). * $p < 0.05$ vs. untreated control. † $p < 0.05$ vs. VEGF.

2.4. Effects of EPA on Cell Viability

The cytotoxicity of various doses of EPA to the cultured HUVECs was examined using the MTT assay. The cell viability of HUVECs was not changed by treatment with EPA at doses of less than 100 μmol/L (Figure 4). Although no changes in cell viability were observed in HUVECs at a dose of 100 μmol/L of EPA, we used EPA at doses of 10 and 30 μmol/L instead of 100 μmol/L in the present experiments, considering the concentration used in the previous studies [19].

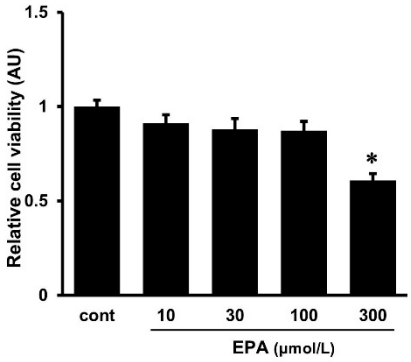

Figure 4. HUVEC viability when subjected to different concentrations (10, 30, 100, 300 μmol/L) of eicosapentaenoic acid (EPA) for 24 h. Cell viability was measured using the MTT assay. The results are expressed as a percentage of the untreated control (cont), and each value represents eight independent experiments ($n = 8$). * $p < 0.05$ vs. untreated control (cont).

2.5. Effects of EPA on the VEGF-Induced Gene Expression and Protein Secretion of MCP-1 in HUVECs

To elucidate the effects of EPA on the VEGF-induced gene expression and protein secretion of MCP-1, HUVECs were pretreated with various concentrations of EPA (10 and 30 μmol/L) overnight, followed by stimulation with VEGF for 4 h to examine *MCP-1* gene expression in HUVECs and for 24 h to measure MCP-1 protein secretion from HUVECs. The treatment with EPA (10 and 30 μmol/L) significantly inhibited the VEGF-induced increase in *MCP-1* gene expression in HUVECs (Figure 5A). On the other hand, the VEGF-stimulated increase in MCP-1 protein secretion from HUVECs was significantly suppressed only at the dose of 30 μmol/L of EPA (Figure 5B).

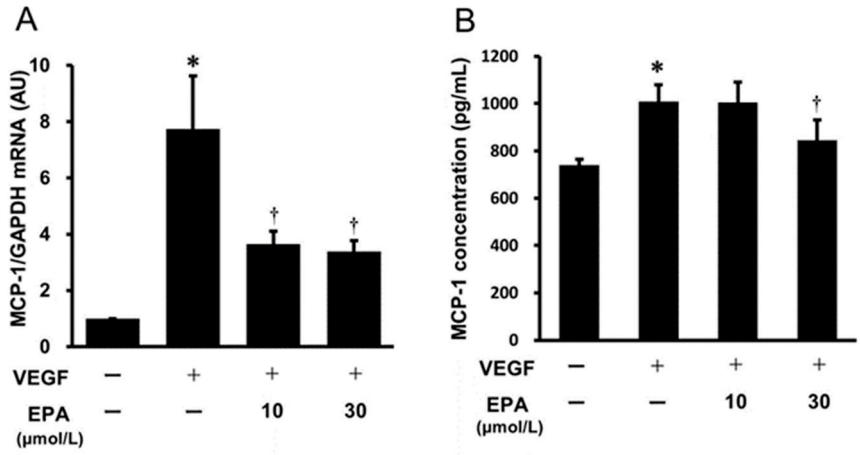

Figure 5. Effects of EPA on the gene expression and protein secretion of MCP-1 in HUVECs. VEGF-induced *MCP-1* mRNA (**A**) and MCP-1 protein concentration (**B**) were suppressed by EPA. HUVECs were treated with VEGF (10 ng/mL) for 4 h (**A**) or 24 h (**B**) with or without pretreatment with EPA (10 and 30 μmol/L). Bars represent *MCP-1* mRNA after normalization to *GAPDH* mRNA and relative to the untreated control in (**A**). Bars represent MCP-1 protein concentrations in (**B**). * $p < 0.05$ vs. untreated control. † $p < 0.05$ vs. VEGF.

2.6. Effects of SB203580, BAY11-7085, and EPA on the VEGF-Induced Gene Expression of IL-6 and IL-8 in HUVECs

Real-time PCR demonstrated that VEGF significantly increased the gene expression of *IL-6* and *IL-8* in HUVECs. SB203580 (p38 MAPK inhibitor), BAY11-7085 (NF-κB inhibitor), and EPA significantly inhibited the VEGF-stimulated gene expression of *IL-6* (Figure 6A) and *IL-8* (Figure 6B) in HUVECs.

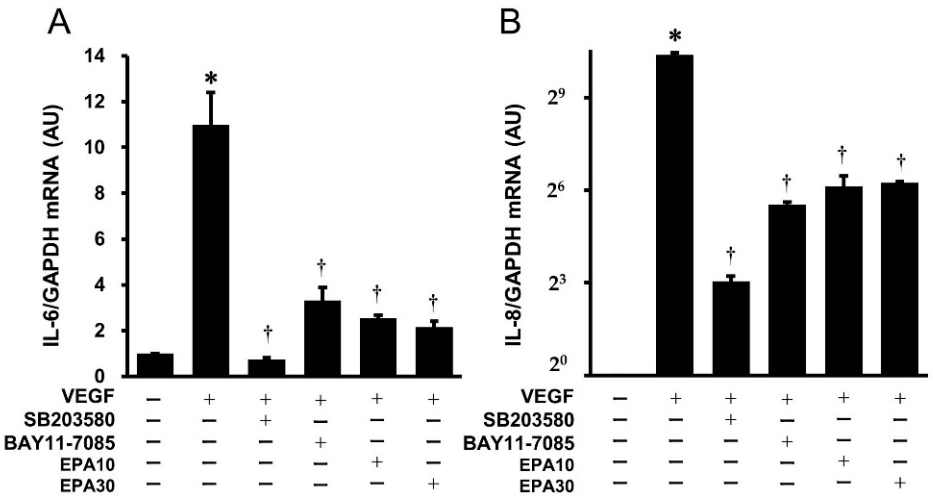

Figure 6. Effects of SB203580, BAY11-7085, and EPA on the VEGF-stimulated gene expression of *IL-6* mRNA (**A**) and *IL-8* mRNA (**B**) in HUVECs. HUVECs were preincubated with SB203580 (10 μmol/L) or BAY11-7085 (10 μmol/L) for 2 h each and EPA (10 and 30 μmol/L) overnight, then stimulated using VEGF (10 ng/mL) for 4 h to examine gene expression of *IL-6* and *IL-8*. Bars represent *IL-6* mRNA (**A**) and *IL-8* mRNA (**B**) after normalization to *GAPDH* mRNA and relative to the untreated control. * $p < 0.05$ vs. untreated control. † $p < 0.05$ vs. VEGF.

2.7. Effects of EPA on the VEGF-Stimulated Phosphorylation of p38 MAPK in HUVECs

To investigate whether the VEGF-induced phosphorylation of p38 MAPK was suppressed by EPA, HUVECs were pretreated with various concentrations of EPA (10 and 30 μmol/L) overnight, followed by stimulation with VEGF for 5 min. Western immunoblot analysis revealed that EPA slightly but significantly inhibited the VEGF-induced phosphorylation of p38 MAPK (Figure 7).

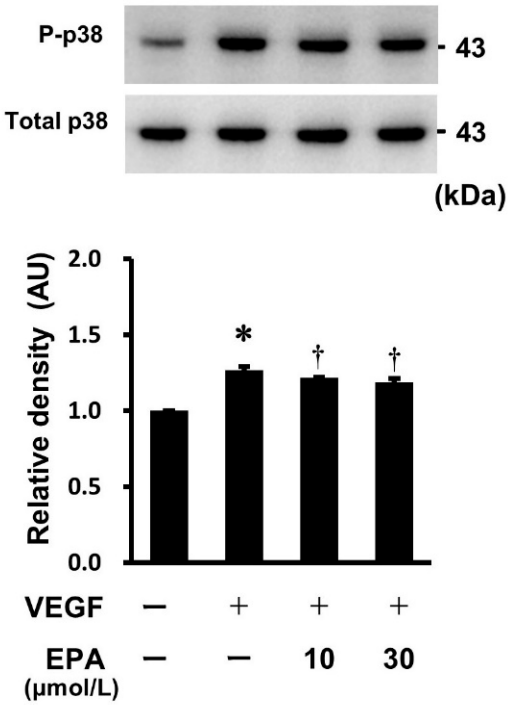

Figure 7. Effects of EPA on the VEGF-induced phosphorylation of p38 MAPK. EPA suppressed the phosphorylation of p38 MAPK in HUVECs. HUVECs were pretreated with EPA (10 and 30 μmol/L) overnight, then incubated with VEGF (10 ng/mL) for 5 min. Bars represent the results from the densitometric analyses of each phosphorylation signal after normalization to total protein and relative to the untreated control. Blots are representative of three independent experiments. * $p < 0.05$ vs. untreated control. † $p < 0.05$ vs. VEGF.

2.8. Immunofluorescence Staining

Immunofluorescence staining was used to examine whether EPA affects the translocation of phospho-p65 to the nucleus by suppressing VEGF-stimulated p65 phosphorylation. HUVECs were pretreated with EPA or Bay11-7085, followed by treatment with VEGF for 60 min. The immunofluorescence signal of phospho-p65 was localized in the nuclei of HUVECs after incubation with VEGF for 60 min compared with untreated control cells. VEGF-induced phospho-p65 activation was inhibited by EPA at the dose of 30 μmol/L (Figure 8). Similarly, Bay11-7085 attenuated the VEGF-induced translocation of phospho-p65 to the nucleus.

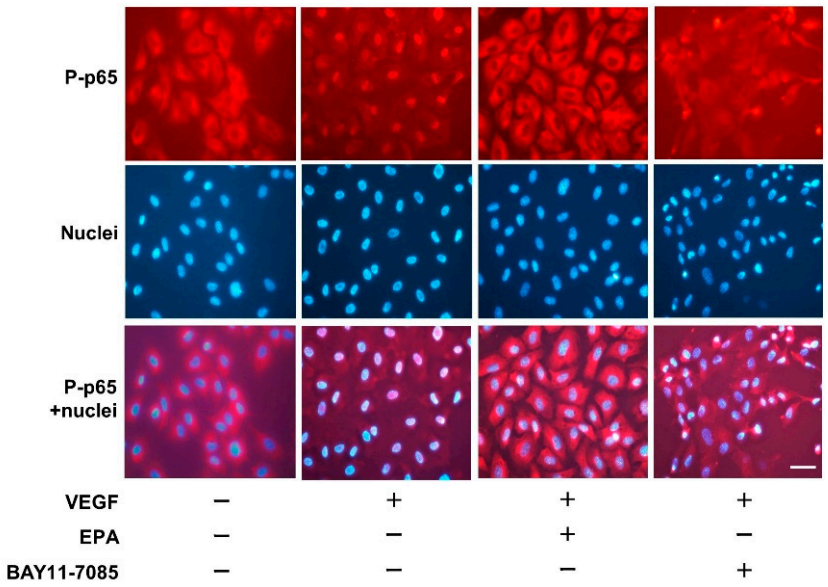

Figure 8. Effects of EPA and BAY11-7085 on VEGF-induced translocation of phospho-p65 to the nucleus, as determined by immunofluorescence staining. HUVECs were pretreated with EPA (30 μmol/L) or BAY11-7085 (10 μmol/L), followed by an additional incubation with VEGF (10 ng/mL) for 60 min. Representative immunofluorescence image showing the localization of phospho-p65 in HUVECs. Red staining indicates the specific Alexa staining for phospho-p65, and blue staining indicates the nuclei (Hoechst 33342). Original magnification, ×400. Scale bar = 50 μm.

3. Discussion

Atherosclerosis is characterized by chronic inflammation of the vessel wall [1]. Neoangiogenesis in atherosclerotic plaques is associated with unstable plaque formation and consequent rupture risk. VEGF plays a pivotal role in angiogenesis, causing recruitment of inflammatory cells to the injury site, and is involved in the development of atherosclerosis and furthers cardiovascular diseases [5]. EPA, a representative of the omega-3 polyunsaturated fatty acids, is known to reduce plaque instability and plaque inflammation [20]. The current study has demonstrated that EPA significantly inhibited the VEGF-stimulated activation of proinflammatory cytokines and chemokines in the vascular endothelial cells and provides new insights into the roles of EPA in the pathophysiology of vascular inflammation and atherosclerosis.

MCP-1 and IL-8 are the chemokines that recruit monocytes/macrophages and neutrophils to the sites of action, respectively. MCP-1 is a member of the CC class of chemokine supergene family, whereas IL-8 is of the CXC class, both of which play important roles in the inflammatory diseases [11] and are implicated in atherogenesis [12]. On the other hand, IL-6 is a multi-functional proinflammatory cytokine that is involved in immune regulation, inflammation, metabolism, and tissue regeneration [21,22]. Recently, a causal role for IL-6 in systemic atherothrombosis and aneurysm formation and the potential role of IL-6 inhibition in stable coronary disease, acute coronary syndromes, heart failure, and the atherothrombotic complications associated with chronic kidney disease and end-stage renal failure have been reported [13]. In the present study, EPA effectively suppressed the VEGF-induced activation of chemokines (MCP-1 and IL-8), as well as a proinflammatory cytokine (IL-6), in the vascular endothelial cells. EPA inhibits monocyte recruitment to the atherosclerotic lesions and subsequent conversion to macrophages and foam cells, reducing atherosclerotic plaque formation and the vulnerability to rupture [17,20]. These beneficial actions of EPA may be related to the suppressing effects of EPA on the VEGF-induced activation of chemokines (MCP-1 and IL-8) and a proinflammatory cytokine (IL-6), as shown in the present study.

The current study showed that VEGF stimulated MCP-1 gene expression and protein secretion in the human vascular endothelial cells. We sought to investigate the signal transduction pathways involved in the VEGF-induced MCP-1 activation and found that VEGF-induced MCP-1 activation occurred through activation of the p38 MAPK and NF-κB pathways in the human vascular endothelial cells. The finding that VEGF induces MCP-1 expression in the vascular endothelium is supported by previous studies [6,8]. Marumo et al. demonstrated that VEGF induced the gene expression and protein secretion of MCP-1 via the activation of NF-κB and activator protein (AP)-1 binding activity in bovine retinal endothelial cells, suggesting an important role for VEGF-induced MCP-1 in the development of microvascular angiopathy. Using the selective ERK1/2 inhibitor PD98059, the authors also found that induction of MCP-1 expression by VEGF was also dependent on the ERK1/2 pathway [6]. Yamada et al. revealed that MCP-1 was an important factor in the angiogenesis process and the vascular leakage induced by VEGF and that AP-1 was directly involved in the VEGF-induced MCP-1 expression in the vascular endothelium [8]. On the other hand, several investigations have reported MCP-1-induced VEGF activation in the literature. Parenti et al. showed that MCP-1 increased the expressions of *VEGF* mRNA and protein and that MCP-1 stimulated proliferation and migration of rat vascular smooth muscle cells through the activation of endogenous VEGF [10]. Other investigators have demonstrated that MCP-1 stimulated VEGF production through the activation of ERK1/2 in human aortic endothelial cells [9]. These findings reveal that angiogenic VEGF induces chemotactic MCP-1 expression and that MCP-1 also induces VEGF in an opposite fashion, delineating a positive feedback regulatory loop between VEGF and MCP-1 in the vascular endothelium. Crosstalk between VEGF and MCP-1 is intriguing and needs further investigation.

EPA, a representative of the omega-3 polyunsaturated fatty acids, has been clinically prescribed in patients with hyperlipidemia. EPA has a variety of pharmacological properties including lowering triglycerides [23], improvement of endothelial function via nitric oxide production [24], vasodilatation [24,25], and anti-inflammatory actions [26]. MCP-1 is an important chemokine that plays a crucial role in pathological conditions, such as cardiovascular diseases including atherosclerosis, brain pathologies, bone and joint disorders, respiratory infections, endothelial dysfunction, and cancer [7]. In this study, EPA treatment effectively inhibited VEGF-mediated MCP-1 induction by suppressing the signal transduction systems of the p38 MAPK and NF-κB signaling pathways. Previous studies also investigated the inhibitory properties of EPA on MCP-1 expression. Matsumoto et al. conducted a study on a mouse model of hyperlipidemia and demonstrated that the administration of EPA reduced the development of atherosclerotic lesions in this animal model [17]. The atherosclerotic plaques of EPA-fed mice revealed a stable morphology in association with a lower deposition of lipids and a reduced accumulation of macrophages and an increase in smooth muscle cells and collagen content. In addition, EPA treatment attenuated the TNF-α-induced up-regulation of adhesion molecules and MCP-1 in HUVECs [17]. EPA effectively decreased LPS-induced NF-κB activation and MCP-1 expression in human proximal tubular cells [27]. Akekura et al. demonstrated that EPA inhibited the LPS-induced phosphorylation of the NF-κB p65 subunit in a mouse monocyte/macrophage cell line [28]. EPA partially but significantly suppressed LPS-induced MCP-1 gene expression in these cells in vitro. The authors also showed that MCP-1 expression was induced in the adventitia of intracranial aneurysm and that its expression was remarkably suppressed in the intracranial aneurysm lesions from EPA-treated rats [28]. EPA suppressed TNF-α-stimulated MCP-1 transcription by preventing NF-κB activation in an ERK-dependent fashion in the cultured rat mesangial cells [29]. In addition, Koto et al. performed in vitro experiments and showed that EPA treatment led to a significant inhibition of the mRNA expression and protein levels of MCP-1 in TNF-α-stimulated murine brain-derived capillary endothelial cells and decreased *VEGF* mRNA and protein secretion in LPS-stimulated murine macrophages [18].

Other investigators have also reported on the biological properties of EPA to suppress VEGF expression. Yang et al. demonstrated that treatment with EPA for 48 h resulted in a dose-dependent suppression of VEGF-induced proliferation in bovine carotid artery endothelial cells [30]. VEGF-activated MAPK was also inhibited by treatment with EPA in these cells [30]. Serum-starvation-induced constitutive VEGF expression was reduced by treatment with EPA through inhibition of the ERK1/2 signaling pathway in human colon cancer cells [19]. EPA dose-dependently suppressed cell proliferation and wound repair in cultured human microvascular endothelial cells, and EPA significantly suppressed the gene expression and protein secretion of VEGF in both normoxia and hypoxia culture conditions [31]. Tevar et al. investigated the effects of supplemental dietary EPA in an animal model of progressive malignancy and found that EPA supplementation inhibited tumor growth, potentially through alterations in the expression of the pro-angiogenic VEGF [32]. These findings demonstrate that EPA inhibits MCP-1 and/or VEGF and might play an important role in the underlying mechanisms of the beneficial effects in the treatment of vascular inflammation and atherosclerosis. Further studies are required to investigate the role of EPA in vascular inflammation and atherosclerosis.

Although the present study indicates a plausible role for EPA in the VEGF-induced activations of MCP-1, IL-6, and IL-8 in vascular endothelial cells, it has some limitations. First, we used HUVECs as representative vascular endothelial cells in the current study. However, there is significant endothelial cell phenotype heterogeneity across the vascular tree [33]. At present, no single endothelial cell line is representative of the endothelium in all blood vessels [34] and HUVECs are commonly used in in vitro experiments for endothelial-derived gene expression and the protein secretion of cytokines, such as IL-8 [35], GRO-α [36], and MCP-1 [37]. Second, the current study is an in vitro cell culture study and does not involve preclinical or clinical data. Inflammation is central to the pathophysiology of atherosclerosis. The present study demonstrated that EPA suppressed the VEGF-induced activation of a proinflammatory cytokine (IL-6) and some chemokines (MCP-1 and IL-8), delineating a possible role for EPA in the treatment of atherosclerosis due to anti-inflammatory properties. Third, secretion studies of IL-6 and IL-8 are lacking because of the depletion of the supernatant samples. However, it is likely that the secretion pattern of IL-6 and IL-8 resembles that of MCP-1, because the gene expression of these interleukins is similar to that of MCP-1. Further studies using ELISA are needed to confirm the secretion of IL-6 and IL-8 in HUVECs stimulated by VEGF in the presence and absence of EPA.

4. Materials and Methods

4.1. Regents

Recombinant human VEGF was obtained from PeproTech (Rocky Hill, NJ, USA). The rabbit polyclonal antibodies for p38, phospho-p38 (Thr180/Tyr182), IκB, phospho-IκB (Ser32/36), and phospho-p65 (Ser536) were obtained from Cell Signaling Technology (Beverly, MA, USA). The rabbit polyclonal anti-GAPDH antibody was from Santa Cruz Biotechnology (Heidelberg, Germany). Pharmacological inhibitors SB203580 (p38 MAPK inhibitor) and BAY11-7085 (NF-κB inhibitor) were purchased from FUJIFILM Wako Pure Chemical (Osaka, Japan) and Cayman Chemical (Ann Arbor, MI, USA), respectively. EPA was purchased from Merck (Darmstadt, Germany).

4.2. Cell Culture of HUVECs

HUVECs were purchased from Kurabo (Osaka, Japan), seeded in plastic plates pre-coated with type I collagen (Asahi Techno Glass, Nagoya, Japan), and maintained in medium 199 (Life Technologies, Carsbad, CA, USA) supplemented with 10% heat-inactivated fetal calf serum, 0.5 μg/mL fungizone, 0.25 μg/mL amphotericin B, 100 μg/mL streptomycin, 100 U/mL penicillin (all Life Technologies, Carlsbad, CA, USA), 14 U/mL heparin (Ajinomoto, Tokyo, Japan), 20 μg/mL endothelial cell growth supplement (Kohjin

Bio, Saitama, Japan), and 10 μg/mL human epidermal growth factor (PeproTech, Rocky Hill, CT, USA). HUVECs were cultured at 37 °C in 5% CO_2 and 95% air in a humidified atmosphere.

4.3. Total RNA Extraction and Real-Time RT-PCR

Total RNA was extracted from HUVECs using the Pure Link RNA Mini Kit (Invitrogen, Carlsbad, CA, USA). The cDNA was synthesized using the Superscript VILO cDNA Synthesis kit (Invitrogen, Carlsbad, CA, USA). Real-time PCR using Power SYBR Green PCR Master Mix (Applied Biosystems, Warrington, UK) was carried out on a CFX connect thermal cycler (Bio-Rad, Hercules, CA, USA). The value of each cDNA was calculated using the ΔΔCq method and normalized to the value of the housekeeping gene *GAPDH*.

Oligonucleotide PCR primers targeting human *MCP-1* mRNA were designed according to a previous report [37] and primers targeting human *GAPDH* mRNA were purchased from TaKaRa (Shiga, Japan); the specificity of the primer sets was verified by a basic local alignment search tool (BLAST) search and melting-curve analysis. The primer sequences and accession numbers are shown in Table 1. The reaction conditions were as follows: an activation step at 95 °C for 10 min, followed by 40 cycles of denaturation at 95 °C for 15 s and annealing/extension at 60 °C for 1 min.

Table 1. Primers for real-time RT-PCR.

Gene Name	Primer Sequences (Forward/Reverse)	Accession Number
MCP-1	F: 5′-CATAGCAGCCACCTTCATTCC-3′ R: 5′-TCTCCTTGGCCACAATGGTC-3′	NM_002982.3
IL-6	F: 5′-ACTCACCTCTTCAGAACGAATTG-3′ R: 5′-CCATCTTTGGAAGGTTCAGGTTG-3′	NM_000600.3
IL-8	F: 5′-AAGAAACCACCGGAAGGAAC-3′ R: 5′-ACTCCTTGGCAAAACTGCAC-3′	NM_000584.3
GAPDH	F: 5′-GCACCGTCAAGGCTGAGAAC-3′ R: 5′-TGGTGAAGACGCCAGTGGA-3′	NM_002046

4.4. Enzyme-Linked Immunosorbent Assay (ELISA)

The concentrations of MCP-1 in the culture medium were determined by using a human MCP-1 ELISA kit (R&D Systems, Minneapolis, MN, USA) according to the manufacturer's protocol. The optical densities of the samples and standards were measured spectrophotometrically with an iMark microplate reader (BIORAD, Hercules, CA, USA). MCP-1 concentrations were evaluated by comparing the optical density with the standard curve.

4.5. Western Immunoblot Analysis

Western immunoblot analysis was performed as previously reported, with some modifications. HUVECs were harvested in ice-cold cell lysis buffer together with phenylmethylsulphonyl fluoride and a protease inhibitor cocktail. The proteins were resuspended in sodium dodecyl sulfate sample buffer and dithiothreitol, sonicated, and boiled for 5 min. They were separated by 4–12% NuPAGE Bis-Tris gels (Life Technologies, Carlsbad, CA, USA) and transferred to a polyvinylidene difluoride membrane with a Trans-Blot Turbo Transfer System (Bio-Rad, Hercules, CA, USA) for 7 min. The membrane was soaked in a 5% nonfat dry milk blocking buffer. The membrane was then incubated with the primary antibody overnight at 4 °C in the concentrations suggested by the manufacturer, followed by 1 h incubation with horseradish-peroxidase-conjugated secondary antibody (Cell Signaling Technology, Beverly, MA, USA). ECL prime (GE Healthcare, Buckinghamshire, UK) was used to visualize the protein bands, and the intensities of the blots were quantified by a ChemiDoc Touch Imaging System (Bio-Rad, Hercules, CA, USA).

4.6. Cell Viability

Cell viability was assessed using the MTT assay (Roche, Mannheim, Germany). HUVECs were treated with 10, 30, 100, or 300 μmol/L of EPA overnight, after which 0.5 mg/mL MTT solution was added to the culture medium and then the samples were incubated for 4 h. After they were incubated with dimethyl sulfoxide overnight, the cell viability was measured with an iMark microplate reader (BIORAD, Hercules, CA, USA). The survival rates of the EPA-treated cells were compared with those of the untreated control cells.

4.7. Immunofluorescence Staining

After fixation with 1% paraformaldehyde, HUVECs were permeabilized with 0.1% Triton X-100 and blocked with normal horse serum for 30 min. The cells were incubated with a rabbit p65 antibody at a 100-fold dilution overnight. They were then washed and incubated with anti-rabbit IgG-Alexa (Cell Signaling Technology, Beverly, MA, USA) at a dilution of 250-fold for 1 h, and the nuclei were counterstained using Hoechst 33342 (Invitrogen, Carlsbad, CA, USA). Images were analyzed using a fluorescence microscope (Olympus, Tokyo, Japan).

4.8. Statistical Analysis

Data are shown as mean ± SD. The average of three to eight independent experiments were represented in each data point. The statistical significance of the data was assessed using one-way ANOVA with Tukey–Kramer's post hoc test. A p value < 0.05 was considered statistically significant.

5. Conclusions

The present study has demonstrated that VEGF induces MCP-1 expression via the p38 MAPK and NF-κB signaling pathways and that EPA inhibits these signaling pathways and suppresses VEGF-induced MCP-1 expression in the human vascular endothelial cells. This study supports the properties of EPA as a beneficial anti-inflammatory and anti-atherogenic drug in the treatment of vascular inflammation and atherosclerosis.

Author Contributions: M.J. supervised and conceived the project. M.J., A.T. and Y.T. designed the experiments. A.T. and Y.T. performed data curation. A.T. and Y.T. performed the experiments. M.J., A.T. and Y.T. interpreted data. A.T. and Y.T. contributed reagents/analytic tools. A.T. and Y.T. wrote the original draft. M.J. reviewed and edited. All authors have read and agreed to the published version of the manuscript.

Funding: This research was funded by a grant from National Hospital Organization Collaborative Clinical Research.

Institutional Review Board Statement: Not applicable.

Informed Consent Statement: Not applicable.

Data Availability Statement: The data that support the findings of this study are available from the authors upon reasonable request.

Acknowledgments: We thank Ku Sudou for technical assistance.

Conflicts of Interest: The authors declare no conflict of interest.

Abbreviations

AP-1	activator protein-1
BLAST	basic local alignment search tool
CCL2	CC-motif ligand 2
ELISA	enzyme-linked immunosorbent assay
EPA	eicosapentaenoic acid
ERK	extracellular signal-regulated kinase

GAPDH	glyceraldehyde-3-phosphate dehydrogenase
HUVECs	human vascular endothelial cells
IκB	inhibitor of nuclear factor-kappa B
LPS	lipopolysaccharide
MAPK	mitogen-activated protein kinase
MCP-1	monocyte chemoattractant protein-1
NF-κB	nuclear factor-kappa B
PI3K	phosphoinositide-3-kinase
RT-PCR	reverse transcription polymerase chain reaction
TNF	tissue necrosis factor
VEGF	vascular endothelial growth factor

References

1. Libby, P.; Ridker, P.M.; Maseri, A. Inflammation and atherosclerosis. *Circulation* **2002**, *105*, 1135–1143. [CrossRef]
2. Apte, R.S.; Chen, D.S.; Ferrara, N. VEGF in Signaling and Disease: Beyond Discovery and Development. *Cell* **2019**, *176*, 1248–1264. [CrossRef]
3. Melincovici, C.S.; Boşca, A.B.; Şuşman, S.; Mărginean, M.; Mihu, C.; Istrate, M.; Moldovan, I.M.; Roman, A.L.; Mihu, C.M. Vascular endothelial growth factor (VEGF)—Key factor in normal and pathological angiogenesis. *Rom. J. Morphol. Embryol.* **2018**, *59*, 455–467. [PubMed]
4. Shibuya, M. Structure and function of VEGF/VEGF-receptor system involved in angiogenesis. *Cell Struct. Funct.* **2001**, *26*, 25–35. [CrossRef] [PubMed]
5. Dabravolski, S.A.; Khotina, V.A.; Omelchenko, A.V.; Kalmykov, V.A.; Orekhov, A.N. The Role of the VEGF Family in Atherosclerosis Development and Its Potential as Treatment Targets. *Int. J. Mol. Sci.* **2022**, *23*, 931. [CrossRef] [PubMed]
6. Marumo, T.; Schini-Kerth, V.B.; Busse, R. Vascular endothelial growth factor activates nuclear factor-kappaB and induces monocyte chemoattractant protein-1 in bovine retinal endothelial cells. *Diabetes* **1999**, *48*, 1131–1137. [CrossRef]
7. Singh, S.; Anshita, D.; Ravichandiran, V. MCP-1: Function, regulation, and involvement in disease. *Int. Immunopharmacol.* **2021**, *101 Pt B*, 107598. [CrossRef]
8. Yamada, M.; Kim, S.; Egashira, K.; Takeya, M.; Ikeda, T.; Mimura, O.; Iwao, H. Molecular mechanism and role of endothelial monocyte chemoattractant protein-1 induction by vascular endothelial growth factor. *Arterioscler. Thromb. Vasc. Biol.* **2003**, *23*, 1996–2001. [CrossRef]
9. Hong, K.H.; Ryu, J.; Han, K.H. Monocyte chemoattractant protein-1-induced angiogenesis is mediated by vascular endothelial growth factor-A. *Blood* **2005**, *105*, 1405–1407. [CrossRef] [PubMed]
10. Parenti, A.; Bellik, L.; Brogelli, L.; Filippi, S.; Ledda, F. Endogenous VEGF-A is responsible for mitogenic effects of MCP-1 on vascular smooth muscle cells. *Am. J. Physiol. Heart Circ. Physiol.* **2004**, *286*, H1978–H1984. [CrossRef]
11. Mukaida, N.; Harada, A.; Matsushima, K. Interleukin-8 (IL-8) and monocyte chemotactic and activating factor (MCAF/MCP-1), chemokines essentially involved in inflammatory and immune reactions. *Cytokine Growth Factor Rev.* **1998**, *9*, 9–23. [CrossRef]
12. Boisvert, W.A. Modulation of atherogenesis by chemokines. *Trends Cardiovasc. Med.* **2004**, *14*, 161–165. [CrossRef] [PubMed]
13. Ridker, P.M.; Rane, M. Interleukin-6 Signaling and Anti-Interleukin-6 Therapeutics in Cardiovascular Disease. *Circ. Res.* **2021**, *128*, 1728–1746. [CrossRef]
14. Budoff, M. Triglycerides and Triglyceride-Rich Lipoproteins in the Causal Pathway of Cardiovascular Disease. *Am. J. Cardiol.* **2016**, *118*, 138–145. [CrossRef]
15. Hilleman, D.; Smer, A. Prescription Omega-3 Fatty Acid Products and Dietary Supplements Are Not Interchangeable. *Manag. Care* **2016**, *25*, 46–52.
16. Crupi, R.; Cuzzocrea, S. Role of EPA in Inflammation: Mechanisms, Effects, and Clinical Relevance. *Biomolecules* **2022**, *12*, 242. [CrossRef] [PubMed]
17. Matsumoto, M.; Sata, M.; Fukuda, D.; Tanaka, K.; Soma, M.; Hirata, Y.; Nagai, R. Orally administered eicosapentaenoic acid reduces and stabilizes atherosclerotic lesions in ApoE-deficient mice. *Atherosclerosis* **2008**, *197*, 524–533. [CrossRef] [PubMed]
18. Koto, T.; Nagai, N.; Mochimaru, H.; Kurihara, T.; Izumi-Nagai, K.; Satofuka, S.; Shinoda, H.; Noda, K.; Ozawa, Y.; Inoue, M.; et al. Eicosapentaenoic acid is anti-inflammatory in preventing choroidal neovascularization in mice. *Investig. Ophthalmol. Vis. Sci.* **2007**, *48*, 4328–4334. [CrossRef]
19. Calviello, G.; Di Nicuolo, F.; Gragnoli, S.; Piccioni, E.; Serini, S.; Maggiano, N.; Tringali, G.; Navarra, P.; Ranelletti, F.O.; Palozza, P. n-3 PUFAs reduce VEGF expression in human colon cancer cells modulating the COX-2/PGE2 induced ERK-1 and -2 and HIF-1alpha induction pathway. *Carcinogenesis* **2004**, *25*, 2303–2310. [CrossRef]
20. Cawood, A.L.; Ding, R.; Napper, F.L.; Young, R.H.; Williams, J.A.; Ward, M.J.; Gudmundsen, O.; Vige, R.; Payne, S.P.; Ye, S.; et al. Eicosapentaenoic acid (EPA) from highly concentrated n-3 fatty acid ethyl esters is incorporated into advanced atherosclerotic plaques and higher plaque EPA is associated with decreased plaque inflammation and increased stability. *Atherosclerosis* **2010**, *212*, 252–259. [CrossRef]
21. Ishihara, K.; Hirano, T. IL-6 in autoimmune disease and chronic inflammatory proliferative disease. *Cytokine Growth Factor Rev.* **2002**, *13*, 357–368. [CrossRef]

22. Kang, S.; Tanaka, T.; Narazaki, M.; Kishimoto, T. Targeting Interleukin-6 Signaling in Clinic. *Immunity* **2019**, *50*, 1007–1023. [CrossRef]
23. Patel, A.A.; Budoff, M.J. Effects of eicosapentaenoic acid and docosahexaenoic acid on lipoproteins in hypertriglyceridemia. *Curr. Opin. Endocrinol. Diabetes Obes.* **2016**, *23*, 145–149. [CrossRef]
24. Tagawa, H.; Shimokawa, H.; Tagawa, T.; Kuroiwa-Matsumoto, M.; Hirooka, Y.; Takeshita, A. Long-term treatment with eicosapentaenoic acid augments both nitric oxide-mediated and non-nitric oxide-mediated endothelium-dependent forearm vasodilatation in patients with coronary artery disease. *J. Cardiovasc. Pharmacol.* **1999**, *33*, 633–640. [CrossRef]
25. Bercea, C.I.; Cottrell, G.S.; Tamagnini, F.; McNeish, A.J. Omega-3 polyunsaturated fatty acids and hypertension: A review of vasodilatory mechanisms of docosahexaenoic acid and eicosapentaenoic acid. *Br. J. Pharmacol.* **2021**, *178*, 860–877. [CrossRef]
26. Wardhana; Surachmanto, E.S.; Datau, E.A. The role of omega-3 fatty acids contained in olive oil on chronic inflammation. *Acta Med. Indones.* **2011**, *43*, 138–143. [PubMed]
27. Li, H.; Ruan, X.Z.; Powis, S.H.; Fernando, R.; Mon, W.Y.; Wheeler, D.C.; Moorhead, J.F.; Varghese, Z. EPA and DHA reduce LPS-induced inflammation responses in HK-2 cells: Evidence for a PPAR-gamma-dependent mechanism. *Kidney Int.* **2005**, *67*, 867–874. [CrossRef] [PubMed]
28. Abekura, Y.; Ono, I.; Kawashima, A.; Takizawa, K.; Koseki, H.; Miyata, H.; Shimizu, K.; Oka, M.; Kushamae, M.; Miyamoto, S.; et al. Eicosapentaenoic acid prevents the progression of intracranial aneurysms in rats. *J. Neuroinflamm.* **2020**, *17*, 129. [CrossRef] [PubMed]
29. Diaz Encarnacion, M.M.; Warner, G.M.; Cheng, J.; Gray, C.E.; Nath, K.A.; Grande, J.P. n-3 Fatty acids block TNF-α-stimulated MCP-1 expression in rat mesangial cells. *Am. J. Physiol. Renal Physiol.* **2011**, *300*, F1142–F1151. [CrossRef] [PubMed]
30. Yang, S.P.; Morita, I.; Murota, S.I. Eicosapentaenoic acid attenuates vascular endothelial growth factor-induced proliferation via inhibiting Flk-1 receptor expression in bovine carotid artery endothelial cells. *J. Cell. Physiol.* **1998**, *176*, 342–349. [CrossRef]
31. Zhuang, W.; Wang, G.; Li, L.; Lin, G.; Deng, Z. Omega-3 polyunsaturated fatty acids reduce vascular endothelial growth factor production and suppress endothelial wound repair. *J. Cardiovasc. Transl. Res.* **2013**, *6*, 287–293. [CrossRef] [PubMed]
32. Tevar, R.; Jho, D.H.; Babcock, T.; Helton, W.S.; Espat, N.J. Omega-3 fatty acid supplementation reduces tumor growth and vascular endothelial growth factor expression in a model of progressive non-metastasizing malignancy. *JPEN J. Parenter. Enteral Nutr.* **2002**, *26*, 285–289. [CrossRef] [PubMed]
33. Aird, W.C. Endothelial cell heterogeneity. *Cold Spring Harb. Perspect. Med.* **2012**, *2*, a006429. [CrossRef] [PubMed]
34. Robinson, A.T.; Cook, M.D.; Lane-Cordova, A.D. Making cell culture more physiological: A call for a more comprehensive assessment of racial disparities in endothelial cell culture studies. *Am. J. Physiol. Cell Physiol.* **2020**, *318*, C238–C241. [CrossRef] [PubMed]
35. Umebashi, K.; Tokito, A.; Yamamoto, M.; Jougasaki, M. Interleukin-33 induces interleukin-8 expression via JNK/c-Jun/AP-1 pathway in human umbilical vein endothelial cells. *PLoS ONE* **2018**, *13*, e0191659. [CrossRef]
36. Yamamoto, M.; Umebashi, K.; Tokito, A.; Imamura, J.; Jougasaki, M. Interleukin-33 induces growth-regulated oncogene-alpha expression and secretion in human umbilical vein endothelial cells. *Am. J. Physiol. Regul. Integr. Comp. Physiol.* **2017**, *313*, R272–R279. [CrossRef]
37. Umebashi, K.; Yamamoto, M.; Tokito, A.; Sudou, K.; Takenoshita, Y.; Jougasaki, M. Inhibitory Effects of Simvastatin on IL-33-Induced MCP-1 via the Suppression of the JNK Pathway in Human Vascular Endothelial Cells. *Int. J. Mol. Sci.* **2023**, *24*, 13015. [CrossRef]

編集後記

令和 5 年度（2023 年 4 月～2024 年 3 月）の臨床研究部の活動をまとめた「研究業績集 第 24 号」が完成いたしました。本業績集には、臨床研究や治験の成果をはじめ、英文原著論文、和文原著論文、学会発表、研究会、学術講演会など、多岐にわたる研究実績を掲載しています。

コロナ禍からの回復が進むこの 1 年、職員各位が研究活動の維持と発展に力を注いだ結果、英文原著論文の掲載数は 27 編に達し、一昨年度の 24 編、昨年度の 25 編から着実に増加しました。中でも、職員が筆頭著者を務めた原著英文論文は 7 編、原著以外の英文論文が 5 編と、いずれも一昨年度と昨年度を大きく上回ったことは、当施設の研究の質の向上と国際的な認知度の高まりを示す成果です。これらの業績は、日々の臨床業務と研究活動を両立させている職員各位の努力の賜物であり、深く感謝申し上げます。

2024 年度から私が臨床研究部長を拝命しまして、倫理性と科学的妥当性のある質の高い臨床研究を円滑かつ安全に推進できる環境の整備に取り組んでいます。当施設が、地域や社会の健康向上に寄与する研究成果をさらに多く生み出せるよう、引き続き尽力してまいります。この業績集が、当施設の研究活動の現状を広くご理解いただくとともに、新たな研究交流や協力関係の構築につながることを願っております。また、当施設の研究が地域の皆様の生活の質向上に貢献できるよう、職員一同一層努力してまいります。

最後に、本業績集の作成に多大な尽力をいただいた臨床研究部スタッフならびに関係各位に心より御礼申し上げます。

令和 6 年 3 月吉日

国立病院機構鹿児島医療センター

臨床研究部長 松下 茂人